SCIENCE & TECHNOLOGY

ARS JOURNAL

A PUBLICATION OF THE AMERICAN ROCKET SOCIETY

VOLUME 31 NUMBER 10 OCTOBER 1961

LOS ANGELES PUBLIC LIBRARY
OCT 20 1961

BIND

SURVEY ARTICLE

Motion and Heating of Lifting Vehicles During Atmosphere Entry . . . Alfred J. Eggers Jr. and Thomas J. Wong 1364

CONTRIBUTED ARTICLES

Measurement of Heat Flux From Initiators for Solid Propellants . . . J. A. Keller and N. W. Ryan 1375

Detonability of Solid Composite Propellants . . . W. H. Andersen and R. F. Chaiken 1379

Combustion of Carbon in an Air Stream . . . Jeffrey A. Moore and Martin Zlotnick 1388

Effect of Fuel Composition on High Frequency Oscillations in Rocket Motors Burning Premixed Hydrocarbon Gases and Air . . . J. R. Osborn and J. M. Bonnell 1397

Combustor Similitude Study . . . E. C. Woodward 1401

Problems Associated With Multiple Engine Starts in Spacecraft . . . William F. Radcliffe and John R. Transue 1408

Vehicle Motion in the Equatorial Plane of a Planet: a Second Order Analysis in Ellipticity . . . Maurice L. Anthony and Lawrence M. Perko 1413

Recent Developments in Bio-Medical Instrumentation . . . H. L. Wolbers 1422

Optimum Conditions for Photosynthesis in Optically Dense Cultures of Algae . . . A. G. Fredrickson, A. H. Brown, R. L. Miller, and H. M. Tsuchiya 1429

TECHNICAL NOTES

Choice of Unperturbed Orbit in the Use of Encke's Method for the Effects of Oblateness and Drag . . . N. S. Hall, H. F. Gawlowicz, and E. J. Wallman 1436

Geomagnetic and Geoelectric Activity as a Function of Magnetic Latitude . . . Robert Sanders 1438

High Temperature Fission Chambers and Ionization Chambers . . . G. M. B. Bouricius 1439

Thermal Diffusion Ratio in Dissociated Air . . . Sinclaire M. Scala 1441

Vacuum-Air Missile Boost . . . James J. Murray and Sudhir Kumar 1443

Attitude Control of Rotating Satellites . . . Ray Dale Cole, Mary Elizabeth Ekstrand, and Michael R. O'Neill 1446

Preliminary Thrust-Time Curve for a Spherically Shaped Solid Propellant Rocket Motor . . . Howard M. Segal 1447

Limitations on Space Vehicles Imposed by Communications Requirements . . . R. W. Sanders 1450

Streamlines in Boundary Layers on Flat and Concave Surfaces in Hypersonic Flow . . . Robert H. Johnson and Elwin C. Sigelow 1452

One-Dimensional Overtaking of a Shock Wave by a Rarefaction Wave . . . I. I. Glass, L. E. Hoeckreth, and S. Molder 1453

One-Dimensional Overtaking of a Rarefaction Wave by a Shock Wave . . . G. F. Bremner, J. K. Dukowicz, and I. I. Glass 1455

Method for Determining Scale Heights in the Atmosphere . . . S. Rubin 1456

Measurement of Heat Transfer in a Graphite Rod Heat Exchanger . . . Charles B. Johnson and Frank L. Clark 1458

Surface Behavior of Boron Nitride in High Temperature Arc Heated Gases . . . P. Dyo and S. Steinberg 1460

Effect of Earth's Oblateness on the Anomalistic Period of a Satellite . . . M. M. Mee and E. E. Karp 1462

Capture Problem in Gravitational Attitude Control of Satellites . . . E. E. Zajac 1464

DEPARTMENTS

Technical Comments . . . 1466

Patents . . . 1470

Technical Literature Digest . . . 1471

A Note of Appreciation to Dr. von Kármán . . . 1481

ARS SPACE FLIGHT REPORT TO THE NATION

OCTOBER 9-15, 1961

Session Outline

	MONDAY	TUESDAY	WEDNESDAY	THURSDAY	FRIDAY	SATURDAY	SUNDAY
9:00 MORNING	**Robot Exploration** (Jack Froehlich) 4 **Logistics and Operational Problems of Very Large Booster Systems** (Phillip F. Fahey) 3 **Structures and Materials** (Ernest E. Sechler) 5 **Power Sources for Electric Propulsion** (John Evvard) 6 **Nuclear Rocket Mission Applications** (Robert Trapp) 2 **Astrodynamics** (Samuel Herrick) 1	**Human Factors and Bioastronautics** (Brig. Gen. Charles Roadman) 3 **Missiles and Space Vehicles** (Maxwell Hunter) 4 **Power Systems** (Major W. G. Alexander) 5 **Electrothermal and Electromagnetic Thrust Generation** (Mark Ghai) 6 **Nuclear Instrumentation** (Andrew M. Koonce) 2 **Hypersonic Heat Transfer and Vaporization Ablation** (C. F. Hansen) 1	**Missiles and Space Vehicles** (Carl Kober) 4 **Environment of Space** (Joseph Kaplan) 3 **Electric Propulsion Missions** (Capt. Richard Hayes) 5 **Guidance and Control, State-of-the Art Review** (James S. Farrior) 6 **New Liquid Rocket Techniques** (Paul D. Castenholz) 2 **Hypersonics** (William H. Dorrance) 1	**Communication Satellite Future Programs** (Frank Lehan) 4 **Environment of Space** (Sidney Sternberg) 3 **Advanced Guidance Devices** (Charles E. Durham) 5 **Design of Electric Propulsion Spacecraft** (Geoffrey Robillard) 6 **NASA Program Report** (Milton Rosen) 2 **Space Propulsion and Components** (H. G. Jones) 1	**Propulsion System Selection** (Arch C. Scurlock) 4 **Environment of Space** (Jack Ruina) 3 **Propellant Technology for Space Application** (Gerald Morrell) 5 **Magnetohydrodynamics** (Milton M. Slawsky) 6 **Space Law and Sociology** (Robert D. Crane) 2 **Post Injection Guidance Considerations** (Charles E. Durham) 1	SPACE EDUCATION DAY	FINAL DAY OF EXHIBITS
12:15	LUNCHEON	LUNCHEON	LUNCHEON	LUNCHEON	LUNCHEON		
2:30 AFTERNOON	**Instrumentation for Manned Space Flights** (Col. John P. Stapp) 4 **Current State-of-the-Art of Missile and Space Vehicle Flight Testing** (Lt. Col. P. B. Peabody) 3 **Structures and Materials** (Ernest E. Sechler) 5 **Electrostatic Thrust Generation** (A. T. Forrester) 6 **Propulsion Reactor Op. Problems & Facilities** (Gaylord Newton) 2 **Astrodynamics** (G. Leitmann) 1	**Human Factors and Bioastronautics** (Brig. Gen. Ted Bedwell, Jr.) 4 **Military Program Review** (Col. Harry Evans) 3 **Power Systems** (U. B. Thomas) 5 **Electric Propulsion Testing** (Robert Supp) 6 **Communication Satellite Current Programs** (William Pickering) 2 **Hypersonics** (Walter R. Warren) 1	**Space Flight Report Panels** **The Vehicles** (Krafft Ehricke) **The Missions** (Arthur Kantrowitz) **The Global Effects** (James Doolittle)				
7:30 EVENING	**Evolution of American Liquid Propellant Rocket Engines** (Robert C. Truax) 4 **Continuing Education** (Vince Haneman) 3 **Electric Propulsion Panel** (Ernst Stuhlinger) 5 **Astrodynamics** (Robert M. L. Baker, Jr.) 2	**Human Factors Panel** (Eugene B. Konecci) 4 **Space Law and Sociology** (Andrew G. Haley) 3 **Technical Information: The Paper Curtain** (Sheldon Isaacson) 5 **Power Systems** (G. M. Anderson) 2		**The U.S. and U.S.S.R. Space Programs: A Critical Evaluation**	**SFRN BANQUET**		

Session Chairmen denoted by parentheses ( ) Numerals indicate Session Rooms.

ARS JOURNAL

A PUBLICATION OF THE AMERICAN ROCKET SOCIETY

EDITOR — Martin Summerfield
ASSOCIATE TECHNICAL EDITOR — Irvin Glassman
MANAGING EDITOR — Margaret Sherman
STAFF EDITOR — Barbara Nowak
ART EDITOR — John Culin

ASSOCIATE EDITORS

Igor Jurkevich, *G. E. Space Sciences Laboratory, Russian Supplement;* George F. McLaughlin, *Patents;* Charles J. Mundo, Jr., *Raytheon Co., Guidance;* Bernard H. Paiewonsky, *Aeronautical Research Associates of Princeton, Flight Mechanics;* M. H. Smith, *Princeton University, Technical Literature Digest*

ASSISTANT EDITORS

Carol Falcetti, Norma Herrin, Carol Rubenstein

DIRECTOR OF MARKETING

Owen A. Kean

ADVERTISING PRODUCTION MANAGER

Walter Brunke

ADVERTISING REPRESENTATIVES

New York
D. C. Emery and Thomas Harford
400 Madison Ave., New York, N. Y.
Telephone: Plaza 9-7460

Los Angeles
James C. Galloway and Co.
6335 Wilshire Blvd., Los Angeles, Calif.
Telephone: Olive 3-3223

Chicago
Thomas M. Bryne, Jr.
2316 Sherman Ave., Evanston, Ill.
Telephone: 869-1831

London
B. C. Nichols
151 Fleet St.
London E. C. 4, England

American Rocket Society

500 Fifth Avenue, New York 36, N. Y.

Founded 1930

OFFICERS

President	Harold W. Ritchey
Vice-President	William H. Pickering
Executive Secretary	James J. Harford
Treasurer	Robert M. Lawrence
General Counsel	Andrew G. Haley
Director of Publications	Irwin Hersey

BOARD OF DIRECTORS

(Terms expire on dates indicated)

Ali B. Cambel	1962	Samuel Herrick	1963
Richard B. Canright	1962	Arthur Kantrowitz	1963
William J. Cecka, Jr.	1963	A. K. Oppenheim	1961
James R. Dempsey	1961	Simon Ramo	1963
Herbert Friedman	1962	David G. Simons	1961
George Gerard	1961	John L. Sloop	1961
Robert A. Gross	1962	Martin Summerfield	1962
		Abe M. Zarem 1963	

TECHNICAL COMMITTEES AND CHAIRMEN

Astrodynamics, Robert M. L. Baker, Jr.
Communications and Instrumentation, Frank W. Lehan
Electric Propulsion, Ernst Stuhlinger
Guidance and Control, James S. Farrior
Human Factors and Bioastronautics, Eugene B. Konecci
Hypersonics, William H. Dorrance
Liquid Rockets, Martin Goldsmith
Magnetohydrodynamics, Milton M. Slawsky
Missiles and Space Vehicles, William M. Duke
Nuclear Propulsion, Robert W. Bussard
Physics of the Atmosphere and Space, Herbert Friedman
Power Systems, John H. Huth
Propellants and Combustion, Peter L. Nichols, Jr.
Ramjets, William H. Avery
Solid Propellant Rockets, G. Daniel Brewer
Space Law and Sociology, Andrew G. Haley
Structures and Materials, George Gerard
Test, Operations, and Support, Bernhardt L. Dorman
Underwater Propulsion, Herman E. Sheets

A Note of Appreciation

In the preceding issue of the JOURNAL, Dr. Theodore von Kármán wrote a congratulatory message that was addressed to me but which clearly concerned the American Rocket Society as a whole. The occasion, which would have otherwise slipped by unnoticed, was the tenth year of the "new style" JOURNAL and the tenth year of my service as Editor.

Needless to say, it is not an editorial practice of mine to feature personal messages of self-praise in the JOURNAL. In bypassing me, however, Dr. von Kármán apparently found willing accomplices in the Publications Department who engineered the deed in secret. Now that it is done, I will confess that my embarrassment upon seeing it in print was mixed with a deep feeling of gratitude, not only toward Dr. von Kármán, whose judgments have always been of the highest importance to me, but also toward my colleagues in the Publications Department and among the Society's officers who cared enough to see it done.

Although it may seem trite, I must nevertheless say to Dr. von Kármán that he can never really know as I know, nor can any outsider, how much the build-up of the JOURNAL was due to the painstaking, unselfish efforts of a group of editors —not one—who determined collectively to create a responsible scientific medium of publication for their profession; nor can he know, as I do, of the courageous administrative and financial decisions of the succession of Boards of Directors who guided the Society's publications. An institution like ARS JOURNAL is the product of many talents and labors. In placing this response on the masthead page, I wish to draw attention once again to the names of my colleagues.

Dr. von Kármán, your generous judgment, that "ARS JOURNAL is the outstanding journal of its kind in the world today," will serve to inspire the Society and its editors for years to come.

Martin Summerfield

Submit manuscripts in duplicate (orginal plus first carbon, with two sets of illustrations) to the Managing Editor, ARS JOURNAL, 500 Fifth Avenue, New York 36, N.Y.

ARS JOURNAL is published monthly by the American Rocket Society, Inc. and the American Interplanetary Society at 20th & Northampton Sts., Easton, Pa., U. S. A. Editorial offices: 500 Fifth Ave., New York 36, N. Y. Price: $18.00 per year, $3.00 per single copy. Second-class postage paid at Easton, Pa., with additional entry at New York, N. Y. This publication is authorized to be mailed at the special rates of postage prescribed by Section 132.122. Notice of change of address should be sent to the Secretary, ARS, at least 30 days prior to publication.

Opinions expressed herein are the authors' and do not necessarily reflect the views of the editors or of the Society. © Copyright 1961 by the American Rocket Society, Inc.

CREATIVE ELECTRONICS BY RCA

NORAD ON THE ALERT

Inputs from BMEWS Provide Instantaneous Missile Data Direct to NORAD Headquarters

From our vast outer defense perimeter, over thousands of miles, to the nerve center of the North American Air Defense Command at Colorado Springs, the most advanced concept of data handling and checkout is being utilized in the BMEWS system. The stakes are high, for the purpose is defense of the North American Continent.

At BMEWS installations operated by USAF Air Defense Command, computers read out missile tracking data from giant radars. This information is simultaneously relayed to NORAD's Combat Operations Center.

The Radio Corporation of America is prime systems contractor for BMEWS. At the COC, RCA's Display Information Processor computing equipment automatically evaluates missile sightings, launch sites and target areas. By means of data processing and projection equipment installed by RCA and a team of other electronics manufacturers, the findings are displayed on huge, two-story high map-screens in coded color symbols, providing the NORAD battle staff with an electronic panorama of the North American and Eurasian land masses.

The handling of BMEWS inputs at NORAD is an example of how RCA data processing capabilities are assuring the high degree of reliability so vital to continental defense.

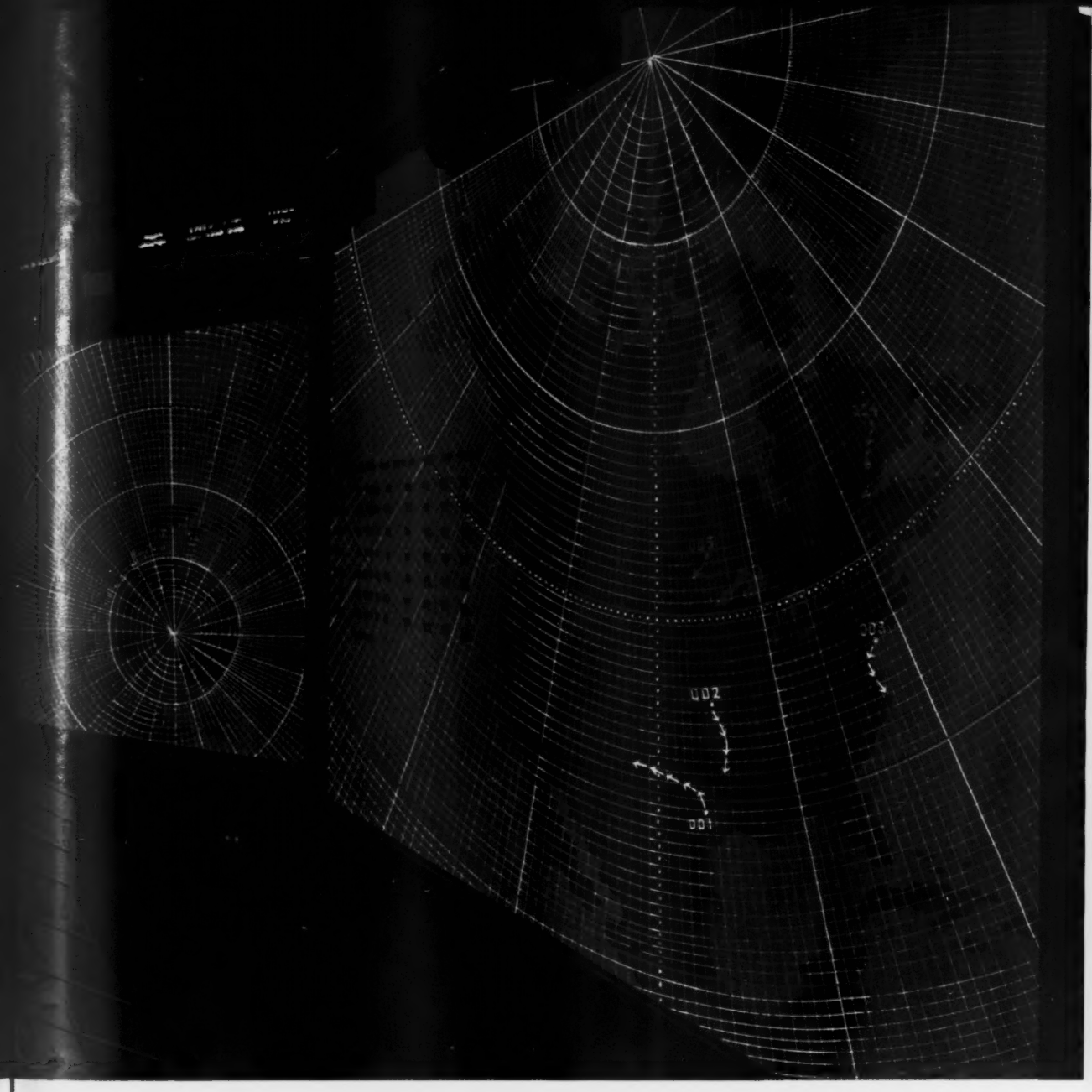

NORAD Headquarters, RCA computing equipment, the Display Information Processor (control console shown here) receives sightings data from BMEWS and processes it for automatic readout.

RCA is prime system contractor for the sprawling BMEWS three-site radar network whose probing electronic fingers reach deep into space to provide early warning of missile attacks.

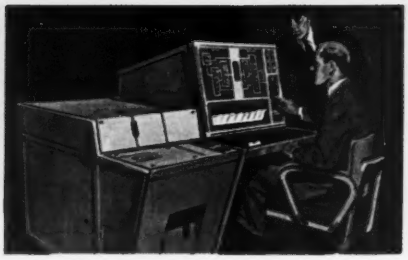

RCA's Automatic Checkout & Monitoring equipment continuously tests and checks performance of portions of the system and alerts an operator when a monitored signal exceeds certain limits.

ut of th defense needs of today a new generation of RCA electronic data rocessing equipments has been born. For tomorrow's needs RCA offers one of e nation s foremost capabilities in research, design, development and produc- on of dat processing equipment for space and missile projects. For information n these and other new RCA scientific developments, write Dept. 434, **Defense lectronic Products,** Radio Corporation of America, Camden, N. J.

RCA®

The Most Trusted Name in Electronics

RADIO CORPORATION OF AMERICA

Motion and Heating of Lifting Vehicles During Atmosphere Entry

ALFRED J. EGGERS Jr.
THOMAS J. WONG

NASA Ames Research Center
Moffett Field, Calif.

CURRENT knowledge of the motion and heating of lifting vehicles entering the Earth's atmosphere is reviewed with primary emphasis on grazing entry trajectories. The review proceeds from methods of analysis to results calculated thereby, and in the course of events attention is called to dominant effects of vehicle aerodynamic characteristics on entry motion and heating. Thus, for example, it is observed that increased lift-drag ratio at small angles of entry tends to decrease deceleration and increase maneuverability and total heat load, whereas increased lift and drag tend to decrease heating rate. Certain dominant design trends are also noted. Thus, for example, if heat shielding is by absorption (whatever the technique) then minimum total heat load contributes to reduced heat shield weight, and this tends to be achieved by making entry vehicles as small as practical consistent with their payload. Such vehicles appear suitable for entry at satellite and supersatellite speeds. If heat shielding is by radiation from the surface, relatively large vehicles are required for a given payload to limit surface temperatures, and such vehicles with a high lift and/or drag capability appear to be applicable at satellite entry speeds. With increasing entry speed, however, heating rates become especially severe and radiation cooling may become impractical.

Examination of heating and flow domains during entry indicates that the assumption of continuum flow in motion and heating studies is largely valid at speeds up to parabolic and probably well into the hyperbolic regime. On the other hand, the assumption of equilibrium flow may be somewhat in error even at subsatellite speeds, and nonequilibrium dissociation and association phenomena in combination with other nonideal gas behavior, notably ionization and radiation, can markedly influence heat transfer at supersatellite speeds. Of these several phenomena, equilibrium and nonequilibrium radiation demonstrate perhaps the most marked tendency to dominate heat transfer under hyperbolic entry conditions, and in this event it is indicated that relatively less blunt vehicles may be required to minimize heat transfer. Vastly more research is required, however, to grasp the full significance of these equilibrium and nonequilibrium phenomena in supersatellite entry.

Some consideration is given to configurations suitable for entry at satellite and supersatellite speeds, and it is noted that an exceptionally wide variety of such configurations have been considered to date. It is undertaken to point out some of the advantages and problems of several example configurations. Also suggested is a novel variable geometry shape with wings that are folded during entry to provide a compact configuration, unfolding after deceleration down to supersonic speeds to provide a relatively efficient configuration with a conventional subsonic landing capability.

The paper concludes with a comparative discussion of the problems of motion and heating of lifting vehicles entering the atmospheres of planets adjacent to Earth.

A SPACE vehicle suitable for entering the Earth's atmosphere must satisfy a minimum of two major requirements. First, the vehicle must have a heat shield which is capable of preventing overheating of the load carrying structure and internal contents during entry. Second, the vehicle must have sufficient maneuverability to prevent overstressing the structure and contents during entry and to permit landing at the desired location. Unfortunately considerations of heating and maneuverability frequently introduce conflicting design requirements, which become increasingly severe with increasing entry speed. It is precisely this combination of severe and conflicting requirements which limits our choice of structures and materials for entry vehicles and which, more generally, dictates the need

Presented at the ARS Conference on Lifting Re-Entry Vehicles, Palm Springs, Calif., April 4–6, 1961.

Dr. Alfred J. Eggers Jr., Chief, Vehicle-Environment Div., NASA Ames Research Center, Moffett Field, Calif., joined the research staff in October 1944, after receiving a B. A. from the University of Omaha. Subsequently he completed graduate studies at Stanford University, receiving an M. S. in 1949 and a Ph.D. in 1956. Before assuming his present position in November 1959, he was Chief of the 10×14-In. Supersonic Wind Tunnel Branch of NASA. Dr. Eggers, who has contributed to hypersonic flow theory and the understanding of motion and heating during atmosphere entry, has also conceived and developed specialized research equipment, including hypersonic wind tunnels and an atmosphere entry simulator, and has produced novel aircraft and lifting re-entry vehicle concepts having practical application. Dr. Eggers is a member of the Scientific Advisory Board of the U. S. Air Force, a Fellow of the Institute of Aeronautical Sciences and the ARS, and a former National Director of the ARS. He is a member of the Society of Sigma Xi, Tau Beta Pi, the American Association for the Advancement of Science, and the American Ordnance Association. He is the holder of several awards for his contributions in the aerospace field.

Thomas J. Wong, Research Scientist of the NASA Ames Research Center, was graduated from the University of Minnesota with a B. S. in Aeronautical Engineering in 1944. After later graduate study, he was awarded an M. S. degree in Aeronautical Engineering by the University of Minnesota in 1949. He has been a member of the staff of the NASA Ames Research Center since 1949, specializing in hypersonic aerodynamics, re-entry mechanics, and aerothermodynamics and space mechanics. Mr. Wong is a member of the ARS and Tau Omega.

for a large body of knowledge on the aerothermodynamics of entry to insure successful vehicle design.

The first purpose of this paper is to review the current status of this knowledge, placing primary emphasis on grazing entry trajectories because of their suitability for exploiting the maneuvering capabilities of entry vehicles in general and manned vehicles in particular. Subsequent to this review, heating and flow domains are examined with the aim of highlighting phenomena which may emerge importantly in entry at supersatellite speeds and which require additional research to be well understood. Attention is then directed to entry configuration concepts and some of the specialized motion and heating problems they may encounter. The paper concludes with a comparative discussion of motion and heating during entry into the atmospheres of planets near Earth.

Analysis

In studying the motion of a lifting vehicle during entry into a planetary atmosphere we will proceed with the following notations and basic Eqs. 1–4.

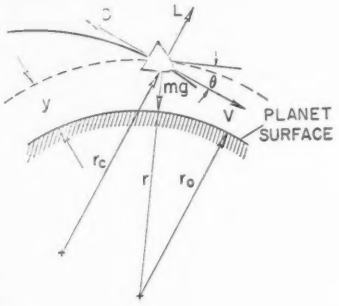

Normal Plane

$$L - mg\left(\frac{r_0}{r}\right)^2 \cos\theta = -\frac{mV^2}{r_c} \qquad [1]$$

$$D + mg\left(\frac{r_0}{r}\right)^2 \sin\theta = -\frac{m}{2}\frac{dV^2}{dS} \qquad [2]$$

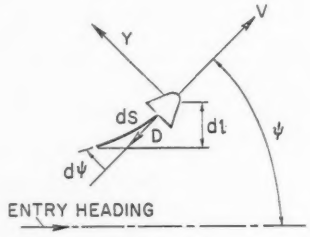

Lateral Plane

$$Y = mV^2\frac{d\psi}{dS} \qquad [3]$$

$$dl \approx dS \sin\psi \qquad [4]$$

Treating the planet and its atmosphere as stationary, a balance of the forces and accelerations in the lift and drag directions yields Eqs. 1 and 2, respectively, where the angle θ to the local horizontal is negative downwards, g is gravity acceleration, and S is arc length in the direction of motion. (See Appendix for complete list of symbols.) Balancing the side force Y with the corresponding acceleration yields Eq. 3, where lateral displacement dl is proportional to the sine of the lateral flight path angle ψ, as shown in Eq. 4, provided that this displacement is small compared with the longitudinal displacement dS.

Numerous methods of combining and transforming these equations have been used to facilitate the study of entry motion. See, for example, (1–14).[1] We are primarily interested in the case of small entry angles, and with this limitation plus the assumption that entry occurs when drag predominates over the colinear component of weight, Eqs. 1 and 2 can be combined into the single second-order differential Eq. 5, and Eq. 3 transforms to Eq. 6.

Normal Plane

$$\frac{1}{C_DA}\frac{d}{dz}\left(C_DA\frac{df}{dz}\right) + \frac{I}{f}(1 - e^{-z}) + J = 0 \qquad [5]$$

Lateral Plane

$$\frac{d\psi}{dz} + \frac{1}{2}\frac{Y}{D} = 0 \qquad [6]$$

where

$$f = \frac{1}{\alpha}\frac{\rho}{\rho_0} = e^{-\beta y} \qquad z = \ln \overline{V}^2$$

$$I = \frac{\beta}{r_0}\left(\frac{m}{C_DA\rho_0\alpha}\right)^2 \qquad J = \frac{\sqrt{I\beta r_0}}{2}\left(\frac{L}{D}\right)$$

$$\theta = \frac{1}{\sqrt{I\beta r_0}}\frac{df}{dz} \qquad \overline{V} = V/\sqrt{gr_0}$$

and

$$G = \frac{1}{2}\sqrt{\frac{\beta r_0}{I}}fe^z\sqrt{1 + \left(\frac{L}{D}\right)^2 + \left(\frac{Y}{D}\right)^2} \qquad [7]$$

It is noted in Eqs. 7 that the density variable f is proportional to the ratio of density at altitude ρ to density at sea level ρ_0, and to a good degree of approximation this ratio varies exponentially with altitude y in Earth's atmosphere. The independent variable z equals $\ln\overline{V}^2$ where $\overline{V}$ is the ratio of flight velocity to near Earth satellite velocity. The parameters I and J are functions of planet and atmosphere properties along with the mass and drag characteristics of a vehicle in the case of I, and the lift characteristics in the case of J. Note too the dependence of flight path angle θ and resultant deceleration G on these quantities.

We can now attach physical significance to the terms in Eq. 5. The first term is proportional to the rate of change of flight path angle with velocity, and it is usually small in the case of relatively steep entry of a ballistic vehicle (1). The second term is proportional to the difference between weight and centrifugal force in flight essentially parallel to the curved surface of a planet, and it is usually negligible in a very strong skip (2) or relatively steep ballistic entry. The third term, which is proportional to lift-drag ratio, will play a dominant role in our study.

A particularly instructive approximate solution to Eq. 5 corresponds to Sanger's equilibrium gliding flight (6), in which case the first term is negligible and the second and third terms balance to equate the sum of lift, weight, and centrifugal force to zero. Thus there is obtained $f = -I/J(1 - e^{-z})$; under these circumstances we obtain with the aid of Eqs. 6 and 7 the following results for satellite entry with constant force coefficients (3):

$$G_{max} = \sqrt{1 + \left(\frac{D}{L}\right)^2 + \left(\frac{Y}{L}\right)^2} \qquad [8]$$

$$S_{max} = \frac{r_0}{2}\frac{L}{D}\ln\left(\frac{1}{1 - \overline{V}_E^2}\right) \to \infty \quad \text{as } \overline{V}_E \to 1 \qquad [9]$$

[1] Numbers in parentheses indicate References at end of paper.

and

$$l_{max} = \frac{\pi^2}{48} r_0 \left(\frac{L}{D}\right)_0^2 + \ldots \qquad [10]$$

when the vehicle bank angle is 45°, and where the subscript 0 on $(L/D)^2$ in Eq. 10 denotes the value of this quantity at zero bank. Now Eqs. 8 and 9 lose validity as $L/D \to 0$, and Eq. 10 loses accuracy at values of $(L/D)_0$ in excess of about 1. Nevertheless these equations provide a valuable guide for our thinking about the effect of lift, drag, and side force on entry motion. Thus increased lift-drag ratio decreases deceleration and increases both longitudinal and lateral range. Moreover, since maximum lateral range is achieved at 45° bank angle it corresponds to the case of side force equal to lift force. Now it is noteworthy that longitudinal range tends to be far more sensitive to entry velocity than to L/D and this fact, coupled with the additional powerful capability to change longitudinal range by changing entry time, permits special emphasis on the use of L/D to achieve lateral range by banking.

Returning our attention to Eq. 5, it should be noted that it is equally valid with constant or variable force coefficients, and it has been found (3–5) to be especially suited for obtaining simplified series solutions of f as a function of z in the case of entry with constant lift and drag coefficients.[2] Observe too that Eq. 6 for lateral motion is relatively simple; thus for a constant value of Y/D it is clear that the change in the lateral direction of motion is directly proportional to Y/D and the net change in z during entry, irrespective of the type of entry.

Motion and heating during entry are, of course, intrinsically related. Consider therefore the form taken by the convective heating equation in terms of the f and z variables and the other parameters of this analysis. We will allege now and verify later (3,4,8,9) that flight Reynolds numbers during severe heating are usually on the order of a million or less. Under these circumstances the boundary layer at the surface of a vehicle frequently tends to be largely laminar. In this event the equation for heating rate can be written in the following form:

$$\dot{q} = C_q (\alpha\rho_0)^{1/2} (gr_0)^{3/2} \left(\frac{f}{d}\right)^{1/2} e^{3z/2} \qquad [11]$$

where C_q is a constant depending on body shape and properties of the atmosphere (3).[3] It is easily demonstrated (see for example, Refs. 3 and 8) that laminar heat transfer rate varies directly as the square root of atmosphere density, inversely as the square root of the pertinent body dimension, and directly as the cube of the flight velocity. This variation reflects directly in the functional dependence of $\dot{q}$ on f, z, and the pertinent body dimension d in Eq. 11. Now, it is convenient to transform this equation to a differential equation with z as the dependent variable:

$$\frac{dq}{dz} = -C_q \frac{gr_0}{(\alpha\rho_0)^{1/2}} \frac{m}{C_D A} \frac{e^z}{(fd)^{1/2}} \qquad [12]$$

This equation, combined with solutions to Eq. 5 relating f to z, makes it possible to calculate integrated heat transfer per unit area and total heat transfer to a vehicle during atmosphere entry.

As in the case of entry motion, it is instructive to examine the entry heating equations for lifting vehicles in an equilibrium glide from satellite speed. These equations are shown (3) to take the following form

$$\dot{q}_{max} = C_q \frac{2\sqrt{2}}{3\sqrt{3}} g^{3/2} r_0 \sqrt{\frac{m}{C_L A d}} \qquad \text{at } \bar{V} = \sqrt{\frac{2}{3}} \qquad [13]$$

$$q = C_q \frac{\pi}{2\sqrt{2}} g r_0^{3/2} \sqrt{\frac{L}{D}\left(\frac{m}{C_D A d}\right)} \qquad [14]$$

$$Q = C_Q \frac{\pi}{2\sqrt{2}} g r_0^{3/2} \sqrt{\frac{L}{D}\left(\frac{md}{C_D}\right)} \qquad [15]$$

First we note from Eq. 13 that heating rate $\dot{q}$ varies directly as the square root of the mass per unit lifting area and inversely as the square root of the lift coefficient and pertinent dimension of the vehicle. Thus to reduce heating rate for a given mass, it appears desirable to increase the size and lift coefficient developed by a vehicle. It is seen from Eq. 14 that net heat transfer per unit area q is also reduced by increasing size. In addition q is decreased by decreasing the lift-drag ratio and increasing the drag coefficient of a vehicle. Finally it is observed that Q, the total heat transfer to a vehicle, is also reduced by reducing lift-drag ratio; however, unlike the situation with $\dot{q}$ and q, total heat transfer is further reduced by *decreasing* the dimensions and hence the size of the vehicle. Generally speaking, then, it can be suspected that, for a given mass, a radiation cooled vehicle will be relatively large and have relatively high lift capability, whereas a vehicle with an absorption type of heat shield will be of relatively small size, with high drag and with low lift-drag ratio.

To better understand the effects of these parameters on heating and temperatures during entry it is necessary to proceed to a more precise and enlarged understanding of entry motion. This subject will be developed in the following paragraphs, first in the case of satellite entry and then in the case of supersatellite entry.

The majority of motion results to be presented and discussed were selected from (3–5), which employed Eqs. 5 and 6 setting $\alpha = 0.715$ and $\beta = 1/24{,}800$ ft to conform with the ARDC model atmosphere for Earth (3), and setting $r_0 = 21 \times 10^6$ ft. Additional results obtained with the aid of Eqs. 5 and 6 will also be presented along with pertinent IBM calculations from the extensive entry studies of Chapman (8, 9), who employed an alternate form of Eq. 5. The heating results to be presented and discussed were obtained with the aid of Eqs. 11 and 12 in combination with the motion results, and with the assumption of chemical equilibrium in the flow about a vehicle.

Satellite Entry

The effect of lift-drag ratio on maximum decelerations and

---

[2] In the case of grazing entry a useful series solution (3) is

$$= k_0\sqrt{I}e^{-z_0/2}\left[1 - \frac{1}{2k_0^2}\left(e^{z_0} - 1 + k_0 e^{z_0/2}\frac{J}{\sqrt{I}}\right)(z - z_0)^2 - \frac{1}{6k_0^2}(z - z_0)^3\right]$$

where

$$k_0^2 - \frac{k_0}{2} e^{z_0/2}\frac{J}{\sqrt{I}}(z_E - z_0)^2 - \left[\frac{e^{z_0} - 1}{2}(z_E - z_0)^2 + \frac{1}{6}(z_E - z_0)^3\right] = 0$$

and the subscript 0 corresponds to conditions at the bottom of a graze. As noted in (4) for grazing entries at parabolic speed with positive lift, it is generally sufficient to retain only the first two terms in the above series. For parabolic grazes with negative lift, it is again sufficient to retain only two terms, provided that $z_E - z_0 \ll 1$.

[3] The values used here for C_q in air are as follows (15)

Stagnation Region

$C_q = 1.75 \times 10^{-8}$ Btu-sec^2/slug$^{1/2}$-ft^3 for $\bar{V}_E = 1.0$

$= 2.15 \times 10^{-8}$ Btu-sec^2/slug$^{1/2}$-ft^3 for $\bar{V}_E = \sqrt{2}$

Conical Surface Area

$C_q = 1.4 \times 10^{-8} \sin\delta\sqrt{\cos\delta}$ Btu-sec^2/slug$^{1/2}$-ft^3

where δ is the surface angle to the flight direction.

In the case of the stagnation region and conical surface area, the characteristic dimension d is the nose radius of curvature and the base radius of curvature, respectively. Density ρ_0 is evaluated at sea level.

lateral maneuverability during entry at satellite speed near θ_E of zero is shown on Fig. 1. It is evident that maximum decelerations at zero L/D are not prohibitively large even for manned vehicles, and at lift-drag ratios the order of $\frac{1}{2}$ and greater these decelerations are reduced to levels approaching those of conventional flight. Note too the relatively accurate prediction of G_{max} by equilibrium glide theory at the higher values of L/D. Now the increase in maximum lateral range with increasing $(L/D)_0$ up to 1 is—as was also expected from equilibrium glide theory—quadratic, yielding values of $(l/r_0)_{max}$ of about 0.2 or less, which corresponds to $\frac{1}{2}$ or less of the orbit shift distance. To maneuver laterally the order of the orbit shift distance, lift-drag ratios of the order of $1\frac{1}{2}$ are required.

Calculations of the heating of flat top, half cone configurations entering at satellite speed near θ_E of zero are shown in Fig. 2.[4] These configurations were chosen to facilitate the calculations (3) without obscuring the essential dependence of heating on mass, size, and aerodynamic characteristics of entry vehicles.

It is observed in Fig. 2 that heating rate and net heat transfer per unit area are substantially more severe in the stagnation region than on an average surface element aft of the nose. Evidently increasing L/D for a fixed C_DAd/m markedly reduces maximum stagnation and average heating rates, and to a lesser but nevertheless significant extent the corresponding equilibrium surface temperatures are reduced. In practice of course, C_DAd/m is usually not fixed, and the effect of L/D on average heating rates may be changed and even reversed, depending on the variation of C_DAd/m with L/D. Stagnation region heating rates and equilibrium surface temperatures are, however, as was noted with the equilibrium glide theory, generally minimized at maximum lift, which occurs with the study configuration and many other configurations at lift-drag ratios the order of $\frac{1}{2}$. In any case Fig. 2 suggests that maximum equilibrium surface temperatures may not exceed the order of 3500° to 4000°R in the stagnation region, and they may be as low as the order of 2000° to 2500°R on an average surface element during satellite entry. The higher temperatures may not exceed the range of application of ceramic and coated refractory materials, whereas super alloys may be suitable for use at the lower temperatures. Accordingly we can appreciate the possibility of employing radiation cooled vehicles for satellite entry. It is evident from Fig. 2 that, as was anticipated, unit heat transfer and total heat transfer increase substantially with increasing L/D. In view of the large values of heat transfer associated with entry at the higher values of L/D, it can be suspected that radiation cooling may be essential to minimize heat shield weight under these circumstances. At lower values of L/D, however, unit and total heat transfer are not prohibitively larger than those for ballistic vehicles, and therefore ablation heat shields, for example, should have practical application.

It is pertinent to inquire how maneuvering affects these heating results and certain of the motion results. To this end the effects of bank angle of a vehicle on G, S, $\dot{q}$, q and Q are shown in Fig. 3. It appears that these effects are not inordinately large at bank angles up to 45°, which corresponds to that for maximum lateral range. For example, maximum deceleration is increased by not more than about 40%, longitudinal range is decreased by only about 30%, heating rates are increased by only about 20%, and net heat transfer is decreased by about 15%. In all probability these effects are wholly or in part less severe than those which may be encountered following an aborted launch, and for which any satellite vehicle must of course be designed. Accordingly

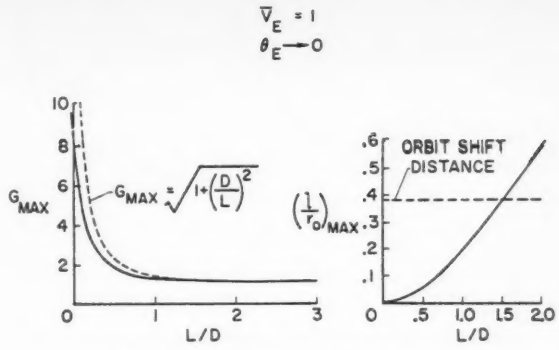

Fig. 1 Deceleration and lateral range

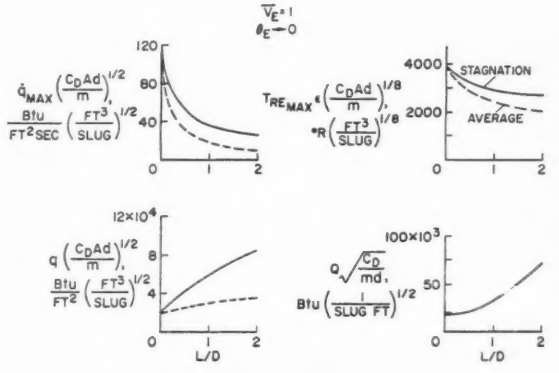

Fig. 2 Maximum heating and temperatures

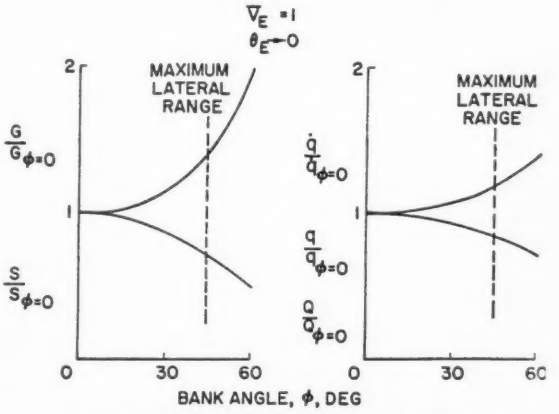

Fig. 3 Effect of bank on motion and heating

normal entry maneuvering requirements should be well within design capabilities of a satellite vehicle whether, for example, it be of the relatively low L/D ablation cooled type or relatively high L/D radiation cooled type.

The fact that a satellite vehicle must be capable of operating over a spread of altitudes and speeds about those characteristic of a nominal entry has led to the adoption of the corridor concept (14) illustrated in Fig. 4. If the upper boundary of the corridor is exceeded in flight below satellite speed, the entry vehicle is flying too slowly to sustain altitude and is unable to check its descent before passing through the lower boundary. Below the lower boundary the vehicle is flying too fast to maintain decelerations and/or heating rates at tolerably low values. These boundaries, then, define speed-altitude limits beyond which a satellite entry vehicle should not fly, whether in the course of returning from orbit or subsequent to an aborted boost into orbit. The concept

[4] These conical configurations are assumed to have their axes of revolution parallel to the flight direction; thus, for small nose bluntness their Newtonian aerodynamic characteristics are approximated by

$$C_L = (4/\pi) \sin \delta \cos \delta\, L/D = (2/\pi) \cot \delta$$

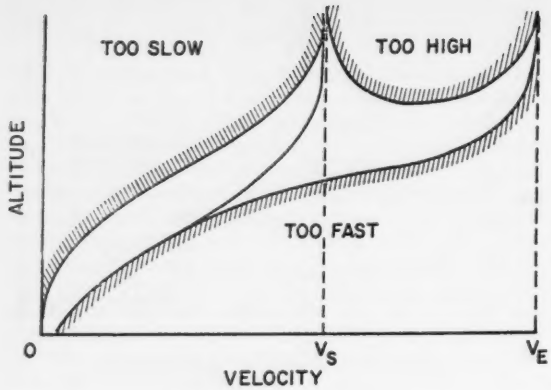

Fig. 4 Corridor concept

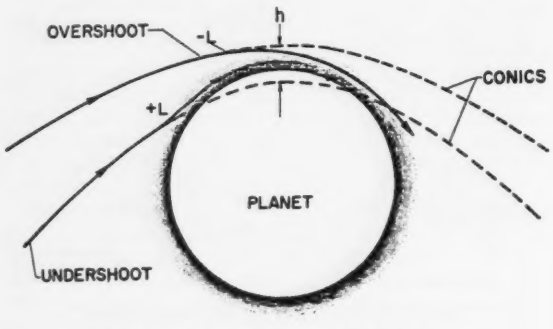

Fig. 5 Supersatellite corridor definition

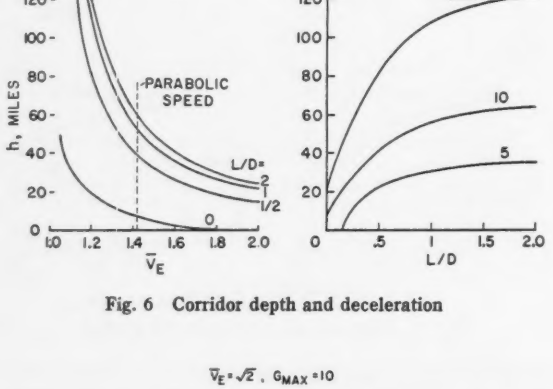

Fig. 6 Corridor depth and deceleration

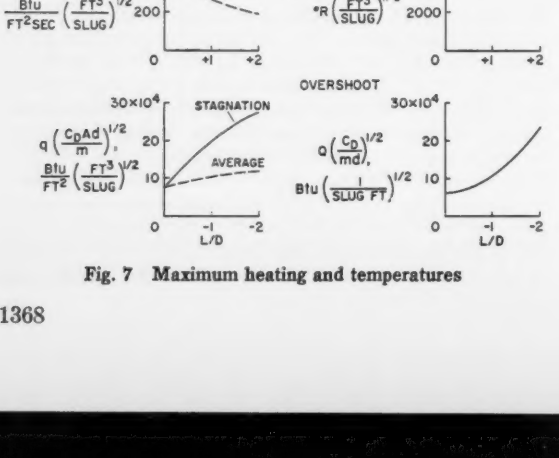

Fig. 7 Maximum heating and temperatures

has proved useful in satellite vehicle design studies, and it has a logical extension to the case of supersatellite entry.

Supersatellite Entry

If a vehicle flies at supersatellite speeds above the upper boundary of the entry corridor shown in Fig. 4, it is unable to decelerate sufficiently to avoid exiting the atmosphere and proceeding possibly vast distances back into space. This latter result appears undesirable and may be unacceptable as normal procedure in manned flight. On the other hand, if supersatellite entry leads to flight below the lower boundary, speed is so high that a vehicle is unable, as in the subsatellite case, to avoid excessive deceleration and/or heating. In order to formalize this description of supersatellite corridors it is instructive to consider Fig. 5, which shows a planetary approach along an overshoot and an undershoot boundary. The solid lines are the actual flight trajectories of a vehicle in the atmosphere, whereas the dashed lines are the fictitious conic trajectories that would be followed if the planet and its atmosphere were removed and replaced with an equivalent point mass. Now it is convenient (9) to define the corridor depth h, measured in miles, as the difference between the virtual perigees of the overshoot and undershoot conics. The larger the value of h, the less stringent is the guidance accuracy requirement during planetary approach. Corridor depth can be increased as suggested in Fig. 5 by employing negative lift along the upper boundary to avoid exiting at supersatellite speed, and by employing positive lift along the lower boundary to avoid penetrating to too low an altitude at too high speed. The achievable values of h are, of course, connected (see, for example, Refs. 4 and 9) with both the force and mass characteristics of entry vehicles, and with the heating and deceleration limitations of their structures and payloads. Maximum decelerations are encountered at the lower boundary of the corridor; the connection between these decelerations and corridor depths is shown in Fig. 6 for supersatellite entry into Earth's atmosphere over a range of speeds and vehicle lift-drag ratios. In obtaining the corridor depths presented in Fig. 6, L/D was held constant and negative down to satellite speed in flight along an overshoot boundary; a positive L/D of the same absolute magnitude[5] was employed in calculating the descending portion of the undershoot boundary to at least zero flight-path angle. Along the subsequent portion of the undershoot boundary it was assumed that force coefficients may be modulated as required (10) to avoid exiting at supersatellite speed. Note first that for $G_{max} = 10$, which may be acceptable for manned vehicles, there is a marked reduction in h with increasing entry speed. There is, on the other hand, a sizable increase in h with increasing L/D, especially from zero to $\frac{1}{2}$; this effect is shown on the right of Fig. 6 for several values of G_{max} at parabolic entry speed. Clearly, increasing L/D can markedly increase h irrespective of the value of G_{max}, and even small values of L/D provide sizable entry corridors if G_{max} is not too small. Thus, for example, if a permissible G_{max} is 10, a vehicle with $L/D = \frac{1}{2}$ may provide in excess of a 40-mile deep entry corridor at parabolic approach speed, and with reasonable guidance capabilities (see, for example, Refs. 4, 9 and 16) this depth should be ample for lunar return and other relatively near Earth missions. In the case of deeper space missions characterized by hyperbolic flight speeds in return to Earth, corridor depths for an entry vehicle of $L/D = \frac{1}{2}$ will be substantially reduced, approaching the order of 15 miles for a G_{max} of 10 at $\overline{V}_E = 2$ (see Fig. 6). It has been estimated, however, that such corridors are well within the accuracy capabilities that should evolve from advanced guidance systems (16).

It is appropriate now to inquire about the heating experienced by vehicles flying along the corridor boundaries.

[5] Values of m/C_DA were considered to be identical in flights characterized by the same absolute magnitude of L/D.

Maximum convective heating rates are usually encountered on entry trajectories characterized by maximum deceleration, whereas net heat transfer tends to be a maximum on entry trajectories characterized by minimum deceleration. Accordingly we are particularly interested in investigating heating rates and equilibrium surface temperatures along the undershoot boundaries, whereas heat transfer per unit area and total heat transfer to a vehicle are of special interest on the overshoot boundary. These quantities are shown in Fig. 7 for the case of entry at parabolic speed in a corridor limited at the lower boundary by $G_{max} = 10$, and at the lower and upper boundary by the requirement for exit speed not to exceed satellite speed. The values of net heat transfer for entry along the overshoot boundary also include heating for the final descent from satellite speed at the corresponding positive L/D. It is interesting to note in Fig. 7 that the effects of L/D on heating are qualitatively similar to those observed in Fig. 2 for satellite entry. The magnitude of the heating problem in parabolic entry is clearly much more severe, however, than in the satellite entry case. It can be seen, for example, that maximum heating rates along the undershoot boundary may be an order of magnitude greater than those encountered in satellite entry, with the result that maximum equilibrium surface temperatures may be the order of 50 to 100% higher than those for the same vehicle in a satellite entry. Indeed these surface temperatures appear so high, e.g., from 4500° to 6000°R, that it almost certainly will prove difficult if not altogether impractical to employ radiation cooling in parabolic entry near the undershoot boundary. Let us consider next flight along the overshoot boundary. Fig. 7 indicates in this case that unit and total heat loads are several times those encountered in a satellite entry, and they increase markedly with increasing L/D. Accordingly, if heat shielding by radiation is impractical due to the exceptionally high heating rates encountered in the lower portion of the entry corridor, then low lift-drag ratios may be mandatory, especially in flight near the overshoot boundary, in order to minimize absorption[6] heat shield weight.

In the light of these considerations it is pertinent to consider the heating histories of a low L/D vehicle flying along its overshoot and undershoot boundaries. These histories are shown in Fig. 8 for the stagnation regions of a vehicle developing an L/D of $\frac{1}{2}$, characterized by a value of $m/C_DAd = 3$ slugs/ft^3, and entering the atmosphere at parabolic speed. It is observed that in decelerating from parabolic speed to satellite speed along the undershoot boundary, maximum stagnation heating rates reach the order of 1100 Btu/ft^2-sec and the total heating time is only about 200 sec. Total heating time along the overshoot boundary is more than 4 times greater; however the maximum heating rates are considerably less, being only about 300 Btu/ft^2-sec. In the final descent from satellite speed, heating rates and heating times along overshoot and undershoot trajectories bear about the same relation as in the supersatellite portion of flight, although as expected the rates are considerably lower than those encountered at supersatellite speeds. It is evident too, as was suggested earlier, that net heat transfer along an overshoot boundary is considerably greater than that along an undershoot boundary.

Up to now we have considered motion and heating during supersatellite entry in terms of extreme conditions encountered at vertical corridor boundaries. It is to be expected that conditions encountered in flight within the boundaries will normally lie between these extremes. In the light of our findings on satellite entry, it is to be expected further that maneuvering laterally will not alter the order of the motion and heating problems. It is instructive nevertheless to consider lateral maneuvering briefly, especially in terms of the comparative effectiveness of maneuvering in the atmosphere and maneuvering in space by means of rocket thrust. To this end, the change in the lateral direction of flight ψ as a function of the ratio of side force to drag force is shown in the upper left of Fig. 9 for deceleration during entry from parabolic speed to satellite speed. This change in direction can be interpreted as a rotation of the plane of the orbit; the corresponding rotation due to the application of lateral rocket thrust[7] in space is shown in the upper right of Fig. 9. It is evident that large rotation could be achieved aerodynamically with large values of Y/D. We have already observed, however, that the severity of the overall heating problem during parabolic entry may preclude the use of high L/D entry vehicles. There will tend to be a corresponding restriction on Y/D; in this event lateral maneuvering by aerodynamic means to rotate the orbit by more than a few tenths of a radian may not be practical. On the other hand, if orbit rotation is achieved by rocket thrust early in the approach trajectory, large rotation may be practical. Thus, for example, if these maneuvers are initiated at a distance the order of 50 radii from Earth, the order of $\frac{1}{2}$ a radian

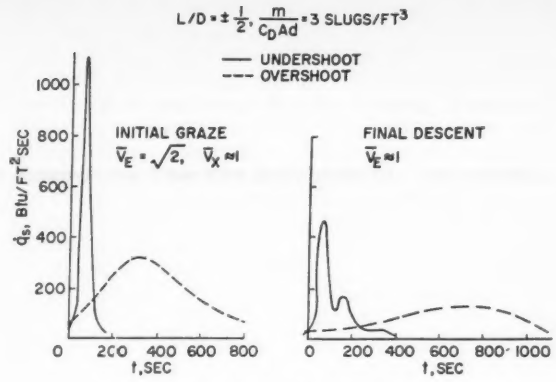

Fig. 8 Heating histories

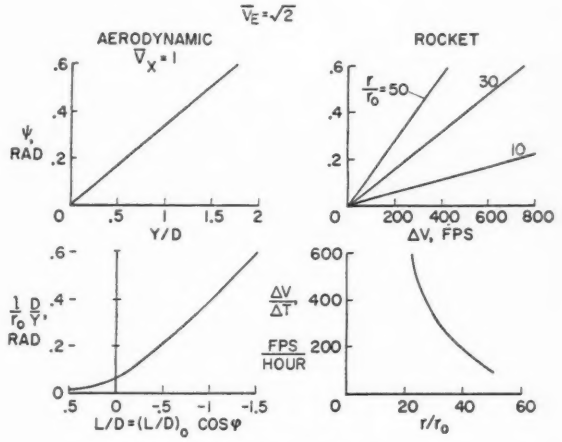

Fig. 9 Maneuvering

[6] The term absorption as employed here and elsewhere in this paper is intended to encompass ablation, et al. At this point too it bears remarking that combined absorption-radiation heat shields are, of course, feasible and might have attractive application to parabolic entry vehicles.

[7] Lateral rocket thrust and resultant velocity increment are applied in the plane normal to the radius r at the angle $(\pi + \psi)/2$ relative to the initial orbit plane in order to rotate the orbit through the angle ψ without changing virtual perigee.

rotation appears to be achievable with a lateral velocity increment the order of 300 fps; this would seem to be a nominal rocket requirement. It may logically evolve therefore that large orbit rotation maneuvers are most effectively performed by means of rocket thrust at large distances from Earth, whereas relatively small lateral maneuvers for fine entry trajectory control can be performed aerodynamically during entry. In connection with such aerodynamic maneuvers it is interesting to note from the calculated results presented in the lower left of Fig. 9 that maximum lateral displacement in a parabolic entry is the same order as that in a satellite entry if these displacements are achieved at the upper boundary of the corridor. Lateral displacements decrease markedly with decreasing altitude in the corridor, however, being as much as perhaps an order of magnitude less at the lower boundary. Finally, and of very considerable importance is the effect of rocket thrust on time of arrival at Earth (see lower right of Fig. 9). If this thrust is applied essentially along the radius r connecting the center of Earth and the vehicle, the change in virtual perigee can be reduced to essentially zero. At the same time, as shown in Fig. 9, a velocity increment of a few hundred feet per second can change the time of arrival by the order of an hour if the increment is applied at relatively large distances from Earth. Remembering that a point on Earth is displaced as much as 1000 mph due to Earth rotation, it is evident that changing arrival time by application of rocket thrust in space can provide a means of achieving substantial lateral as well as longitudinal range control, depending on the inclination of the approach trajectory to the Equator. An analogous maneuver, of course, is to hold in a near Earth satellite orbit and simply let Earth rotate under the vehicle. With these various techniques available for maneuvering in space, it seems unlikely that large amounts of lateral maneuvering will be required during supersatellite entry.

We have, however, in the course of reviewing our knowledge of entry motion and heating, made a number of assumptions which bear examination to determine their limitations, and this is the matter we shall take up next.

Examination of Assumptions

Valuable information on the validity of our assumptions can be obtained by examining heating and flow domains during atmosphere entry. These domains are shown on Fig. 10 in the altitude-velocity coordinate system (17). It appears reasonable to assume (18) that continuum flow will prevail about practical size vehicles where the mean free path of air molecules in the atmosphere does not exceed the order of a hundredth of a foot. This condition is satisfied at altitudes

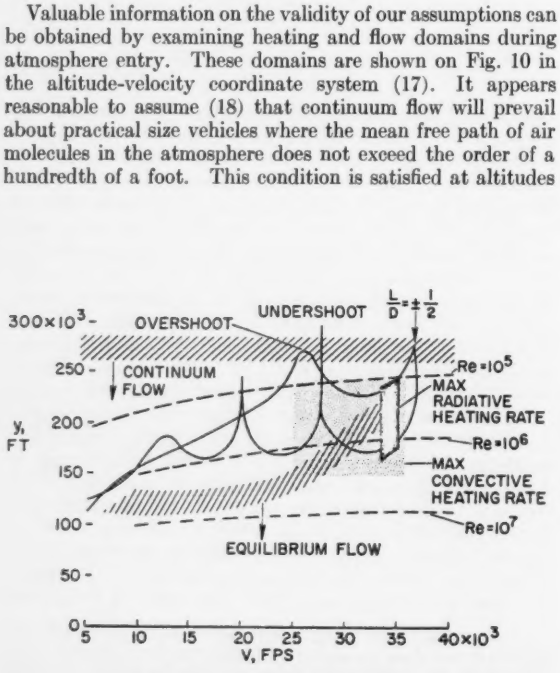

Fig. 10 Flow and heating domains

in the neighborhood of and below about 250,000 ft, and deceleration and heating of relatively compact entry vehicles tend to occur largely below these altitudes. This observation is generally substantiated by Fig. 10, which shows the region of maximum heating rates for a wide class of such vehicles entering at parabolic speed, including the $L/D = \frac{1}{2}$ vehicle that was considered in Fig. 8. It is evident too from Fig. 10 that the assumption of flight Reynolds numbers being the order of or less than a million is largely valid.[8] At this point, however, a word of caution is in order, because some shock tube experiments on blunt shapes in relatively high enthalpy air flow corresponding to $V \leq 13{,}600$ fps (19) indicate that transition Reynolds numbers may be in the range from half a million to a million. In this event substantial turbulent boundary layer flow may occur on entry vehicles in flight near their lower boundary. Accordingly, heating rates and hence net heat transfer at the lower boundary may be substantially higher than was estimated earlier herein assuming laminar boundary layer flow. Indeed in the limiting case of all turbulent flow over the $L/D = \frac{1}{2}$ vehicle of Figs. 8 and 10, it is estimated that net heating in flight along the undershoot boundary may be the same order as that for laminar flow along the overshoot boundary. Under such circumstances ablation heat shield requirements could be more severe along the undershoot than along the overshoot boundary, since the effective heat capacity of ablators tends to be reduced because of reduced "blowing" effectiveness in turbulent flow (20). These observations serve to point up the important need for additional experimental data on transition, turbulent heating and ablation heat shield effectiveness under Reynolds number and enthalpy conditions encountered in satellite and supersatellite entry.

Let us inquire now whether the assumption of chemical equilibrium is valid in the disturbed flow about an entry vehicle. It appears probable (17) that this assumption will tend to break down first in the boundary layer. Note that the lower shaded band in Fig. 10 is centered on a line for which laminar convective heating may be decreased by nonequilibrium effects to the order of 70% of the equilibrium value. Note too that the entry corridor of the $L/D = \frac{1}{2}$ vehicle is largely at a higher altitude than this band, as is the general area in which maximum convective heating rates occur. Nonequilibrium effects tend to become more pronounced, of course, with decreasing density and hence increasing altitude. Accordingly nonequilibrium boundary layer phenomena may significantly reduce convective heating during atmosphere entry; hence they deserve careful study. Important progress has already been made on this problem, and recently Chung, Anderson and Goodwin (21, 22) completed calculations of nonequilibrium heating during parabolic entry along overshoot and undershoot boundaries. Typical results of these calculations over a range of values of L/D are shown in Fig. 11 for the case of stagnation region heating rates; it will be observed that with a noncatalytic wall these rates may be reduced the order of 60% along an overshoot boundary, and the order of 30% along an undershoot boundary. Comparable reductions in net heat transfer may be expected; however, the key to either of these reductions is to obtain a noncatalytic wall. One method for obtaining such a wall may be to use silicon oxide coatings; however, Goodwin and Chung point out (22) that even at the higher altitudes of entry the presence of a reasonably cold wall, and possibly ablated material in the boundary layer may encourage the association of atoms near the wall which would increase heating towards the equilibrium value (22–26). Additional investigations are clearly required to fully understand these nonequilibrium boundary layer and wall reaction phenomena.

Returning to Fig. 10, we are reminded of the fact that radiation heating may not be negligible in supersatellite

[8] Reynolds numbers presented in Fig. 10 are based on vehicles with a typical dimension of 10 ft.

entry. Specifically it will be noted that maximum radiative heating rates for parabolic entry tend to occur during the descent in the first graze, and they overlap the region of maximum convective heating rates. Equilibrium radiation from the "hot gas cap" between the bow shock wave and surface of a body has been the subject of considerable theoretical and experimental study at subsatellite speeds (27–29), but relatively little research has been completed on this subject at supersatellite speeds. The dearth of experimental data on equilibrium radiation is especially notable at supersatellite speeds, and our knowledge of nonequilibrium radiation at both subsatellite and supersatellite speeds is only now beginning to develop. Such information as we have on supersatellite radiation is therefore largely theoretical in nature, and it probably should be considered little better than qualitative at this stage. Nevertheless theory in combination with available experiment can prove useful in clarifying our thinking on the order of supersatellite radiation and the dependence of this phenomena on vehicle parameters and flight trajectories. With this in mind, Yoshikawa of Ames Research Center has calculated equilibrium radiation heating rates for a hemispherical stagnation region. His results are summarized on the left of Fig. 12; see also (12) and (30). It is indicated that these rates increase relative to equilibrium convective heating rates as the radius of curvature of the body increases, as flight altitude decreases corresponding to increasing density and, especially, as flight speed increases.[9] Indeed, with entry speeds well into the hyperbolic regime, it appears altogether possible that radiative heating may predominate over convective heating, depending on vehicle shape and trajectory. On the other hand it is indicated in Fig. 12 that in parabolic entry equilibrium radiative heating may be a very small fraction of equilibrium convective heating in the stagnation region of an example vehicle with R = 1 ft, $L/D = \frac{1}{2}$, and $m/C_DA = 3$ slugs/ft^2. However, this possibility requires careful qualification on several counts. First, it certainly may not hold for another entry vehicle that has a substantially larger nose radius and/or a deeper entry. Second, although the amount of heat transferred by radiation may be considerably smaller than that transferred by convection, it may complicate heat shielding problems (20).[10] Third, the amount of radiative heat transfer may be significantly increased if nonequilibrium radiation occurs. This possibility is pointed up by the results shown on the right of Fig. 12 which were recently obtained by Camm, Kivel, Taylor and Teare (31) at satellite speed. It is evident that nonequilibrium radiation at this speed can easily be an order of magnitude more intense than equilibrium radiation in the altitude range of atmosphere entry. Moreover, there is a mounting body of evidence that it occurs in like manner at supersatellite speed. Clearly then, we must obtain considerably more information on radiation heat transfer at supersatellite speeds before we can accurately evaluate this phenomenon for any entry shape. This observation applies, of course, not only to the stagnation region but also to the afterbody.

It is true too, of course, that when radiation assumes major proportions in air, there tends also to be a sizable degree of ionization. Hansen (32) was among the first to observe that in this event free electrons could be present in and near the boundary layer in large numbers, and because of their high mobility they could cause large increases in thermal conductivity. Accordingly there could be an increase in energy

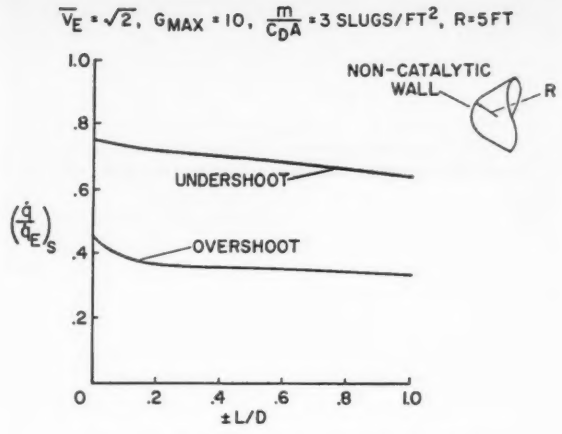

Fig. 11 Nonequilibrium convective heating

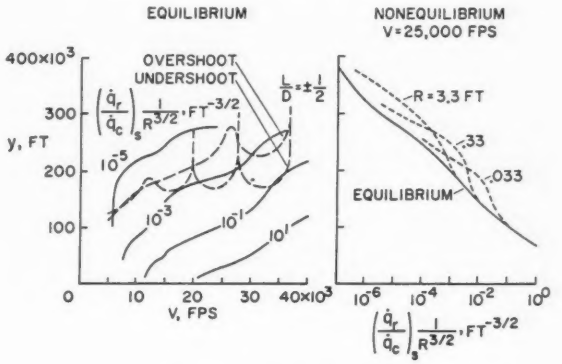

Fig. 12 Radiative heating

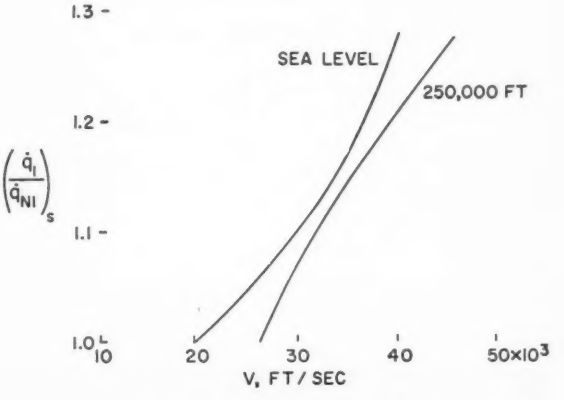

Fig. 13 Ionization heating effects

transport to the surface, which means of course additional heating. Adams (33) has recently investigated this possibility including diffusion effects of ion-electron pairs; his estimates of the contribution of ionization heating effects to total convective heating of a stagnation region are summarized in Fig. 13. It is indicated that this contribution may be nontrivial at speeds in excess of 30,000 fps; at speeds in excess of 40,000 fps it may exceed the order of 30%, which becomes a matter of major concern.[11] Accordingly ioniza-

[9] Indeed in the region of maximum heating (see Fig. 10) these results are correlated approximately by the expression

$$(\dot{q}_r/\dot{q}_c)_s = KR^{3/2}\rho^{5/4}V^{15}$$

[10] Thus, for example, an ablation heat shield might be particularly effective in blocking convective heat transfer, but relatively transparent to radiative heat transfer, unless it is naturally (e.g., possibly by charring) or artificially altered in some manner to block the radiation.

[11] These results were obtained assuming recombination at or near the wall, so it is noteworthy that the possibility of obtaining a noncatalytic wall is of interest here just as in the case of the nonequilibrium boundary layer effects discussed earlier.

tion heating effects must be added to the list of important phenomena which need further study to fully understand the overall heating problem during supersatellite entry.

Turning our attention now to the question of motion, it is significant to note that our calculations to this point have consistently contained the assumption of flight at constant force coefficients during descent through the atmosphere. It is pertinent to inquire, therefore, about the effects of modulating force coefficients on this portion of entry flight, and a limited study of such modulation was made by Lees, Hartwig and Cohen (10). Grant (34) has treated the problem more recently and extensively, and some results of his analysis of entry corridor depths are presented in Fig. 14. It is indicated that for parabolic entry with G_{max} limited to 10 along the lower boundary, so-called "full modulation" from $C_{L_{max}}$ in the early phase of descent to zero C_L (and $C_{D_{min}}$) at the end of descent may increase corridor depths by a factor of from 3 to 4 for values of $(L/D)_{max}$ in the neighborhood of 3. As would be expected, less modulation produces smaller increases in corridor depth for a given $(L/D)_{max}$, and the smaller $(L/D)_{max}$ is, the smaller is the effect of modulation. Thus at values of $(L/D)_{max}$ in the neighborhood of $\frac{1}{2}$ and less, modulation is indicated to have relatively little effect on corridor depths.

It is usually true, as we observed before and as we see also in Fig. 14,[12] that increasing corridor depth increases the severity of heating, and heating is, of course, severe at best in parabolic entry. Accordingly we are reminded of our earlier conclusion that parabolic entry may tend to be restricted to the limited corridors achievable with values of L/D the order of $\frac{1}{2}$ or less. In this event, while modulation is apparently not capable of largely increasing corridor depth, it may be neither required nor for that matter desired to. On the other hand, if in the course of events systems are evolved which can efficiently shield against the widely varied and generally intense heating encountered in relatively deep corridors, then modulation in combination with higher values of L/D appears to be an effective technique for obtaining such corridors. Substantially more research is in order, therefore, on problems of motion and heating in modulated entries.[13]

Already, of course, we have collected a sizable body of knowledge on general problems of motion and heating during entry, and this knowledge has been employed to evolve numerous entry configurations. It is beyond the scope of this paper to consider all these configurations, or for that matter any one of them in detail; however, it is instructive to consider a few of them with a view to better appreciating some of the more specific advantages which may be achieved, and problems which may be encountered with different entry vehicles.

[12] Note that the values of relative q_s in this figure include convective heating to the bottom of the undershoot descent only, and the velocities at this point are not all the same.

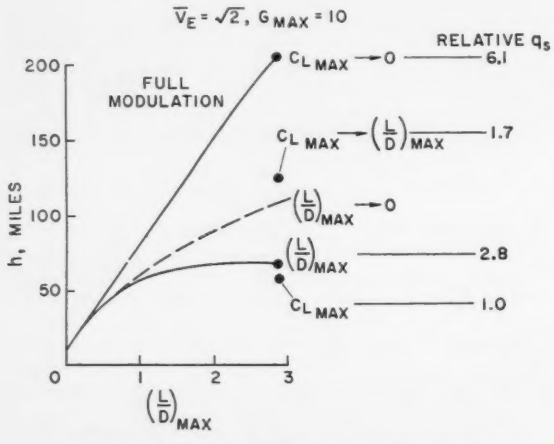

Fig. 14 Effect of modulation on corridor depth

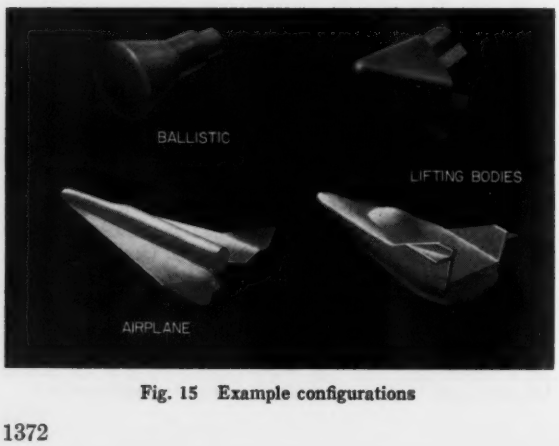

Fig. 15 Example configurations

Configurations

Some examples of the types of entry configurations that have been considered to date are illustrated in Fig. 15. They include a ballistic configuration of the Mercury type; two lifting bodies, the blunter one capable of a maximum L/D the order of $\frac{1}{2}$ and the more slender one capable of a maximum L/D the order of $1\frac{1}{2}$; and an airplane configuration of the Dyna Soar type capable of somewhat higher L/D. Many variations on these configurations have, and/or are being studied, including the limiting cases of the ballistic shape essentially reversed and the lifting bodies and the airplane essentially inverted. The ballistic configuration as shown, however, has advantageous qualities. Among the foremost of these is the almost flat face which increases drag coefficient and decreases convective heat transfer and hence heat shield weight. Terminal recovery of the vehicle would, of course, be by parachute or some other comparably lightweight device. The conical lifting bodies tend to be compact, and capable of developing high lift and high drag to reduce heating and hence heat shield weight. Likewise they tend to be both statically and dynamically stable over the speed range with the slender configuration having qualities suitable for more or less conventional flight and landing at low speeds. The airplane configuration has essentially a flat bottom, which is well suited for radiation shielding, with the body in the relatively cool flow environment on the leeward side of the wing at high angles of attack during entry. This configuration should, of course, be relatively well-suited for conventional flight and landing at low speeds.

The controls for lifting configurations deserve special comment. Careful attention to their design is required to insure their adequate effectiveness over the speed, altitude and attitude range of flight. Moreover it must be recognized that controls may encounter especially severe heating when extended to perform sharp maneuvers or to sizably increase the drag. This fact is emphasized by the photograph in Fig. 16 showing hypervelocity flow about a lifting body with controls extended and thereby immersed in a very hot and radiating gas cap.

All of the lifting configurations we have discussed have basically a fixed geometry. The designs of such configurations must, of course, be compromised to one degree or another when acceptable entry characteristics and conventional low speed flying qualities are required. With increasing entry

[13] The very recent work of Bryson, Denham, Carroll and Mikami (35) is indicated to be a contribution in this area.

Fig. 16 Flow about a lifting body

Fig. 17 Variable geometry configuration; wing folded

speed this compromise may become increasingly difficult to achieve because of the tendency of the severe heating environment to force designs in the direction of compact low L/D shapes, which are relatively unsuited for conventional low speed flight. If such flight is important, it may be desirable to achieve it with the aid of variable geometry configurations. The use of variable geometry for entry configurations is, of course, by no means a novel idea; however it is a matter of some interest to explore the possibility of devising a variable geometry configuration which is suitably compact and blunt in the one limit of, say, parabolic entry flight and which is suitably extended and slender in the other limit of low speed flight. A possible configuration of this type might have its wings folded on the leeward side of a compact body during entry as shown in Fig. 17 and have its wings unfolded to provide relatively good flying qualities after deceleration down to low speed, as shown in Fig. 18. Such a configuration might, in fact, have relatively good supersonic performance if the nose cap were ejected to expose an inlet for jet engine operation and if the unfolded wing panels were configured, as they tend naturally to be in this case, to interfere favorably with the pressure field generated by the body (36).

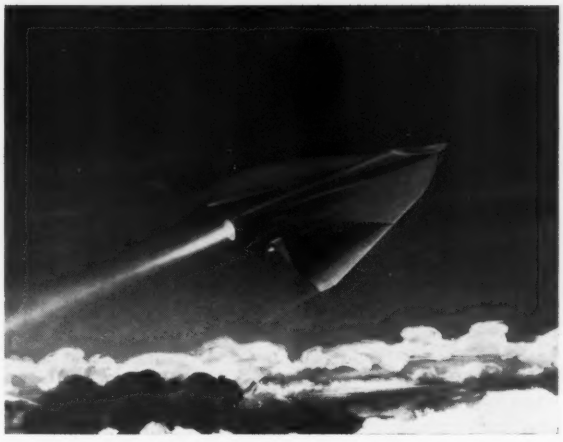

Fig. 18 Variable geometry configuration; wing unfolded

SATELLITE ENTRY	G	$\dot{q}$	q,Q
EARTH	1	1	1
MARS	.4	.1	.2
VENUS	.9	.8	.9
JUPITER	2.6	50	100

PARABOLIC ENTRY	G	h	$\dot{q}$	q,Q
EARTH	1	1	1	1
MARS	1	12	.5	.2
VENUS	1	1	.9	1
JUPITER	1	2	40	130

Fig. 19 Relative deceleration and heating

Entry Into Planetary Atmospheres

We have to this point confined our attentions either implicitly or explicitly to problems of entry into Earth's atmosphere. As a final point it is pertinent to inquire briefly about problems of entry into the atmospheres of other planets in our solar system. We will give particular attention to the relatively near Earth planets and how their entry problems compare with those in Earth's atmosphere. To this end it is instructive to consider Fig. 19 which relates deceleration and heating in the atmospheres of Mars, Venus and Jupiter to the corresponding quantities in the Earth's atmosphere for the cases of satellite entry and parabolic entry.[14] It is indicated that satellite entry into the Martian atmosphere may be characterized by less than half as severe a deceleration problem, and perhaps an order of magnitude less severe heating problem than in the Earth's atmosphere. On the other hand, satellite entry into the Venusian atmosphere may be characterized by the same order of deceleration and heating problems, while the corresponding entry into Jupiter's atmosphere may be characterized by severalfold higher decelerations, and from 1 to 2 orders of magnitude higher heating than in the Earth's atmosphere. If the restriction is imposed that the deceleration limits be the same in all the planetary atmospheres considered, and if it is required that exit be at satellite speed in all cases, then it is indicated that the parabolic corridor depths in the Venusian atmosphere are about the same as those in the Earth's atmosphere, whereas the corridor depths in Jupiter's atmosphere may be the order of twice as great, and those in the Martian atmosphere may be an order of magnitude greater than those in the Earth's atmosphere. Again the heating prob-

[14] See, e.g., (3, 7, 8, 9) for estimated values of planet and atmosphere properties and calculations of entries into these planetary atmospheres.

lem in the Venusian atmosphere may be the same order as that in the Earth's atmosphere, while in the Martian atmosphere it may be substantially less, and in Jupiter's atmosphere it may be one to two orders of magnitude more severe than in the Earth's atmosphere. It would, of course, be very dangerous to attach quantitative significance to the results presented in Fig. 19 inasmuch as our knowledge of the atmospheres of the planets other than Earth is exceedingly limited (see Ref. 37–43).

Concluding Remarks

General features of motion and convective heating during satellite entry appear to be reasonably well understood and supported by a sizable body of reliable theoretical and experimental information. With increasing entry speed, however, additional phenomena which are only partially understood at present may come importantly into play and affect heating in major respects. These phenomena include nonequilibrium chemical behavior in the boundary layer which may reduce convective heating in the presence of a noncatalytic wall; substantial radiation from the hot gas cap which may be largely intensified by nonequilibrium effects; and extensive ionization tending to increase energy transport to, and hence heating of, a wall. Of these several phenomena radiation heating demonstrates perhaps the most pronounced tendency to increase in intensity with increasing speed, and it may in fact tend to dominate the heating problem during hyperbolic entry (see Fig. 12). In this event relatively less blunt shapes may be required than those which derive from considerations of convective heating alone. It also appears that the assumption of laminar boundary layer flow during atmosphere entry of lifting vehicles near their undershoot boundary may be marginal, and experimental study of transition and turbulent flow under corresponding supersatellite entry conditions is therefore required. It is evident too that more attention should be given to both motion and heating under conditions of a modulated entry.

In the area of entry configurations it is notable that both fixed and variable geometry types may have application; however, the primary need now and for some time to come is doubtless in the realm of detailed aerodynamic and heating data on typical shapes with suitable controls.

In so far as entry into other planetary atmospheres is concerned, it is indicated for example that motion and heating problems in the Martian atmosphere should be substantially less severe than those in the Earth's atmosphere, whereas corresponding problems in the Venusian atmosphere may be about the same order of severity as those in the Earth's atmosphere. Entry into Jupiter's atmosphere appears almost without exception to be vastly more severe than entry into the Earth's atmosphere. A reliable quantitative understanding of these entry problems must await, however, the development of a far better understanding of these atmospheres.

Nomenclature

A = reference area for aerodynamic force coefficients
C_D = drag coefficient, $2\,\text{drag}/\rho V^2 A$
C_L = lift coefficient, $2\,\text{lift}/\rho V^2 A$
C_q = unit heat transfer constant, Btu-sec^2/slug$^{1/2}$-ft^3
C_Q = total heat transfer constant, Btu-sec^3/slug$^{1/2}$-ft^3
d = characteristic dimension, ft
D = drag, lb
e = Naperian logarithm base
f = density variable (see Eqs. 5 and 7)
g = sea level gravity acceleration, 32.2 ft/sec^2
G = resultant deceleration, g
h = corridor depth, miles
I,J = drag and lift parameter (see Eq. 7)
k_0 = constant proportional to density ratio at minimum altitude in a graze
l = lateral range, ft
L = lift, lb
L/D = lift to drag ratio
$(L/D)_0$ = $\sqrt{(L/D)^2 + (Y/D)^2}$
m = vehicle mass, slug
$\dot{q}$ = heating rate, Btu/ft^2-sec
q = unit heat transfer load, Btu/ft^2
Q = total heat transfer load, Btu
r = radius from center of planet, ft
r_0 = mean radius of planet surface, ft
r_c = radius of curvature of flight path in normal plane, ft
R = radius of curvature of stagnation region, ft
S = distance traveled along flight path, ft
T = time of flight to virtual perigee, hr
V = velocity, fps
$\bar{V}$ = ratio of velocity to near Earth satellite speed, $V/\sqrt{gr_0}$
$\bar{V}_E$ = entry velocity ratio
$\bar{V}_x$ = exit velocity ratio
y = altitude, ft
Y = side force
Y/D = side force to drag force ratio
z = $\ln \bar{V}^2$
α = constant in exponential atmosphere (see Eq. 7), 0.715 for Earth
β = density decay parameter in exponential atmosphere (see Eq. 7), 4.03×10^{-5} ft^{-1} for Earth
δ = cone semivertex angle, radian
θ = flight-path angle relative to local horizontal, negative downward, radian
ϕ = vehicle bank angle, deg
ρ = atmosphere density, slug/ft^3
ρ_0 = sea level atmosphere density, 0.002378 slug/ft^3 for Earth
ψ = lateral flight-path angle measured relative to entry heading, or orbit rotation angle relative to initial orbital plane, radian

Subscripts

E = equilibrium
I = ions
NI = no ions
S = stagnation region

References

1 Allen, H. J. and Eggers, A. J., Jr., "A Study of the Motion and Aerodynamic Heating of Missiles Entering the Earth's Atmosphere at High Supersonic Speeds," NACA TN 4047, October 1957.

2 Eggers, A. J., Jr., Allen, H. J. and Neice, S. E., "A Comparative Analysis of the Performance of Long-Range Hypervelocity Vehicles," NACA TN 4046, October 1957.

3 Eggers, A. J., Jr., "The Possibility of a Safe Landing," Chap. 13 in *Space Technology* (Howard Seifert, ed.), John Wiley & Sons, Inc., New York, 1959.

4 Wong, T. J. and Slye, R. E., "The Effect of Lift on Entry Corridor Depth and Guidance Requirements for the Return Lunar Flight," NASA TR R-80, 1960.

5 Slye, R. E., "An Analytical Method for Studying the Lateral Motion of Atmosphere Entry Vehicles," NASA TN D-325, September 1960.

6 Sanger, E. and Bredt, J., "A Rocket Drive for Long Range Bombers," Technical Information Branch, Navy Department, Trans. CGD-32, 1944.

7 Gazley, C., Jr., "Deceleration and Heating of a Body Entering a Planetary Atmosphere From Space," RAND Corp. paper P-955, 1957.

8 Chapman, D. R., "An Approximate Analytical Method for Studying Entry Into Planetary Atmospheres," NACA TN 4276, May 1958.

9 Chapman, D. R., "An Analysis of the Corridor and Guidance Requirements for Supercircular Entry into Planetary Atmospheres," NASA TR R-55, 1959.

10 Lees, L., Hartwig, F. W. and Cohen, C. B., "Use of Aerodynamic Lift During Entry Into the Earth's Atmosphere," ARS JOURNAL, vol. 29, no. 9, 1959, pp. 633–641.

11 Hildebrand, R. B., "Manned Re-Entry at Super-Satellite Speeds," IAS Rep. no. 60–83, 1960.

12 Brunner, M. J., "The Aerodynamic and Radiant Heat Input to Space Vehicles Which Re-Enter at Satellite and Escape Velocity," presented at ARS 15th Annual Meeting, Washington, D. C., Dec. 5–8, 1960 (ARS preprint 1681-61).

13 Mandell, D. S., "A Study of the Maneuvering Performance of Lifting Re-Entry Vehicles," presented at 15th ARS Annual Meeting, Washington, D. C., Dec. 5–8, 1960 (ARS preprint 1555-60).

14 Masson, D. J. and Gazley, C., Jr., "Surface Protection and Cooling Systems for High-Speed Flight," *Aero. Engr. Rev.*, vol. 15, November 1956, pp. 46–55.

15 Eggers, A. J., Jr., Hansen, C. F. and Cunningham, B. E., "Stagnation-Point Heat Transfer to Blunt Shapes in Hypersonic Flight, Including Effects of Yaw," NACA TN 4229, April 1958.

16 Friedlander, A. L. and Harry, D. P., III, "Requirements of Trajectory Corrective Impulses During the Approach Phase of an Interplanetary Mission," NASA TN D-255, 1960.

17 Wong, T. J., Goodwin, G. and Slye, R. E., "Motion and Heating During Atmosphere Reentry of Space Vehicles," NASA TN-D-334, September 1960.
18 Hayes, W. D. and Probstein, R. F., "Hypersonic Flow Theory," *Appl. Math. and Mech.*, vol. 5, Academic Press, New York, 1959.
19 Stetson, K. F., "Boundary Layer Transition on Blunt Bodies With Highly Cooled Boundary Layers," IAS Rep. no. 59-36, 1959.
20 Georgiev, S., "The Relative Merits of Various Test Facilities With Regard to Simulation of Hypersonic Ablation Phenomena," *Proc.* of the Hypervelocity Techniques Symposium, Denver, Colo., Oct. 20–21, 1960, pp. 102–169.
21 Chung, P. M. and Anderson, A. D., "Heat Transfer Around Blunt Bodies With Nonequilibrium Boundary Layers," presented at 1960 Heat Transfer and Fluid Mechanics Inst.
22 Goodwin, G. and Chung, P. M., "Effects of Nonequilibrium Flows on Aerodynamic Heating During Entry Into the Earth's Atmosphere from Parabolic Orbits," presented at Second International Congress for Aeronautical Sciences, Zurich, Switzerland, September 1960.
23 Lees, L., "Convective Heat Transfer with Mass Addition and Chemical Reactions," *Third AGARD Combustion and Propulsion Panel Colloquium*, Palermo, Sicily, March 17–21, Pergamon Press, New York, 1958, pp. 451–498.
24 Lees, L., "Laminar Heat Transfer Over Blunt-Nosed Bodies at Hypersonic Flight Speeds," JET PROPULSION, vol. 26, no. 4, April 1956, pp. 259–269.
25 Fay, J. A. and Riddell, F. R., "Theory of Stagnation Point Heat Transfer in Dissociated Air." *J. Aeronaut. Sci.*, vol. 25, no. 2, February 1958, pp. 73–85, 121.
26 Kemp, N. H., Rose, P. H. and Detra, R. W., "Laminar Heat Transfer Around Blunt Bodies in Dissociated Air," *J. Aerospace Sci.*, vol. 26, no. 7, July 1959, pp. 421–430.
27 Kivel, B. and Bailey, K., "Tables of Radiation from High Temperature Air," Res. Rep. 21, Contracts AF 04(645)-18 and AF 49(638)-61, AVCO Res. Lab., December 1957.
28 Kivel, B., "Radiation from Hot Air and Stagnation Heating," Avco-Everett Research Lab., Res. Rep. 79, (1959), AFBMD-TR-59-20, ASTIA AD-232 836, *J. Aerospace Sci.*, November 1960.
29 Keck, J., Camm, J., Kivel, B. and Wentink, T., Jr., "Radiation from Hot Air, Part II," Avco-Everett Res. Lab., February 1959, Everett, Mass.: Res. Rep. 42, *Annals of Physics*, vol. 7, May 1959.
30 Kivel, Bennett, "Radiation From Hot Air and Its Effect on Stagnation-Point Heating," *J. Aerospace Sci.*, vol. 28, no. 2, February 1961, pp. 96–102.
31 Camm, J. C., Kivel, B., Taylor, R. L. and Teare, J. D., "Absolute Intensity of Non-Equilibrium Radiation in Air and Stagnation Heating at High Altitudes," Avco-Everett Res. Lab., Res. Rep. 93, December 1959.
32 Hansen, C. F., "Approximations for the Thermodynamic and Transport Properties of High-Temperature Air," NACA TN 4150, March 1958.
33 Adams, M. C., "A Look at the Heat Transfer Problem at Super Satellite Speeds," presented at ARS 15th Annual Meeting, Washington, D. C., Dec. 5–8, 1960 (ARS preprint 1556-60).
34 Grant, F. C., "Analysis of Low-Acceleration Lifting Entry from Escape Speed," NASA TN D-249, June 1960.
35 Bryson, A. E., Denham, W. F., Carroll, Frank J. and Mikami, K., "Determination of the Lift or Drag Program that Minimizes Re-Entry Heating With Acceleration or Range Constraints Using a Steepest Descent Computation Procedure," presented at IAS 29th Annual Meeting, New York January 23–25, 1961 (IAS paper 61-6).
36 Eggers, A. J., Jr. and Syvertson, C. A., "Aircraft Configurations Developing High Lift-Drag Ratios at High Supersonic Speeds," NACA RM A55L05, 1956.
37 Dole, S. H., "The Atmosphere of Venus," The RAND Corp., paper p-978, Oct. 12, 1956.
38 Kuiper, G. P. (ed.), *The Atmospheres of the Earth and Planets*, University of Chicago Press, revised ed., 1952, p. 295.
39 Hess, S. L., Some Aspects of the Meteorology of Mars, *J. Meteorol.*, vol. 7, 1950, pp. 1–13.
40 Kopal, Z., "Aerodynamic Effects in Planetary Atmospheres," presented at IAS National Summer Meeting, Los Angeles, Calif., June 28-July 1, 1960 (IAS paper 60-74).
41 Sagan, C., "The Radiation Balance of Venus," JPL TR No. 32-24.
42 Opik, E. J., "Aeolosphere and Atmosphere of Venus," presented at the 42nd Annual Meeting of the American Geophysical Union.
43 DeVaucouleurs, G., *Physics of the Planet Mars*, Faber and Faber, Ltd., 1954.

Measurement of Heat Flux From Initiators for Solid Propellants[1]

J. A. KELLER[2]
N. W. RYAN[3]

University of Utah
Salt Lake City, Utah

Thin film resistance thermometers have been applied to the measurement of heat flux from two types of initiators for solid propellants. The theory of heat conduction to a semi-infinite body was used for translating temperature-time histories to heat flux vs. time relationships. Studies on ignition of propellant indicate that results of independent investigations on igniters and propellants can be correlated.

IN SO far as propellant ignition can be regarded as a purely thermal process in which external application of heat produces decomposition of and reaction between propellant ingredients, the two phases of ignition can be studied separately. The second phase, response of the propellant to external heat, has recently received intensive study by McAlevy, Baer, Beyer, and others (1).[4] Except by Nanigian (2), the heat supply aspect of ignition has not been studied with very fast response instrumentation. No study in which both phases of the ignition process have been correlated in terms of heat flux has been reported.

This article reports a study of heat flux from two kinds of igniters, and a preliminary attempt to correlate the results with propellant response data reported by Baer, Ryan, and

Presented at the ARS Solid Propellant Rocket Conf., Salt Lake City, Utah, Feb. 1–3, 1961.
[1] This work was supported by subcontract to Thiokol Chemical Corp. under Air Force Contract AF 33 (600)-36514.
[2] Dept. of Chemical Engineering. Member ARS.
[3] Professor, Dept. of Chemical Engineering. Member ARS.

[4] Numbers in parentheses indicate References at end of paper.

Salt (3). The essential feature of the study is the heat flux gage, a rugged platinum film resistance thermometer, with the thin film bonded to a ceramic substrate which serves as a semi-infinite body. The gage is mounted in the wall of a test chamber and exposed to the action of an igniter. The temperature-time data obtained are translated into heat flux-time results.

Calculation of Heat Flux

The instruments employed produce an oscilloscope trace showing surface temperature as a function of time. The problem is to translate this into surface heat flux as a function of time. From the theory of heat transfer to a semi-infinite body initially at uniform temperature, one obtains (4)

$$q(t) = \frac{\Gamma}{\sqrt{\pi}} \frac{\partial}{\partial t} \int_0^t \frac{T(\lambda)}{\sqrt{t-\lambda}}\, d\lambda \qquad [1]$$

Integration by parts followed by the indicated differentiation gives, provided $T(0) = 0$

$$\frac{\sqrt{\pi}}{\Gamma} q(t) = \int_0^t \frac{dT}{d\lambda} \frac{d\lambda}{\sqrt{t-\lambda}} \qquad [2]$$

Eq. 2 is the starting point of Nanigian (2), who develops further the equations employed to analyze the data presented here. The procedure is to approximate the temperature trace by n straight-line segments bounded by $\lambda = 0, \theta_1, \theta_2, \ldots, \theta_n$, where $\theta_n = t$. The slope of the ith segment is

$$\left(\frac{dT}{d\lambda}\right)_i = \frac{T_i - T_{i-1}}{\theta_i - \theta_{i-1}} = m_i \qquad [3]$$

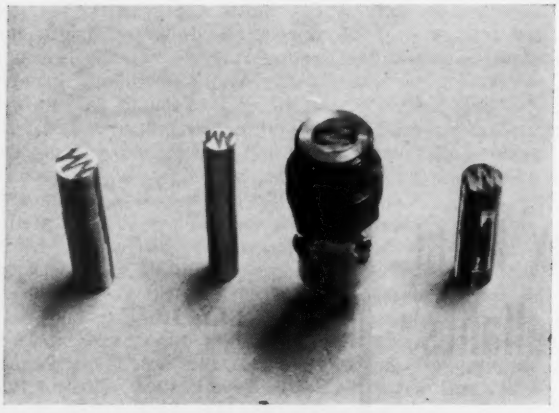

Fig. 1 Zircon and Vycor heat flux gage elements

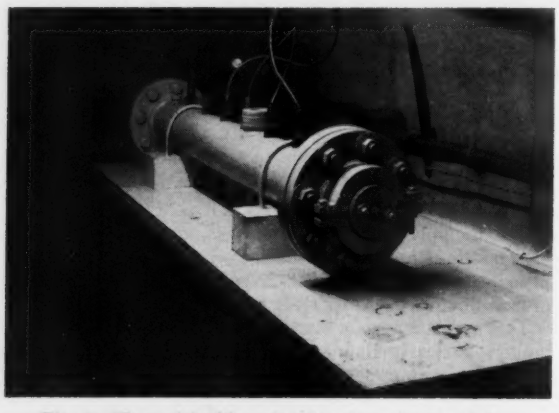

Fig. 2 View of ignition chamber from igniter end

Eq. 2 becomes

$$\frac{\sqrt{\pi}}{\Gamma} q(t) = \sum_{i=1}^{n} m_i \int_{\theta_{i-1}}^{\theta_i} \frac{d\lambda}{\sqrt{t-\lambda}} = 2 \sum_{i=1}^{n} m_i(\sqrt{t-\theta_{i-1}} - \sqrt{t-\theta_i}) \qquad [4]$$

Eq. 4, supplemented by the definition of m_i, (Eq. 3), is the equation employed in this study.

Heating after passage of a shock wave or detonation wave at time zero is an interesting and sometimes important special case. As $T(+0)$ is finite, Eq. 2 is not applicable. Eq. 1 is employed, assuming that T is constant at T_0 to θ_1.

$$\frac{\sqrt{\pi}}{\Gamma} q(t) = T_0 \frac{\partial}{\partial t} \int_0^{\theta_1} \frac{d\lambda}{\sqrt{t-\lambda}} + \frac{\partial}{\partial t} \int_{\theta_1}^{t} \frac{T(\lambda)}{\sqrt{t-\lambda}}\, d\lambda$$

$$= \left[\frac{T_0}{\sqrt{t}} - \frac{T_0}{\sqrt{t-\theta_1}}\right] + \left[\frac{T_0}{\sqrt{t-\theta_1}} + \int_{\theta_1}^{t} \frac{dT}{d\lambda} \frac{d\lambda}{\sqrt{t-\lambda}}\right]$$

$$= \frac{T_0}{\sqrt{t}} + 2 \sum_{i=2}^{n} m_i(\sqrt{t-\theta_{i-1}} - \sqrt{t-\theta_i}) \qquad [5]$$

Since there is no commitment as to the magnitude of θ_1, it can be made vanishingly small. The derivation can be modified to account for shocks at later times in the heating process.

Heat Flux Gages

The choice of temperature sensors for accurately measuring heat flux is limited to those types which give temperature-time histories that are directly convertible to heat flux. For this reason, only two basic designs of sensing devices are presently available for determining heat flux from igniters, i.e., the surface calorimeter, and a temperature sensor mounted on a semi-infinite body. For the calorimeter, temperature is measured by mounting a thermocouple in the calorimeter, or using the calorimeter metal as a resistance thermometer. The first is best suited for measurement of heat fluxes of 1000 Btu/ft²-sec or greater, because its sensitivity is less than that of the second. The second type of sensing device gives temperature-time histories which are translated to heat fluxes by application of the theory of heat conduction to a semi-infinite body as discussed in the preceding section. For the second type, the temperature of the sensor surface faithfully follows the temperature-time history of the environment to which it is exposed if the film is thin.

The second type of sensor, subsequently referred to as a heat flux gage, was selected for these studies because of its excellent sensitivity and rapid response to temperature changes. For the heat flux gage, either a thermocouple or a resistance thermometer can be used for measuring temperature changes. In these studies, a thin film resistance thermometer on a substrate of zircon or Vycor was used. The most useful reference to this type of resistance thermometer is a report by Vidal of the Cornell Aeronautical Laboratory (5). The thermometer was later applied to measurement of heat fluxes in a shock tube by Baer of the University of Utah (3,6). The greater sensitivity of the resistance thermometer gives it advantage over the thermocouple. The sensitivities of the resistance thermometers used in this work were as great as 1 mv/°C. The sensitivities of conventional thermocouples range from 0.005 to 0.05 mv/°C.

The thin platinum film, about 1-μ thick, is applied to an insulator, such as zircon or Vycor, by painting with Liquid Bright Platinum No. 05-X, manufactured by Hanovia Chemical and Manufacturing Company. The gages are then fired in an oxygen rich atmosphere at temperatures of

600° to 800°C to decompose and oxidize the organic material in the paint. This leaves a thin film of platinum securely bonded to the insulator.

In the manufacture of heat flux gages for these studies, cylinders of Vycor or zircon $\frac{1}{2}$-in. diam replaced the element in a C-75 spark plug. The platinum resistance element was painted on one face of the cylinder and electrical leads painted down the sides as shown in Fig. 1. Since the platinum film is very thin (0.1 to 1.0 μ), the surface temperature of the gage is very nearly that of the substrate material (5). The temperature at the gage surface is then measured by placing the gage in a suitable electrical circuit and measuring emf drop across the gage as the resistance of the platinum film changes with temperature.

Before temperature measurements are made, determinations are made of the coefficient of the platinum film and of the thermal responsivity Γ of the gage. Thermal responsivity is the square root of the product of thermal conductivity, density, and heat capacity for the gage. Values of thermal responsivity were 4.2 and 10.2 Btu/(hr)$^{1/2}$-ft^2-°F, respectively, for Vycor and zircon heat flux gages. Temperature coefficients were 2.72×10^{-3}/°C for Vycor gages, and varied from 2.5 to 3.2×10^{-3}/°C for zircon gages. The values for zircon gages were found to be dependent on the temperature at which the platinum film was fired.

Some development studies were required to produce a heat flux gage which could withstand the severe environmental conditions imposed by the igniters. Pyrex was originally considered for the substrate material; however, it was found that small surface cracks formed during tests, and the platinum easily eroded from the surface. Vycor, with a very low linear coefficient of thermal expansion (8×10^{-7}/°C in the temperature range 25° to 300°C), and zircon were found to be excellent substrate materials. It was found that for extremely high heat flux environments along with abrasive action of the igniter reaction products, a small amount of platinum film was eroded from gage surfaces during tests. This effect was to increase the resistance of the film which simulated a temperature increase. For all experiments reported here, the change in resistance of the platinum due to abrasion was small relative to the total temperature increase.

Experimental Methods

The chamber used for conducting heat flux studies was fabricated from a section of 4-in. ID-pipe, 4-ft long. Fig. 2 shows a view of the test chamber. The igniters were mounted at one end; ports for heat flux gages and pressure transducers were placed at 3-in. intervals along the chamber wall. A chamber window was used for viewing propellant ignition with high speed photography. The window was placed opposite a gage position so that heat flux could be measured at the same position as propellant ignition was observed.

Two types of solid propellant initiators were studied: pyrotechnics and propellant gas generators. Only one pyrotechnic composition, with pellet form as the variable, was studied. The pyrotechnic pellet forms were cylinders, $\frac{1}{8}$-in. diam by $\frac{1}{4}$-in. long, and pills, $\frac{1}{4}$-in. diam by approximately $\frac{1}{8}$-in. deep. Charge weights tested were 40 gm for pills and 50 gm for cylinders of pyrotechnic composition.

The gas generator discharged gases through a 0.4-in. diameter orifice into the ignition chamber. The pyrotechnic igniter was enclosed by a 2-in. diam perforated plate.

Results of Heat Flux Study

Heat flux-time relationships for igniters were obtained from oscilloscope records of temperature-time data by the method described in a previous section. Temperature-time traces for a run with the gas generator type igniter in a nozzled chamber are shown in Figs. 3. The maximum chamber

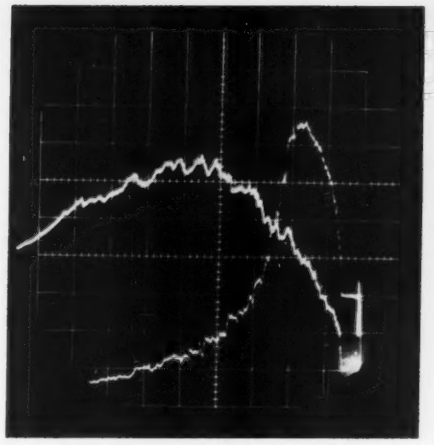

Fig. 3a Temperature-time traces for gas generator
Temperature: 100°C/div (vertical)
Time: 50 millisec/div (horizontal, right to left)
Upper trace: 11 in. from igniter
Lower trace: 20 in. from igniter

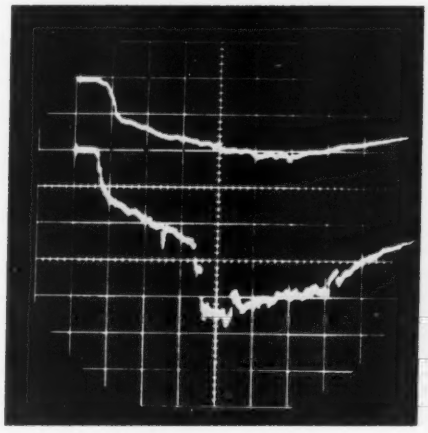

Fig. 3b Temperature-time traces for gas generator
Temperature: 100°C/div (vertical)
Time: 50 millisec/div (horizontal, right to left)
Upper trace: 29 in. from igniter
Lower trace: 38 in. from igniter

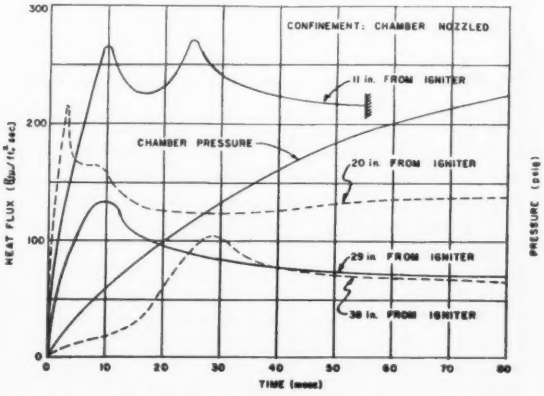

Fig. 4 Heat flux pattern for gas generator

pressure during the run was 360 psig and occurred 220 millisec after the start of igniter action. Heat flux gage positions were 11, 20, 29, and 38 in. from the igniter orifice. For the gage position 11 in. from the igniter (Fig. 3a) it was noted that after approximately 55 millisec of igniter action, the tempera-

ture-time trace exhibited what appeared to be a rapid decrease in temperature. It was found that this anomalous behavior resulted from the deposition of a thin conducting film of igniter reaction products on the face of the heat flux gage. The conducting film lowered the resistance across the gage giving the appearance of a rapid temperature drop.

Fig. 4 shows the heat flux pattern in the test chamber for the temperature-time data of Fig. 3. As expected, the highest heat flux occurred at the gage position nearest the igniter orifice. However, the slope of the heat flux-time curve was steeper for the gage in the second position. This indicates that the initial discharge of hot gases from the gas generator orifice, which includes reaction products from the pyrotechnic initiators, transfers a greater amount of heat downstream of the first gage position. As the pressure in the chamber increased, the position of highest heat flux moved closer to the igniter orifice. The heat flux curve for the gage 37 in. from the igniter showed that only a small amount of heat was transferred to this position for the first 20 millisec of igniter action. This effect can probably be attributed to reduced velocities of hot gases at the far end of the chamber during initial pressurization.

The effect of igniter confinement (nozzled and open chamber) is illustrated by Fig. 5. The curve for open chamber condition with the gas generator shows a high initial heat flux. This initial peak can be attributed to reaction products from the pyrotechnic initiator used for igniting the gas generator propellant and also to slight overignition of the gas generator. For the open chamber condition, the gas generator exhibited an almost uniform heat flux pattern for all gage positions.

Heat fluxes from different igniters are compared in Fig. 6. The curves for the pyrotechnic igniters illustrate the variation

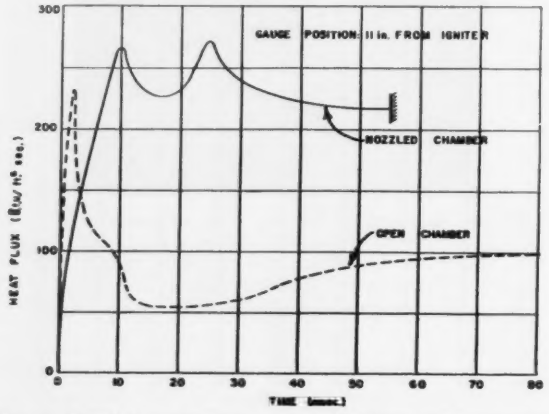

Fig. 5 Effect of confinement on heat flux from gas generators

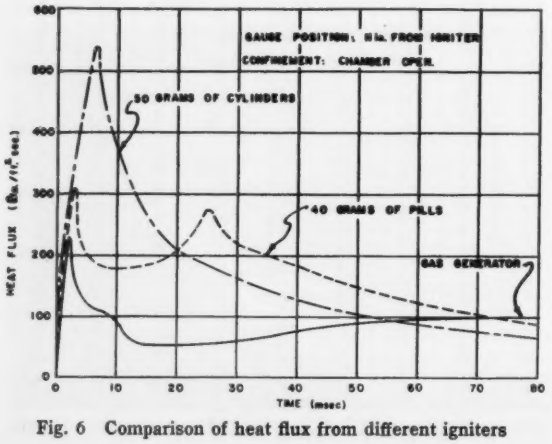

Fig. 6 Comparison of heat flux from different igniters

in igniter properties that can be achieved by pellet design alone.

Fig. 7 shows the effect on the heat flux pattern in the chamber resulting from radial deflection of igniter reaction products. The use of the radial deflector increased the heat transfer rate for positions close to the igniter.

Correlation With Propellant Ignition

Eq. 4 permits calculating $q(t)$ for a heat flux gage exposed to igniter action. There remains the problem of interpreting the result in terms of heat flux to propellant. If the mechanism is radiation, and if propellant and gage have the same absorptivity, the flux calculated for one applies to the other. With practical igniter systems, ignition occurs before surface temperature to the fourth power becomes comparable to source temperature to the fourth power.

On the other hand, if convection is important, the change in surface temperature rise, usually not negligible compared to the source surface temperature difference, alters $q(t)$. It is evident that to employ the results of heat flux measurement to describe propellant ignition, one must have some knowledge or make reasonable assumptions about the mechanism of heat transfer.

For the purposes of the correlation with ignition data reported here, it is assumed that the heat flux to the gage is approximately the same as the heat flux to the propellant. The propellant specimen (polysulfide-ammonium perchlorate) was mounted in the wall of the ignition chamber 14 in. from the orifice of a gas generator. The specimen was photographed at 2100 frames per sec through a window on the opposite side of the chamber. Nearly simultaneous ignition at many points on the propellant was observed about 20 millisec after the pyrogen was activated.

An identical test with a heat flux gage replacing the sample showed an average heat flux of about 180 Btu/ft²-sec, the average pressure level being about 50 psig. Baer (3,6) reports for this same propellant and same heat flux at 300 psig, an ignition time of about 10 millisec. Wright (7) indicates that a factor of about two must be applied to correct for the difference in pressure. The agreement obtained indicates that results of independent igniter and propellant studies can be correlated.

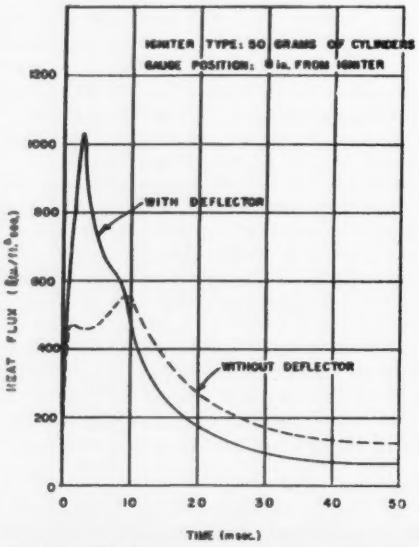

Fig. 7 Effect of radial deflection of igniter reaction products on heat flux from pyrotechnic igniters

Conclusions

The thin film platinum resistance thermometer (heat flux gage) has been successfully applied to measurement of heat fluxes from initiators for solid propellants. Heat fluxes measured were as high as 1000 Btu/ft²-sec from hot, particle-laden reaction products of pyrotechnic igniters. Results of heat flux studies and ignition of propellants by these igniters show good agreement with independent propellant ignition studies in shock tubes and radiation furnaces.

Nomenclature

H = heat or energy
θ = time
T = temperature
L = length
} Dimensions

m_i = slope of the ith straight line segment, $T\theta^{-1}$
$q(t)$ = heat flux at time t from start of igniter action, $HL^{-2}\theta^{-1}$
t = time from start of igniter action, θ
T_i = temperature at the terminus of the ith straight line segment, T
T_0 = temperature at zero time, T
Γ = thermal responsitivity (square root of the product of density, heat capacity, and thermal conductivity) $HL^{-2}\theta^{-1}t^{-1/2}$
θ_i = time at terminus of the ith straight line segment, θ
θ_n = time at the terminus of last straight line segment ($\theta_n = t$), θ
λ = time variable of integration, θ

References

1 Summerfield, M., (ed)., "Solid Propellant Rocket Research," *Progress in Astronautics and Rocketry*, Academic Press, N. Y., Vol. 1, 1960.

2 Nanigian, J., Crookston, N. J., Jr. and Michelson, A., "Instantaneous Heat Transfer, Pressure, and Surface Temperature Characteristics of Solid Propellant Igniters," U. S. Naval Propellant Plant Technical Memorandum Rep. 178, April 1960.

3 Baer, A. D., Ryan, N. W. and Salt, D. L., "Propellant Ignition by High Convective Heat Fluxes," presented at the ARS Solid Propellant Rocket Conf., Princeton, N.J., Jan. 28–29, 1960 (ARS preprint 1059-60).

4 Carslaw, H. S. and Jaeger, J. C., *Conduction of Heat in Solids*, Clarendon Press, Oxford, 2nd ed., 1959.

5 Vidal, R. J., "Model Instrumentation Techniques for Heat Transfer and Force Measurements in a Hypersonic Shock Tunnel," Cornell Aeronaut Lab. Rep. no. AD-917-A-1, WADC-TN-56-315, ASTIA no. AD-9723,-1956.

6 Baer, A. C., "Ignition of Composite Rocket Propellants," Ph.D. Thesis, Univ. of Utah, August 1959.

7 Wright, D. W., "Thermal Ignition Delay of Composite Rocket Propellants, B.S. Thesis, Univ. of Utah, June 1959.

Detonability of Solid Composite Propellants[1]

W. H. ANDERSEN[2]
Aerojet-General Corp.
Downey, Calif.

R. F. CHAIKEN[3]
Aerojet-General Corp.
Azusa, Calif.

A theoretical model of propagation of detonation in propellants is presented. This model is based on the hypothesis that detonation is propagated by the same rate controlling chemical reactions that occur during normal burning of the propellant. In particular, it is assumed that a grain burning of the oxidizer occurs and that the rate of linear-surface decomposition (pyrolysis) of the oxidizer can be used to describe the rate of detonation reaction. Kinetic data on the surface decomposition of ammonium perchlorate, which were obtained by the hot plate-linear pyrolysis technique, suggests that sublimation of ammonium perchlorate (with an apparent activation energy of ~22 kcal/mole) is the rate controlling step in the surface decomposition of this oxidizer. A discussion is presented on how these data can be used in conjunction with the detonation model to calculate the minimum (critical) diameters at which detonation can propagate in a cylindrical charge of solid propellant. The possible effect of various propellant parameters, i.e., oxidizer binder ratio, oxidizer particle size, confinement, etc., on the detonation process is discussed. The role of ignition, diffusion and heat conduction processes in the detonation and rapid deflagration of solid composite propellants is discussed. A preliminary theoretical approach to accelerating burning in porous propellant is also presented. This approach indicates that porous burning in rocket motors containing solid composite propellants can lead to very rapid chamber pressure build-up, so that an explosion could occur within several milliseconds after porous burning begins.

Presented at the Solid Propellant Rocket Conf., Feb. 1–3, 1961, Salt Lake City, Utah.
[1] This work was supported by the Special Projects Office Bureau of Naval Weapons, Dept. of the Navy.

[2] Technical Specialist, Ordnance Div.
[3] Technical Specialist, Chemical Div.

COMPOSITE solid propellants have an energy density which is comparable to, or higher than, so-called high explosives. However, the detonability characteristics of most composite propellants are considerably different from those of high explosives. These differences arise from the fact that during detonation, the rate at which the energy can be released in a composite propellant is controlled by factors somewhat different from those which occur in many conventional explosives. Firstly, composite propellants are heterogeneous and require the fuel or binder to be evaporated and mixed with the gaseous products of the oxidizer before the potential energy of the binder can be liberated. (This process requires time, and therefore effectively restricts the amount of energy from these reactions that can be made available for supporting the initiating mechanism of detonation.) Secondly, composite propellants contain very little porosity. This results in a relatively low efficiency toward initiation of the propellant by shock heating, in the time necessary for propagating detonation, to the high temperatures which would normally occur in regions surrounding air or gas pockets. The concentration of hot spots produced by shock passage in an essentially nonporous propellant would be considerably less than the concentration produced in a granular explosive charge which is packed to a density of about 95% or less of theoretical density. Thirdly, the fundamental decomposition kinetics during explosion of monopropellant type oxidizers, which are used in typical composite propellants, viz., ammonium perchlorate and ammonium nitrate, are generally considerably slower than those involved in typical high explosives.

This paper discusses the above physicochemical factors in greater detail and indicates how they influence the detonation and rapid (explosive) deflagration characteristics of composite solid propellants. Particular emphasis is placed on propellants which contain ammonium perchlorate and a conventional oxygen lean binder.

Detonation Process

The general model which will be assumed to describe detonation in composite propellants is as follows: A shock wave (whose initial origin will be discussed later) is considered to initiate self-supporting chemical reaction at the surface of the oxidizer grains by compressional heating of the propellant. This occurs in a time t_i from the moment of passage of the shock front. The oxidizer then pyrolyzes in a grain-burning fashion in its own monopropellant redox flame which may, under suitable conditions, be perturbed by reaction of the binder in the monopropellant flame. The total time to consume the oxidizer grain is given by R_g/Lk_s (1)[4] where R_g is the average radius of the oxidizer grains, L is the thickness of the monomolecular surface layer on the grain, and k_s is the specific rate constant of the rate-controlling surface reaction. After complete pyrolysis of the oxidizer, the binder undergoes further reaction with the oxidizer pyrolysis products. It is expected that many of these reactions take place in the gas phase. The time to complete the combustion of the binder after consumption of the oxidizer grains is taken as t_g. Thus the total time τ_t to release all of the specific energy in a propellant during detonation is simply

$$\tau_t = t_i + R_g/Lk_s + t_g \qquad [1]$$

Concurrent with the initial shock compression and reaction of the propellant, rarefaction waves move into the detonation reaction zone of the charge from its external surfaces and reduce the local pressure and temperature. This in effect will remove a portion of the liberated specific chemical energy from supporting the initiating shock front. The portion of energy dissipated will depend in part on τ_t. Approximate treatments of the influence of reaction kinetics on the detonation process, i.e., nonideal detonation, have been given by Jones (2), Eyring et al. (1) and Cook (3). It follows from these treatments, i.e., the so-called diameter theories, that in the nonideal detonation region, any factor which tends to increase the total energy release time, Eq. 1, will tend to decrease the hydrodynamic properties of the detonation, e.g., velocity, pressure, temperature, including the initiating shock strength. When the initiating shock strength becomes sufficiently weak, detonation will fail to propagate.

Initiation

The shock initiation of the oxidizer surface in the propellant probably proceeds through a hot spot mechanism involving rapid compression of gases or solids, intergranular friction, and possibly rapid viscous flow (4). However, little is known quantitatively about these hot spots. Experimental evidence (Ref. 5 and other unpublished works) suggests that the detonation initiation time of cylindrical charges of pure ammonium perchlorate is negligible compared with the grain consumption time when the charge densities are $\sim$1.3 gm/cm^3 or lower (particle radius $\leqslant 30\ \mu$). Above this density and particle size the initiation time appears to increase. Embedding the oxidizer in a polymeric binder has somewhat the same influence as increasing the charge density, since in each case the total concentration of voids, which can form *hot spots* from the passage of a shock, is decreased. However, in the case of the propellant, the concentration of load-bearing contact points between oxidizer particles, which can yield hot spots by intergranular friction, are also decreased. This can cause a possible further decrease in the ease of initiation by shock. Thus, although t_i is small compared with R_g/Lk_s for low density charges of pure AP, its value may become large compared with the grain burning time when the AP is embedded in a polymeric binder which has essentially no porosity.

Unfortunately, present knowledge does not allow an a priori calculation of t_i; however this term may be the controlling factor in determining the detonability of a composite propellant. The value of t_i is probably related to the concentration and distribution of porosity and oxidizer present in the propellant, the burning additives (catalysts) present in the propellant and the strength of the initiating shock.

Grain Burning

In the Eyring grain burning theory of detonation, the reaction of the individual grains of a detonating explosive consists of a surface burning in which a layer of molecules is not ignited until the previous layer is consumed. The theory implies that the detonation reaction zone consists of a finite region in which granules of explosive undergo layerwise decomposition at the surface. The time τ required for complete reaction is taken as simply the time required for the surface reaction to traverse the grain radius, i.e.

$$\tau = R_g/Lk_s \qquad [2]$$

It is noted by comparing Eqs. 1 and 2 that the Eyring expression for the detonation reaction time would be applicable to propellant detonation if both t_i and t_g were negligible when compared to R_g/Lk_s. However, if $t_g \gg R_g/Lk_s$, the Eyring expression would still be applicable provided that one assumes that the t_g time period occurs in the region of Taylor expansion. In other words, the energy liberated by chemical reaction during the t_g time period occurs behind the Chapman-Jouguet plane and therefore lends no support to propagation of the detonation front. It is believed that this condition prevails during detonation of AP propellants containing conventional binders with low oxygen content.

In connection with the chemical reactions occurring at the surface of a burning solid propellant, it has been hypothesized (6) that the rate controlling reaction occurs in the mono-

[4] Numbers in parentheses indicate References at end of paper.

molecular surface layer exposed to the flame zone and not below this surface layer. Experimental data by the hot plate method which was first devised at Aerojet by Schultz and Dekker (7)[5] for studying the linear pyrolysis rate of solids as a function of surface temperature have demonstrated the validity of this hypothesis. It is believed that the conditions at the hot plate solid interface approximate those which occur at the solid surface during burning. The use of the concept of surface decomposition kinetics and experimentally obtained linear pyrolysis rates led to the formulation of new theoretical models for describing the mechanism of combustion of composite propellants containing ammonium nitrate (8,9) and AP (10) as the oxidizer. Of particular importance to this discussion is the fact that the rate controlling mechanism of surface decomposition of certain solids has been found experimentally to be different from that of decomposition in the bulk phase under isothermal conditions. This duality of thermal decomposition has been demonstrated with ammonium nitrate (11) and typical polymeric binders (8,12), where it was shown that at high surface temperatures endothermic surface vaporization or dissociative sublimation is apparently rate determining. The duality of the reaction mechanism (bulk and surface) in ammonium nitrate is related to the manner in which thermal energy is supplied to the solid. Under the conditions of the high heat flux at the solid surface (such as occurs during hot plate pyrolysis or burning of the NH_4NO_3), endothermic surface desorption involving dissociative sublimation can compete with, and is faster than, exothermic bulk decomposition as the rate controlling step in the regression of the solid surface.

In a previous publication (13) the authors have utilized the concept of surface decomposition kinetics and experimental linear pyrolysis data to describe the detonation reaction time in granular ammonium nitrate. The suggested detonation model, which is based on earlier hypotheses (1,3,14) that the grain burning detonation is merely a surface deflagration at an extremely high temperature and pressure, correlates quite well with reaction times determined from detonation velocity vs. charge diameter data. Since the detonation pressure is very high, the surface temperature of the decomposing explosive particles will be nearly identical with that of the gas temperature in the reaction zone. It was therefore concluded (13) that there should be one unique rate controlling reaction in grain burning detonation, and it should be equal to the linear pyrolysis rate B of the explosive particles, i.e., $B = Lk_s$; therefore

$$\tau = R_0/B \qquad [3]$$

The kinetic expression for B is obtained experimentally by the hot plate-linear pyrolysis technique (15,16) and is generally expressed as an Arrhenius and/or Absolute Rate expression.

Surface Decomposition Kinetics of Ammonium Perchlorate

Preliminary data for the linear pyrolysis rate of ammonium perchlorate have been obtained using the hot plate apparatus described in (15, 16). The data[6] are shown in Fig. 1. A reasonable correlation with the data can be obtained using the following rate expression

$$B = 31T_s \exp(-22{,}000/RT_s) \quad \text{cm/sec} \qquad [4]$$

where T_s is the surface temperature.

It is interesting to note that Eq. 4 predicts surface temperatures of burning pure AP which are consistent with those measured experimentally by Friedman et al. (18).

It is believed that, during the linear thermal decomposition of ammonium perchlorate, the linear rate of regression of the surface is controlled by an endothermic sublimation process, represented by the following equation

$$NH_4ClO_4(s) \rightarrow HClO_4(g) + NH_3(g) \qquad [5]$$

The activation energy for bulk sublimation in vacuo was found to be 21.5 ± 2.8 kcal (19), which is in reasonable agreement with the pyrolysis rate data of Fig. 1. Eq. 5 probably involves a proton transfer process at the solid surface followed by desorption of $HClO_4$ and NH_3 from the surface. Because of the high temperatures encountered in propellant combustion, rapid redox reactions between the gas products occur; hence Eq. 5 is essentially irreversible. Preceding and/or in the surface (where Eq. 5 occurs) is a small region where there is partial decomposition caused by exothermic solid reactions. These reactions occur in the so-called intermosaic (defect lattice) material. The heat released in this material lowers the apparent value of the endothermicity of the overall surface reaction. The kinetics of the exothermic solid reactions depend on the crystal structure of the oxidizer while it is decomposing (19,20,21). The rates are expressed by the following Arrhenius expressions

Orthorhombic crystals, temperatures below 513° K
$B = 1.5 \times 10^5 \exp(-31500/RT_s)$ cm/sec

Cubic crystals, temperatures above 513° K
$B = 25 \exp(-16200/RT_s)$ cm/sec

No information is available for the rate of the crystal transition. However, additives which will influence the rate of this transition should influence the extent of the overall endothermicity of the surface reaction and hence the burning characteristics of NH_4ClO_4. The solid decomposition probably proceeds through an electron transfer process (19,20). Thus additives which will influence electron transfer might influence the surface endothermicity and enhance the burning characteristics of NH_4ClO_4.

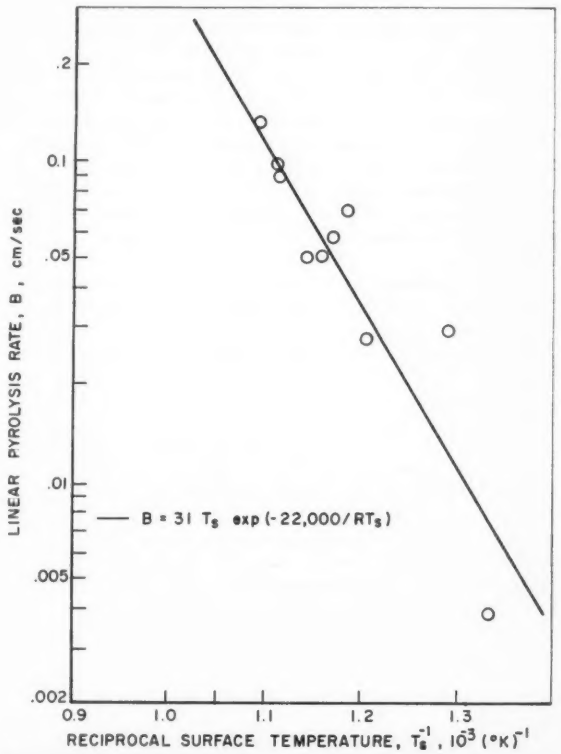

Fig. 1 Linear surface pyrolysis rate of ammonium perchlorate

[5] This method involves the measurement of the linear rate of surface regression of a solid which is undergoing gasification by being pressed against a heated surface.

[6] These data were obtained utilizing strands of pressed AP supplied by R. Friedman of Atlantic Research Corp. Details concerning the strands are described in (17).

Table 1 Calculated detonation reaction times and critical diameters of uncased pure ammonium perchlorate

ρ_0, gm/cm³	R_g, μ =	6	50	100
0.6	τ (μsec)	3.6	26	52
	d_c (in.)	0.5	3.8	7.6
1.0	τ	2.8	23	46
	d_c	0.6	4.7	9.5
1.4	τ	2.0	16.5	33
	d_c	0.5	4.4	9.7

Reaction Times and Critical Diameters of AP

Andersen and Pesante (5) have shown that Eqs. 3 and 4 will explain the detonation reaction time of low density small particle size AP, as obtained by analyzing the experimental detonation velocity vs. charge diameter data by means of the Eyring curved front theory (1). Examples of the reaction times computed in this manner for pure AP of various charge densities and particle sizes are given in Table 1. The Chapman-Jouguet (CJ) detonation temperatures computed in (5) were used in these calculations.

In the curved front theory the analytical expression, relating the detonation velocity D at charge diameter d with the ideal (infinite diameter) detonation velocity D_i and the reaction zone length a, is given for unconfined cylindrical charges as

$$D/D_i = 1 - a/d \qquad [6]$$

From (1)

$$a = \frac{\rho_0}{\rho} D\tau \simeq 0.75\, D\tau \qquad [7]$$

where ρ_0 is the initial charge density and ρ is the CJ density.

The minimum (critical) charge diameter d_c at which steady state detonation can propagate depends upon the rate at which energy is being liberated in the detonation reaction zone and the rate at which energy is being dissipated from the reaction zone by lateral expansion. An exact description of this process would require a solution to the time dependent, three-dimensional hydrodynamic shock equations with nonlinear energy source terms. This is a formidable task. However, it is possible to obtain an estimate of the critical diameter of a cylindrical charge of explosive from the following arguments.

Lateral expansion in the reaction zone of a detonating charge results in a rarefaction wave sweeping inward and forward from the external surface of the charge. This rarefaction wave will travel in the reaction zone with the local velocity of sound C laterally to the detonation front and with the velocity $(C + W)$ laterally to the charge, where W is the mass particle velocity. Since the local velocity of the rarefaction wave is greater than the detonation velocity, such a rarefaction wave will slow down the detonation front. The general influence of the charge diameter and reaction zone length on this process is assumed to be given by Eq. 6. Detonation failure should occur at approximately the moment when the rarefaction wave overtakes the detonation front at its midpoint, since the rarefaction will have then effectively quenched the entire wave front. The distance that the rarefaction must travel for complete quenching of the detonation front is

$$s = [(d_c/2)^2 + (fa)^2]^{1/2} \qquad [8]$$

where f is a proportionality factor. The average value of C in the reaction zone is about 1.375 D, and the average value of $(C + W)$ is 1.75 D. This follows (1) from the fact that the value of $(C + W)$ at the shock front is about 2.5 D, and at the CJ surface it is 1.0. Geometrical considerations then show that $f = 0.786\ s/a$, which combined with Eq. 8 gives $s = 0.81\ d$. It can be shown that the value of f is usually slightly greater than unity, and hence to a good approximation $s = (C^2 + W^2)^{1/2} f\tau \simeq (C + W)\tau$, where τ is the reaction time. Combining this expression with Eqs. 6 and 7 then gives

$$d_c = 0.55\, D_i\tau \quad \text{in.} \qquad [9]$$

where D_i is in cm/sec and τ is in sec. Examples of d_c computed by Eq. 9 for pure AP are shown in Table 1. The calculated values are in fairly good agreement with those determined experimentally (5). Eq. 9 appears to also predict d_c adequately for many conventional high explosives.

Role of Binder

The binder may influence the detonation characteristics of a composite propellant in several ways: 1) the shock initiation process of the oxidizer may be altered; 2) the binder may influence the effective temperature which determines the surface pyrolysis rate of the oxidizer; 3) the gas-phase reaction time between oxidizer and binder pyrolysis products may be changed. The shock initiation process was considered in a previous section and will not be discussed further at this time.

The binder can influence the surface temperature of the deflagrating oxidizer, i.e., the value of B, through a perturbation of the monopropellant thermal layer surrounding the decomposing oxidizer particles (10). However, for relatively unreactive binders, e.g., low oxygen content, it is believed that the perturbation depends primarily on gaseous diffusion and/or on heat conduction processes between the binder and the monopropellant flame. Since it is assumed that the high pressures in detonation allow the oxidizer surface temperature to be identified with the detonation reaction zone temperature, i.e., the CJ temperature, it is possible to estimate the effect of the binder by approximate considerations of the total energy release within the detonation reaction zone.

The extent to which the binder heats up and vaporizes in the detonation reaction zone should be intimately tied up with the extent of its diffusing with the gaseous oxidizer. This may be seen from the following considerations. Upon ignition of grain burning at the oxidizer-binder interface, a few monolayers of the binder will immediately heat up and vaporize. This will drastically lower the effective thermal gradient into the solid binder and therefore decrease the rate of temperature rise and vaporization of the solid binder. However, if sufficiently rapid diffusion of vaporized binder and oxidizer takes place, the enthalpy of the flame zone surrounding the solids will be increased by exothermic oxidizer-binder reactions. This will result in a higher CJ temperature (also a higher oxidizer surface temperature), and hence shorter detonation reaction times. It is important to note that, while the increased flame temperature in the reaction zone would tend to increase the rate of vaporization of binder, the decrease in detonation reaction tends to decrease the time available for gaseous diffusion to occur. Thus the effect of binder on τ depends on how these two effects balance themselves.

Now the rate of chemical reaction between gaseous oxidizer and binder at temperatures of 2000° K or greater should be fast compared to the rate of gaseous diffusion. Therefore, by estimating the extent of gaseous diffusion it should be possible to estimate the possible increase in the CJ temperature due to binder reaction. The extent of reaction of gaseous oxidizer and binder N_b in the detonation reaction zone

Table 2 Extent of binder reaction N_b for various times of diffusion τ (Eq. 13)[a]

τ, sec =	10^{-5}	10^{-4}	$3(10^{-4})$	$6(10^{-4})$	10^{-3}	$2(10^{-3})$	$2.5(10^{-3})$
N_b =	$4(10^{-3})$	0.04	0.12	0.24	0.40	0.81	1.0
d_c, ft[b] =	0.37	2.2	6.9	15	28	67	90

[a] Reaction zone conditions: $T = 2000°$ K, $P = 34{,}000$ atm, and $R_g = 50\ \mu$.
[b] d_c is the critical diameter for a composite propellant with a heat of combustion of 900 cal/gm which contains 80% oxidizer and having a reaction time τ calculated on the assumption that the shock initiation time is very small.

can be defined as

$$N_b = f_{bd}/f_b \qquad [10]$$

where f_{bd}/f_b is the fraction of the initial amount of solid binder which diffuses with the oxidizer pyrolysis products. To a good approximation, $f_{bd} \simeq f_b\,\tau/t_d$, where τ, the detonation reaction time, is the time available for diffusion in the reaction zone and t_d is the time required for complete mixing of the oxidizer and binder gases. Therefore, N_b can be expressed as

$$N_b \simeq \tau/t_d \qquad \tau \leq t_d \qquad [11]$$

For the present purpose, it should be suitable to treat the spherical boundary of the oxidizer-binder interface as a plane, so that for essentially complete diffusional mixing the expression given by Rice (22) can be used, i.e.

$$t_d = \frac{0.5\ \delta_d{}^2}{D_0}\,[T_0/T]^{1.75}\,(P/P_0) \qquad [12]$$

where D_0 = the diffusion coefficient at normal pressure P_0 and temperature T_0, and δ_d = the average diffusional distance. The value of D_0 may be taken as about 0.1 cm²/sec, and δ_d as about $R_g/8$. This latter expression follows from the fact that about 90% of the mass of a spherical particle is contained in the outer half of the radius of the particle, and that the average binder thickness between oxidizer particles is very small.

$$N_b \simeq 5.84\ (10^{-4})\ \frac{T^{1.75}\tau}{R_g{}^2 P} \qquad [13]$$

where P is in atmospheres, R_g is in centimeters, and τ is in seconds.

From the preceding considerations, the perturbation of the monopropellant flame temperature due to oxidizer-binder reaction can be written as

$$T_s \simeq T_{f0} + (e/C_v)N_b\Delta E_{0b} \qquad [14]$$

where T_s is the oxidizer surface temperature (also the CJ gas temperature), T_{f0} is the CJ detonation flame temperature of the pure oxidizer at the same charge density as it is present in the propellant, ΔE_{0b} is standard specific heat of combustion of the solid binder with the gaseous pyrolysis products of the oxidizer, C_v is an averaged heat capacity at constant volume, and e is an approximately constant parameter which is used to account for the entropy increase in the binder and its products due to the shock front and reaction in the reaction zone. A reasonable value of e/C_v in Eq. 14 is ~5.

Detonation Reaction Times and Critical Diameters of Propellants

The equations presented in the previous sections may be used to estimate reaction times and critical diameters for propagation of steady state detonation in propellants if the assumption is made that the shock initiation time of the oxidizer is negligibly small. This assumption is probably realistic if the propellant contains a reasonably high degree of homogeneously distributed porosity or cracks, or if it has been ground up. It seems unlikely that the assumption is even approximately true if the propellant is essentially nonporous. However, the calculations help to define lower limits on the critical diameter for propagating detonation in composite propellants and may serve to help guide future studies relating to the shock initiation of the oxidizer in a propellant.

An examination of Eq. 13 shows that under high pressure conditions, such as occur during detonation, the extent of the gaseous oxidizer-binder reaction is very small for short diffusion times. Table 2 illustrates the extent of the binder reaction as a function of time under typical detonation conditions. The oxidizer-binder gas reaction energy released in a diffusion time greater than the detonation reaction time cannot contribute toward the propagation of detonation in a composite propellant. Thus, the energy release rate of the oxidizer-binder gas reactions is diffusion controlled at very high pressures, e.g., during detonation, and hence will contribute very little toward propagating detonation. This is in agreement with experience. It is interesting to note, however, that much of this energy will be available for supporting air blast, since much of the energy will be liberated in the Taylor expansion region behind the reaction zone.

Since the gas reactions of the monopropellant oxidizer, e.g., NH_4ClO_4, will be the principal contributing energy reaction during a propagating detonation, it is doubtful if a propellant employing mainly a non-monopropellant oxidizer, e.g., $KClO_4$, can propagate a true detonation under any conditions. This, of course, does not exclude a thermal explosion due to a large specific burning surface.

Examples of the calculated detonation reaction times and critical diameters for composite propellants of various oxidizer concentrations and particle sizes are given in Table 3. It is again emphasized that these computations ignore the shock initiation time of Eq. 1. The computed critical diameters will thus be *minimum* values. The calculations also ignore the N_b term in Eq. 14, and the t_d term in Eq. 1, since they have been shown to be of negligible importance in most instances toward influencing the detonation process. It should also be noted that the value for D_i to be used in Eqs. 6, 7 and 9 is that which is consistent with the energy release

Table 3 Detonation reaction times and critical diameters of uncased composite propellants calculated on the assumption that the shock initiation time is very small[a]

f_0[a]	ρ_{0x}, gm/cm³	τ, 10^{-6} sec	R_g = 50 μ d_c in.	R_g = 100 μ d_c in.
0.9	1.48	15.9	4.4	8.8
0.8	1.31	18.3	4.6	9.2
0.7	1.15	20.7	4.7	9.4
0.6	0.99	23.4	4.7	9.4

[a] f_0 is the weight fraction of the oxidizer in the propellant, and ρ_{0x} is the corresponding oxidizer concentration.

in the detonation reaction zone. For the above calculations only the monopropellant oxidizer energy is involved.

The calculated critical diameters shown in Table 3 deserve some comment. These calculated values are at least several factors lower than what experience suggests are the critical diameters of typical composite propellants. A part of this discrepancy may be due to the inadequacy of the proposed theory, including Eq. 14. However, it is believed that this discrepancy primarily indicates the importance of the time for shock initiation of the oxidizer in an essentially nonporous propellant. A small diameter propellant which contains a high degree of porosity (from grinding) will propagate steady state detonation. However, a considerably larger diameter propellant of the same composition but containing no porosity will not propagate steady state detonation. The supposedly long shock initiation time of composite propellants is not surprising in view of the fact that the initiating shock will be relatively weak, since the energy is supplied only from the monopropellant oxidizer. This suggests that if the charge diameter of the nonporous propellant were increased sufficiently to allow the diffusion controlled reactions to liberate their energy in a time short enough for them to support the initiating shock, then the shock initiating time may be considerably shortened. Examples of the critical diameter calculated for various values of N_b are shown in Table 2. The initiating shock strength (temperature) will be reasonably high only when the extent of binder reaction is about 0.4 or higher. It is seen that the critical diameters under this condition will be very large. It is reasonable to assume that nominal diameter composite propellant will never propagate steady state detonation if the propellant is essentially nonporous.

Influence of Other Propellant Parameters on Critical Diameters for Detonation

Confinement

The function $D(d)$ for moderately confined charges as given by the curved front theory (1) is

$$D/D_i = 1 - \frac{2.17\ \rho_e a^2}{\sigma_c d} \qquad [15]$$

where σ_c is the mass per unit area of casing and ρ_e is the density of the explosive (oxidizer in this case). The critical diameter may be obtained by substituting in this equation the expressions given in the section on the detonation process. The results show that nominal confinement will decrease the critical diameter of small particle size pure AP and propellant, but that it has no appreciable influence on the critical diameters under conditions where the reaction time is large. This means that the natural mass confinement of materials having very large detonation reaction times is large compared with the artificial confinement.

Propellant porosity, geometry, ambient temperature, binder composition and metal additives

A tacit assumption underlying all of the preceding arguments concerning the detonation reaction time and critical diameter is that a surface deflagration of the oxidizer is initiated by a shock wave, i.e., the detonation front. This initiation process is usually considered to proceed through a hot spot mechanism involving rapid compression of gases or solids, intergranular, friction and/or rapid viscous flow. When the shock initiation time to grain burning is small compared with the detonation reaction time, the arguments presented in the previous sections should be reasonably valid. However, it is possible that for a given propellant and shock strength there may be an insufficient number of high temperature hot spots to cause rapid initiation of grain burning. For example, this possibility might arise in a solid composite propellant with no porosity and where each oxidizer particle is in intimate contact with the binder. In these cases, the initiation process would be rate controlling, and the previous calculations of the reaction time would not apply. It could be expected that the critical diameters would be larger than those suggested in Table 3. Also, if the shock strength required to initiate a reaction in a given propellant is greater than that which can be supplied by the detonation reaction, it is obvious that the propellant will never propagate a detonation. Many composite propellants in use have experimental densities which are greater than 99% of their theoretical densities (at normal temperatures). It is not known whether this small degree of porosity (surface area unknown) is sufficient to help produce enough hot spots to allow ignition by the shock strength corresponding to that calculated on the basis of the rate of chemical reaction and the hydrothermodynamics of the system.

Some ammonium perchlorate composite propellants, which have been previously mascerated, e.g., by mechanical grinding, can be made to undergo steady state detonation when packed into small, e.g., ~2-in. diam, steel tubes. In addition, the experimental evidence indicates that the detonation velocity (between 2000 to 4000 m/sec) goes through a maximum as the packing density is increased. At high packing densities, which approach that of the unmascerated propellant, the cylindrical charge fails to propagate a detonation. This phenomenon is somewhat analogous to that of "dead pressing" in certain common explosives. The explanation of the detonation behavior of mascerated propellants is probably related to the initiation problem discussed in the previous section.

In view of the discussions above, it is apparent that any prevailing conditions which would increase propellant porosity or introduce oxidizer-binder separations in a propellant might tend to sensitize the propellant toward detonation and/or influence the critical diameter for propagative detonation. Such conditions would undoubtedly involve uneven strains or stresses set up in the propellant, possibly as a result of environmental pressure and/or temperature changes. It can be expected that propellant geometry and confinement would also be important factors. Unfortunately, little is known quantitatively concerning the formations of voids in a propellant or their role in propellant detonation.

The presence of oxygen in a binder might well be expected to be of considerable importance in influencing the detonability of a composite propellant. This is because diffusion would be of less importance in limiting the energy release rate of the binder. Critical diameters of propellants containing large amounts of oxygen will undoubtedly be small.

The presence of metals in a propellant should generally increase the critical diameter, since detonation reaction zone temperatures are not usually high enough to rapidly burn the metal.

Nonsteady Deflagrative Processes

Porosity in Propellants at Lower Temperature

Studies at Aerojet and other laboratories suggest that explosions encountered in low temperature rocket motor firings of AP-composite propellant are due to a rapid deflagration via a bulk burning mechanism involving an increase in the surface area available for instantaneous burning. This increased surface area may arise from any internal imperfection in the propellant grain such as pores, cracks and fissures. Although such rapid deflagrations are not detonations in the strict sense of the word, the possible destructive violence of such deflagrations, even with relatively small propellant masses, can be seen from the fact that the measured TNT equivalence of the explosions is sometimes high.

A concept of *frozen* porosity may be used to explain qualitatively some of the observed effects of configuration and low temperature on the explosion sensitivity of rocket motors containing solid composite perchlorate propellant. This

concept involves the formation of voids by the separation of oxidizer and binder, i.e., blanching, or the formation of cracks in the propellant grain during low temperature conditioning, e.g., −75°F of the propellant. The influence of chamber pressure during burning can cause the voids produced from the blanching or cracking to collapse or remain open, depending upon the compressibility of the propellant at the particular firing temperature. Normally, for most composite propellants, compressibility decreases rapidly with decreasing temperature below 0°F. Since the separation of oxidizer and binder at low temperature results from internal strain caused by differential thermal contraction of the propellant constituents, it is seen that confinement of the propellant grain, e.g., case bonding, could increase the internal strain and hence the degree of porosity.

In addition to frozen porosity, micro-cracks, small fissures, pores, etc., could develop in a propellant due to large temperature and pressure gradients which exist during ignition and burning of the propellant grain in a rocket motor. Porosity formed in this manner might well be called a *dynamically induced* porosity, to distinguish it from the porosity present under low temperature ambient conditions, and may be the controlling factor in the explosive deflagration of a propellant. It would not be unreasonable to expect that if the operating pressure of the propellant is increased sufficiently, the formation of new surface area available for instantaneous burning would increase, independent of whether or not the propellant grain is at a low ambient temperature.

Role of Porosity in Rocket Motor Explosions

The role of porosity in causing rocket motor explosions after normal ignition would involve a gas flow into the interior of the propellant in the direction of the flame front. In a sense, this type of gas flow is somewhat analogous to that required by the hydrodynamic-thermodynamic equations for detonation. The normal burning front might be compared with the CJ plane of detonation and the penetration front compared with the shock front of detonation. Penetration of hot gases into the propellant could essentially increase the burning area, which in turn would increase the pressure. The pressure would then increase the linear burning rate and further increase the penetration, and the process would be self accelerating.

A simple model of porous burning is presented which attempts to correlate the physicochemical parameters which control the rate of pressure build-up in a rocket motor. The treatment, while crude and approximate, is useful as a starting point for a more exact investigation.

Briefly, it is assumed: 1) the burning area S is directly proportional to the chamber pressure P, $S = aP$; 2) the confinement of the chamber is such that the rate of pressure rise is directly proportional to the rate of gasification, $dP/dt = bdm/dt$; 3) the Muraour burning rate equation $v = \alpha + \beta P$ cm/sec describes the linear rate of surface regression of the oxidizer particles. For these conditions, and the condition that the chamber pressure is normal P_0 at the onset of porous burning

$$\frac{dP}{dt} = \theta P(1 + \phi P) \qquad [16]$$

and

$$P = \frac{P_0}{(1 + \phi P_0)e^{-\theta t} - \phi P_0} \qquad [17]$$

where

$\phi = \beta/\alpha$
$\theta = ab\,\rho_s\alpha$
ρ_s = density of the oxidizer particles

It is seen from Eq. 17 that the pressure goes to infinity in a finite time t_e

$$t_e = \frac{1}{\theta} \ln\left[\frac{1 + \phi P_0}{\phi P_0}\right] \qquad [18]$$

Fig. 2 shows a plot of Eq. 17 on a dimensionless time scale $\xi = \tau/\tau_e$ for various values of ϕ. It is apparent that the shape of the pressure-time curve is relatively insensitive to variations in ϕ. Now the value for ϕ for AP composite propellant with a conventional binder has been estimated to be ~0.1 (10). For this value, the pressure-time curve of Fig. 2 goes through an apparent induction period prior to the rapid pressure rise to explosion. This type of pressure increase is consistent with the explosion phenomena observed with certain motors which were fired at approximately −75°F.

The following sections are devoted to a more detailed examination of parameters in Eq. 17.

Propellant Permeability

The microscopic scale combustion model of the thermal layer mechanism of propellant combustion (9,10) describes the combustion in terms of individual oxidizer particles which undergo surface decomposition. Thus, for a close-particle packing arrangement, the burning area S, which results from penetration of hot gases, can be related to the normal burning area S_0 by the expression

$$S = S_0\left(1 + \frac{x}{2R_a}\right) \qquad [19]$$

where

x = penetration in advance of the normal burning surface, cm
R_a = average radius of the oxidizer particle, cm

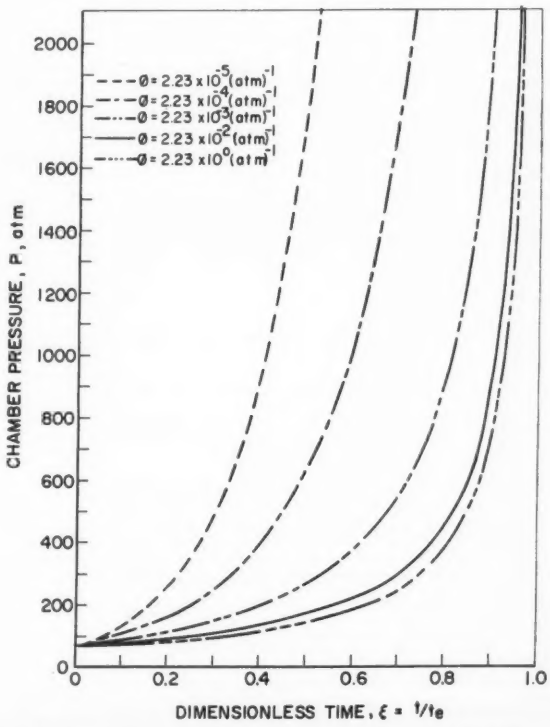

Fig. 2 Pressure vs. dimensionless time for porous burning

Vest, Baer and Geene (23) utilized Aronofsky's (24) equations for flow through a porous bed to estimate the gas penetration factor in a porous propellant. From their calculations, it can be approximated that the instantaneous linear penetration distance is directly proportional to the instantaneous chamber pressure $x = cP$. For the condition $cP \gg 2R_g$, the increase in burning area with chamber pressure can be expressed as $s = aP$, which is in accordance with our original assumption. The proportionality factor a would depend in part upon the porosity and permeability of the propellant and the viscosity of the combustion gas. Since the permeability of a substance is an empirical quantity, experimental studies of the penetration of gas into porous propellants would be of great value in helping to define the effects of porous burning.

It should be noted that Eq. 19 implicitly assumes that the ignition of internal oxidizer particles by the penetrating hot gases occurs rapidly with induction times less than the period for a valid penetration pressure proportionality assumption. It is obvious that a relatively large induction time to ignition would have the effect of decreasing the dependence of the internal burning area on the penetration of hot gas.

Burning Rate Parameters

The thermal-layer mechanism of combustion (9,10) offers a means of analyzing the constants of the Muraour burning rate equation $v = \alpha + \beta P$ in terms of the chemical kinetics of the combustion process. Steady state combustion is described as a feedback system between an endothermic surface gasification (linear pyrolysis) and an exothermic redox reaction between the gaseous pyrolysis products. Although the surface gasification of ammonium perchlorate is apparently complicated by solid phase exothermic reactions (as discussed previously), the feedback system, which controls the normal burning rate, is described (10) as

1) NH_4ClO_4 (s) + heat → $NH_3(g)$ + $HClO_4$ (g)
2) NH_3 (g) + $HClO_4$ (g) → Oxidizer pyrolysis products + heat
3) oxidizer pyrolysis products + binder pyrolysis products $\xrightarrow[\text{in thermal layer}]{\text{partial reaction}}$ products + heat

According to the Thermal Layer Mechanism (9,10), the propellant burning rate can be expressed as

$$v \simeq \frac{\sigma(T_{f0} - T_s + \epsilon)(1 + \phi_0 P)}{\rho_s \Delta H R_g} \qquad [20]$$

$$\phi_0 = \frac{R_g}{RT_g}\left[\frac{C_p k_g}{2\pi\sigma}\right]^{1/2} \qquad [21]$$

where

σ = average thermal conductivity of the pyrolysis gas products
T_{f0} = adiabatic flame temperature for the reaction between NH_3 and $HClO_4$ the increase in temperature of the thermal layer due to reaction step 3.
ρ_s = density of oxidizer particles
ΔH = endothermicity of the oxidizer pyrolysis reaction
T_s = oxidizer surface temperature
T_g = a constant temperature near T_{f0}
C_p = average heat capacity of pyrolysis product gases
k_g = rate constant for the gas-phase reaction of reaction step 2 above.

Comparing the Muraour equation to Eqs. 20 and 21 indicates that the parameters α and β can be described as

$$\alpha = \frac{\sigma(T_{f0} - T_s + \epsilon)}{\rho_s \Delta H R_g} \qquad [22]$$

and

$$\beta = \alpha\phi_0 = \alpha\phi \qquad [23]$$

There is evidence (10) that ϵ decreases with pressure and becomes relatively small above 100 atm.

It is seen that both α and β tend to decrease as P increases; however, their ratio ϕ is relatively constant. The use of Eqs. 21, 22 and 23 for expressing the parameter θ in Eq. 16 would result in a nonlinear expression for the rate of pressure rise in porous burning. It is apparent that accurate knowledge of the kinetics of the surface gasification of ammonium perchlorate is necessary for describing the explosion time of porous burning.

Confinement Parameters

Very little is known concerning the effective confinement of combustion gas in a rocket motor which explodes in the order of 10^{-2} sec after ignition. It can be expected that under high rates of pressure build-up, the inertia of the propellant mass and chamber wall will result in chamber pressures far exceeding the hydrostatic burst strength of the motor. In addition, the heat loss by expansion of gas through the nozzle may approach zero (adiabatic condition) during the burning time to explosion. As seen from Eq. 17, confinement (parameter b) is important in determining the pressure-rise time to explosion via porous burning. In view of the sensitivity of the pressure-time curve to θ, and hence b, a more detailed description of rapid deflagration in a rocket motor would require adequate information on rocket chamber conditions during high rate gas pressurization. However, for the purpose of estimating a constant value for b, it might be assumed that the ideal gas law adequately describes the rocket chamber conditions. Therefore

$$b \simeq \frac{RT_{fi}}{MV_{0c}} \simeq \text{const} \qquad [24]$$

where

T_{fi} = normal burning adiabatic flame temperature
V_{0c} = initial volume of rocket combustion chamber
M = average molecular weight of combustion products

Calculated Explosion Lines

In view of the discussions in the previous sections, Eq. 18 for t_e can be used to estimate the explosion time from the onset of porous burning. Here the parameter $\theta = ab\rho_s\alpha$ can be expressed as

$$\theta = \left[\frac{S_0 c}{2 R_g}\right]\left[\frac{RT_{fi}}{MV_{0c}}\right]\left[\rho_s\right]\left[\frac{\sigma(T_{f0} - T_s + \epsilon)}{\rho_s \Delta H R_g}\right] \qquad [25]$$

or

$$\theta = 0.5\left[\frac{R}{M}\right]\left[\frac{S_0}{V_{0c}}\right]\left[\frac{\sigma T_{fi}(T_{f0} - T_s + \epsilon)}{\Delta H}\right]\frac{c}{R_g^2} \qquad [26]$$

Table 4 Parameter values for estimating porous burning explosion times

R/M	= 2 atm-cm³/gm-deg	
S_0/V_{0c}	= 2 cm^{-1}	
σ	= 2×10^{-4} cal/cm-sec/deg	Ref. (10)
T_{f0}	= 1360° K	Ref. (10)
T_s	= 1060° K	Ref. (10)
ϵ	= 200° K	Ref. (10)
ΔH	= 530 cal/gm	Ref. (10)
ϕ	= 56.7 R_g = 0.14 atm^{-1}	Ref. (10)
T_{fi}	= 3000° K	
P_0	= 70 atm	
R_g	= 2.5×10^{-3} cm	

It is interesting to note that θ is directly proportional to the initial surface to volume ratio of the combustion chamber and indirectly proportional to the square of the oxidizer particle size.

Utilizing the parameter values listed in Table 4, the explosion time from Eqs. 18 and 26 becomes

$$t_e = 5.35 \times 10^{-7} c \quad \text{sec} \qquad [27]$$

where c is the penetration factor.

The calculations of Vest et al. (23) indicate that the value of c for a solid propellant with a porosity of ~10% will be in the range of 10^{-2} cm/atm for a total pressure drop of 10 atm. For propellants with less porosity and greater driving pressures it may not be unreasonable to expect an effective penetration of 10^{-4} to 10^{-3} cm/atm. This will yield an explosion time of 0.5 to 5 millisec. This range of values for t_e is consistent with that observed at Aerojet from high speed motion picture studies of explosions of small rocket motors.

Deflagration to Detonation Transition (DDT)

The theoretical and experimental work discussed support the hypothesis that detonation does not occur in small diameter, nonporous propellant. The theoretical work suggests that detonation may occur in sufficiently large diameter charges, however. The possibility of a DDT requires conditions which will allow an accelerating deflagration to build up to a propagating detonation. The conditions necessary are those which will create a very rapid pressure build-up so as to form a shock wave. High local temperatures (hence fast chemical reactions) and proper confinement and geometry are requisites for a rapid pressure increase. An internal or bulk surface burning of a propellant rather than a purely exterior propellant surface burning is generally required to make conditions suitable for detonation. Thus, the accelerating porous burning previously discussed could initiate a DDT if the conditions, e.g., charge diameter, permit a propagative detonation. If the conditions are not proper to permit a propagative detonation, e.g., too small a charge diameter, then a thermal explosion will occur. The mechanism of a DDT, therefore, probably involves a gas penetration being some function of the instantaneous pressure. The burning rate will thus be accelerating. The simple calculations presented for porous burning are suggestive of the approach necessary for the DDT, but further study is necessary.

Acknowledgment

The authors wish to express their appreciation for the encouragement given to them during the course of this work by L. Zernow and E. Mishuck of Aerojet-General Corp.

References

1 Eyring, H., Powell, R. E., Duffy, G. H. and Parlin, R. B. "The Stability of Detonation," *Chem. Rev.*, vol. 45, 1949, pp. 69–181.

2 Jones, H., "A Theory of the Dependence of the Rate of Detonation of Solid Explosives on the Diameter of the Charge," *Proc. Roy. Soc.*, vol 189A, 1947, pp. 415–426.

3 Cook, M. A., *The Science of High Explosives*, Reinhold Publishing Corp., New York, 1958.

4 Bowden, F. B. and Yoffe, A. D., *Initiation and Growth of Explosion in Liquids and Solids*, University Press, Cambridge, Mass., 1952.

5 Andersen, W. H. and Pesante, R. E., "Reaction Rate and Characterstics of Ammonium Perchlorate in Detonation," to be published in the *Eighth International Combustion Symposium*.

6 Wilfong, R., Penner, S. S. and Daniels, F., "An Hypothesis for Propellant Burning," *J. Phys. Chem.* vol. 54, 1950, pp. 863–872.

7 Schultz, R. D. and Dekker, A. O., "The Absolute Thermal Decomposition Rates of Solids," *Fifth International Symposium on Combustion*, Reinhold, New York, 1955, pp. 260–267.

8 Andersen, W. H., Bills, K. W., Mishuck, E., Moe, G. and Schultz, R. D., "A Model Describing Combustion of Solid-Composite Propellants Containing Ammonium Nitrate," *Combustion and Flame*, vol. 3, 1959, pp. 301–318.

9 Chaiken, R. F., "A Thermal Layer Mechanism of Combustion of Solid Composite Propellants: Application to Ammonium Nitrate Propellants," *Combustion and Flame*, vol. 3, 1959, pp. 285–300.

10 Chaiken, R. F. and Andersen, W. H., "The Role of Binder in Composite Propellant Combustion," *Solid Propellant Rocket Research*, Academic Press, New York 1960, pp. 227–244.

11 Andersen, W. H., Bills, K. W., Dekker, A. O. Mishuck, E., Moe, G. and Schultz, R. D., "The Gasification of Solid Ammonium Nitrate," JET PROPULSION, vol 28, 1958, pp. 831–832.

12 Chaiken, R. F., Andersen, W. H., Barsh, M. K., Mishuck, E., Moe, G. and Schultz, R. D., "Kinetics of the Surface Degradation of Polymethylmethacrylate," *J. Chem. Phys.*, vol. 32, 1960, pp. 141–146.

13 Andersen, W.H. and Chaiken, R. F., "Application of Surface Decomposition Kinetics to Detonation of Ammonium Nitrate," ARS JOURNAL, vol. 29, 1959, pp. 49-51.

14 Kistiakowsky, G. B., "Initiation of Detonation of Explosives," *Third Symposium on Combustion and Flame and Explosion Phenomena*, The Williams and Wilkins Co., Baltimore, Md., 1959, pp. 560–565.

15 Barsh, M. K., Andersen, W. H., Bills, K. W., Moe, G. and Schultz R. D., "Improved Instrument for the Measurement of Linear Pyrolysis Rates of Solids," *Rev. Scien. Instr.*, vol. 29, 1958, pp. 392–395.

16 Chaiken, R. F. and Van de Mark, D. K., "Thermocouple Junction for a Hot-Plate Linear Pyrolysis Apparatus," *Rev. Scien. Instr.*, vol. 30, 1959, pp. 375–376.

17 Friedman, R., Nugent, R. G., Rumbel, K. E. and Scurlock, A. C. "Deflagration of Ammonium Perchlorate," *Sixth Symposium (International) on Combustion*, Reinhold Publishing Corp., New York, 1957, pp. 612–618.

18 Friedman, R., Levy, J. B. and Rumbel, K. E., "The Mechanism of Deflagration of Pure Ammonium Perchlorate," AFOSR TN-59-173, Atlantic Research Corp., February 1959.

19 Bircumshaw, L. L. and Phillips, T. R., "The Kinetics of the Thermal Decomposition of Ammonium Perchlorate," *J. Chem. Soc.*, 1957, pp. 4741–4747.

20 Bircumshaw, L. L. and Newman, B. H., "The Thermal Decomposition of Ammonium Perchlorate," Parts 1 and 2, *Proc. Royal Soc.*, vol. A227, 1954, pp. 115–132, 228–241.

21 Schultz, R. D. and Dekker, A. O., "Transition-State Theory of the Linear Rate of Decomposition of Ammonium Perchlorate," *Sixth International Combustion Symposium*, Reinhold Publishing Corp., New York, 1958, pp. 618–626.

22 Rice, O. K., "Theory of Burning of Rocket Powders," OSRD Rep. 5574, 1945.

23 Vest, D. C., Baer, P. G. and Geene, R. W., *Bulletin of the 12th ANAF Meeting of the Solid Propellant Group*, Vol. 2, 1956, pp. 319–336.

24 Aronofsky, J. S. and Jenkins, R., "Unsteady Flow of Gas Through Porous Media, One-Dimensional Case," *Proc.* 1st U.S. National Congress Applied Mechanics, *Amer. Soc. of Mech. Engrs.*, New York, 1952, p. 763.

1961–62 ARS Meeting Schedule

Date	Meeting	Location	Abstract Deadline
1961			
Oct 9–15	ARS SPACE FLIGHT REPORT TO THE NATION	New York, N.Y.	Past
1962			
Jan. 24–26	Solid Propellant Rocket Conference	Waco, Tex.	Oct. 20
March 14–16	Electric Propulsion Conference	Monterey, Calif.	Nov. 20
April 3–5	Launch Vehicles Structures and Materials Conference	Phoenix, Ariz.	Sept. 15

Combustion of Carbon in an Air Stream[1]

JEFFREY A. MOORE[2]
MARTIN ZLOTNICK[3]

AVCO Research and
Advanced Development Div.
Wilmington, Mass.

An investigation was made to determine the combustion rate of carbon operating at a surface temperature between 1000° and 3000 °K in a stream of air. Relatively general forms of the surface reaction rate equations were used in the analysis, with the boundary layer equations simplified by letting $Le_i = Pr = 1$, so that the effect of the chemical kinetics could be elucidated. The results of the analysis can be used to make rapid estimates of mass loss rate for a wide range of free stream conditions. The accuracy of these estimates is limited primarily by the accuracy of the reaction rate parameters used rather than by the approximations used in the boundary layer equations, except when the combustion rate is controlled solely by diffusion and convection. Specific calculations, involving the graphical solution of two algebraic equations, were made at the stagnation point and a downstream station on a blunted slender body for a flight Mach number of 15 and an altitude of 100,000 ft. The ablation rate for porous carbon approached the diffusion (transport) controlled value at the stagnation point for nose radii greater than 1 cm. However, the rate of carbon removal was found to be governed only by the heterogeneous kinetics 16 cm downstream of the stagnation point (small bodies), and between the two limiting cases of reaction rate controlled and diffusion controlled at a distance of 400 cm downstream of the stagnation point (large bodies). The ablation rate for nonporous carbon, however, was reaction rate controlled for every station and geometry considered.

IN THE design of graphite rocket nozzles and some reentry vehicle heat shields, carbon combustion is often an important factor. This paper reports a computational scheme and some general results that may be useful in predicting the rate of the carbon combustion.

The rate of combustion depends on the rates of the following five processes: 1) transport of reactants to the surface (including any reactant supplied by gas phase reactions); 2) adsorption of reactants impinging on the surface; 3) chemical reaction between a reactant adsorbed on the surface and a surface molecule; 4) desorption of products from the surface; 5) transport of products away from the surface. See (1, 2).[4]

When one of the transport processes, items 1) or 5), is very much slower than the other processes it determines the ablation rate, and the true surface kinetics are irrelevant. When one of the surface kinetic processes, 2), 3) or 4), is the slowest, the reactant concentration at the surface is approximately that of the free stream, and boundary layer analysis is not required to determine the ablation rate. Between these two extremes there is an intermediate regime in which the transport rates and surface kinetic rates are comparable, so that the ablation rate is determined both by the aerothermochemistry of the boundary layer and the true kinetics at the solid surface.

An analysis of the intermediate regime was made in 1934 by Tu, Davis and Hottel (3). In this early work, which predated many modern developments in boundary layer theory, convection and gas phase reactions in the boundary layer were not considered. As a result, the final formulation lacked generality and, in fact, contained constants (other than chemical rate constants) that had to be determined empirically. Other authors have been more sophisticated in their treatment of the boundary layer, but they have considered only the limiting case in which surface combustion is controlled by diffusion and convection (4–9).

This work analyzes the interaction of surface chemical kinetics with the boundary layer transport processes to determine under what circumstances one or the other controls the rate of ablation. Effects of the chemical kinetics in the intermediate regime referred to previously are elucidated by introducing well-understood approximations that simplify the aerodynamics and leave the surface chemistry as general as possible. Nevertheless, it is expected that the accuracy of the results is limited more by the accuracy of the chemical rate data than by that of the boundary layer calculations. The computational scheme is general and simple enough so that comparable results can be readily derived from whatever data on surface kinetics is available.

The Model

Fig. 1 shows a schematic diagram of the physicochemical model in which partially dissociated air flows over a carbon surface. The surface temperature is between 1000° and 3000° K, and the static pressure is between 10^{-5} and 10^{3} atm.

Oxygen is convected and diffused to the surface with which it reacts to form carbon monoxide. The carbon monoxide is transported away from the surface and reacts with oxygen in the boundary layer to form carbon dioxide. The carbon dioxide is then transported back to the surface where it reacts to form more carbon monoxide. Thus the surface reacts with three species: the atomic and molecular oxygen originally in the boundary layer and the carbon dioxide formed by the

Received June 30, 1961.
[1] This work was sponsored by the Ballistic Systems Div., Air Force Systems Command, U. S. Air Force, under Contract No. AF 04(647)-305.
[2] Senior Scientist, Theoretical Aerodynamics Group. Member ARS.
[3] Assistant Section Chief, Aerodynamics.
[4] Numbers in parentheses indicate References at end of paper.

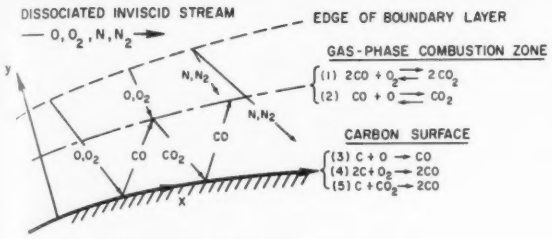

Fig. 1 Physicochemical model

gas phase reaction of oxygen with the carbon monoxide. Carbon monoxide is the primary product of both surface reactions (see the Appendix). In the gas phase, the chemical formulas are

$$2CO + O_2 \rightleftarrows 2CO_2 \qquad [1]$$

$$CO + O \rightleftarrows CO_2 \qquad [2]$$

and at the surface[5]

$$C + O \rightarrow CO \qquad [3]$$

$$2C + O_2 \rightarrow 2CO \qquad [4]$$

$$C + CO_2 \rightarrow 2CO \qquad [5]$$

As shown in Fig. 1, reactions 1 and 2 are assumed to occur at the same gas phase reaction surface.

Conditions under which there would be an appreciable concentration of carbon vapor have been excluded from consideration, and effects of NO and CN formation are neglected.[6] Kinetics are discussed in the Appendix.

Reynold's analogy between mass and energy transfer is assumed to be valid in the boundary layer. For a laminar boundary layer, this implies that the Prandtl and Lewis numbers are equal to one and all of the species have equal gas phase diffusion coefficients. Moreover, the gas phase reactions must occur within infinitesimally thin surfaces. Under these conditions it follows (11, 12) that the stagnation enthalpy and species concentrations are linearly related everywhere in the boundary layer if they are constant at the wall and at the outer edge. Thus the present work can be confined to determining concentration profiles and rates of mass flux in terms of stagnation enthalpy profiles and heat flux rates obtained elsewhere. To be consistent, the latter should be obtained from so-called locally similar solutions of the laminar boundary layer equations (13).[7] For some practical purposes, however, boundary layer data obtained from other calculations or from experiment may be used. For example, it would not be unreasonable, in the absence of a better model, to use turbulent boundary layer data in an effort to obtain qualitative information for turbulent boundary layer ablation, as in (14).

[5] Only the forward reactions are relevant at the surface since the high bond energy of the carbon monoxide molecule makes release of the oxygen atom and re-adsorption of the carbon atom improbable in the temperature range considered here.

[6] The equilibrium-air mole fraction of NO does not exceed 8% for temperatures below 8000° K and densities below 1 atm (see Ref. 10 and footnote 16 in the Appendix).

[7] These can be solutions for arbitrary local pressure gradient rather than for zero pressure gradient only. The relation between species concentration and stagnation enthalpy was used, rather than the more common one between concentration and velocity, because of this additional generality and because heat flux is calculated more often than shear stress in connection with ablation problems.

Derivation of the Equations

The reactions in the gas and at the wall serve as sources and sinks for the chemical species involved. The strength of these sources and sinks will be written as a function of the species concentrations and their derivatives. These equations, the equations stating that atomic species are conserved, and the statement of the boundary conditions will complete the formulation.

At each reaction surface

$$\left\{\begin{matrix}\text{net mass flux of species } i \\ \text{particles out of the reaction} \\ \text{surface, per unit area per unit time}\end{matrix}\right\} =$$

$$\left\{\begin{matrix}\text{net mass of species } i \\ \text{particles convected away} \\ \text{from the reaction surface,} \\ \text{per unit area per unit time}\end{matrix}\right\} +$$

$$\left\{\begin{matrix}\text{net mass of species } i \text{ particles} \\ \text{diffused away from the reaction surface,} \\ \text{per unit area per unit time.}\end{matrix}\right\}$$

Consistent with the classical laminar boundary layer approximations, it is assumed that only the y-component of the mass average velocity and the average diffusion velocity contribute to the net flux of each species out of the reaction surface. That is, the species mass source relation becomes

$$\dot{m}_{i,*} = [(\rho_i v)_+ - (\rho_i v)_-]_* + [(\rho_i \underline{v}_i)_+ - (\rho_i \underline{v}_i)_-]_* \qquad [6]$$

where

$(\ )_+$ = quantities evaluated just above the reaction surface

$(\ )_-$ = quantities evaluated just below the reaction surface

From Ficks law, assumed valid for a multicomponent mixture (12), since $\mathrm{Pr} = \mathrm{Le}_i = 1$ and $C_i = C_i(H)$

$$\underline{v}_i \simeq -\frac{D_i}{C_i}\frac{\partial C_i}{\partial y} = -\frac{1}{\rho_i}\frac{\dot{q}'}{H_t}\frac{dC_i}{d\bar{H}}$$

where

$$\dot{q}' \equiv \frac{k}{\bar{C}_p}\frac{\partial H}{\partial y}$$

But by continuity

$$(\rho v)_+ = (\rho v)_-$$

Also, since the function $\dot{q}'$ and the gas species concentrations must be continuous

$$(\dot{q}')_+ = (\dot{q}')_- \qquad (C_i)_+ = (C_i)_-$$

Hence, at any gas phase reaction surface

$$\dot{m}_{i,*} = -\frac{\dot{q}'}{H_t}\left[\left(\frac{dC_i}{d\bar{H}}\right)_+ - \left(\frac{dC_i}{d\bar{H}}\right)_-\right]_* \qquad [7]$$

Similarly, at the wall or reacting surface of the body[8]

$$\dot{m}_{i,w} = C_{i,w}(\rho v)_w - \frac{\dot{q}_w'}{H_t}\left(\frac{dC_i}{d\bar{H}}\right)_w \qquad [8]$$

where the subscript i in these equations refers to each of the chemical species, N, O, CO and CO_2.[9]

[8] Note that $\dot{q}_w' = \dot{q}_w = (k\partial T/\partial y)_w$. Also, see (4, 15) for another derivation of the relations which are analogous to Eqs. 7 and 8, obtained for the special case of zero pressure gradient.

[9] As discussed in the Appendix, only the total concentrations of nitrogen atoms and oxygen atoms need to be described, independently of whether these are in atomic or molecular form. It follows that it is not necessary to explicitly describe the location of the dissociation and recombination surfaces.

At the gas phase combustion zone, the amount of carbon dioxide formed is limited either by the amount of oxygen or carbon monoxide available. Since the location of this zone has not been specified, it is necessary to consider both possibilities. For reaction surface locations where there is an abundance of oxygen, the amount of carbon monoxide remaining above the reaction surface after the reaction is specified by the parameter θ

$$C_{CO,*} = \theta C_{CO_2,*} \quad [9]$$

Where there is an abundance of carbon monoxide, the amount of oxygen remaining below the reaction surface after the reaction is given by the parameter ϵ

$$C_{O,*} = \epsilon C_{CO_2,*} \quad [10]$$

That is, the reciprocals of the parameters θ and ϵ vary linearly with the reaction surface sink strengths. Compatibility of these relations at the stoichiometric point gives the relation

$$\theta = (M_{CO}/M_O)\epsilon \quad [11]$$

The description of the gas phase combustion zone is completed by Eq. 7 and by the statement of atomic species conservation, viz.

$$\dot{m}_{CO,*} = + \frac{M_{CO}}{M_O} \dot{m}_{O,*} \quad [12a]$$

$$\dot{m}_{CO_2,*} = - \frac{M_{CO_2}}{M_O} \dot{m}_{O,*} \quad [12b]$$

$$\dot{m}_{N,*} = 0 \quad [12c]$$

At the wall, the species mass fluxes $\dot{m}_{i,w}$ are related to the ablation rate $\dot{m}_w$ by employing conservation of atomic species. That is

$$\dot{m}_{O,w} = -(1 - \beta)\dot{m}_w \frac{M_O}{M_C} \quad [13a]$$

$$\dot{m}_{CO,w} = (1 + \beta)\dot{m}_w \frac{M_{CO}}{M_C} \quad [13b]$$

$$\dot{m}_{CO_2,w} = -\beta \dot{m}_w \frac{M_{CO_2}}{M_C} \quad [13c]$$

$$\dot{m}_{N,w} = 0 \quad [13d]$$

where

$$(\rho v)_w = \frac{R_C M_C}{N} = \sum_i \dot{m}_{i,w} = \dot{m}_w \quad [14]$$

The quantity R_C is the total rate of carbon atom consumption per unit area per unit time, i.e., R_5, R_6 or R_8, as given in the Appendix. The function β is defined as the ratio

$$\beta \equiv \frac{\left\{\begin{array}{c}\text{carbon atoms consumed as a result of the capture} \\ \text{of oxygen atoms from carbon dioxide molecules}\end{array}\right\}}{\left\{\begin{array}{c}\text{total number of carbon atoms} \\ \text{removed from the wall}\end{array}\right\}}$$

As seen from the rate equations derived in the Appendix, β must represent the three ratios

$$\beta = R_3/R_5,\ R_4/R_6 \text{ or } \frac{(R_8 - R_7)}{R_8}$$

which are expressed as functions of the concentrations as follows

$$\beta = \frac{\left(\frac{M_O}{M_{CO_2}} \frac{C_{CO_2,w}}{C_{O,w}}\right)^{l=1/2,3/2}}{1 + \left(\frac{M_O}{M_{CO_2}} \frac{C_{CO_2,w}}{C_{O,w}}\right)^{l=1/2,3/2}}$$

$$\text{or} \quad \frac{\left(\frac{M_O}{M_{CO_2}}\right)^{1/4} \left(\frac{M_O}{M_{CO_2}} \frac{C_{CO_2,w}}{C_{O,w}}\right)^{l=3/4}}{1 + \left(\frac{M_O}{M_{CO_2}}\right)^{1/4} \left(\frac{M_O}{M_{CO_2}} \frac{C_{CO_2,w}}{C_{O,w}}\right)^{l=3/4}} \quad [15]$$

where the appropriate value of l depends upon the rate equations which are applied to the problem.

Eq. 8 with Eqs. 13, 14 and 15 complete the description of conditions at the wall.

Finally, the boundary conditions at the outer edge of the boundary layer are imposed

$$C_{O,e} = \alpha \qquad C_{N,e} = 1 - \alpha \qquad C_{CO,e} = 0 \qquad C_{CO_2,e} = 0 \quad [16]$$

where C_O and C_N are the total concentrations of oxygen atoms and nitrogen atoms, respectively, including those associated in molecular form.

Solution of the Equations

Defining the nondimensional "blowing" parameter ξ and the Stanton number C_H in the usual manner

$$\xi = \frac{\dot{m}_w}{\rho_e u_e C_H} \quad [17]$$

$$C_H = \frac{\dot{q}_w}{\rho_e u_e (h_{s,e} - h_{s,w})} \quad [18]$$

the mass concentrations of each species at the wall can be written in terms of the gas phase reaction surface concentrations as follows

$$C_{O,w} = \frac{C_{O,*} - \bar{H}_* (1 - \beta) \frac{M_O}{M_C} \xi}{(1 + \bar{H}_* \xi)} \quad [19a]$$

$$C_{CO,w} = \frac{C_{CO,*} + \bar{H}_* (1 + \beta) \frac{M_{CO}}{M_C} \xi}{(1 + \bar{H}_* \xi)} \quad [19b]$$

$$C_{CO_2,w} = \frac{C_{CO_2,*} - \bar{H}_* \beta \frac{M_{CO_2}}{M_C} \xi}{(1 + \bar{H}_* \xi)} \quad [19c]$$

$$C_{N,w} = \frac{C_{N,*}}{(1 + \bar{H}_* \xi)} \quad [19d]$$

The remainder of the solution, which gives the mass concentrations of each species at the reaction surface $\bar{H} = \bar{H}_*$, is divided into two regimes (see Eqs. 9 and 10)

$\bar{H}_* \geq \bar{H}_*'$

$$C_{CO,*} = \theta C_{CO_2,*} \quad [9]$$

$$C_{O,*} = \frac{\alpha \frac{M_{CO_2}}{M_O} (1 + \bar{H}_* \xi) - (1 - \bar{H}_*) \frac{M_{CO_2}}{M_C} \xi - \frac{1}{1 + \theta} [\alpha + \xi(1 - \bar{H}_* + \alpha \bar{H}_*)]}{(1 + \xi) \left(\frac{M_{CO_2}}{M_O} - \frac{1}{1 + \theta}\right)} \quad [20a]$$

$$C_{CO_2,*} = \frac{(1 - \bar{H}_*)\frac{M_{CO_2}}{M_O}\frac{M_{CO}}{M_C}\left(\frac{1}{1+\theta}\right)\xi}{(1+\xi)\left(\frac{M_{CO_2}}{M_O} - \frac{1}{1+\theta}\right)} \quad [20b]$$

$$C_{N,*} = \frac{(1-\alpha)(1+\bar{H}_*\xi)}{(1+\xi)} \quad [20c]$$

$\bar{H}_* \leq \bar{H}_*'$

$$C_{O,*} = \epsilon C_{CO_2,*} \quad [10]$$

$$C_{CO,*} = \frac{\frac{M_{CO_2}}{M_C}\xi(1-\bar{H}_*) - \frac{1}{1+\epsilon}[\alpha(1+\bar{H}_*\xi) + \xi(1-\bar{H}_*)]}{(1+\xi)\left(\frac{M_{CO_2}}{M_{CO}} - \frac{1}{1+\epsilon}\right)} \quad [21a]$$

$$C_{CO_2,*} = \frac{\left(\frac{1}{1+\epsilon}\right)\left[\alpha\frac{M_{CO_2}}{M_{CO}}(1+\bar{H}_*\xi) - \frac{M_{CO_2}}{M_C}\frac{M_O}{M_{CO}}(1-\bar{H}_*)\xi\right]}{(1+\xi)\left(\frac{M_{CO_2}}{M_{CO}} - \frac{1}{1+\epsilon}\right)} \quad [21b]$$

$$C_{N,*} = \frac{(1-\alpha)(1+\bar{H}_*\xi)}{(1+\xi)} \quad [21c]$$

where $\bar{H}_*'$ is the location of the stoichiometric line in the $(\bar{H}, C_i)$ plane, and is given by the expression

$$\bar{H}_* \equiv \bar{H}_*' = \frac{\xi - \frac{\alpha M_C}{2M_O}}{\xi\left(1 + \frac{\alpha M_C}{2M_O}\right)} \quad [22]$$

The stoichiometric reaction surface will move to the solid carbon surface when

$$\xi \equiv \xi' = \frac{\alpha M_C}{2M_O} \quad [23]$$

A qualitative description of the concentration profiles in the enthalpy plane is shown in Figs. 2–5.

It can be demonstrated that the maximum obtainable value of the nondimensional blowing rate is only a function of the free stream oxygen concentration, and is given by the relation

$$\xi \equiv \xi_{max} = \frac{\alpha M_C}{M_O} \quad [24]$$

This corresponds to all of the oxygen and carbon dioxide at the wall being consumed; that is, this is the case of a diffusion controlled reaction. Except for the special case $\theta = 0$ and $\bar{H}_* < (\bar{H}_*')_{\xi=\xi_{max}}$, the species mass concentrations $C_{O,w}$ and $C_{CO_2,w}$ will become zero simultaneously for all values of the blowing parameter ξ (see Figs. 2–5). Finally, from Eqs. 22 and 24, the value of $(\bar{H}_*')_{\xi=\xi_{max}}$ is

$$(\bar{H}_*')_{\xi=\xi_{max}} = \frac{1}{2 + \frac{\alpha M_C}{M_O}} \quad [25]$$

Hence, upon specifying the free stream oxygen concentration α, the reaction surface location $\bar{H}_*$,[10] and the parameter

[10] Alternately, $\bar{H}_*$ could be obtained as a function of θ or ϵ if it is required, for example, that thermodynamic equilibrium exists "just above" the reaction surface. Cohen, et al. (4) located the reaction surface by specifying either an ignition temperature (which is analogous to a specification of $\bar{H}_*$) or that the reactants exist in stoichiometric proportions at the reaction surface.

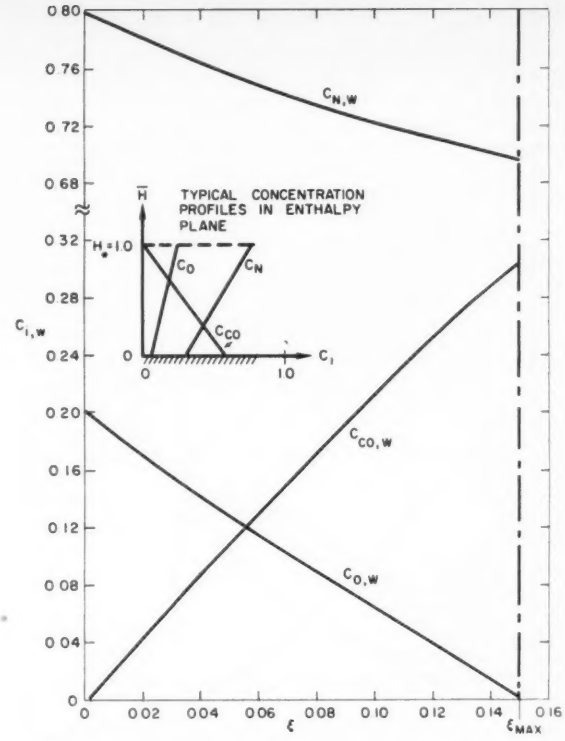

Fig. 2 Species mass concentration at the wall as a function of the nondimensional blowing rate for $\bar{H}_* = 1.0$

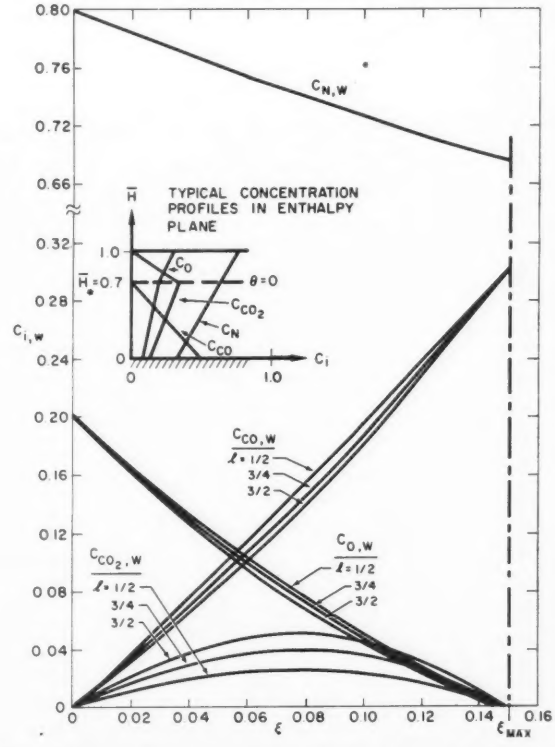

Fig. 3 Species mass concentration at the wall as a function of the nondimensional blowing rate for $\bar{H}_* = 0.7$ and $\theta = 0$

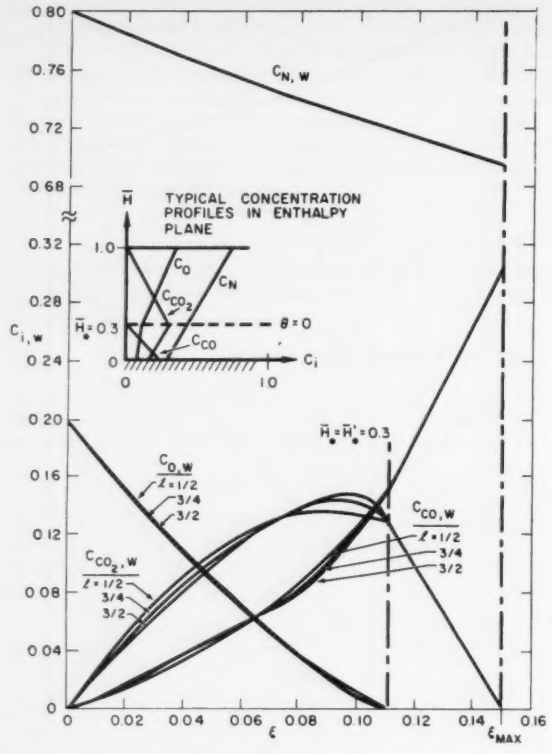

Fig. 4 Species mass concentration at the wall as a function of the nondimensional blowing rate for $\bar{H}_* = 0.3$ and $\theta = 0$

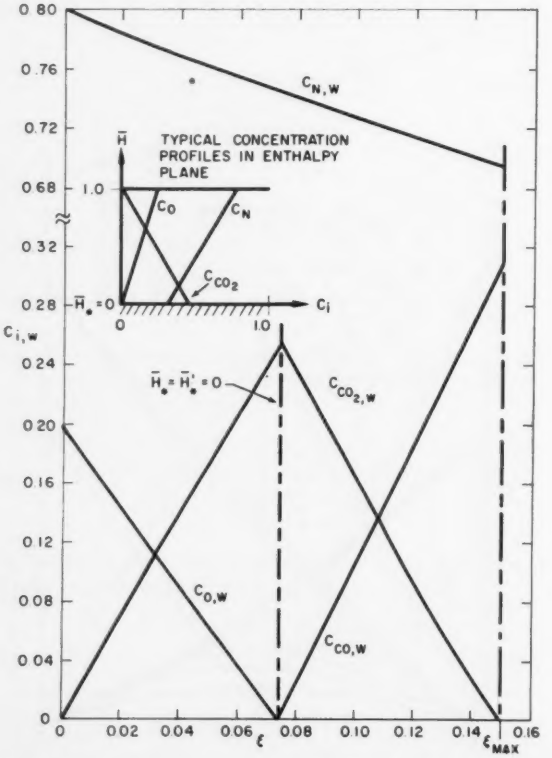

Fig. 5 Species mass concentration at the wall as a function of the nondimensional blowing rate for $\bar{H}_* = 0$ and $\theta = 0$

θ or ϵ, it is possible to calculate the variation of $C_{i,w}$ with the parameter ξ. This variation will be different for each form of the reaction rate R_c because the parameter β enters into the solution (see Eqs. 13 and 15, and Fig. 6). Typical variations of $C_{i,w}$ with ξ are given in Figs. 2–5.

Employing the semi-empirical relation, for example, (12)[11]

$$C_H/C_H^0 = \left(1 - \eta \frac{\dot{m}_w}{\rho_e u_e C_H^0}\right) \quad [26]$$

(with the superscript denoting conditions without blowing), and the definition of the blowing parameter ξ, we obtain the expressions

$$C_H/C_H^0 = \frac{1}{1 + \eta\xi} \quad [27]$$

$$\dot{m}_w = \frac{M_C R_C}{N} = \frac{\rho_e u_e C_H^0 \xi}{1 + \eta\xi} \quad [28]$$

where, for laminar flow, $\eta \simeq 0.7$.

In addition, we modify the reaction rate laws R_i given in the Appendix as follows

$$r_5 = \frac{R_5}{P_w^{1/2} T_w e^{-E/RT_w}} = K_1 \left[\left(\frac{\bar{M}_w}{M_O} C_{O,w} \right)^{1/2} + \left(\frac{\bar{M}_w}{M_{CO_2}} C_{CO_2,w} \right)^{1/2} \right] \equiv f_5(\xi) \quad [29a]$$

$$r_8 = \frac{R_8}{P_w^{1/2} T_w e^{-E/RT_w}} = K_1 \left[\left(\frac{\bar{M}_w}{M_O} C_{O,w} \right)^{3/2} + \left(\frac{\bar{M}_w}{M_{CO_2}} C_{CO_2,w} \right)^{3/2} \right] \equiv f_8(\xi) \quad [29b]$$

[11] A study of similar solutions indicates that this formulation is substantially correct for $[\dot{m}_w/\rho_e u_e C_H^0] < 1.0$.

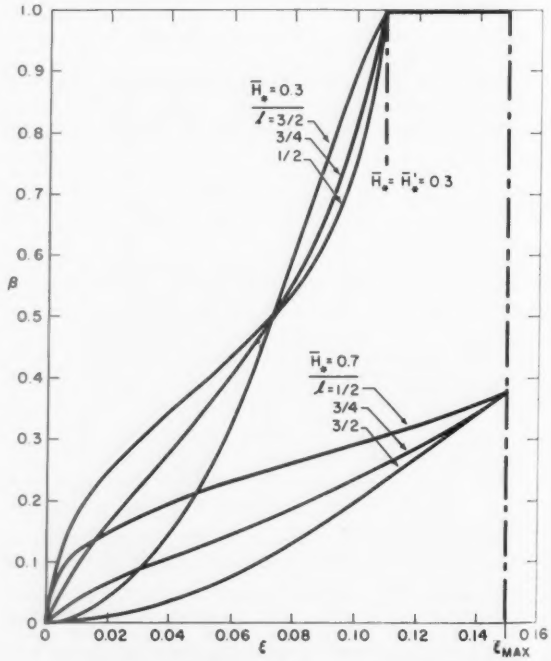

Fig. 6 Parameter β as a function of the nondimensional blowing rate for $\bar{H}_* = 0.3$, 0.7, and $\theta = 0$

for nonporous carbon surfaces, and

$$r_6 = \frac{R_6}{\phi(1-\phi)^{1/2}P_w^{3/4}T_w^{1/4}e^{-E/2RT_w}} = K_2\left[\left(\frac{\bar{M}_w}{M_O}C_{CO,w}\right)^{3/4} + \left(\frac{M_O}{M_{CO_2}}\right)^{1/4}\left(\frac{\bar{M}_w}{M_{CO_2,w}}C_{CO_2,w}\right)^{3/4}\right] \equiv f_6(\xi) \quad [29c]$$

for porous carbon surfaces. Utilizing the definition of $\bar{M}$, Eqs. 19, 9 or 10 and either 20 or 21, the variation of r_j, the modified reaction rate laws, with the blowing parameter ξ can be obtained independently of the specific application or flight conditions. This function $r_j = f_j(\xi)$ is shown in Fig. 7.

Also, from Eq. 28 and the rate Eqs. 37, 38 and 40

$$r_3 = r_3 = \frac{\rho_e u_e C_H{}^0}{P_w^{1/2}T_w e^{-E/RT_w}}\frac{N}{M_C}\left(\frac{\xi}{1+\eta\xi}\right) \equiv g_3(\xi) = g_3(\xi) \quad [30a,b]$$

$$r_6 = \frac{\rho_e u_e C_H{}^0}{\phi(1-\phi)^{1/2}P_w^{3/4}T_w^{1/4}e^{-E/2RT_w}}\frac{N}{M_C}\left(\frac{\xi}{1+\eta\xi}\right) \equiv g_6\xi \quad [30c]$$

Eqs. 30a,b,c give $r_j = g_j(\xi)$ if $\rho_e u_e C_H{}^0$, P_w, and T_w are known, The intersection of the curve $g_j(\xi)$, defined by Eqs. 30a,b,c, and $f_j(\xi)$, given in Fig. 7, will yield values for r_j and ξ. From the definition of either of these quantities the value of the ablation rate $\dot{m}_w$ can be determined.

Results and Discussion

Results of ablation rate calculations, with and without gas phase reaction surfaces, will be described and discussed. Some details of the calculations are included.

No Gas Phase Reaction Surface

We consider first a stagnation point with a sufficiently high wall temperature (say, greater than 2000° K) which would probably not give rise to a carbon dioxide producing reaction in the gas. Specifying a flight Mach number of 15 at an altitude of 100,000 ft, the following quantities are calculated for the stagnation point (16, 17, 18)

$$P_w = 3.385 \times 10^6 \quad \text{dynes/cm}^2$$

$$\rho_e u_e C_H{}^0 = 3.03 \times 10^{-3}\, a^{-1/2} \quad \text{gm/cm}^2\text{-sec}$$

where the nose radius a is expressed in centimeters and we stipulate that

$$2000°\text{K} \leq T_w \leq 3000°\text{K}$$

$$C_{CO_2}(\bar{H}) = 0 \text{ (i.e., } \bar{H}_* = 1 \quad \text{(see Fig. 2)}$$

$$\phi = 0.40 \qquad \alpha = 0.20$$

where the above value of α reflects an attempt to incorporate the effects of nitric oxide formation (i.e., $\alpha \simeq 0.232$ for undissociated air).

Employing Eq. 30c

$$g_6 = 6.22 \times 10^{15}\frac{a^{-1/2}}{T_w^{1/4}\,e^{-500/T_w}}\left(\frac{\xi}{1+0.7\xi}\right) \quad [31]$$

The $g_6(\xi)$ curves can now be plotted on the $r_6(\xi)$ diagram (Fig. 7b) for representative values of both wall temperature T_w and nose radius a. Eqs. 30a,b can be used in a similar fashion. The various solutions for $g_j(\xi) = f_j(\xi)$ are shown in Fig. 7 and the results are summarized in Fig. 8.

It is evident from Figs. 7a and 7c that both the $\frac{1}{2}$-order and $\frac{3}{2}$-order (nonporous) surface reactions are essentially rate controlled for a nose radius a of less than 100 cm. The dependence of the ablation rate on wall temperature, as given in Fig. 8, is dictated by the rate relations given in Eqs. 37 and 40. Finally, returning to Fig. 7b, the $\frac{3}{4}$-order

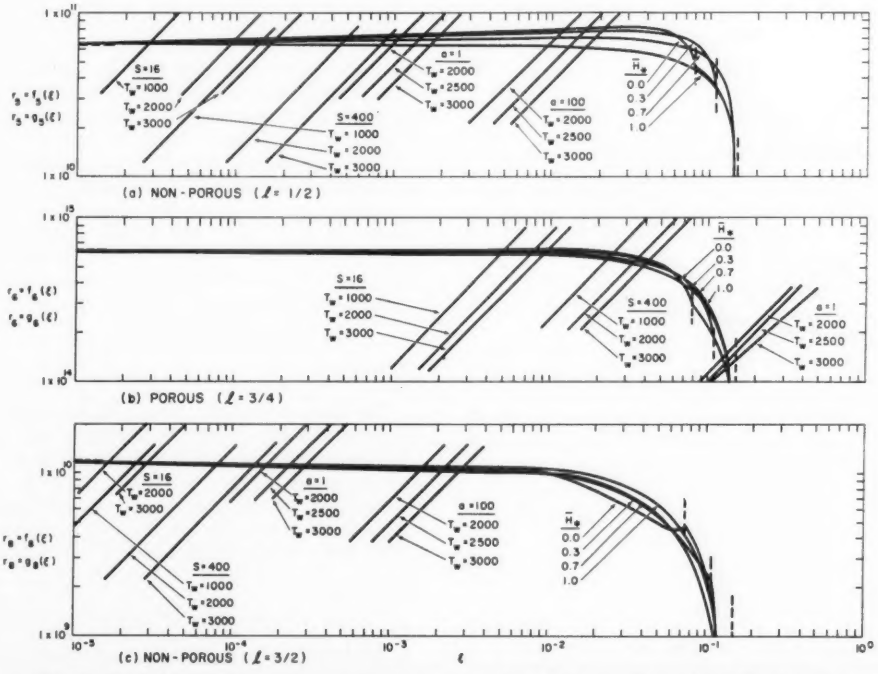

Fig. 7 Modified reaction rate parameters as a function of the nondimensional blowing rate

(porous) surface reaction is seen to approach quickly a transport controlled reaction with increasing nose radius. For this limiting case, the mass flux (depicted in Fig. 8) is independent of surface temperature and inversely proportional to the square root of the nose radius, as given by Eq. 31. That is, although stagnation point flow favors the convection of reactant (oxygen) to the surface and thus encourages a kinetically controlled process, the porous carbon reaction rate is more sensitive to pressure ($R_\theta \sim P_w^{3/4}$) than the nonporous rate (R_s, $R_g \sim P_w^{1/2}$) so that the process is driven toward the diffusion controlled limit.

Single Gas Phase Reaction Surface

Three combustion surface locations, or values of $\bar{H}_*$, are considered with the parameter $\theta = 0$. Only one value of the parameter θ was chosen because making $\theta = 0$ has the same qualitative effect on the wall mass loss rate as increasing $\bar{H}_*$. An increase in either $\bar{H}_*$ or θ corresponds to a decrease in the source-sink strength of the reaction surface.

Postulating, again, a flight Mach number of 15 at an altitude of 100,000 ft, the mass loss rate at representative stations downstream of the stagnation point on two blunted bodies will be calculated, where it is assumed that the concept of local similarity is applicable.

Assuming a Mach number of 4 at the edge of the laminar boundary layer, and local properties corresponding to an isentropic expansion of stagnation conditions, we find that (16, 17, 19)

$$P_w = 1.89 \times 10^3 \qquad \text{dynes/cm}^2$$

$$\rho_e u_e C_H{}^0 = 3.35 \times 10^{-3}\, s^{-1/2} \qquad \text{gm/cm}^2\text{-sec}$$

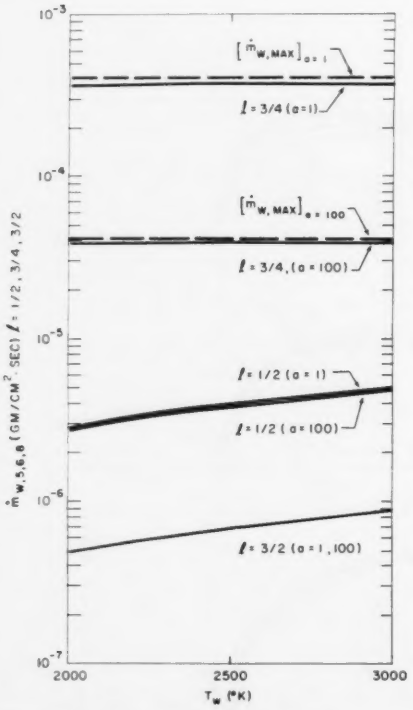

Fig. 8 Stagnation point ablation rate as a function of wall temperature for porous (l = ¾) and nonporous (l = ½, ⅜) carbon

where

$$1000°\text{K} \leq T_w \leq 3000°\text{ K} \qquad 0.25 \leq T_w/T_e \leq 1.5$$

$$\bar{H}_* = 0.7,\ 0.3,\ \text{and}\ 0.0\ \text{(Figs. 3, 4, 5, respectively)}$$

$$\phi = 0.40 \qquad \alpha = 0.20$$

and s is the distance downstream of the stagnation point in centimeters. Substituting the above values into Eqs. 30a,b,c, as before, we obtain $g_i(\xi)$ for $s = 16$ cm (small bodies) and 400 cm (large bodies), which are shown in Fig. 7.

It is clear from Figs. 7a and 7c that the nonporous wall reactions are definitely rate controlled for distances downstream of the stagnation point well in excess of 400 cm and wall temperatures as great as 3000° K. The true ablation rate in this case is substantially independent of the transport processes, and hence of the geometry. The temperature dependence is as given in the rate equation, Eqs. 37 and 40.[12] These results do not significantly depend upon either the location or the strength of the gas phase reaction surface (see Figs. 9a and 9c), and thus the simplified treatment of the carbon dioxide producing reaction has been justified for a nonporous wall.

The ablation rate of a porous surface is seen in Fig. 7b to be a rate controlled process for distances downstream of the stagnation point of less than 16 cm (i.e., small bodies), but lies between the rate controlled and diffusion controlled limits for the relatively large body corresponding to $s = 400$ cm. Fig. 9b also depicts the variation of the wall mass loss rate with wall temperature for porous carbon at distances of 16 cm and 400 cm downstream of the stagnation point. It can be seen that these results also have only a weak dependence on the value of $\bar{H}_*$.

Concluding Remarks

From the preceding analysis one may conclude that the ablation rate of a nonporous carbon surface, moving at hypersonic velocities, approaches the reaction rate controlled limit, this rate being less than the transport controlled value by a factor of 10 to 10^4 (depending on the geometry and location on the body). On the other hand, the rate of consumption of a porous carbon wall was found, at the stagnation point, to be controlled by the transport of oxygen to the surface, and to be between the two limiting cases of transport and reaction rate controlled at large distances downstream of the stagnation point. These conclusions are contingent on confirmation of the surface kinetics data used in the analysis.

Finally, the ablation rate of nonporous carbon was found to be rather sensitive to the order of the reaction and the surface temperature. Hence, the possibility exists of obtaining more fundamental information on the actual surface kinetics from experiments on carbon specimens immersed in a high energy air stream.

Appendix

The heterogeneous kinetics are derived from the theoretical and experimental studies of Blyholder and Eyring (20), who considered the kinetics of the oxygen-graphite reaction for temperatures between 900° and 1300° C, and a pressure range of 1 to 100 μ of mercury. At these temperatures, the formation of a carbonyl type bond between an oxygen atom and a surface carbon atom is postulated as the slowest,

[12] Note that the slight increase in r_s over the rate controlled limit, at low values of ξ, is due to the postulated functional form of the rate law, Eq. 38; that is, for the lack of any quantitative data, the rates of the two surface reactions were assumed to be additive.

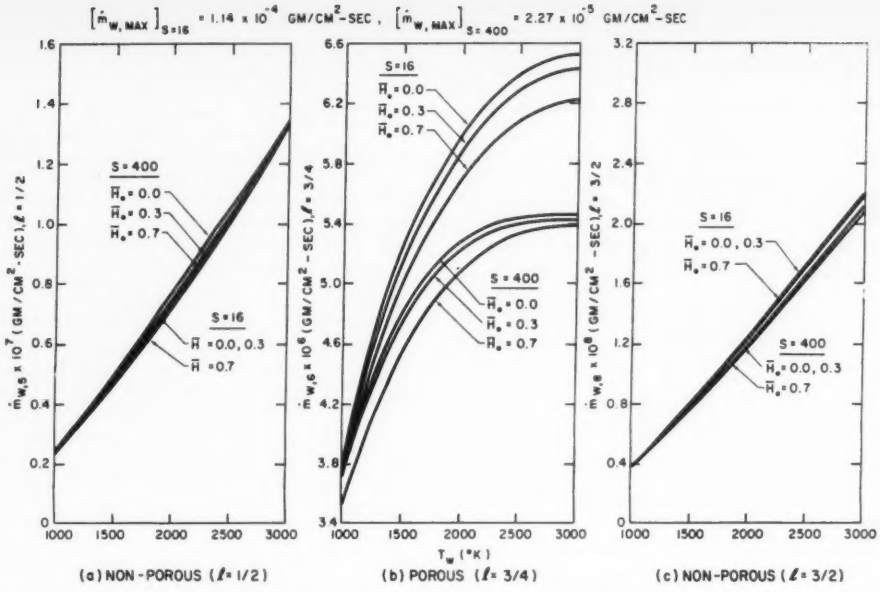
$[\dot{m}_{w,MAX}]_{S=16}$ = 1.14 x 10^{-4} GM/CM^2-SEC, $[\dot{m}_{w,MAX}]_{S=400}$ = 2.27 x 10^{-5} GM/CM^2-SEC
S = 400
$\bar{H}_e$ = 0.0
$\bar{H}_e$ = 0.3
$\bar{H}_e$ = 0.7
S = 16
$\bar{H}$ = 0.0, 0.3
$\bar{H}$ = 0.7
$\dot{m}_{w,5}$ x 10^7 (GM/CM^2-SEC), ℓ = 1/2
$\dot{m}_{w,6}$ x 10^6 (GM/CM^2-SEC), ℓ = 3/4
$\dot{m}_{w,8}$ x 10^8 (GM/CM^2-SEC), ℓ = 3/2
T_w (°K)
(a) NON-POROUS (ℓ = 1/2)
(b) POROUS (ℓ = 3/4)
(c) NON-POROUS (ℓ = 3/2)

Fig. 9 Downstream surface ablation rate as a function of wall temperature for porous (l = ¾) and nonporous (l = ½, 3/2) carbon

and thus reaction rate controlling, step.[13] The carbon to carbon bond then quickly decomposes to yield a carbon monoxide molecule, with the reverse process being very unlikely.[5] Preceding the formation of the carbonyl bond, the oxygen atom hops along the surface by forming only a single bond with a succession of adjacent carbon atoms. Further, since Blyholder and Eyring propose that the adsorption of an oxygen atom from an oxygen molecule is relatively fast in comparison with the other microscopic rate processes at the surface, it may be assumed that the overall reaction rate is independent of the degree of oxygen dissociation.

To include the possibility of a reaction between a carbon dioxide molecule (formed in the gas phase) and the carbon surface,[14] it is assumed that one of the oxygen atoms can be captured by a carbon site (viz., adsorbed) and that this process is at least as fast as the capture of an oxygen atom from an oxygen molecule.[15] This assumption implies, in turn, the direct application of the reaction rate law derived for the oxygen-carbon system to a carbon dioxide-carbon system. Finally, it is assumed that the nitrogen atoms and molecules are completely inert, behaving neither as a catalyst nor as an active participant in a gas phase or gas-solid reaction.[16]

Postulating that the reaction rate controlling mechanisms at surface temperatures up to 3000° K will continue to be the capture of mobile oxygen atoms, the following equivalent form of the rate law given in (20) is proposed for the temperature range of 1000° to 3000° K

$$R_1 = K_1 P_w^{1/2} T_w e^{-E/RT_w} \left[\frac{\bar{M}_w}{M_O} C_{O,w}\right]^{1/2} \quad \frac{\text{carbon atoms}}{\text{cm}^2\text{-sec}} \qquad [32]$$

where

E = activation energy = 2 kcal/mole

If the pressure is expressed in dynes per cm^2 and the temperature in °K

$$K_1 = 1.55 \times 10^{11}$$

It follows from the reactions given in Eqs. 1–4 and the above discussion that it is only necessary to retain a description of the concentration of oxygen atoms; thus the subscript O refers to oxygen atoms in both the atomic and the molecular form. The concentration of nitrogen atoms is treated in an analogous manner. The average molecular weight of the gas mixture is given by

$$\frac{1}{\bar{M}} = \sum_i \frac{C_i}{M_i} \qquad [33]$$

Blyholder and Eyring (20) also derive a rate law for the kinetics of the reaction between oxygen molecules and a pure porous carbon, when the mean free path of the reactant near the wall is much greater than the average pore diameter. Since a much larger number of reactions occur within the pores than on the outer surface because of the much greater internal surface area, they neglect the outer surface reactions. Neglecting the change in effective internal pore structure, which is developed and enlarged by reactions, the declared (20) rate law for the consumption of carbon atoms may be written as

$$R_2 = K_2 \phi(1-\phi)^{1/2} P_w^{3/4} T_w^{1/4} e^{-E/2RT_w} \left[\frac{\bar{M}_w}{M_O} C_{O,w}\right]^{3/4} \quad \frac{\text{carbon atoms}}{\text{cm}^2\text{-sec}} \qquad [34]$$

[13] Blyholder and Eyring (21) have also studied the kinetics of the oxygen-carbon system for the temperature range of 600° to 800°C and found another rate controlling mechanism to apply. Wicke (22) has reviewed the conflicting experimental data of various investigators resulting from impurities present in their carbon specimens. Finally, many gas-carbon reactions are discussed in detail by Walker, et al. (23).

[14] The experimental techniques employed (20) preclude the possibility of carbon dioxide diffusing back to the carbon surface and reacting.

[15] This is supported by the fact that the energy required to remove an oxygen atom is less for the CO_2 molecule than for the O_2 molecule at any given temperature.

[16] Zinman (24) found that atomic nitrogen did not react with (spectrographic) carbon at 800°C, and also stated that the reaction rate between molecular nitrogen and carbon is very slow for temperatures up to 2750°C. Also, only negligible concentrations of such species as CN and C_2N_2 will be formed in the gas phase, since the bond energy of the CO molecule is so high. In fact, equilibrium computations for the air-carbon system gives, at 1 atm and 3000°K, a mole fraction for CN as 5.4×10^{-3} and for C_2N_2 as 3.2×10^{-4}.

where

$K_2 = 2.3 \times 10^{15}$

ϕ = porosity (fraction of surface which is space)

Again, we choose to extend the validity of the governing rate equations to a temperature of 3000°K.

Since the carbon dioxide molecule acts merely as a vehicle for the transport of an oxygen atom from the gas phase reaction plane to the wall, the rate coefficient, activation energy, and temperature dependence for the rate law giving the consumption of carbon atoms on a nonporous surface due to the carbon dioxide reaction is as given in Eq. 32. That is

$$R_3 = K_1 P_w^{1/2} T_w e^{-E/RT_w} \left[\frac{\bar{M}_w}{M_{CO_2}} C_{CO_2,w}\right]^{1/2} \frac{\text{carbon atoms}}{\text{cm}^2\text{-sec}} \quad [35]$$

Since the reactant particle velocity in the pores is contained in the formulation of R_2, application of the porous carbon rate law to the carbon dioxide reaction requires that the rate coefficient be multiplied by the factor $(M_O/M_{CO_2})^{1/4}$, which reflects the difference in average molecular speed of the carbon dioxide molecule and oxygen atom at a given translational temperature. That is

$$R_4 = K_2 \left(\frac{M_O}{M_{CO_2}}\right)^{1/4} \phi(1-\phi)^{1/2} P_w^{3/4} T_w^{1/4} e^{-E/2RT_w} \times \left[\frac{\bar{M}_w}{M_{CO_2}} C_{CO_2,w}\right]^{3/4} \frac{\text{carbon atoms}}{\text{cm}^2\text{-sec}} \quad [36]$$

Hence, if there is an abundance of free carbon surface sites, the rate equations for the total consumption of carbon surface atoms become, for the nonporous surface

$$R_5 = K_1 P_w^{1/2} T_w e^{-E/RT_w} \left[\left(\frac{\bar{M}_w}{M_O} C_{O,w}\right)^{1/2} + \left(\frac{\bar{M}_w}{M_{CO_2}} C_{CO_2,w}\right)^{1/2}\right] \frac{\text{carbon atoms}}{\text{cm}^2\text{-sec}} \quad [37]$$

and for the porous surface

$$R_6 = K_2 \phi(1-\phi)^{1/2} P_w^{3/4} T_w^{1/4} e^{-E/2RT_w} \left[\left(\frac{\bar{M}_w}{M_O} C_{O,w}\right)^{3/4} + \left(\frac{M_O}{M_{CO_2}}\right)^{1/4} \left(\frac{\bar{M}_w}{M_{CO_2}} C_{CO_2,w}\right)^{3/4}\right] \frac{\text{carbon atoms}}{\text{cm}^2\text{-sec}} \quad [38]$$

Finally, it would be desirable to generate a slightly modified form of the reaction rate law to determine the influence of a change in the order of the reaction on the ablation rate. Let the reaction rate for the nonporous carbon be diminished by the factor n_i/n, where species i refers to the reactant particle. This arbitrary adjustment in the reaction rate leads to the following modified forms of the nonporous surface rate laws R_1 and R_5, as given in Eqs. 32 and 37

$$R_7 = K_1 P_w^{1/2} T_w e^{-E/RT_w} \left[\frac{\bar{M}_w}{M_O} C_{O,w}\right]^{3/2} \frac{\text{carbon atoms}}{\text{cm}^2\text{-sec}} \quad [39]$$

$$R_8 = K_1 P_w^{1/2} T_w e^{-E/RT_w} \left[\left(\frac{\bar{M}_w}{M_O} C_{O,w}\right)^{3/2} + \left(\frac{\bar{M}}{M_{CO_2}} C_{CO_2,w}\right)\right]^{3/2} \frac{\text{carbon atoms}}{\text{cm}^2\text{-sec}} \quad [40]$$

To review, the true rates for the (pure) nonporous carbon surface reactions are R_5 and R_8, with the rate for the (pure) porous carbon surface reaction given by R_6.

Acknowledgments

The authors are indebted to H. Emmons of Harvard University for his comments and suggestions. The authors are also grateful to D. Simon and A. Pallone of Avco/RAD for their interest and discussions.

Nomenclature

α	=	mass concentration of oxygen at the edge of the boundary layer
β	=	variable, defined by Eq. 15
ϵ	=	parameter which specifies the gas phase reaction surface sink strength, defined by Eq. 10
θ	=	parameter which specifies the gas phase reaction surface sink strength, defined by Eq. 9
μ	=	coefficient of viscosity of the gas mixture
ξ	=	nondimensional "blowing" rate, defined by Eq. 17
ρ_i	=	density of chemical species $i = n_i m_i$
ρ	=	density of the gas mixture $= \sum_i \rho_i$
ϕ	=	porosity of the surface
C_H	=	Stanton number with blowing, defined by Eq. 18
C_H^0	=	Stanton number without blowing, defined by Eq. 26
$\bar{C}_p$	=	specific heat, at constant pressure, of the gas mixture
C_i	=	mass concentration of chemical species $i = \rho_i/\rho$
D_i	=	effective binary diffusion coefficient of species i into the surrounding gas mixture
E	=	activation energy
h_i	=	enthalpy (chemical and thermal) per unit mass of species i
h	=	enthalpy per unit mass of the gas mixture $= \sum_i h_i C_i$
h_s	=	stagnation enthalpy per unit mass of the gas mixture $= h + (u^2/2)$
H	=	local heat transfer potential $= h_s - h_{s,w}$
H_t	=	total heat transfer potential $= h_{s,e} - h_{s,w}$
$\bar{H}$	=	nondimensional heat transfer potential $= H/H_t$
k	=	coefficient of thermal conductivity of the gas mixture
K_1, K_2	=	rate law coefficients (constants)
Le_i	=	Lewis number of species $i = \dfrac{\rho D_i \bar{C}_p}{k}$
M_i	=	molecular weight of species i
$\bar{M}$	=	average molecular weight of the gas mixture, defined by Eq. 33
m_i	=	mass of a species i particle
$\dot{m}_i$	=	mass flux of species i normal to a gas phase or solid surface
$\dot{m}$	=	mass flux of the gas mixture normal to a gas phase or solid surface
N	=	Avogadro's number, particles per mole
n_i	=	number of species i particles per unit volume
n	=	total number of particles per unit volume in the gas mixture $= \sum_i n_i$
Pr	=	Prandtl number of the gas mixture $= \bar{C}_p \mu/k$
P	=	static pressure
$\dot{q}_w$	=	heat flux to the wall $= \left(k \dfrac{\partial T}{\partial y}\right)_w$
$\dot{q}$	=	variable $= \dfrac{k}{\bar{C}_p} \dfrac{\partial H}{\partial y}$
R	=	universal gas constant
T	=	static temperature
v_i	=	x-component of the average diffusion velocity of species i
v_i	=	y-component of the average diffusion velocity of species i
u	=	x-component of the mass average velocity of the gas mixture
v	=	y-component of the mass average velocity of the gas mixture
x	=	coordinate parallel to the wall
y	=	coordinate normal to the wall

Subscripts

e	=	at the boundary layer edge
i	=	generalized subscript referring to the species O, N, CO and CO_2
j	=	generalized rate law subscript, which may assume the values 1 through 8
l	=	order of the surface reaction
w	=	at the wall
*	=	at the reaction surface

References

1 Glasstone, S., Laidler, K. and Eyring, H., *The Theory of Rate Processes*, McGraw-Hill Book Co., Inc., New York, N. Y., 1st ed., pp. 369-372.

2 Rosner, D. E., "Diffusion and Chemical Surface Catalysis in Flow Systems," AeroChem Research Laboratories, Inc., Technical Publication 14, September 1959.

3 Tu, C. M., Davis, H. and Hottel, H. C., "Combustion Rate of Carbon; Combustion of Spheres in Flowing Gas Streams," *Ind. Engng. Chem.*, vol. 26, July 1934, pp. 749–757.

4 Cohen, C. B., Bromberg, R. and Lipkis, R. P., "Boundary Layers with Chemical Reactions Due to Mass Addition," JET PROPULSION, vol. 28, October 1958, pp. 659–668.

5 Hartnett, J. P. and Eckert, E. R. G., "Mass Transfer Cooling with Combustion in a Laminar Boundary Layer," *Proceedings of the Heat Transfer and Fluid Mechanics Institute*, Stanford Univ. Press, June 1958, pp. 659–668.

6 Bromberg, R. and Lipkis, R. P., "Heat Transfer in Boundary Layers with Chemical Reactions Due to Mass Addition," JET PROPULSION, vol. 28, October 1958, pp. 668–674.

7 Denision, M. B. and Dooley, D. A., "Combustion in the Laminar Boundary Layer of Chemically Active Sublimating Surfaces," *J. Aero. Sci.*, vol. 25, April 1958, pp. 271–272.

8 Scala, S., "Surface Combustion in Dissociated Air," JET PROPULSION, vol. 28, May 1958, pp. 340–341.

9 Emmons, H. W., "The Burning of Carbon," Ramo-Wooldridge Corp., Internal Memo., August 1954.

10 Logan, J. G. and Treanor, C. E., "Tables of Thermodynamic Properties of Air from 3000°K to 10,000°K," Cornell Aeronaut. Lab., Inc., Rep. BE-1007-A-3, January 1957.

11 Hayes, W. D. and Probstein, R. F., *Hypersonic Flow Theory*, Academic Press, New York, 1st ed., Chap. 8.

12 Lees, L. "Convective Heat Transfer with Mass Addition and Chemical Reactions," *Combustion and Propulsion Third AGARD Colloquium*, Palermo 1958, Pergamon Press, New York, pp. 451–498.

13 Kemp, N. H. Rose, P. H. and Detra, R. W., "Laminar Heat Transfer Around Blunt Bodies in Dissociated Air," *J. Aerospace Sci.*, vol. 26, July 1959, pp. 421–430.

14 Denison, M. R., "The Turbulent Boundary Layer on Chemically Active Ablating Surfaces," *J. Aerospace Sci.*, vol. 28, June 1961, pp. 471–479.

15 Eschenroeder, A. Q., "Combustion in the Boundary Layer on a Porous Surface," *J. Aerospace Sci.*, vol. 27, December 1960, pp. 901–906.

16 Feldman, S., "Hypersonic Gas Dynamic Charts for Equilibrium Air," Avco Research Lab. Research Rep. 40, January 1957.

17 Bauer, E. and Zlotnick, M., "Transport Coefficients of Air to 8000° K," ARS JOURNAL, vol. 29, October 1959, pp. 721–728.

18 Fay, J. A. and Riddell, F. R., "Theory of Stagnation Point Heat Transfer in Dissociated Air," *J. Aero. Sci.*, vol. 28, February 1958, pp. 73–85.

19 Van Driest, E. R., "Investigation of Laminary Boundary Layer in Compressible Fluids Using the Crocco Method," NACA TM 2597, January 1952.

20 Blyholder, G. and Eyring, H., "Kinetics of Graphite Oxidation II," *J. Phys. Chem.*, vol. 63, June 1959, pp. 1004–1008.

21 Blyholder, G. and Eyring, H., "Kinetics of Graphite Oxidation," *J. Phys. Chem.*, vol. 61, May 1957, pp. 682–688.

22 Wicke, E., "Contributions to the Combustion Mechanism of Carbon," 1955, *Fifth Symposium (International) on Combustion*, Reinhold, Publishing Corp., New York, 1955, pp. 245–252.

23 Walker, P. L., Rusinko, F. and Austin, L. G., "Gas Reactions of Carbon," *Advances in Catalysis*, Vol. 11, Academic Press, New York, pp. 133–221.

24 Zinman, W. G., "A Study of the Interaction Between Carbon and Dissociated Gases," General Electric Co., Missile and Space Vehicle Dept., Rep. R59SD457, November 1959.

Effect of Fuel Composition on High Frequency Oscillations in Rocket Motors Burning Premixed Hydrocarbon Gases and Air

J. R. OSBORN[1]
J. M. BONNELL[2]

Purdue University
Lafayette, Ind.

The experiments reported herein were concerned with the determination of some of the factors which contribute to the occurrence of transverse and longitudinal modes of combustion oscillation in rocket motors burning gases. Three rocket motors having different combustion chamber geometries were employed, using gaseous hydrocarbon fuels premixed with air as propellants; the fuels were methane, ethane, superheated propane, ethylene and hydrogen. The findings indicated that the incidence and amplitude of the combustion pressure oscillations were profoundly influenced by the coupled effects of the chemical composition of the fuels and the aspect ratio of the cylindrical combustion chamber. The results also indicated that the following measures of the behavior of combustion oscillations were functions of the chemical differences of the fuels: 1) the relative ability of the different gaseous propellant combinations to support combustion oscillations; 2) the shape and origin of the instability region of the transverse modes, and the amplitudes of the oscillations within that region; 3) the combustion chamber length below which longitudinal oscillations will not occur (the lower critical length); 4) the tendency for interactions between transverse and longitudinal modes to occur; and 5) the mode of oscillation.

Received July 24, 1961.
[1] Professor of Mechanical Engineering. Member ARS.
[2] Research Assistant. Member ARS.

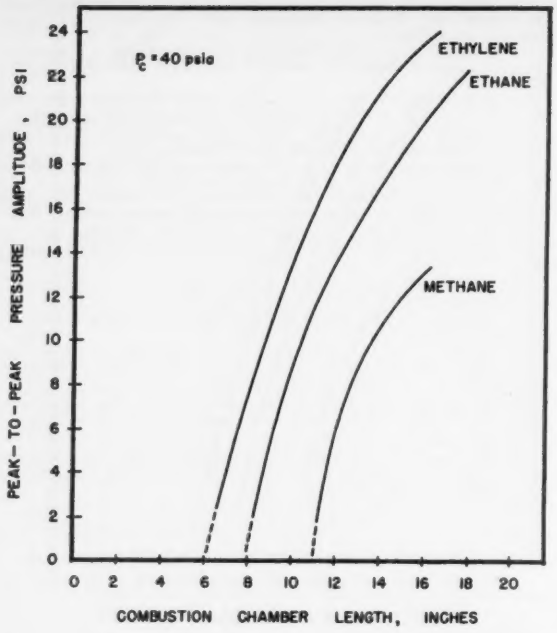

Fig. 1 Amplitude of oscillations of the longitudinal mode vs. chamber length

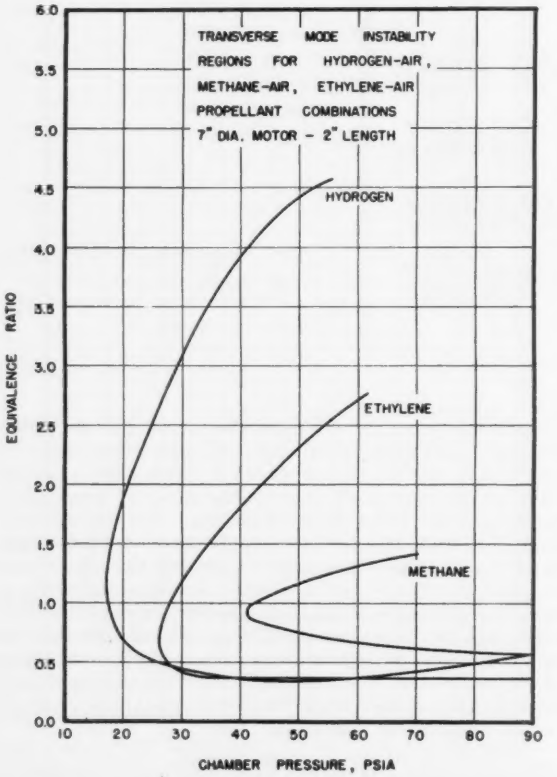

Fig. 2 Transverse mode instability regions of several propellant combinations

A SERIES of experiments was recently conducted to determine the influence of the chemical composition of different gaseous hydrocarbon fuels (burned with air) upon high frequency combustion oscillations in a rocket motor. In all cases the fuel and air were premixed before being injected into the combustion chamber, thereby eliminating the effects of such variables as atomization, vaporization, sublimation, mixing, etc., which enter into the combustion of liquid and solid propellants.

Because the rocket motors employed in the experiments had combustion chambers of different diameters and lengths for determining the effects of combustion chamber geometry, the effects due to the chemical differences of the fuels cannot be completely segregated from those due to the aforementioned differences in geometry. In this paper, however, the major emphasis will be placed upon the effect of the fuel composition. The influence of differences in combustion chamber geometry is presented in (1).[3]

Experimental Apparatus

The rocket motor utilized in studies of the longitudinal mode of combustion oscillation had a combustion chamber diameter of $3\frac{3}{8}$ in. The two motors utilized in the transverse mode investigations had combustion chambers of 7- and 14-in. ID. In all cases the lengths of the combustion chamber were altered by adding spacers.

The pressure oscillations were sensed by Photocon pressure transducers mounted in the wall of the combustion chamber. A complete description of the instrumentation, rocket motors, and all other test apparatus is found in (2–5).

Air was used as the oxidizer with the following gaseous fuels: methane, ethane, superheated propane, ethylene, and hydrogen. All of the fuels were technical grade of 95% purity except hydrogen, which was 99.5% pure.

Experimental Results

Longitudinal Mode Results

References (4, 5) present the results of the studies of the longitudinal mode of combustion pressure oscillation for the following propellant combinations: superheated propane and air, ethane and air, methane and air, and ethylene and air. The fuels were selected for their different degrees of saturation and relative chemical reactivities. Several indices of reactivity as used in this paper are: 1) laminar flame velocity, 2) chemical reaction rate, or heat release rate, and 3) activation energy. Similar definitions of reactivity are presented in (6). Thus, in considering two different fuel-air combinations, the more reactive combination would have a higher laminar flame velocity, a higher heat release rate, and a lower activation energy.

These experiments determined the *lower critical lengths*[4] for the longitudinal mode for the aforementioned propellant combinations. Fig. 1 presents the maximum amplitude[5] of longitudinal pressure oscillations as a function of the chamber length for ethylene-air, ethane-air and methane-air propellants, for a steady state combustion pressure of 40 psia. The combustion chamber lengths at which the amplitudes of the oscillations approach zero are the lower critical lengths.

Transverse Mode Results

The experiments concerned with the transverse modes of oscillation were conducted with methane, ethylene and hy-

[3] Numbers in parentheses indicate References at end of paper.

[4] The lower critical length is the combustion chamber length below which longitudinal oscillations will not occur.

[5] The maximum amplitude refers to the maximum amplitude at a given chamber pressure without restriction on equivalence ratio.

drogen as the fuels. In general, the relative effects of the differences in the chemistry of the propellants noted in the experiments with the 7-in. diam motors were the same as those observed for the 14-in. diam motors. Consequently, the discussion will be restricted to results obtained with the 7-in. diam motors.

Fig. 2 presents the instability boundary curves[6] for hydrogen, ethylene, and methane. The boundary curves are plots of equivalence ratio as a function of chamber pressure and were obtained with the 7-in. diam motor, 2-in. length. The instability regions for methane and ethylene fuels are discussed in greater detail in (1–3).

Fig. 3 presents the peak to peak pressure amplitude as a function of the combustion chamber length and illustrates the effect of chamber length upon the maximum amplitudes of the pressure oscillations. The experiments were conducted at a steady state combustion pressure of 160 psia burning methane-air and ethylene-air as the propellants. It is seen that in the case of ethylene-air there is a shift in trend of the oscillation amplitude at the 6-in. length; for the methane-air propellants no comparable shift was found. The same type of amplitude shift for ethylene-air was also observed with the 14-in. diam motor. Experiments conducted with steady combustion chamber pressures other than 160 psia gave the same trends for the oscillation amplitudes but, of course, different magnitudes for the maximum amplitudes.

Fig. 4 presents the maximum amplitude of the pressure oscillations as a function of steady combustion chamber pressure for the hydrogen-air, ethylene-air and methane-air propellant combinations.

In (1–3) the instability regions for different chamber lengths of the 7-in. and the 14-in. diam motors were presented for the methane-air and ethylene-air propellants. It was observed that, for methane-air, increasing the chamber length caused the toes of the instability regions for the transverse modes to be displaced to higher chamber pressures in all cases. For ethylene-air, however, in both the 7-in. and 14-in. diam motors, the toes of the instability regions moved to higher chamber pressures until a length/diameter ratio of approximately 1.0 was reached. At that length the toe of the instability region occurred at a lower chamber pressure, and then the toes of the regions again progressed toward higher chamber pressures as chamber length increased.

Another interesting result of the effect of chemical composition is that certain types of transverse modes were characteristic for a given propellant combination within the range of chamber pressures investigated. For the methane-air propellant combination, the mode of oscillation was almost exclusively the first tangential.[7] For ethylene-air propellants the modes were chiefly the first tangential, the first tangential with a superimposed radial, and an occasional trace of a second tangential. For hydrogen-air propellants, the first and second tangential modes were common, with traces of a superimposed radial mode.

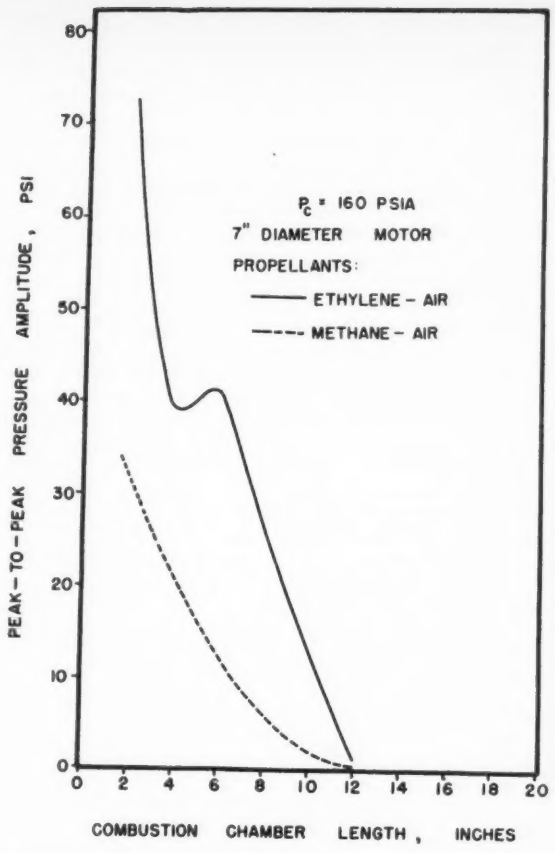

Fig. 3 Amplitude of oscillations of transverse mode vs. chamber length

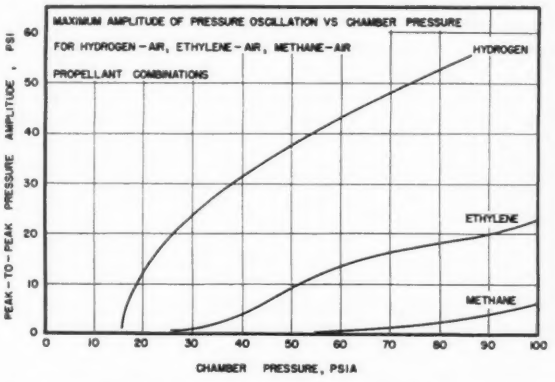

Fig. 4 Amplitude of oscillations of transverse mode vs. chamber pressure

Discussion of Results

A discussion of the effects due to chemical differences in the fuels is facilitated by considering a mechanism presented in (4, 5) which was postulated to explain the initiation and propagation of a longitudinal mode; it is believed that the mechanism also explains the initiation and propagation of the transverse modes. In substance, the mechanism states that in a combustion chamber a pressure wave is initiated by some pressure disturbance, and the subsequent passage of the pressure wave through the burning and unburned propellants adiabatically compresses these hot gases. The increased temperature and pressure of the gases causes an accelerated chemical reaction rate (or heat release rate) behind the pressure front, which drives and sustains the pressure wave. As has been stated, this mechanism was employed (4) for explaining the existence of the lower critical length as shown in Fig. 1 and for postulating the probable existence of the upper critical length (5). The experiments of (7, 8) with liquid propellants demonstrate the existence of a lower and an upper critical length.

[6] The boundary curve for an instability region denotes unstable combustion to the right of the boundary and either stable combustion or no combustion to the left of the boundary curve.

[7] The classification of "tangential" type modes used herein includes both "standing" and "traveling" waves.

Consideration of the reactivities (defined previously in this paper) for the different propellants can explain the relative position of the curves of Fig. 1 as well as the relative values for the lower critical lengths. In a rocket motor having a short tubular combustion chamber, the time for a pressure disturbance to travel twice the length of the combustion chamber is short. Consequently, only a small amount of combustible mixture is injected into the combustion chamber during the time required for two successive reflections of a pressure wave from the face of the injector. Therefore, the shorter the length, the smaller the quantities of the unburned and burning propellants traversed by a pressure disturbance, and the smaller the excess energy release for driving the disturbance. As a result, the peak to peak amplitude of the combustion pressure oscillations also becomes smaller. If the chamber is short enough, the amplitude of the oscillations may become insignificant. Since the more reactive fuels (those with a lower activation energy) require less preparation time than the relatively unreactive fuels, more energy may be added per oscillation, thereby permitting the lower critical length of the chamber to be shorter. Moreover, for a given length, the more reactive fuels will produce higher amplitude oscillations for the above reasons.

The heat release rate can be employed for explaining the fact that the instability region for a more reactive fuel (higher heat release rate) is larger than that for a less reactive fuel. An expression for the heat release rate as a function of laminar flame velocity and propellant density as derived by Spalding (9) is

$$q''' = \frac{C_p(\rho_u S_u)^2 \, m_{fu} H}{2k} \qquad [1]$$

where C_p is the specific heat at constant pressure, H is the heat of combustion, k is the thermal conductivity, m_{fu} is the mass concentration of fuel in unburned propellants, S_u is the laminar flame velocity, q''' is the average heat release rate in the reaction zone, and ρ_u is the density of unburned reactants.

Fig. 5 is a qualitative presentation of the heat release rates vs. the equivalence ratio for different hydrocarbon-air combinations at a constant combustion pressure. Eq. 1 is the basis of these curves, since the laminar flame velocity is a function of equivalence ratio.

If a datum line (shown as a horizontal broken line in Fig. 5 for the sake of simplicity) may be assumed such that the rate of energy release at the line is that required to maintain steady combustion, then the heat release rates above the line are excessive and may produce combustion pressure oscillations. Thus, the intersections of the datum line and the heat release rate curves denote the points where pressure oscillations would become negligible and thereby define the equivalence ratio limits of an instability region. For example, from Fig. 2, for methane-air, the instability limits on equivalence ratio are 0.6 and 1.35 for a mean chamber pressure of 65 psia.

Since the curves of Fig. 5 are drawn for a specific value of mean chamber pressure, different curves will need to be drawn for each value of mean chamber pressure. It is believed that the datum line, however, should remain at approximately the same value of heat release rate because it is related to the balance between the driving forces and the dissipative forces. Therefore, at some mean chamber pressure lower than that for the curves of Fig. 5, the heat release rate curves will be shifted downward, and the datum line will then be tangent to the peak of the heat release rate curve for one of the propellant combinations. The point of tangency defines the toe of the instability region for that particular propellant combination. For example, from Fig. 2, for methane-air, the toe is at an equivalence ratio of 0.9 and a mean chamber pressure of 41 psia, which is lower than the 65 psia of above.

It is evident from Fig. 5 that for the given datum line (that is, for given driving and dissipative forces) the bounds of the instability regions of the fuels of higher heat release rate should cover a wider range of equivalence ratio. That is, it would be expected that the propellant combination of hydrogen and air would have a larger instability region than methane and air. This is demonstrated experimentally by the data of Fig. 2, where hydrogen-air, having the greatest reactivity, has the largest instability region. Methane-air is the least reactive and has the smallest region.

In (1-3) the shift of instability for ethylene-air propellants was explained as being due to an interaction between longitudinal and transverse modes at a length/diameter ratio of approximately 1.0. It appears reasonable that the same type of interaction caused the amplitude shift for the ethylene-air combination as observed in Fig. 3. The methane-air propellants did not exhibit such shifts (Fig. 3) thus demonstrating another influence of the effect of the differences in reactivity of the propellant combinations.

Using the proposed combustion oscillation mechanism, the amplitudes of the pressure oscillations are dependent upon the amount of the excess heat release rate. Since the heat release rates are larger for the more reactive fuels, the amplitudes of oscillation should be proportional to the fuel reactivity, as is indicated in Fig. 4. It is also apparent from Fig. 4 that the amplitudes of the oscillations for all propellants increase with chamber pressure. This may be attributed to the increase in heat release rate due to the increase in propellant density at the increased chamber pressures.

It is interesting to note that as the steady chamber pressure increases, the ratio of the maximum amplitudes of oscillation for any two of the propellant combinations converges to a nearly constant value, which closely approximates the ratio of laminar flame velocities of the propellants, the latter being determined at a stoichiometric fuel/air ratio. In other

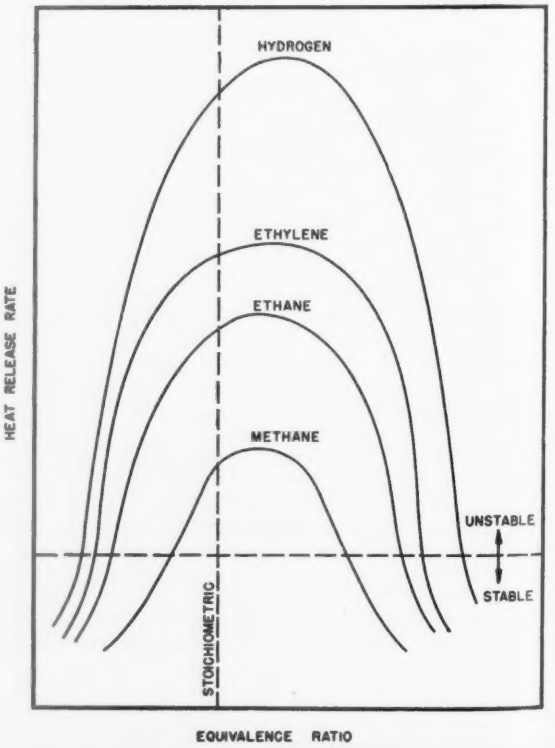

Fig. 5 Heat release rate vs. equivalence ratio for four propellant combinations

words, at a chamber pressure where the amplitude ratio has met the above condition of convergence

$$\frac{P_a}{P_b} = K\frac{S_{ua}}{S_{ub}} \qquad [2]$$

where P is the amplitude of the pressure oscillation, S_u is the laminar flame velocity, and K is the proportionality constant. Subscripts a and b refer to propellant combinations A and B, respectively, where combination A has a higher laminar flame velocity than B. For the range of chamber pressures and the propellant combinations investigated, the value of K was very nearly 1.0.

It is also interesting to note that the results indicate that the number of different transverse modes which a propellant combination is capable of sustaining appears to be a function of the reactivity of the fuel as well as a function of the combustion chamber geometry. In the chamber pressure range investigated, the saturated hydrocarbon (methane) sustained only the fundamental transverse modes, while the unsaturated hydrocarbon (ethylene) and also hydrogen were capable of sustaining combinations of modes and modes higher than first order.

Conclusions

Consideration of the relative reactivities and heat release rates of the fuels used in these experiments explain the following combustion oscillation phenomena for premixed gaseous propellant systems: 1) saturated hydrocarbons exhibit less tendency to cause oscillations than the unsaturated hydrocarbons and hydrogen; 2) the magnitude of the lower critical length for the longitudinal mode of oscillation is smaller for the more reactive fuels; 3) when the lower critical length of the longitudinal mode is exceeded, it is highly probable that for the more reactive fuels there will be an interaction between the longitudinal and transverse modes which will cause a shift in the location of the instability region and an increase in the amplitudes of oscillation; 4) the characteristics of the instability region are influenced by differences in the chemistry of the fuels; and 5) whereas relatively unreactive saturated hydrocarbon fuels may support a single fundamental transverse mode, more reactive fuels are capable of sustaining more than one fundamental mode simultaneously as well as second order modes.

Acknowledgments

The authors wish to thank M. J. Zucrow, Atkins Professor of Engineering, Purdue University, for his helpful guidance and counsel throughout the course of the investigation.

Acknowledgment is also given to the Office of Naval Research, Contract N7 onr 39418, and the Air Force Office of Scientific Research, Contract AF 49(638)-756 under whose sponsorship the research reported herein was conducted. Reproduction in full or in part is permitted for any use of the U. S. Government.

References

1 Osborn, J. R. and Bonnell, J. M., "Importance of Combustion Chamber Geometry in High Frequency Oscillations in Rocket Motors," ARS JOURNAL, vol. 31, no. 4, April 1961, p. 482.

2 Bonnell, J. M., "An Experimental Investigation of Transverse Mode Combustion Oscillations in Premixed Gaseous Bipropellant Rocket Motors," M.S. Thesis, Purdue University, January 1960.

3 Osborn, J. R. and Bonnell, J. M., "An Experimental Investigation of Transverse Mode Combustion Oscillations in Premixed Gaseous Bipropellant Rocket Motors," Purdue University Rep. I-60-1, January 1960.

4 Zucrow, M. J. and Osborn, J. R., "An Experimental Study of High Frequency Combustion Pressure Oscillations," JET PROPULSION, vol. 28, no. 10, October 1958, p. 654.

5 Osborn, J. R. and Schiewe, R. M., "An Experimental Investigation of High Frequency Combustion Pressure Oscillations in a Gaseous Bipropellant Rocket Motor," Purdue University Rep. I-58-1, June 1958.

6 Lewis, B. and von Elbe, G., *Combustion, Flames and Explosions of Gases*, Academic Press, N. Y., 1951, p. 180.

7 Crocco, L., Grey, J. and Harrje, D. T., "On the Importance of the Sensitive Time Lag in Longitudinal High-Frequency Rocket Combustion Instability," JET PROPULSION, vol. 28, no. 12, December 1958, p. 841.

8 Crocco, L., Grey, J. and Harrje, D. T., "Theory of Liquid Propellant Rocket Combustion Instability and Its Experimental Verification," ARS JOURNAL, vol. 30, no. 2, February 1960, p. 159.

9 Spalding, D. B., *Some Fundamentals of Combustion*, Butterworths' Scientific Publications, London, 1955, p. 194.

Combustor Similitude Study

E. C. WOODWARD[1]

University of South Carolina
Columbia, S. C.

A geometrically similar family of three idealized combustors is investigated over a wide range of Reynolds numbers at different inlet temperatures and fuel-air ratios. The data are used to determine the validity of an approximate similitude law based upon the concept of an effective overall reaction order. The results of this investigation indicate that under conditions of geometric similarity of combustors, constant inlet temperature of fuel and air, specified gaseous fuel, specified gaseous oxidant, low velocity flow, absence of body forces, and negligible heat losses to the walls, a reasonable degree of similarity will exist if one maintains constant the ratio of chemical reaction time to mixture residence time, the fuel-air ratio, and the Reynolds number for a model and a prototype. Results taken at conditions where high heat losses prevail would not be expected to yield a correlation which would prove satisfactory. The concept of the effective overall reaction order is shown to be useful in describing the complex reactions occurring in hydrocarbon-air systems.

Received June 22, 1961.

[1] Professor and Head, Department of Mechanical Engineering. Member ARS.

THE COMPLEXITY of practical combustion systems prompts the question, "Is there a law of similarity for combustion processes with fluid flow?" or, phrased differently, "Is there a set of dimensionless operating parameters for a family of geometrically similar combustors such that the dimensionless performance parameters, e.g., efficiency, will depend invariably on such operating variable parameters?" It is understood that the number of dimensionless operating parameters must be less than the number of independent physical variables. If this goal cannot be realized 100%, it is of interest to find to what extent it may be approximately achieved for engineering purposes.

Some progress in the field of scaling and similitude in systems involving chemical reactions has been made in recent years (1–5).[2] More recent treatments, in the form of general review studies, clearly define the currently accepted laws of similitude, as well as emphasize the great need for more immediate experimental investigation in the scaling of both liquid and gaseous fired systems (6–9).

This study is experimental in nature and may be considered a continuation of a study reported earlier by the author (10). Data obtained from a geometrically similar family of gaseous fired (propane-air), idealized combustors operating at various inlet conditions are presented. The data are used to test the validity of an approximate similitude law based upon the concept of an effective overall (global) reaction order.

Although the data are obtained from combustors of a very idealized nature, the results should be applicable in land, aviation, and marine gas turbine combustor development. They may also shed some light on the problem of rocket-chamber similarity. While restricted to gaseous systems, the results should prove of interest in any analysis of liquid fired systems.

The direction of attention to the important dimensionless operating parameters, which is one of the objectives of this study, does not hinge upon a particular type of design of the experimental combustion system; it is only necessary that the system involve all the processes which one may wish to encompass, such as flow and mixing processes, gaseous diffusion, chemical reaction, and heat transfer from one part of the fluid to another.

Similitude Law Based on Theory

The results of theoretical approaches to a similitude law (8,9) may be summarized as follows: 1) Perfect similitude of gaseous fired combustion systems is impossible. 2) Under conditions of geometric similarity, constant inlet temperature (fuel and oxidant), specified gaseous fuel, specified gaseous oxidant, low velocity (Mach number) flows, absence of body forces, and negligible heat losses to the walls, one expects a reasonable degree of similarity by maintaining constant the ratio of the chemical reaction time to the mixture residence time, the fuel-air ratio, and the Reynolds number for a model and a prototype. A reasonable degree of success may be expected from this approximate similitude law provided the various reactions occurring in the multicomponent mixture depend upon pressure, and upon each other, in such a manner that they may be lumped together to yield an effective overall reaction rate.

As shown elsewhere (10), the ratio of the chemical reaction time to the mixture residence time is proportional to a term β where

$$\beta = W/P^n D^3 \qquad [1]$$

Here, W is the total mass flow rate into the combustor, P is the combustor inlet pressure, D is a characteristic dimension of the combustor, and n is the effective overall reaction order.

Note that β is not a dimensionless variable; its value will depend upon the system of units employed.

One would expect a dependent dimensionless system variable, say the combustion efficiency η, to be a function of the above described terms when conditions set down in item 2 are fulfilled. Hence

$$\eta = \varphi(\mathrm{Re}, W_f/W_a, \beta) \qquad [2]$$

where Re is the Reynolds number, W_f is the fuel mass flow rate to the combustor, and W_a is the air mass flow rate to the combustor.

This investigation is not concerned with the determination of an explicit functional relation between the combustion efficiency and the terms shown in Eq. 2, either empirically or otherwise. The primary objective is to show that, through the introduction of the terms Re and β, two geometrically similar combustors 1 and 2 operating under specified conditions, as in item 2 above, at a constant value of W_f/W_a should exhibit a reasonable degree of similitude of flow and combustion processes if

$$\mathrm{Re}_1 = \mathrm{Re}_2 \qquad \beta_1 = \beta_2 \qquad [3]$$

A secondary objective is to determine the most appropriate n value for gaseous fired, nonpremixed combustors of the general type used in this study. This n value will most certainly depend on fuel type and may also be expected to depend somewhat on fuel-air ratio and inlet temperature.

Description of Experimental Apparatus

The details of the combustor geometry used in this investigation may be found in Fig. 1. The choice of a spherical dome was not made to achieve any resemblance to spherical "homogeneous reactors" used by some investigators, but was selected on the basis of what was considered good design for the purposes for which the combustor was intended. A geometrically similar family of three combustors having actual diameters D of 3.90, 5.89, and 8.83 in. was constructed. All dimensions were a function of D as shown in the table of dimensions in Fig. 1. Henceforth, each combustor will be

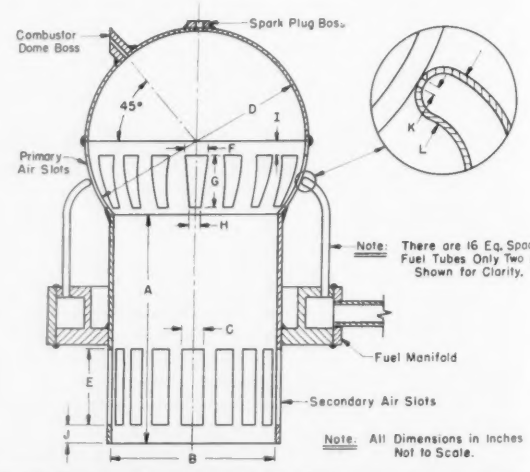

Nominal D	4	6	9	Nominal D	4	6	9
A	4.890	7.375	11.060	G	0.911	1.375	2.062
B	2.930	4.422	6.633	H	0.207	0.3125	0.469
C	0.223	0.337	0.505	I	0.248	0.375	0.562
D	3.900	5.890	8.830	J	0.331	0.500	0.750
E	1.325	2.000	3.000	K	0.0465	0.070	0.1065
F	0.414	0.625	0.937	L	0.092	0.139	0.2085

Fig. 1 Spherical dome combustor details

[2] Numbers in parentheses indicate References at end of paper.

referred to by the nominal diameter, i.e., the 3.90-in. diam combustor will be referred to as the 4-in. combustor. Careful construction preserved geometric similarity of the combustors.

Details of the test passage in which the combustors were placed may be found elsewhere (10,11). However, a few comments may be appropriate. A completely independent control of primary and secondary air was possible. The primary fuel-air ratio could be varied independently of the overall fuel-air ratio. The fuel jets injected directly into the combustor, preventing flashback and assuring a certain degree of diffusion type burning. A radial flow of primary air and fuel occurred, assuring a very high degree of mixing in the primary zone and encouraging recirculation of the combustion products. A relatively large primary combustion volume was available, which helped assure realistic values of combustion efficiency. The cool secondary air was injected in such a manner as to promote rapid mixing with the hot combustion products. For the measurement of combustion product temperature, use was made of six aspirating thermocouples located at the center of six equal annular areas. The temperature measuring section was insulated to prevent appreciable heat losses. Observation ports were provided for viewing the flame extending from the combustor. All dimensions of the test passage were scaled as a function of the combustor diameter D. An electric heater in the primary air supply maintained a constant inlet temperature.

Description of Test Procedure

For a particular combustor, a Reynolds number and primary and overall fuel-air ratios were chosen. The primary air was preheated to a constant inlet temperature T_{ip}. The mass flow rates of primary air W_{ap} and secondary air W_{as} were adjusted to satisfy the fuel-air ratios. The combustor dome pressure P_d was adjusted to the desired value. Ignition was supplied. Fuel mass flow rate W_f was adjusted to satisfy fuel-air ratios. After the ignition system was turned off, 15 to 30 min were allowed for thermal equilibrium to be established. All readings were recorded and the steps repeated for a new system pressure.

If investigating in the direction of decreasing pressures, tests continued to "blowout." If investigating in the direction of increasing pressures, tests continued until a desired pressure range had been explored.

Description of Test Data

The primary objective of this study was to provide extensive data from each of the three combustors operating under conditions of: gaseous injection of a given fuel, constant primary fuel-air ratio, constant ratio of secondary to primary air, constant inlet temperature, and low velocity flows.

The fuel used throughout the investigation was commercial propane having a guaranteed composition of a minimum of 95% propane, the remaining gases being ethane and butane. Injection of propane in the gaseous state was assured by operating at low injection pressures and high fuel temperatures and through visual observation. The fuel temperature was 560°R ± 4%.

Data were taken for each combustor at Reynolds numbers[3] of 20×10^3, 30×10^3, 50×10^3, 70×10^3, 100×10^3, and 130×10^3 while operating under the following conditions: $W_f/W_{ap} = 0.040$, $W_{as}/W_{ap} = 2.0$, and $T_{ip} = 680$°R. Data taken at Re = 20,000 are shown in Fig. 2 as combustion efficiency vs. combustor pressure.

A secondary objective was to provide some data which would show effects of changes in W_f/W_{ap}, T_{ip} and W_{as}/W_{ap}.

[3] The Reynolds number used throughout this investigation is based on inlet conditions to the primary zone and on the actual inside diameter of the spherical dome portion of the combustor.

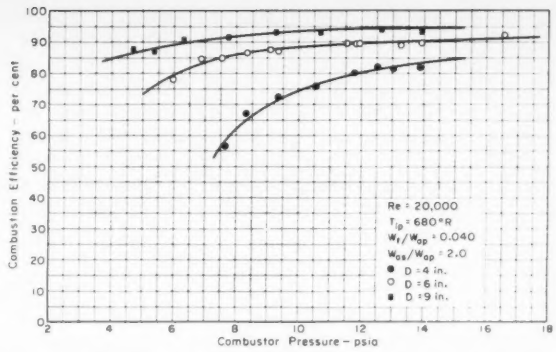

Fig. 2 Variation of combustion efficiency with combustor pressure

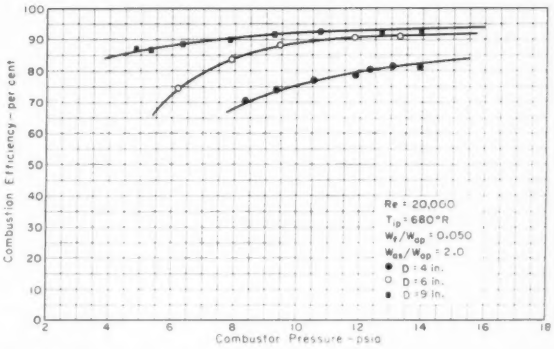

Fig. 3. Variation of combustion efficiency with combustor pressure

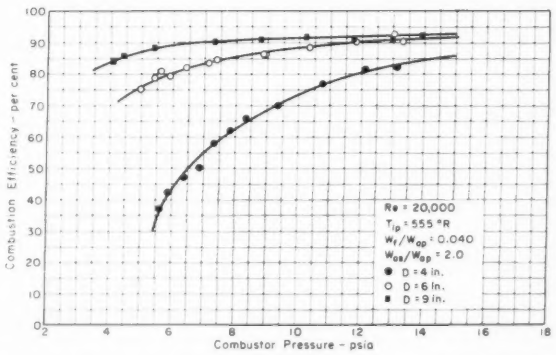

Fig. 4 Variation of combustion efficiency with combustor pressure

The tests described below were therefore made.

Data were taken for each combustor at Reynolds number of 20×10^3, 30×10^3, 50×10^3 and 70×10^3 while operating under conditions of: $W_f/W_{ap} = 0.050$, $W_{as}W_{ap} = 2.0$ and $T_{ip} = 680$°R. Data taken at Re = 20,000 are shown in Fig. 3 as combustion efficiency vs. combustor pressure.

Two series of tests were performed for each combustor at only one Reynolds number (20,000) to obtain the effect of changes in inlet temperature and in the ratio of secondary to primary air with a fixed primary fuel-air ratio. Fig. 4 shows the variation of combustion efficiency with combustor pressure for conditions of: $T_{ip} = 555$°R, $W_f/W_{ap} = 0.040$

and $W_{as}/W_{ap} = 2.0$. Fig. 5 shows the variation of combustion efficiency with combustor pressure for conditions of: $T_{ip} = 680°R$, $W_f/W_{ap} = 0.050$ and $W_{as}/W_{ap} = 2.75$.

Each point shown in Figs. 2 through 5 represents an experimentally determined point. Experimental data obtained at Reynolds numbers greater than 20,000 are not presented here as combustion efficiency vs. combustor pressure. Complete data of the investigation for all Reynolds numbers are available elsewhere (11). However, experimental data at all values of Re investigated are used to determine the results shown in Figs. 7 and 9.

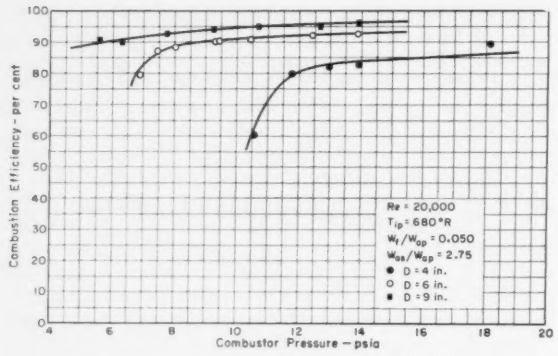

Fig. 5 Variation of combustion efficiency with combustor pressure

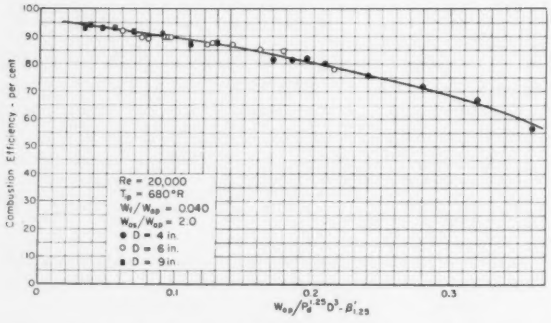

Fig. 6 Combustion efficiency dependence on β'_n

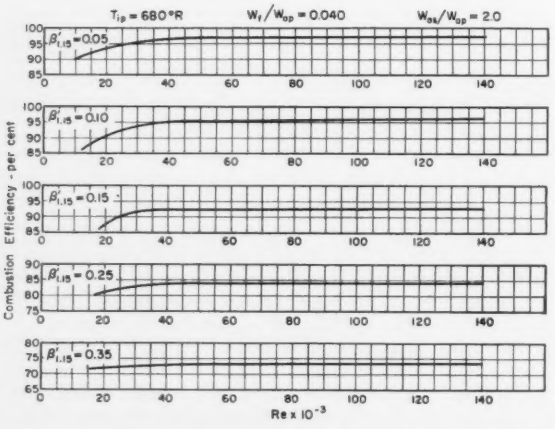

Fig. 7 Combustion efficiency dependence on Re for some arbitrary values of a constant β'_n

Operating conditions were maintained to within 2% of the nominal values shown with the following exception: three tests employing the 9-in. combustor at the higher values of Re had inlet temperature variations of 7% or less from the figure 680° R.

The largest value of Reynolds number obtained at $W_f/W_{ap} = 0.040$ for the 9-in. combustor was set by the maximum delivery of the compressors supplying the air. The largest value of Reynolds number that could be obtained for any size combustor at $W_f/W_{ap} = 0.050$ was limited by the combustion product temperatures. An upper limit of 1800°R was set to prevent excessive damage to the test passage. Neither of the restrictions imposed severe limitations on the desired range of experimental investigation, as shown. The Mach number in all tests was less than 0.30.

The combustion efficiency was computed from

$$\eta = C_h \frac{W_{ap}(h_{ep} - h_{ip}) + W_{as}(h_{ep} - h_{is}) + W_f h_{ep}}{W_f H_l} \quad [4]$$

Here, h_{ep}, h_{ip} and h_{is} represent enthalpies of air at average combustion product, primary air inlet, and secondary air inlet temperatures, respectively. The quantity C_h represents an enthalpy correction factor to correct partially for the fact that the products are not all air. At a value of $W_a/W_f = 75$, $C_h = 1.027$, for example. The lower heating value is represented by H_l.

During each run of every test a visual check was made through the observation ports to determine that the flame was burning in the combustor and that no luminous portion of the flame extended beyond the plane of the thermocouples (considered the downstream boundary of the secondary zone).

The mixing section effected a very uniform combustion product temperature profile. The variation across the stream was, in general, less than 10% of the average product temperature.

The extreme low pressure point in all series of tests was determined either by the blowout point or a flame instability. At the latter condition the flame would fail to anchor in the combustor and would anchor in the mixing zone. Data at these conditions are not shown.

The results could be reproduced to within ±1%. Check points were taken on days other than the day the regular test was performed. Check points are shown in Figs. 2–5 and appear as overlapping or closely adjacent (pressure-wise) to another point.

Discussion of Experimental Results

Eq. 2 predicts that the experimental data from a geometrically similar family of gaseous fired combustors operating under conditions of constant inlet temperature, primary fuel-air ratio, ratio of secondary to primary air, and Reynolds number, should correlate with the combustion efficiency as a function of the parameter β. In effect, this requires the data of Fig. 2 to fall along a common curve. In view of the approximate nature of the similitude law presented, one should not expect a perfect correlation.

A method of data correlation has been devised to treat the data of the problem under discussion (11). The method does not require the specification of the form of the curve which one attempts to fit to the data. It requires only the very reasonable assumption that data from several similar systems will obey some general unspecified functional relation between a dependent system variable and an independent system variable.

The data of Fig. 2, correlated by the above method, appear as Fig. 6; β_n' is $W_{ap}/P_d{}^n D^3$ in. (pph)/(psia)^n(in.)^3. The reader is cautioned against arbitrarily comparing values of

β_n' from systems having different primary and/or overall fuel-air ratios. One should compare values of β in such cases. The relation between β and β_n' is

$$\beta = \left\{1 + \frac{W_{as}}{W_{ap}} + \frac{W_f}{W_{ap}}\right\} \beta_n' \qquad [5]$$

The n value for Re = 20,000 is 1.25. The curve shown has been faired in.

The data at higher Reynolds numbers were correlated either as in Fig. 6 or by trial and error methods, depending upon the slope. The n values ranged from 1.10 to 1.25 under conditions: $W_f/W_{ap} = 0.040$, $W_{as}/W_{ap} = 2.0$ and $T_{ip} = 680°R$. In general, the trend of the data of this investigation shows a small decrease in n with increases in Re. This is consistent with the results of Tobey and Raymond (12).

The results of Fig. 6 may be considered as verification of the approximate similitude law described earlier and represented in Eq. 2. Clearly, a very reasonable degree of success has been obtained for the stated conditions.

To find the effect of changes in Reynolds number on combustion efficiency for constant values of the parameter β_n', the data of Fig. 2 as well as the data obtained at the higher values of Re may be cross-plotted using an average value of n.[4] For an average n of 1.15, some curves of efficiency vs. Re are shown in Fig. 7 for several arbitrary values of $\beta_{1.15}'$. Reference to these curves shows the particular combustor geometry investigated to be relatively insensitive to changes in Re over most of the range of investigation for a given value of β_n'. (No significance should be attached to the slight extension of these faired in curves beyond the actual limits of the investigation.) When the parameter β_n' is maintained constant, one cannot arbitrarily increase Re by changes in P_d or velocity separately. An increase in velocity decreases the residence time for a given combustor. If velocity is increased, an increase must be made in P_d to effect an increase in the reaction rate and a corresponding reduction in reaction time. Hence, as one goes in the direction of increasing Re for a given D on Fig. 7, both residence time and reaction time are changing to maintain the ratio constant.

The combustion efficiency is seen to depend very slightly on Reynolds number over most of the range of investigation and to depend rather markedly on the ratio of reaction time to residence time.

The data representing the effects of changes in primary fuel-air ratio (Fig. 3) were correlated as described above and are shown in Fig. 8 for Re = 20,000. The range of n values for the data at higher Reynolds numbers was from 1.10 to 1.40, the n value, in general, decreasing with increasing Re.

It is of interest to compare the results shown in Fig. 8 with those of Fig. 6. It should be noted, however, that results shown in these figures are not from similar systems, since the primary and overall fuel-air ratios are not maintained constant. Reference to Figs. 2 and 3 shows that at a given value of P_d approximately the same values of efficiency are found for the conditions $W_f/W_{ap} = 0.04$ and 0.05. One expects the flame temperature in the system of richer primary fuel-air ratio to be greater than that in the leaner case (both fuel-air ratios being less than the stoichiometric value) for a constant inlet temperature. Such is actually the case, the difference in average combustion product temperatures ranging from 200° to 350°F over the range of investigation. Since we are considering a constant pressure P_d and a constant Re, the higher average combustion product temperature in the richer system results in a lower density in the combustor. This causes the velocity of the richer system to be greater than in the lean case, since the mass flows in

[4] The value of n yielding the best correlation for a given Re varied, as noted, with Re. Although a change in n from, say, 1.15 to 1.20 would not affect any appreciable change in the "appearance" of a given set of data, the exact n determined is always shown. When cross-plotting, it is necessary to arrive at an average value of n.

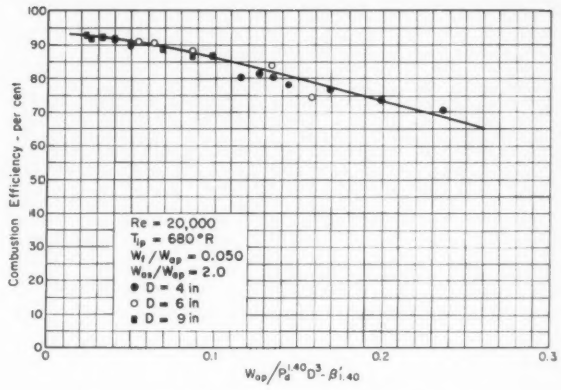

Fig. 8 Combustion efficiency dependence on β'_n

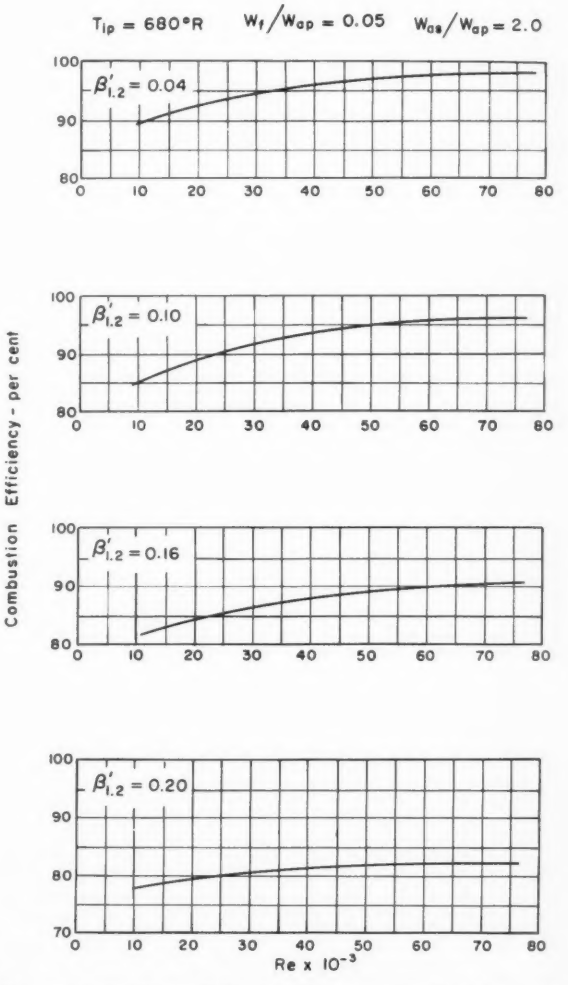

Fig. 9 Combustion efficiency dependence on Re for some arbitrary values of a constant β'_n

the primary zone are the same (actual difference is 1%) for both systems. This means the actual residence time in the richer system is less than that in the leaner system for a given size combustor. Since the efficiencies are essentially the same in the two systems at a constant value of P_d, the system having the lower residence time must have a higher reaction rate (or lower required reaction time). Since P_d is fixed, this requires the reaction sequence in the richer system to have a higher apparent overall reaction order. The effective overall reaction orders for the systems having $W_f/W_{ap} = 0.04$ and 0.05 are 1.25 and 1.40, respectively, as shown by Figs. 6 and 8. This observation is also in line with what one might expect from kinetic considerations. At higher temperatures the first-order reactions, associated with fuel decomposition, tend to go much faster, so that the overall process tends to proceed at a rate determined to a larger extent by the second-order reactions. The overall reaction order thus moves closer to two.

Again, the data at the various values of Re have been plotted using an average n value of 1.20. Such plots permit one to present the curves shown in Fig. 9 of efficiency vs. Re for several arbitrary values of $\beta_{1.2}'$. Here, efficiency is somewhat more sensitive to changes in Re than the lean data previously discussed. This is not too surprising for, when the mixing is less than perfect (instantaneous), the introduction of additional fuel at a given level of turbulence means that a larger fraction of the available residence time must be alloted to mixing phenomena. One would still expect the efficiency to become essentially insensitive to changes in Re at large values of Re. This trend is shown in Fig. 9.

The correlation shown in Fig. 10 may be compared with that shown in Fig. 6 to investigate effects of changes in inlet temperature, other conditions remaining constant, as indicated. In addition to the very successful correlation shown in Fig. 10, one may note the n value of 1.30 as compared to the n value of 1.25 for $T_{ip} = 680°R$ for Re = 20,000.

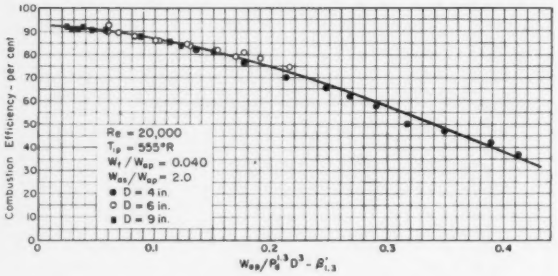

Fig. 10 Combustion efficiency dependence on β'_n

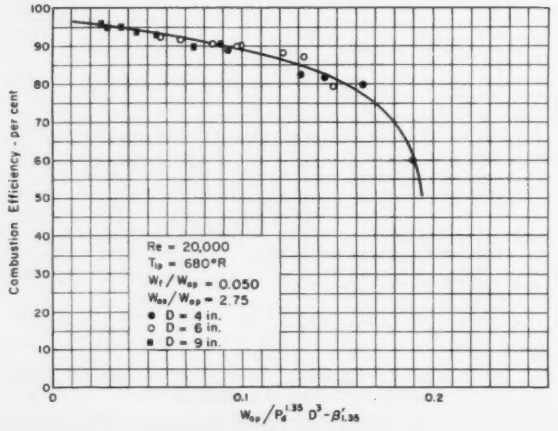

Fig. 11 Combustion efficiency dependence on β'_n

One may compare the results shown in Fig. 11 with those of Fig. 6 to see the effects of a change in primary fuel-air ratio, the overall fuel-air ratio and inlet temperature remaining constant. A comparison of Fig. 11 with Fig. 8 shows the effects of a change in overall fuel-air ratio, the primary fuel-air ratio and inlet temperature remaining constant. Note that none of the three systems are similar throughout.

Reference to the data of Figs. 2 and 5 shows that over most of the range of P_d the efficiency of the richer primary fuel-air ratio system is somewhat better than that of the leaner system. The richer system does have a more narrow stability limit, which may be attributed to the higher flow velocities (at the lower pressures) caused by the higher flame temperatures (in the primary zone), as described previously. At a given value of P_d, one can reason as before that, for a given T_{ip} and Re, the residence time available in the leaner system is greater than that available in the richer system. Since the effective reaction order of the lean system is smaller than that for the rich system, 1.25 vs. 1.35, respectively, one has the case of a system with a low residence time and high reaction rate yielding efficiencies which are comparable to one having a high residence time and low reaction rate, relatively speaking. This is a perfectly reasonable situation. Also, one would expect n to be larger for the higher primary zone temperature because of the increased relative importance of the rates of the second-order reactions, as mentioned previously.

Reference to the data of Figs. 3 and 5 shows that over most of the range of P_d the efficiencies of the two described systems are comparable, those of the system having the larger overall air-fuel ratio being slightly greater. The more narrow stability limit of the leaner fuel-air system can be explained as in the above described case. The primary zone conditions of these two systems are identical at a given P_d. The differences arise in the secondary zone. As shown, for a given Re the secondary air mass flow rate of the leaner system is about 38% greater than that for the richer system. As one would expect, under these conditions the combustion product outlet temperatures of the richer case are greater than those of the leaner case. (Raw data show the differences to be about 14%.) This means the density in the secondary zone of the richer system is less than that of the leaner system. Since the W_{as} of the richer system are 38% less and the density about 14% less than the leaner system, the velocities of the richer system are less than those in the leaner system. The n value of the richer system is 1.40 as compared to a value of 1.35 in the leaner system. Hence, again, one finds a system having a low residence time and high reaction rate yielding efficiencies comparable to a system having a high residence time and low reaction rate, relatively speaking.

It is worth noting that the data mentioned above indicate that a significant amount of afterburning is present in the secondary zone. The fact that this section was accurately scaled should add confidence to the results presented.

Fig. 11 shows the effect of quenching by the larger amount of secondary air when we have a high primary zone loading factor β_n'.

In summary, the results presented indicate that combustion efficiency should correlate well with a loading parameter of W/P^nD^3. Though not novel to this investigation, this parameter compares with that found by Greenhough and Lefebvre (13) and Longwell and Weiss (14,15). Probert (16), describing the work of White and Lewis (17), reports a slightly different form of $W/P^nD^{2.4}$. Table 1 summarizes the n values obtained.

The reader is reminded that the low n values of (10,11) were obtained from a nonpremixed, diffusion type system. All others except those of (13) came from completely premixed

Table 1 Effective overall reaction orders

Reference	Values of n
(10)[a]	1.64, 1.28
(11)[b]	1.10–1.40
(13)	1.75
(14)	1.80
(15)	1.80
(16)	1.50
(18)	1.50–4.0

[a] Contains results from two different geometries.
[b] Corresponds to results presented in this paper.

gaseous systems. The value shown for (13) came from a system employing liquid fuel injection.

The author cannot explain the large spread between the low n values and those grouped nearer the accepted value of 1.8 to 2.0. However, the physical significance attached to n (both here and elsewhere) has been that it represents an effective (or apparent) overall reaction order or some physical rate constant slightly modified by the chemical kinetics. Hence, it appears that anything which alters the various chemical reactions would reflect itself in the ultimate value of n determined. It seems plausible that such factors as geometry and fuel injection methods could easily effect changes in the pattern of reaction kinetics.

Conclusions

Under conditions of geometric similarity of combustors, constant inlet temperature of fuel and air, specified gaseous fuel, specified gaseous oxidant, low velocity (Mach number) flows, absence of body forces, and negligible heat losses to the walls, a reasonable degree of similarity will exist if one maintains constant the ratio of reaction time to residence time, the fuel-air ratio, and the Reynolds number for a model and a prototype. Results taken at conditions where high heat losses prevail, e.g., small combustor operating at very high pressure, would not be expected to yield a correlation which would prove satisfactory.

The concept of the effective overall reaction order is useful in describing the complex reactions occurring in hydrocarbon-air systems. Approximate similitude laws based on this concept appear to be well founded as evidenced by the strong experimental support offered here.

The effects of Reynolds number on combustion efficiency appear rather slight over the Reynolds number range 20,000 to 130,000 for a primary fuel-air ratio of 0.040 for the particular combustors investigated. A more significant effect of changes in Reynolds number in the range 20,000 to 70,000 is evident for a primary fuel-air ratio of 0.050. The preponderant influence of the ratio of reaction time to residence time on the combustion efficiency is shown clearly in both cases.

The effects of changes in inlet temperature, primary fuel-air ratio, and overall fuel-air ratio on combustion efficiency appear slight for the particular combustors investigated.

A range of values for the apparent overall reaction order for the diffusion type propane-air flame employed exists for the many different inlet conditions investigated. Values range from 1.10 to 1.40, the majority falling near 1.20.

Experiments as here described appear to yield results which should prove useful in future scaling predictions. They support the procedure of changing pressure and velocity, while testing a scale model, in such a way as to simulate the performance of a prototype combustor and to indicate the manner in which this should be done.

Acknowledgment

This investigation was performed in the Westinghouse Research Laboratories. The author is particularly indebted to S. Way of these laboratories for his discussions and assistance during the investigation and to H. G. Wolfhard.

References

1 Damkohler, G., "Einflusse der Stromung, Diffusion und des Warmeuberganges auf die Leistung von Reaktionsofen," *Zeitschr. f. Elektrochemie*, vol. 42, 1936, p. 846.

2 Edgeworth-Johnstone, R., "The Transference of Chemical Processes from Small to Large Scale Operation," *Trans. Inst. Chem. Engineers*, vol. 17, 1939, p. 129.

3 Bosworth, R. C. L., "Chemical Similarity in Heterogeneous Catalysts," *Trans. Faraday Soc.*, vol. 43, 1947, p. 399.

4 Putnam, A. A. and Jensen, R. A., "Application of Dimensionless Numbers to Fash-Back and Other Combustion Phenomena," *Third Symposium on Combustion, Flame and Explosion Phenomena*, Williams and Wilkins, Baltimore, Md., 1949, p. 89.

5 Wolfhard, H. G., "Die Eigenschaften Stationarer Flammen im Unterdruck," *Z. tech. Phys.*, vol. 24, 1943, p. 206.

6 Weller, A. E., "Similarities in Combustion, A Review," *Selected Combustion Problems*, vol. 2, Butterworths Scientific Publications, London, 1956, pp. 371–384.

7 Stewart, D. G., "Scaling of Gas Turbine Combustion Systems," *Selected Combustion Problems*, vol. 2, Butterworths Scientific Publications, London, 1956, pp. 384–414.

8 Way, S., "Similitude Considerations in Turbojet Engines," JET PROPULSION, vol. 27, February 1957, pp. 162–169.

9 Penner, S. S., "Similarity Analysis and the Scaling of Liquid Fuel Rocket Engines," *Combustion Researches and Reviews 1955*, Butterworths Scientific Publications, London, 1955, Chap. 12.

10 Woodward, E. C., "Similitude Study of Idealized Combustors," *Sixth Symposium (International) on Combustion*, Reinhold Publishing Co., New York, 1957, pp. 849–859.

11 Woodward, E. C., "An Investigation of Similitude Considerations for a Family of Geometrically Similar Combustors," Ph.D. Thesis, Univ. of Pittsburgh, Pittsburgh, August 1958.

12 Tobey, A. C. and Raymond, P. M., "Similated High Altitude Combustion Research," M.I.T. Quar. Status Rep. No. 12, Contract AF 33(616)-3037 of WADC, July 1958.

13 Greenhough, V. W. and Lefebvre, A. H., "Some Applications of Combustion Theory to Gas Turbine Development," *Sixth Symposium (International) on Combustion*, Reinhold Publishing Co., New York, 1957, pp. 858–869.

14 Weiss, M. A., and Longwell, J. P., "Low Pressure Performance of Cylindrical Can Burners," JET PROPULSION, vol. 26, September 1956, pp. 749–756.

15 Longwell, J. P., and Weiss, M. A., "High Temperature Reaction Rates in Hydrocarbon Combustion," *Ind. Engng. Chem.*, vol. 47, August 1955, pp. 1634–1643.

16 Probert, R. P., "Application of Research to Gas-Turbine Combustion Problems," paper presented at the ASME-IME Joint Conference on Combustion, London, October 1955.

17 White, S. W. and Lewis, W. G. E., "The Performance of a Multi-Stage Combustion System—Part I. Flame Stability of Recirculation Zones," NGTE Rep. R. 165, May 1955.

18 Personal communication from S. W. White of NGTE, July 25, 1956.

Problems Associated With Multiple Engine Starts in Spacecraft

WILLIAM F. RADCLIFFE[1]
JOHN R. TRANSUE[2]

General Dynamics/Astronautics
San Diego, Calif.

Earth-orbit, lunar and interplanetary missions are briefly reviewed to show that vehicle flexibility can be considerably enhanced if the final stage is capable of multiple engine firings interspersed with periods of gravity free coasting. The space thermal environment during coast is discussed and surface finishes desirable for temperature control are examined. Typical surface finish characteristics are used to estimate the temperature histories and venting rates of stored cryogenic propellants, and data are presented to show the effects of thermal radiation shielding. A limit type of analysis describing the behavior of liquids under zero g is presented with the resulting data used to estimate the collecting accelerations required for subsequent engine starts.

THE SPACE missions thus far accomplished by the U. S. and, so far as we know, by the U. S. S. R. have used launch vehicles comprised of stages which fired only once. However, there are definite advantages in using a final stage which is capable of multiple in-flight engine firings. The fact that vehicles with this capability have not been developed before this time indicates that this development involves the solution of some unique problems—problems which could be avoided by accepting the limitations of single-start vehicles.[3] A few of those problems are: 1) boiling heat transfer under zero g; 2) fluid behavior under zero g; 3) storage of propellants during extended coast periods; 4) venting of propellant tanks during zero g conditions; 5) collection of propellants prior to engine starts; 6) cool-down of propellant lines and turbopumps; and 7) environmental control for equipment.

A discussion of selected problems associated with obtaining multiple-start capability in a launch vehicle is the principal content of this paper. However, in order to fully grasp the necessity of solving these problems and of achieving multiple-start capability, it is important to understand some of the advantages of a multiple-start vehicle. These advantages depend in large measure upon the mission of the vehicle.

Mission Requirements

Earth Satellites

The launching of an Earth satellite can be efficiently accomplished by single-start stages only when the desired orbit is close to the Earth, or when a separate stage with the energy required to supply the appropriate apogee impulse is used. However, the apogee impulse varies with the orbital altitude, so either a number of final stages must be available or the ones available must be used in a nonoptimum manner. Neither alternative is particularly appealing. However, if the final stage is capable of an engine restart, it is possible to use the full capability of the stage for launching to any altitude. This goal is realized simply by providing more propellants in the final stage than are required for the final firing of the most difficult mission, and by using the propellants not needed for the last firing during the previous firing.

The 24-hr circular orbit is much like any other satellite orbit if the inclination of the 24-hr orbit is equal to or greater than the latitude of the launch site. However, an important exception to this condition is the 24-hr equatorial orbit. To establish this orbit from a nonequatorial launch site, at least three firing periods are required. This is illustrated in Fig. 1. The final firing must occur over the Equator and, since transfer is most efficiently realized with a Hohmann transfer ellipse, the entry into the transfer ellipse must also be on the Equator. If the launch site is not on the Equator, the launch is a separate firing, so three firings are required. Since the first firing period would normally use either two or three stages, the complete vehicle must either be a four- or five-stage vehicle or it must use multiple starts of at least one stage. In this case, the multiple-start vehicle has several advantages: 1) fewer stages need to be developed; 2) higher reliability; 3) simpler countdown; 4) fewer interfaces; and 5) a shorter vehicle realized by having fewer adapter sections.

Missions involving rendezvous with an Earth satellite are similar to the 24-hr mission in that they will normally use at least three firing periods. The multiple-start vehicle will be preferable for this type of mission also.

Lunar Missions

It is possible to launch a vehicle on an orbit to the moon by using only one firing period. But to do this efficiently, the launch must be timed so that the moon will be near its maximum declination below the Earth's equatorial plane when the spacecraft arrives (assuming the launch to be from a site north of about 25° N lat). This restricts launch dates to a few days out of each lunar month. However, if the launch could use a parking orbit near the Earth with subsequent departure for the moon, it would be possible to launch any day of the month under near optimum conditions. In fact, there would be two launching opportunities during

Presented at the ARS Semi-Annual Meeting, Los Angeles, Calif., May 9–12, 1960; revision received June 4, 1961.

[1] Chief Development Engineer. Member ARS.

[2] Research Group Engineer.

[3] Concurrent with the preparation of this paper, the Able Star satellite vehicle using nitric acid and UDMH propellants was successfully restarted after extended coast. Restart capability has also been incorporated in the Agena vehicle and two flights have been accomplished where this feature was used.

most days. This great increase in the number of launching opportunities is of immediate importance due to launch pad availability conditions, and it might someday be of great importance for rescue missions and military missions. While this departure from the parking orbit could be performed by a separate, single firing stage, the use of a multiple-start stage would provide a more versatile vehicle in that the departure impulse and, therefore, the transfer time could be selected to best meet the mission objectives rather than to meet the stage impulse constraint.

Interplanetary Missions

Interplanetary missions are another example of missions which can benefit from the use of a parking orbit during the launch. In this case, the benefit is not only an increase in the number of launching opportunities, but also the attainment of a more efficient launch trajectory. Under some circumstances it is impossible to launch with a single firing period. When it is possible, the optimum launch time of day is such that a compromise between optimum launch azimuth and optimum burnout flight path angle is effected. But by using a parking orbit, the burnout flight path angle can always be optimized, so the launch time of day can be selected to optimize just the launch azimuth, and a more efficient trajectory results. Also there are two equally good optimal launch times each day if a parking orbit is used. If the launch azimuth of one of these launch times is α, measured east from north, then the launching azimuth of the other launch time is $(180° - \alpha)$. Having two permissible launch azimuths may be important if range safety considerations place restrictions on the launch azimuth. The advantage of multiple-start capability in the final stage is the same for these missions as for the lunar mission, that is, increased mission versatility.

Vehicle Requirements

The brief mission analysis has indicated that for many vehicle applications, coasting is required between periods of powered flight. This analysis also shows that it is frequently more economical to use a single vehicle with multiple starts than to use separate vehicles and propulsion systems for each firing. Thus, we have to examine the problems associated with multiple engine starts in the space craft. These problems are listed as follows: 1) propellant storage during coast; 2) propellant collection preparatory to firing; 3) propulsion system chilldown and priming prior to firing.

Propellant Environment

Propellant storage depends on environment, and for most propellants the space thermal radiation is most important. Fig. 2 shows pictorially this environment for an altitude of 100 n miles above the Earth. The data is presented in terms of the average heat flux incident on a spherical surface. It is seen that in the Earth's shadow the heat flux is modest, amounting to 24.5 Btu/ft²/hr. In the sunlight, the direct solar radiation amounts to 110.5 Btu/ft²/hr. Bodies shielded from the sun, but exposed to the sunlight reflected from the Earth (albedo) receive about 60% of the sun's direct radiation or 68 Btu/ft²/hr. The heat input due to the Earth's radiation and albedo depend strongly on the geometry of the body; the figures quoted apply only to the average flux on a spherical surface.

In the vicinity of the Earth, the direct solar radiation is essentially constant. However, both the Earth's thermal radiation and its albedo decrease rapidly as we leave the Earth's surface as shown in Fig. 3. At a distance of 16,000 n miles (five Earth radii) both of these sources of heat become negligible.

The energy spectrum of this radiation is of interest since it

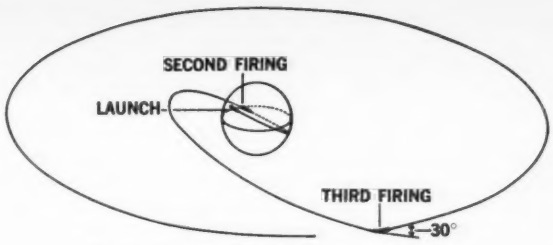

Fig. 1 Typical 24-hr orbit launch trajectory

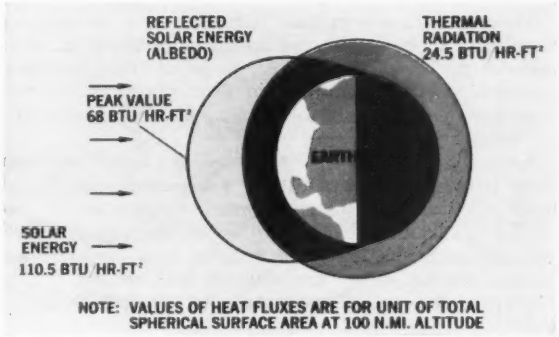
REFLECTED SOLAR ENERGY (ALBEDO)
THERMAL RADIATION 24.5 BTU/HR-FT²
PEAK VALUE 68 BTU/HR-FT²
EARTH
SOLAR ENERGY
110.5 BTU/HR-FT²
NOTE: VALUES OF HEAT FLUXES ARE FOR UNIT OF TOTAL SPHERICAL SURFACE AREA AT 100 N.MI. ALTITUDE

Fig. 2 Space thermal radiation sources

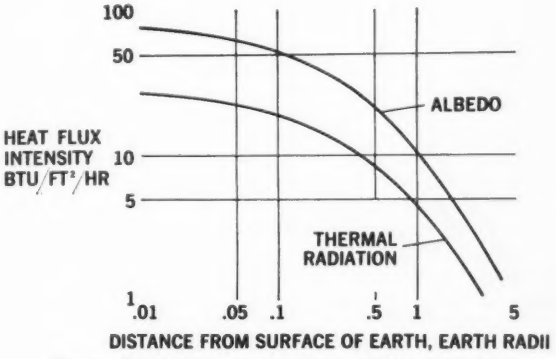

Fig. 3 Earth thermal and albedo radiation intensity

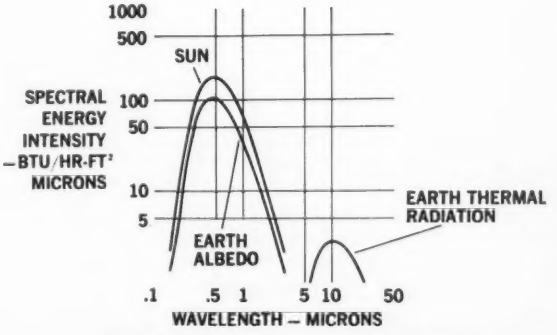

Fig. 4 Spectrum of space radiation sources

governs to some extent the emissivities selected for the vehicle surfaces. Fig. 4 shows the spectral energy density of these three radiation sources, presenting the intensity as a function of wavelength. It is seen that the peak of the sun's spectrum is at 0.5 μ and most of the energy occurs at a wavelength less than 1.2 μ. The spectrum of the albedo is similar to that of the sun, but there is considerable doubt as to its exact nature. On the other hand, the maximum energy of the Earth's radiation is at 10 μ with most of the energy confined to wavelengths less than 24 μ. Since the high intensity radiation has a short wavelength, these spectra indicate the type of surface finish most desirable for the storage tanks. In particular, for cryogenic propellants, the ideal surface would reflect most of the energy in the short wavelength region and emit strongly in the long wavelength region.

The emissivities of various materials as a function of wavelength together with the desired properties of an ideal material are shown in Fig. 5. Some of these materials approach ideal requirements, but further work is required to explore the best means of controlling the surface emissivity for optimum results.

Assuming the satellite has the shape of a sphere and that there is complete heat induction and thermal equilibrium inside the satellite, the equilibrium temperature of the surface can be estimated. Fig. 6 shows the results of such estimates as a function of the distance from the Earth for various orientations of the satellite with respect to the Earth and the sun. These data were prepared using the emissivity data for white paint from Fig. 5.

It is seen that for near Earth orbits, the equilibrium temperature of the spherical satellite varies from $-150°$F in the Earth's shade (position C) to $+20°$F in the full sunlight (position A). At greater distances from the Earth, the equilibrium temperature decreases for positions A and B with these positions approaching a common value of $-75°$F at a distance of five Earth radii. Here in both cases, the effect of the Earth's radiation and albedo are quite small compared to the direct sunlight, so that the condition is representative of free sunlit space.

Position C in the Earth's shadow is completely shielded from the sun, so that the satellite temperature drops rapidly with increasing distance from the Earth. The lowest value shown is $-330°$F at five Earth radii. With the exception of position C at large radii, these results yield temperatures that are too high for cryogenic propellants, but too low for the common storable propellants. For the cryogenic propellants, a highly reflective radiation shield can be inserted to protect the face directed toward the sun. This component with inner surface emissivities of 0.1 produces the temperature shown as curve D in Fig. 6. Generally with this arrangement, a single radiation shield will produce an environment which is almost as good as when the sun is completely shielded by the Earth (orientation C). This latter arrangement is of course a transient condition. With the radiation shield, propellants such as liquid oxygen may be stored when the satellite is more than 16,000 n miles from the Earth's surface. However, since the radiation shield does add weight to the system, and since it is only needed on the side of the satellite directed toward the sun, this suggests the use of only one shield, provided the satellite has the shielded side oriented toward the sun during coast periods. Radiation heating during the short periods of engine operation is negligible, and sun orientation at this time is not required.

Propellant Venting

From curve D of Fig. 6 it is seen that as one leaves the Earth, the equilibrium temperature decreases until conditions representative of outer space are attained. In general, these temperatures exceed the boiling temperatures of most cryogenic propellants except for large distances from the Earth. The propellants, controlled by some pressurization system, will maintain the tank walls at close to the propellant boiling temperature. Thus, in the intermediate region close to the Earth, propellant boiloff will occur. Since the heat input is known, and since the wall temperature for reradiation is established by the propellant temperature, this boiloff can be readily calculated for our spherical satellite. The results in terms of total boiloff for a liquid oxygen tank and a liquid hydrogen tank are shown in Fig. 7. Here as expected, the boiloff rates are high near the surface of the Earth. Initially, the oxygen boiloff exceeds that of hydrogen by approximately two to one because of the higher heat of evaporation of hydrogen. However, as the position in space approaches that where the satellite equilibrium surface temperature is near that of liquid oxygen, most of the incident heat is reradiated and the oxygen boiloff decreases, reaching zero at five Earth radii. Due to the low surface temperature enforced by the liquid hydrogen, very little heat can be reradiated from the hydrogen tank, so that here the boiloff approaches a constant rate as the satellite leaves the Earth. The minimum rate of 0.01 lb/hr/ft^2 of projected area represents the solar heat transmitted through the radiation shield. This boiloff rate is quite low and would be acceptable for a vehicle coast of several hours, but not for coasts of several months. For the latter case, a further optimization would be required to evaluate the merits of additional radiation shields.

Zero G Effects

In addition to providing for adequate thermal environment of the propellants during coast, perhaps the most significant

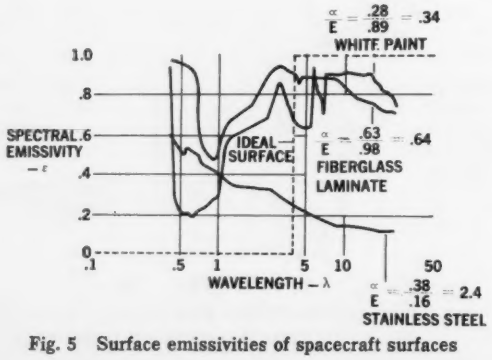

Fig. 5 Surface emissivities of spacecraft surfaces

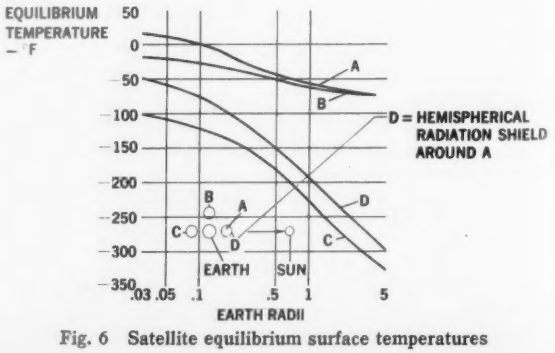

Fig. 6 Satellite equilibrium surface temperatures

problems are those associated with zero g during this period. While these problems may eventually prove to be of little consequence, our complete lack of everyday experience in this area, together with the lack of ready laboratory facilities for testing and observation of the phenomena, have caused some concern over these problems. A brief description of the history of a typical coast phase will illustrate them. For any powered flight preceding coast, the vehicle will be accelerated by the rocket engines to produce an inertia force equivalent to a gravitational field. The propellants will in general have a free surface normal to the thrust vector and, due to attitude control transients, may have a sloshing or oscillatory motion. Further, the mass or weight of the propellants will be reacted by the structure of the tank, which will have elastic stresses induced by the propellant load. Upon engine shutdown, the release of the tank strain energy will accelerate the propellants relative to the tank. Any residual velocity present in sloshing will no longer be restrained and, in general, the propellants will probably float up through the tank. This can be accentuated by any engine thrust transients or attitude control maneuvers at shutdown. If, in addition, the vehicle is to be oriented in some direction, either to the sun or the Earth, there will be further transient forces acting on the fluid. Lastly, some attitude control system would be required to maintain the preferred direction, and the periodic exercise of this system will disturb the fluid throughout the coast period. All of the foregoing effects, with the possible exception of the tank reaction force, are essentially random in nature, so that it is impossible to trace the fluid behavior accurately.

The analysis of the fluid behavior under zero g is further hampered by lack of a simplified physical model to describe the state of the fluid. If thrust shutdown occurs gradually with no transient side forces acting during this period, then the fluid may be assumed to be quiescent with a plane free surface at the start of zero g. Under this assumption, the only forces acting are surface tension of the liquid and capillary attraction between the liquid and the walls of the container. Surface tension exists in all liquids, since it is due to the intermolecular forces which hold the liquid together. While the absolute value of the surface tension varies widely, its general characteristic is such as to contain the liquid and force it to assume a shape of minimum surface for the volume of liquid in question. On the other hand, the capillary attraction between the liquid and the tank wall depends upon both the nature of the liquid and the wall material; this determines whether the liquid "wets" the wall and to what extent. Quantitatively this is established by the angle at which the fluid intersects the containing surface. For liquids which wet the surface, the liquid-wall intersection will move along the wall away from the main body of the liquid. The intersection with the wall will be at some angle α, which may range from 0° to 90°, depending on the liquid and the container material. If the intersection angle α is greater than 0°, the liquid in a partially filled tank will, under zero g, move along the tank wall away from the liquid, stretching the free surface until an equilibrium position is reached. In the event that the intersection angle is zero, the fluid will move along the tank wall until the entire surface is covered, and the vapor in the tank will assume a spherical shape surrounded on all sides by the residual liquid in the tank. This stable configuration was investigated by Li (1)[4] where he developed the results described above. Under these assumptions, the position of the fluid is well established, and collection by low thrust ullage rockets would present no problems.

The surface tension forces, however, are extremely small. For example, the total capilliary attraction force between liquid hydrogen and a 10-ft diam container is 4.1×10^{-3} lb. This is simply the product of the surface tension and the 10-ft diam intersecting line, assuming the wetting angle $\alpha \approx 0$. Similarly, the capilliary force between liquid oxygen and the same container is 2.8×10^{-2} lb. In the absence of external forces on the container, these capillary forces would slowly accelerate the liquids to the final equilibrium position. However, there are usually transient control forces which are large with respect to these capillary and surface tension forces. A complete description of the fluid behavior history resulting from the action of these varied forces is currently beyond the state of the art. Consequently, an alternate and purposely pessimistic approach was taken by J. T. Neu et al. (2). In this analysis, the kinetic energy imparted to the liquid by the transient shutdown and control forces is converted to potential energy of surface tension by breakup of the liquid into small globules. The energy is also dissipated by aerodynamic drag on the resulting droplets. Since the initial liquid velocities were unknown, the problem was approached parametrically so as to establish the maximum initial velocities which could be tolerated. Table 1 shows the impact velocity required to subdivide liquid hydrogen droplets of various radii into two or more particles. It is seen that as the initial droplet decreases in size, the required impact velocity for subdivision into two particles increases by a factor of about three for a tenfold reduction in radius. Similarly, for subdivision into more than two particles, the required impact velocity also increases. Of particular interest are droplets with radii of 0.5 cm and 0.1 cm. To subdivide into two particles, a

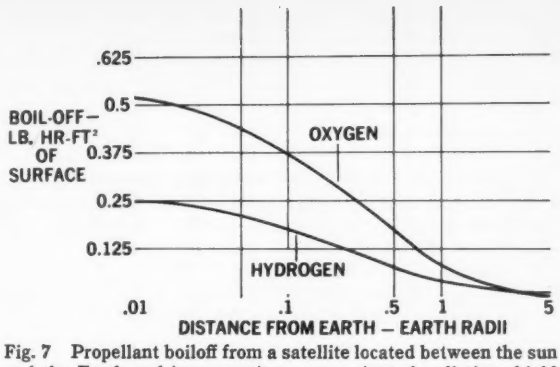

Fig. 7 Propellant boiloff from a satellite located between the sun and the Earth and incorporating a sun oriented radiation shield

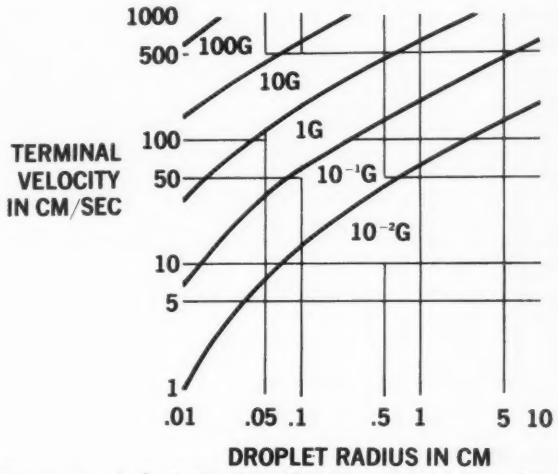

Fig. 8 Terminal velocity of liquid hydrogen droplets in various acceleration fields

[4] Numbers in parentheses indicate References at end of paper.

velocity of 0.32 fps is required for the larger particle, whereas a velocity of 0.72 fps is required for the smaller one. While these are quite low velocities, reference to Table 2 shows that it is unlikely that velocities of this magnitude will occur for impacts on the container walls. The effects of aerodynamic drag were used to estimate the velocities which various size droplets would have after traveling a representative distance of 4.9 ft in the containing propellant tank. The initial velocities were selected to cover a range of possible conditions which might be experienced. It was found that regardless of the initial velocities the particles will eventually stop altogether if the distance of travel is sufficiently great. Considering a droplet size of 0.5-cm radius, which requires an impact velocity of 0.32 fps to subdivide, Table 2 shows that an initial velocity in the tank exceeding 3.26 fps is required to produce this impact velocity. In fact, the initial velocity would have to be approximately 7.0 fps. A droplet of 0.1 cm radius requires an impact velocity of 0.72 fps to subdivide, and Table 2 shows that initial velocities in the tank in excess of 32.6 fps would be required to produce this impact velocity.

The usual engine shutdown procedure will call for a period of low thrust vernier rocket operation to provide for accurate guidance. Accelerations during this period are of the order of 0.1 g or less, so that the forces acting on the fluid are small. It is estimated that the residual strain energy in the tanks would provide propellant velocities of 2 to 3 fps relative to the tanks. Thus, there is insufficient energy imparted to the propellants at engine shutdown to generate droplets of less than 0.1-cm radius. In fact, if droplets are formed, they would probably be 0.5 cm or larger.

Approximate vehicle accelerations required to collect these propellants prior to engine restart are shown in Fig. 8, where droplet terminal velocity is presented in terms of droplet radius and vehicle acceleration. For the droplets of 0.1-cm radius, the terminal velocity is 60 cm/sec at 0.1 g acceleration and 15 cm/sec at 0.01 g acceleration. Thus, an acceleration of between 0.01 and 0.1 g would be required, depending on the desired duration of this collecting period and the size of the tanks.

In the section on propellant environment, it was pointed out that boiloff of propellants would occur during coast in near Earth orbits. If venting of the boiloff gases is prevented, high tank pressures and corresponding high structural weights would result for long coast periods. Thus, tank venting is usually required to prevent excessive pressures. Since zero g conditions will prevail at this time, provisions must be made to prevent venting liquid propellants as well as the boiloff gases.

Currently, the most promising separator is the rotating centrifugal type. This consists of a rotating impeller similar to that of a centrifugal pump. The gas flow, however, is in reverse direction to that of the usual centrifugal pump, and the centrifugal force field prevents the entrance of the heavier liquid droplets. The centrifugal impeller may be driven either by an electric motor or by a turbine operating on the expansion of the vented gases.

Table 1 Impact velocity in fps required to subdivide hydrogen droplets[a]

Radius, cm	Number of resultant particles 2	4	8	16
5.0	0.1	0.15	0.193	0.238
1.0	0.226	0.34	0.44	0.55
5×10^{-1}	0.32	0.49	0.66	0.78
10^{-1}	0.72	1.08	1.42	1.74
5×10^{-2}	1.0	1.51	1.94	2.4

[a] Surface energy for additional particles is supplied by kinetic energy of particle.

Table 2 Velocities of hydrogen droplets after traveling 150 cm (4.9 ft)

Droplet radius, cm	Initial velocity, fps 0.326	3.26	32.6
5×10^{-1}	0.115	0.149	1.49
10^{-1}	0(1.08 ft)[a]	0(2.0 ft)[a]	0.112
5×10^{-2}	0	0	0
10^{-2}	0	0	0

[a] Distance traveled by particle before coming to rest.

Other possible systems can be devised which use the temperature difference between the high pressure mixture of gas and liquid in the tank and a lower pressure, lower temperature enclosure which is filled by expansion of part of the high temperature mixture in the tank. Evaporation of entrained liquid expanding into the low pressure region creates the reduced temperature in the enclosure. Heat transfer between the tank fluids and the low temperature fluids in the enclosure immersed in the primary tank cools the main propellants and provides heat to evaporate all the liquid in the enclosure. The gas so formed is vented to free space as required to maintain the desired tank pressure.

The foregoing discussion has presented some of the salient features associated with multiple engine starts of space vehicles. Some of the problems, such as space environment, are common to all such vehicles, others are more specific to selected vehicles and propellants. The solution of all of these problems will draw heavily on and contribute to our present satellite and space programs.

References

1 Li, Ta, "Liquid Behavior in a Zero-G Field," presented at the IAS 29th Annual Meeting, New York, Jan. 23–25, 1961 (IAS paper 61-20).

2 Neu, J. T., "Condition of Liquid Hydrogen Under Zero "G," Feb. 6, 1959. Convair-Astronautics Rep. AZJ-55-002.

Vehicle Motion in the Equatorial Plane of a Planet: a Second Order Analysis in Ellipticity

MAURICE L. ANTHONY[1]
LAWRENCE M. PERKO[2]

The Martin Co.
Denver, Colo.

This paper presents an approximate analytic solution of the drag-free equations of motion of a particle in the equatorial plane of an oblate spheroid subject only to the gravitational attraction of the spheroid. The solution, correct to second order in the planetary ellipticity ϵ, is obtained using the Poincaré-Lighthill-Kuo perturbation method. Additional results pertaining to the speed, flight-path angle, time, and the escape path are given as functions of angular displacement from an apse. Results are obtained as power series in the oblateness parameters J and D, and are valid for all eccentricities, i.e., no restriction is placed on $|\eta|$. The results agree with similar results given by Tisserand and DeMoraes and offer excellent agreement with numerical data.

THIS paper is intended as a sequel to the reports on planar motions about an oblate planet and escape in the equatorial plane of an oblate planet by Anthony and Fosdick (1,2),[3] extending the equatorial plane results to second order and giving additional information on flight-path angle, time, etc. Analytic results are obtained for the position and velocity of the particle, and its escape in the equatorial plane.

The analysis essentially follows the Poincaré-Lighthill-Kuo perturbation method to solve the equations of the path with motion starting at an apse. No restriction is placed on eccentricity, and results for eccentricity greater than one ($|\eta| > 1$) are given in the section Escape in the Equatorial Plane. Polar coordinates are used throughout.

The gravitational potential function U used to formulate the equations of motion is that given by Jeffreys (3) for the potential outside an ellipsoid of revolution

$$U = -\frac{\mu}{r}\left[1 + \frac{J}{3}\left(\frac{R}{r}\right)^2 + \frac{3}{35}D\left(\frac{R}{r}\right)^4\right] \qquad [1]$$

O'Keefe's pear shape term and all other higher harmonic terms are not carried in the analysis. The coefficients of the second harmonic J and the fourth harmonic D, which appear in the potential function, are given for the Earth by Jeffreys as

$$J = 1.6375 \times 10^{-3}$$

and

$$D = 1.07 \times 10^{-5}$$

King-Hele and Merson (4) derive from recent satellite observations the values

$$J = 1.6246 \times 10^{-3}$$

$$D = (6 \pm 1) \times 10^{-6}$$

which agree with the values given by Garfinkel (5).

Formulation of the Problem

With the potential given by Eq. 1, Newton's second law yields the following equations of motion

$$\ddot{r} - r\dot{\Phi}^2 = -\frac{\mu}{r^2}\left[1 + J\left(\frac{R}{r}\right)^2 + \frac{3}{7}D\left(\frac{R}{r}\right)^4\right] \qquad [2]$$

$$\frac{1}{r}\frac{d}{dt}(r^2\dot{\Phi}) = 0 \qquad [3]$$

The initial conditions, i.e., motion starting at an apse, taken at $t = 0$ are

$$r = r_0 \qquad [4]$$

and

$$\frac{dr}{dt} = 0 \qquad [5]$$

From Eq. 3

$$r^2\dot{\Phi} = h = r_0 v_0 \qquad [6]$$

a constant, from which

$$\frac{d}{dt} = \frac{h}{r^2}\frac{d}{d\Phi} \qquad [7]$$

By the use of Eq. 7 and $u = 1/r$, Eq. 2 reduces to the equation of the path

$$\frac{d^2u}{d\Phi^2} + u = \frac{1}{r_0 c^2}\left[1 + J(Ru)^2 + \frac{3}{7}D(Ru)^4\right] \qquad [8]$$

where

$$c = \frac{v_0}{v_c} = \frac{h}{\sqrt{\mu r_0}} \qquad [9]$$

The initial conditions Eqs. 4 and 5 become

$$u = \frac{1}{r_0} \qquad [10]$$

Presented at the ARS 15th Annual Meeting, Washington, D. C., Dec. 5–8, 1960; revision received July 31, 1961.

[1] Manager, Space Flight Laboratory. Senior Member ARS.

[2] Senior Engineer.

[3] Numbers in parentheses indicate References at end of paper.

and

$$\frac{du}{d\Phi} = 0 \qquad [11]$$

at $\Phi = 0$. The problem then is to find an approximate analytic solution to the second-order nonlinear differential Eq. 8, satisfying the initial conditions of Eqs. 10 and 11.

Method of Determining the Path

The path is obtained by assuming a power series expansion in the parameters J and D for the dependent and independent variables u and Φ of the form

$$u = u_0(\xi) + u_1(\xi)\, J + u_2(\xi)\, J^2 + u_3(\xi)\, D + \ldots \qquad [12]$$

and

$$\Phi = \xi + \Phi_1(\xi)\, J + \Phi_2(\xi)\, J^2 + \Phi_3(\xi)\, D + \ldots \qquad [13]$$

The power series are truncated so as to retain only terms involving the ellipticity ϵ of the oblate spheroid to second and smaller powers.

Using Jeffreys' results for the oblateness parameters

$$J = \epsilon - \frac{m}{2} - \frac{\epsilon^2}{2} + \frac{m\epsilon}{7} \qquad [14]$$

and

$$D = \frac{7}{2}\epsilon^2 - \frac{5}{2} m\epsilon \qquad [15]$$

where

$$\epsilon = \frac{R - R_p}{R} \qquad [16]$$

and

$$m = \frac{\omega^2 R^3 (1 - \epsilon)}{\mu} = \frac{g_e}{g}(1 - \epsilon) \qquad [17]$$

and noting that $m = 0(\epsilon)$ for the planets, we see that only terms of second and smaller powers in J and terms of first power in D need be retained.

Terms of third and higher order have an extremely small effect in the expansions for u and Φ due to the small ellipticity of the planets; hence, they are not carried in the analysis.

The initial conditions, Eqs. 10 and 11, become

$$u_0 = \frac{1}{r_0} \qquad [18]$$

$$u_1 = u_2 = u_3 = 0 \qquad [19]$$

and

$$u_0' = u_1' = u_2' = u_3' = 0 \qquad [20]$$

at $\Phi = \xi = 0$ where the prime indicates differentiation with respect to ξ.

The advantage in assuming a power series expansion for Φ is that through proper choice of Φ_1, Φ_2, and Φ_3 all secular terms[4] in u_1, u_2 and u_3 can be eliminated.

The expansions for $u(\xi)$ and $\Phi(\xi)$ are substituted into the differential Eq. 8, which must be identically satisfied to second order for all values of J and D.

This yields the set of equations

$$u_0'' + u_0 = \frac{1}{r_0 c^2} \qquad [21]$$

$$u_1'' + u_1 = \frac{R^2}{r_0 c^2} u_0^2 - u_0''\Phi_1' + u_0'\Phi_1'' - 3u_0\Phi_1' + \frac{3}{r_0 c^2}\Phi_1' \qquad [22]$$

$$u_2'' + u_2 = \frac{2R^2}{r_0 c^2} u_0 u_1 - u_0''\Phi_2' + u_0'\Phi_2'' - 3u_0\Phi_2' + \frac{3}{r_0 c^2}\Phi_2' - 3u_0\Phi_1'^2 + \frac{3R^2}{r_0 c^2} u_0^2\Phi_1' - u_1''\Phi_1' + u_1'\Phi_1'' - 3u_1\Phi_1' + \frac{3}{r_0 c^2}\Phi_1'^2 \qquad [23]$$

$$u_3'' + u_3 = \frac{3}{7}\frac{R^4}{r_0 c^2} u_0^4 - u_0''\Phi_3' + u_0'\Phi_3'' - 3u_0\Phi_3' + \frac{3}{r_0 c^2}\Phi_3' \qquad [24]$$

This sequence of differential equations with the set of initial conditions, Eqs. 18, 19, and 20, is solvable by elementary methods. The zero-order term is the familiar classical result

$$u_0 = \frac{1}{r_0 c^2}[1 + \eta\cos\xi] \qquad [25]$$

where $\eta = c^2 - 1$.

Upon substituting Eq. 25 into Eq. 22, the differential equation for u_1 becomes

$$u_1'' + u_1 = \frac{1}{r_0 c^2}\left[\left(\frac{R}{r_0 c^2}\right)^2\left(1 + \frac{\eta^2}{2} + \frac{\eta^2}{2}\cos 2\xi\right) + 2\eta\left(\frac{R^2}{r_0^2 c^4} - \Phi_1'\right)\cos\xi - \eta\Phi_1''\sin\xi\right] \qquad [26]$$

Secular terms of the form $\xi\cos\xi$ and $\xi\sin\xi$ are eliminated from u_1 by choosing $\Phi_1(\xi)$ to satisfy

$$\Phi_1''\sin\xi + 2\Phi_1'\cos\xi - 2\left(\frac{R}{r_0 c^2}\right)^2\cos\xi = 0 \qquad [27]$$

The solution of this differential equation satisfying $\Phi_1(0) = 0$ is

$$\Phi_1 = \left(\frac{R}{r_0 c^2}\right)^2 \xi \qquad [28]$$

With this choice of Φ_1, the equation for u_1 becomes

$$u_1'' + u_1 + \frac{1}{r_0 c^2}\left[\left(\frac{R}{r_0 c^2}\right)^2\left(1 + \frac{\eta^2}{2} + \frac{\eta^2}{2}\cos 2\xi\right)\right] \qquad [29]$$

which together with the initial conditions has the solution

$$u_1 = \frac{1}{r_0 c^2}\left(\frac{R}{r_0 c^2}\right)^2\left[\left(1 + \frac{\eta^2}{2}\right) - \left(1 + \frac{\eta^2}{3}\right)\cos\xi - \frac{\eta^2}{6}\cos 2\xi\right] \qquad [30]$$

[4] Terms of the form $\xi^k \times$ (trigonometric function of ξ).

In a similar manner the differential equations for u_2 and u_3 are found to be

$$u_2'' + u_2 = \frac{1}{r_0c^2}\left\{\left(\frac{R}{r_0c^2}\right)^4\left[\left(2 - \eta + \eta^2 - \frac{\eta^3}{3}\right) + \left(-\eta + \eta^2 - \frac{\eta^3}{3}\right)\cos 2\xi - \frac{\eta^3}{6}\cos 3\xi\right] + \eta\left[-2\Phi_2' + 5\left(\frac{R}{r_0c^2}\right)^4\left(1 + \frac{\eta^2}{6}\right)\right]\cos\xi - \eta\Phi_2''\sin\xi\right\} \quad [31]$$

$$u_3'' + u_3 = \frac{1}{r_0c^2}\left\{\frac{3}{7}\left(\frac{R}{r_0c^2}\right)^4\left[\left(1 + 3\eta^2 + \frac{3}{8}\eta^4\right) + \left(3\eta^2 + \frac{\eta^4}{2}\right)\cos 2\xi + \eta^3\cos 3\xi + \frac{\eta^4}{8}\cos 4\xi\right] + \eta\left[-2\Phi_3' + \frac{3}{7}\left(\frac{R}{r_0c^2}\right)^4(4 + 3\eta^2)\right]\cos\xi - \eta\Phi_3''\sin\xi\right\} \quad [32]$$

Elimination of secular terms is accomplished by choosing

$$\Phi_2 = \frac{5}{2}\left(\frac{R}{r_0c^2}\right)^4\left(1 + \frac{\eta^2}{6}\right)\xi \quad [33]$$

$$\Phi_3 = \frac{3}{14}\left(\frac{R}{r_0c^2}\right)^4(4 + 3\eta^2)\,\xi \quad [34]$$

The solutions for u_2 and u_3 are then

$$u_2 = \frac{1}{r_0c^2}\left(\frac{R}{r_0c^2}\right)^4\left[\left(2 - \eta + \eta^2 - \frac{\eta^3}{3}\right) + \left(-2 + \frac{2}{3}\eta - \frac{2}{3}\eta^2 + \frac{29}{144}\eta^3\right)\cos\xi + \frac{1}{3}\left(\eta - \eta^2 + \frac{\eta^3}{3}\right)\cos 2\xi + \frac{\eta^3}{48}\cos 3\xi\right] \quad [35]$$

$$u_3 = \frac{3}{7}\frac{1}{r_0c^2}\left(\frac{R}{r_0c^2}\right)^4\left[\left(1 + 3\eta^2 + \frac{3}{8}\eta^4\right) + \left(-1 - 2\eta^2 + \frac{\eta^3}{8} - \frac{\eta^4}{5}\right)\cos\xi - \left(\eta^2 + \frac{\eta^4}{6}\right)\cos 2\xi - \frac{\eta^3}{8}\cos 3\xi - \frac{\eta^4}{120}\cos 4\xi\right] \quad [36]$$

Substituting these equations into Eq. 12 gives the desired solution for $u(\xi)$. Similarly the expression for $\Phi(\xi)$ is obtained from Eq. 13 and the radius is obtained as a function of ξ by expanding $1/u$ to second order. The results which determine the path of the particle are given by Eqs. 37–39.

$$u = \frac{1}{r_0c^2}\left\{1 + \eta\cos\xi + J\left(\frac{R}{r_0c^2}\right)^2\left[\left(1 + \frac{\eta^2}{2}\right) - \left(1 + \frac{\eta^2}{3}\right)\cos\xi - \frac{\eta^2}{6}\cos 2\xi\right] + J^2\left(\frac{R}{r_0c^2}\right)^4\left[\left(2 - \eta + \eta^2 - \frac{\eta^3}{3}\right) + \left(-2 + \frac{2}{3}\eta - \frac{2}{3}\eta^2 + \frac{29}{144}\eta^3\right)\cos\xi + \frac{1}{3}\left(\eta - \eta^2 + \frac{\eta^3}{3}\right)\cos 2\xi + \frac{\eta^3}{48}\cos 3\xi\right] + \frac{3}{7}D\left(\frac{R}{r_0c^2}\right)^4\left[\left(1 + 3\eta^2 + \frac{3}{8}\eta^4\right) + \left(-1 - 2\eta^2 + \frac{\eta^3}{8} - \frac{\eta^4}{5}\right)\cos\xi - \left(\eta^2 + \frac{\eta^4}{6}\right)\cos 2\xi - \frac{\eta^3}{8}\cos 3\xi - \frac{\eta^4}{120}\cos 4\xi\right]\right\} \quad [37]$$

$$\xi = \frac{\Phi}{1 + J(R/r_0c^2)^2 + \frac{5}{2}J^2(R/r_0c^2)^4[1 + (\eta^2/6)] + \frac{3}{14}D(R/r_0c^2)^4(4 + 3\eta^2)} \quad [38]$$

$$r = \frac{r_0c^2}{1 + \eta\cos\xi}\left\{1 - \frac{J}{1 + \eta\cos\xi}\left(\frac{R}{r_0c^2}\right)^2\left[\left(1 + \frac{\eta^2}{2}\right) - \left(1 + \frac{\eta^2}{3}\right)\cos\xi - \frac{\eta^2}{6}\cos 2\xi\right] - \frac{J^2}{(1 + \eta\cos\xi)^2}\left(\frac{R}{r_0c^2}\right)^4\left[\left(\frac{1}{2} - 2\eta - \frac{2}{3}\eta^3 - \frac{63}{288}\eta^4\right) + \left(\frac{8}{3}\eta + \frac{149}{144}\eta^3\right)\cos\xi + \left(-\frac{1}{2} - \frac{2}{3}\eta - \frac{2}{9}\eta^3 + \frac{2}{9}\eta^4\right)\cos 2\xi - \frac{7}{48}\eta^3\cos 3\xi - \frac{\eta^4}{288}\cos 4\xi\right] - \frac{3D}{7(1 + \eta\cos\xi)}\left(\frac{R}{r_0c^2}\right)^4\left[\left(1 + 3\eta^2 + \frac{3}{8}\eta^4\right) + \left(-1 - 2\eta^2 + \frac{\eta^3}{8} - \frac{\eta^4}{5}\right)\cos\xi - \left(\eta^2 + \frac{\eta^4}{6}\right)\cos 2\xi - \frac{\eta^3}{8}\cos 3\xi - \frac{\eta^4}{120}\cos 4\xi\right]\right\} \quad [39]$$

The results given in Eqs. 37–39 check the original differential Eq. 8 and the initial conditions, Eq. 10 and 11. They also agree with similar results given in the literature. DeMoraes (6) gives a second-order equatorial plane result for u (p. 504) which contains secular terms. Generating secular terms in the expression for u given in Eqs. 37–39 by substituting the expression for $\xi(\Phi)$ into Eq. 37 gives an identical result with the exception of one coefficient. The coefficient of DeMoraes' $\cos 3(\Phi - \Phi_0)$ term must be multiplied by $-1/8$ to have his expression for u satisfy the initial condition $u = 1/r_0$ at $\Phi = \Phi_0$. If this is done, the results agree exactly. Tisserand (7) gives a result for apsidal angle (Tome I, p. 47) which agrees exactly (cf. Appendix A) with the expression obtained from Eq. 38 for nearly circular orbit with $\xi = \pi$.

Additional Analytical Results

Results pertaining to speed, initial speed necessary to have a prescribed apo-distance, flight-path angle, time, and nearly circular orbits are derived and presented in this section.

General Speed

The orbital speed v of the particle is found from the expression

$$v^2 = \dot{r}^2 + (r\dot{\Phi})^2 = h^2\left[\left(\frac{du}{d\Phi}\right)^2 + u^2\right] \quad [40]$$

all expansions being carried out to second order. The result is

$$v = \frac{v_0}{c^2}\sqrt{1+\eta^2+2\eta\cos\xi}\left\{1+\frac{J}{1+\eta^2+2\eta\cos\xi}\left(\frac{R}{r_0c^2}\right)^2\left[\left(1-\eta-\frac{\eta^3}{3}\right)+\left(-1+\eta-\frac{\eta^2}{3}+\frac{\eta^3}{4}\right)\cos\xi+\right.\right.$$
$$\left.\left.\frac{\eta^2}{3}\cos 2\xi+\frac{\eta^3}{2}\cos 3\xi\right]+\frac{J^2}{2(1+\eta^2+2\eta\cos\xi)^2}\left(\frac{R}{r_0c^2}\right)^4[\beta_1(\xi)]+\frac{3D}{14(1+\eta^2+2\eta\cos\xi)}\left(\frac{R}{r_0c^2}\right)^4[\beta_2(\xi)]\right\} \quad [41]$$

where

$$\beta_1(\xi)=\frac{1}{2}\left[\left(9-15\eta+27\eta^2-\frac{91}{6}\eta^3+\frac{131}{12}\eta^4-\frac{229}{72}\eta^5+\frac{39}{72}\eta^6\right)+\left(-9+\frac{83}{3}\eta-\frac{98}{3}\eta^2+\frac{953}{36}\eta^3-\right.\right.$$
$$\frac{817}{72}\eta^4+\frac{395}{72}\eta^5-\frac{25}{72}\eta^6\Big)\cos\xi+\left(-\frac{41}{3}\eta+\frac{26}{3}\eta^2-\frac{80}{9}\eta^3+\frac{225}{72}\eta^4-\frac{89}{72}\eta^5+\frac{35}{144}\eta^6\right)\cos 2\xi+$$
$$\left(\eta-3\eta^2-\frac{19}{12}\eta^3-\frac{5}{3}\eta^4-\frac{41}{72}\eta^5-\frac{2}{9}\eta^6\right)\cos 3\xi+\left(-\frac{5}{6}\eta^3-\frac{37}{36}\eta^4-\frac{5}{18}\eta^5-\frac{5}{24}\eta^6\right)\cos 4\xi-$$
$$\left.\frac{2}{9}\eta^5\cos 5\xi-\frac{\eta^6}{144}\cos 6\xi\right] \quad [42]$$

$$\beta_2(\xi)=\left[\left(2-2\eta+4\eta^2-4\eta^3-\frac{\eta^4}{2}-\frac{2}{5}\eta^5\right)+\left(-2+2\eta-4\eta^2+\frac{13}{4}\eta^3-\frac{2}{5}\eta^4+\frac{\eta^5}{4}\right)\cos\xi+\frac{2}{3}\eta^4\cos 2\xi+\right.$$
$$\left.\left(\frac{3}{4}\eta^3+\frac{1}{8}\eta^5\right)\cos 3\xi+\frac{7}{30}\eta^4\cos 4\xi+\frac{\eta^5}{40}\cos 5\xi\right] \quad [43]$$

Required Injection Speed

The speed required at the initial apse to assure that the path reaches the second prescribed apsidal radius r_π, is found by setting $\xi = \pi$ and $u = 1/r_\pi$ in Eq. 37 and solving for c. A power series is assumed for c^2 in the form $c^2 = c_0 + c_1J + c_2J^2 + c_3D$. The result of substituting this expansion into Eq. 37 with the above substitutions is given by

$$c^2=\left(\frac{v_0}{v_c}\right)^2=\frac{2r_\pi}{r_\pi+r_0}+\frac{2}{3}J\left(\frac{R}{r_0}\right)^2\left[\frac{r_\pi^2+r_\pi r_0+r_0^2}{r_\pi(r_\pi+r_0)}\right]+\frac{6}{35}D\left(\frac{R}{r_0}\right)^4\left[\frac{r_\pi^4+r_\pi^3r_0+r_\pi^2r_0^2+r_\pi r_0^3+r_0^4}{r_\pi^3(r_\pi+r_0)}\right] \quad [44]$$

This yields the following result for v_0, the required injection speed

$$v_0=\sqrt{\frac{2\mu r_\pi}{r_0(r_\pi+r_0)}}\left[1+\frac{J}{6}\left(\frac{R}{r_0}\right)^2\left(\frac{r_\pi^2+r_\pi r_0+r_0^2}{r_\pi^2}\right)+\frac{J^2}{72}\left(\frac{R}{r_0}\right)^4\left(\frac{r_\pi^4+2r_\pi^3r_0+3r_\pi^2r_0^2+2r_\pi r_0^3+r_0^4}{r_\pi^4}\right)+\right.$$
$$\left.\frac{3}{70}D\left(\frac{R}{r_0}\right)^4\left(\frac{r_\pi^4+r_\pi^3r_0+r_\pi^2r_0^2+r_\pi r_0^3+r_0^4}{r_\pi^4}\right)\right] \quad [45]$$

Flight-Path Angle

The flight-path angle α is found noting that

$$\tan\alpha=\frac{\dot r}{r\dot\Phi}=-\frac{1}{u}\frac{du}{d\Phi} \quad [46]$$

so that

$$\alpha=\mathrm{Tan}^{-1}\left[-\frac{1}{u}\frac{du}{d\xi}\frac{d\xi}{d\Phi}\right] \quad [47]$$

The result of carrying out the operations indicated in Eq. 47 to second order is

$$\alpha=\mathrm{Tan}^{-1}\left\{\sin\xi\left\{\frac{\eta}{1+\eta\cos\xi}-\frac{J}{(1+\eta\cos\xi)^2}\left(\frac{R}{r_0c^2}\right)^2\left[\left(1+2\eta+\frac{\eta^2}{3}+\frac{5}{6}\eta^3\right)+\frac{5}{3}\eta^2\cos\xi+\frac{\eta^3}{6}\cos 2\xi\right]-\right.\right.$$
$$\left.\left.\frac{J^2}{(1+\eta\cos\xi)^3}\left[\frac{R}{r_0c^2}\right]^4[\gamma_1(\xi)]-\frac{3D}{7(1+\eta\cos\xi)^2}\left(\frac{R}{r_0c^2}\right)^4[\gamma_2(\xi)]\right\}\right\} \quad [48]$$

where

$$\gamma_1(\xi)=\left(7\frac{1}{2}\eta-3\frac{1}{6}\eta^2+7\frac{5}{72}\eta^3-\frac{3}{2}\eta^4+\frac{95}{144}\eta^5\right)+\left(2\frac{1}{3}-6\eta+12\frac{1}{3}\eta^2-5\frac{4}{9}\eta^3+4\frac{15}{144}\eta^4-1\frac{2}{9}\eta^5\right)\cos\xi+$$
$$\left(-\frac{1}{3}\eta-1\frac{1}{6}\eta^2+\frac{11}{24}\eta^3-1\frac{1}{6}\eta^4+\frac{35}{72}\eta^5\right)\cos 2\xi+\left(-\frac{1}{4}\eta^2+\frac{5}{12}\eta^3-\frac{11}{72}\eta^4+\frac{\eta^5}{36}\right)\cos 3\xi+\frac{1}{48}\eta^5\cos 4\xi \quad [49]$$

$$\gamma_2(\xi)=\left(1+3\eta+2\eta^2+6\frac{3}{4}\eta^3+\frac{1}{5}\eta^4+\frac{97}{24}\eta^5\right)+\left(6\eta^2+2\frac{59}{60}\eta^4\right)\cos\xi+$$
$$\left(1\frac{3}{4}\eta^3+\frac{7}{30}\eta^5\right)\cos 2\xi+\frac{19}{60}\eta^4\cos 3\xi+\frac{1}{40}\eta^5\cos 4\xi \quad [50]$$

Time

The time t is obtained as a function of ξ by integrating Eq. 3 which yields

$$t = \int_0^\xi \left[\frac{d\Phi/d\xi}{hu^2}\right] d\xi \qquad [51]$$

Using the results for $u(\xi)$ and $\Phi(\xi)$ given by Eqs. 37 and 38, this can be put into the form

$$t = K_1 \int_0^\xi \frac{d\xi}{(1 + \eta \cos \xi)^2} + JK_2 \int_0^\xi \frac{(k_0 + k_1 \cos \xi + k_2 \cos^2 \xi + k_3 \cos^3 \xi)\, d\xi}{(1 + \eta \cos \xi)^4} \qquad [52]$$

which can be separated into partial fractions and integrated. The resulting expression is given by

$$t = \sqrt{\frac{r_0^3}{\mu(1-\eta)^3}} \left\{ \sin^{-1} \frac{(1-\eta^2)^{1/2} \sin \xi}{1 + \eta \cos \xi} - \frac{\eta(1-\eta^2)^{1/2} \sin \xi}{1 + \eta \cos \xi} + J \left(\frac{R}{r_0 c^2}\right)^2 \left[\frac{(1+\eta)^3}{(1-\eta^2)} \sin^{-1} \frac{(1-\eta)^{1/2} \sin \xi}{1 + \eta \cos \xi} - \frac{M(\xi) \sin \xi}{(1-\eta^2)^{1/2} (1 + \eta \cos \xi)^2} \right] \right\} \qquad [53]$$

where

$$M(\xi) = (1 + \eta) \left(2 + \eta + \frac{2}{3}\eta^2 + \eta^3 - \frac{2}{3}\eta^4\right) + \left(\eta + \frac{7}{3}\eta^2 + \frac{7}{3}\eta^3 + \frac{5}{3}\eta^4 + \frac{1}{3}\eta^5\right) \cos \xi \qquad [54]$$

The period P defined as the time between two consecutive peri-apsis passages is found by setting $\xi = 2\pi$. It is given by

$$P = \sqrt{\frac{r_0^3}{\mu(1-\eta)^3}} \left[1 + \frac{J}{1-\eta} \left(\frac{R}{r_0}\right)^2\right] 2\pi \qquad [55]$$

Hence, the oblateness of a planet tends to increase the period of a satellite in its equatorial plane by an amount

$$\Delta P = \frac{2JR^2\pi}{\sqrt{\mu r_0 (1-\eta)^5}} \qquad [56]$$

This amounts to approximately 11 sec for Phobos, Mars' inner satellite, 7 sec for Deimos, Mars' outer satellite, and 2.5 min for Satellite V of Jupiter. The oblateness of the Earth would increase the period of a 300-mile satellite to a circular orbit in the equatorial plane by approximately 8.3 sec.

Nearly Circular Orbits

A criterion for a nearly circular orbit is $\eta = 0(J)$ which implies that $|v_0 - v_c| = 0(Jv_c/2)$. If this is the case, the results take on the simplified form given in Eqs. 59–68. Eq. 59 implies that a circular orbit is possible only if $K = 0$ which yields

$$\eta = J \left(\frac{R}{r_0}\right)^2 + \frac{3}{7} D \left(\frac{R}{r_0}\right)^4 \qquad [57]$$

or, equivalently

$$v_0 = v_c \left[1 + \frac{J}{2} \left(\frac{R}{r_0}\right)^2 - \frac{J^2}{8} \left(\frac{R}{r_0}\right)^4 + \frac{3}{14} D \left(\frac{R}{r_0}\right)^4\right] \qquad [58]$$

$$u = \frac{1}{r_0} [1 - K(1 - \cos \xi)] \qquad [59]$$

$$K = \eta(1-\eta) - \left(\frac{R}{r_0}\right)^2 \left[J(1 - 3\eta) + \left(2J^2 + \frac{3}{7} D\right) \left(\frac{R}{r_0}\right)^2\right] \qquad [60]$$

$$\xi = \frac{\Phi}{1 + (R/r_0)^2 \{J(1-2\eta) + [(5/2)J^2 + (6/7)D](R/r_0)^2\}} \qquad [61]$$

$$r = r_0 [1 + \delta_1(\xi) (1 - \cos \xi)] \qquad [62]$$

$$\delta_1(\xi) = \eta(1 - \eta \cos \xi) - \left(\frac{R}{r_0}\right)^2 \left[J(1 - \eta - 2\eta \cos \xi) + J^2 \left(\frac{R}{r_0}\right)^2 (1 + \cos \xi) + \frac{3}{7} D \left(\frac{R}{r_0}\right)^2\right] \qquad [63]$$

$$v = v_0 [1 - \delta_2(\xi) (1 - \cos \xi)] \qquad [64]$$

$$\delta_2(\xi) = \frac{\eta}{2} (2 - 3\eta - \eta \cos \xi) - \left(\frac{R}{r_0}\right)^2 \left[J(1 - 3\eta - \eta \cos \xi) + \frac{9}{2} J^2 \left(\frac{R}{r_0}\right)^2 + \frac{3}{7} D \left(\frac{R}{r_0}\right)^2\right] \qquad [65]$$

$$\alpha = \left\{\eta(1 - \eta \cos \xi) - \left(\frac{R}{r_0}\right)^2 \left[J(1 - 2\eta \cos \xi) + \frac{7}{3} J^2 \left(\frac{R}{r_0}\right)^2 \cos \xi + \frac{3}{7} D \left(\frac{R}{r_0}\right)^2\right]\right\} \sin \xi \qquad [66]$$

$$t = \sqrt{\frac{r_0^3}{\mu}} \left[\left(1 + \frac{3}{2}\eta\right) \xi + J \left(\frac{R}{r_0}\right)^2 (\xi - 2 \sin \xi)\right] \qquad [67]$$

$$P = \sqrt{\frac{r_0^3}{\mu}} \left[1 + \frac{3}{2}\eta + J \left(\frac{R}{r_0}\right)^2\right] 2\pi \qquad [68]$$

Escape in the Equatorial Plane

The oblateness of a planet has several effects on an escaping vehicle. Namely, the minimum speed required for escape v_{0e}, the radial distance to the asymptote p and the angle of the asymptote Φ_∞, are all increased, whereas the speed at infinity v_∞ is decreased. The second order results given in Eqs. 70–73 are obtained using first integrals of the equations of motion. The analysis follows the same methods as those used by Anthony and Fosdick (2).

The speed required for escape from an oblate body exceeds that required for escape from a spherical body by an amount

$$\Delta v_{0e} = \sqrt{2}\, v_c \left[\frac{J}{6}\left(\frac{R}{r_0}\right)^2 - \frac{J^2}{72}\left(\frac{R}{r_0}\right)^4 + \frac{3}{70} D \left(\frac{R}{r_0}\right)^4 \right] \quad [69]$$

This is maximum for $r_0 = R$ and amounts to 9.9064 fps for Earth.

$$v_{0e} = \sqrt{2}\, v_c \left[1 + \frac{J}{6}\left(\frac{R}{r_0}\right)^2 - \frac{J^2}{72}\left(\frac{R}{r_0}\right)^4 + \frac{3}{70} D \left(\frac{R}{r_0}\right)^4 \right] \quad [70]$$

$$p = \frac{r_0 c}{\sqrt{c^2 - 2}} \left[1 + \frac{J}{3(c^2 - 2)}\left(\frac{R}{r_0}\right)^2 + \frac{J^2}{6(c^2 - 2)^2}\left(\frac{R}{r_0}\right)^4 + \frac{3D}{35(c^2 - 2)}\left(\frac{R}{r_0}\right)^4 \right] \quad [71]$$

$$v_\infty = v_c \sqrt{c^2 - 2} \left[1 - \frac{J}{3(c^2 - 2)}\left(\frac{R}{r_c}\right)^2 - \frac{J^2}{18(c^2 - 2)^2}\left(\frac{R}{r_0}\right)^4 - \frac{3D}{35(c^2 - 2)}\left(\frac{R}{r_0}\right)^2 \right] \quad [72]$$

$$\Phi_\infty = \cos^{-1}\left(\frac{-1}{\eta}\right) + \frac{J}{\eta}\left(\frac{R}{r_0 c^2}\right)^2 \left[\sqrt{\frac{\eta + 1}{\eta - 1}} \left(1 - \frac{1}{3}\eta + \frac{2}{3}\eta^2 \right) + \eta \cos^{-1}\left(\frac{-1}{\eta}\right) \right] +$$
$$\frac{J^2}{\eta^2(\eta - 1)}\left(\frac{R}{r_0 c^2}\right)^4 \left[\sqrt{\frac{\eta + 1}{\eta - 1}} \left(-\frac{1}{2} - \eta + \frac{13}{4}\eta^2 - \frac{13}{6}\eta^3 + \frac{55}{36}\eta^4 - \frac{2}{9}\eta^5 \right) + \frac{5}{2}\eta^2 \left(-1 + \eta - \frac{\eta^2}{6} + \frac{\eta^3}{6} \right) \cos^{-1}\left(\frac{-1}{\eta}\right) \right] +$$
$$\frac{3D}{7\eta}\left(\frac{R}{r_0 c^2}\right)^4 \left[\frac{1}{\sqrt{\eta^2 - 1}} \left(1 - \frac{17}{30}\eta + 2\eta^2 + \frac{97}{15}\eta^3 + \frac{1}{5}\eta^4 + \frac{8}{15}\eta^5 \right) + \eta \left(2 + \frac{3}{2}\eta^2 \right) \cos^{-1}\left(\frac{-1}{\eta}\right) \right] \quad [73]$$

Apsidal Motion

A comparison of theoretical and observed data for the apsidal motion of the Martian satellites Phobos and Deimos and Satellite V of Jupiter will be presented in this section. The apsidal motion from Eq. 38 is given by

$$\frac{d\pi}{dt} = \left[J\left(\frac{R}{r_0 c^2}\right)^2 + \frac{5}{2} J^2 \left(\frac{R}{r_0 c^2}\right)^4 \left(1 + \frac{\eta^2}{6} \right) + \frac{3}{14} D \left(\frac{R}{r_0 c^2}\right)^4 (4 + 3\eta^2) \right] n \quad [74]$$

where n is the mean motion of the satellite. To compute the apsidal motion, it will be necessary to first obtain the oblateness parameters J and D for Mars and Jupiter. Values for J and D can be obtained from Eqs. 14–17.

The values used for the constants in the expressions for ϵ and m are not entirely consistent in the literature; however, using values from Allen (8) and Ehricke (9), the following values are obtained for J and D.

Table 1 Oblateness parameters

Planet	ϵ	J	D
Earth	$\frac{1}{297}$	1.637×10^{-3}	1.07×10^{-5}
Mars	$\frac{1}{192}$	3.10×10^{-3}	3.69×10^{-5}
Jupiter	$\frac{1}{15.4}$	2.23×10^{-2} [a]	1.44×10^{-3} [a]
Saturn	$\frac{1}{9.5}$	3.52×10^{-2}	0.80×10^{-3}
Uranus	$\frac{1}{14}$	3.78×10^{-2}	6.23×10^{-3}

[a] Sampson (12) gives values of $J = 2.227 \times 10^{-2}$ and $D = 1.52 \times 10^{-3}$ for Jupiter.

The orbits of a number of satellites in the solar system are inclined only slightly to the equatorial plane of the body around which they revolve. Using the values of the oblateness parameters as given in Table 1, the apsidal motion $d\pi/dt$ was calculated for several of these satellites. The results are given in Table 2.

A direct comparison with observed data shows these results to be very accurate. Wollard (10) gives observed results for the Martian satellites Phobos and Diemos of 158.5 deg/Julian year and 6.54 deg/Julian year, which are very close to the predicted values in Table 2. However, if different values of the oblateness parameters are used for Mars, namely $J = 3.18 \times 10^{-3}$ and $D = 3.70 \times 10^{-5}$, which are within the limits of accuracy to which ϵ and m are known, values of $d\pi/dt = 158.5$ deg/Julian year and $d\pi/dt = 6.53$ deg/Julian year are obtained for Phobos and Deimos, respectively. This indicates that with the proper values for the oblateness parameters J and D the analytic and observed data are in nearly exact agreement for the Martian satellites. Brouwer (11) gives an observed result of 917.4 deg/Julian year for Satellite V of Jupiter, and Sampson (12) a value of 0.40 deg/Julian year for Satellite IV of Jupiter. The value for Satellite V is in excellent agreement with the predicted value in Table 2 (a difference of 0.4%), while that of Satellite IV reflects the increasing effect of the sun as the distance between the satellite and planet becomes larger.

It should be pointed out here that the expression for the apsidal motion given by Eq. 74 is a generalization of Brouwer's result which gives the motion of pericenter for a circular orbit. The result of this paper imposes no restriction on eccentricity other than its being less than 1. The result given in Brouwer's paper is

$$\frac{d\pi}{dt} = \left[J\left(\frac{R}{r_0}\right)^2 - \frac{J^2}{2}\left(\frac{R}{r_0}\right)^4 + \frac{6}{7} D \left(\frac{R}{r_0}\right)^4 \right] n_s \quad [75]$$

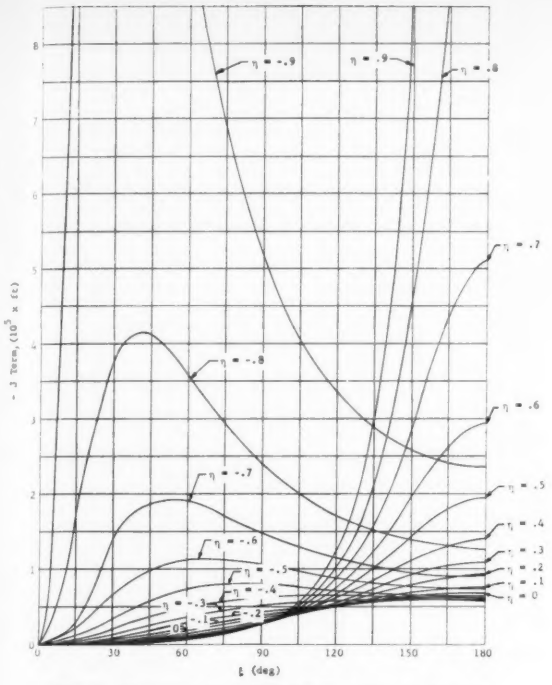

Fig. 1 Decrease in radial distance due to J term

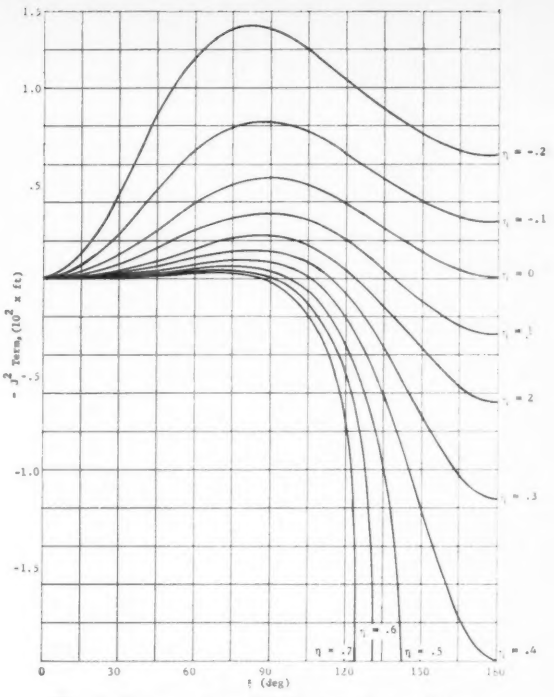

Fig. 2 Decrease in radial distance due to J^2 term

where the mean motion in an inverse-square force field n_s is given by

$$n_s = \frac{2\pi}{P_s} = \sqrt{\frac{\mu}{a^3}} = \sqrt{\frac{\mu(1-\eta)^3}{r_0^3}} \qquad [76]$$

and a is the semimajor axis.

It is not immediately obvious that Eq. 74 reduces to Eq. 75 for a circular orbit. However, noting that in this paper the mean motion is given by

$$n = \frac{2\pi}{P} = \left[1 - \frac{J}{1-\eta}\left(\frac{R}{r_0}\right)^2\right] n_s \qquad [77]$$

Eq. 74 for a circular orbit can be shown to be identical to Brouwer's result (cf. Appendix B).

Magnitudes of Different Order Terms

Figs. 1, 2 and 3 depict the effect of the Earth's oblateness on the radial distance. The effect of the different order terms over a wide range of eccentricities ($-0.9 \leqq \eta \leqq 0.9$) is shown for $r_0 = 21{,}330{,}010$ ft and $R = 20{,}926{,}010$ ft.

Conclusions

This paper presents an approximate analytic solution of the equation of the path of a particle in the equatorial plane of an oblate spheroid. The results, obtained in the form of power series in the oblateness parameters J and D, are correct to second order in the ellipticity.

The close agreement of the calculated and observed data

Table 2 Apsidal motion

Planet	Satellite	$\frac{r_0}{R}$	i	e	$\frac{d\pi}{dt}$ deg / Julian year
Mars:	Phobos	2.79	1°8′	0.021	155
	Deimos	6.93	1°46′	0.003	6.35
Jupiter:	V	2.54	27.′3	0.0028	921
	I	5.905	1.′6	~0	47.7
	II	9.401	28.′1	0.0003	9.36
	III	14.995	11.′0	0.0015	1.83
	IV	26.379	15.′2	0.0075	0.26
Saturn:	Mimas	3.11	1°31′	0.0196	485
	Enceladus	3.99	1.′4	0.0001	208
Uranus:	Ariel	7.35	~0	0.007	32.3
	Umbriel	10.2	~0	0.008	10.1

for the satellites of Mars and Jupiter indicates that the model closely approximates the physical situation.

A first-order result for the time t allows the position of the particle in the path to be determined at any time through numerical or graphical solution for Φ.

Appendix A

Apsidal Angle

The purpose of this appendix is to show that Tisserand's result for apsidal angle agrees with the result of this paper for $\Phi(\xi)$ obtained from Eq. 38 for a nearly circular orbit with $\xi = \pi$. Tisserand (7) gives the general result

$$\Phi = \frac{\pi}{\sqrt{1 - a(\Psi''/\Psi')}}\left[1 + \frac{a\delta^2}{48(\Psi' - a\Psi'')}\left(\frac{a\Psi''^2}{\Psi' - a\Psi''} + 3\Psi^{iv} - \frac{4\Psi''\Psi'''}{\Psi'}\right)\right] \quad [A\text{-}1]$$

as a power series in δ, where

$$\delta = \frac{r_\pi - r_0}{2r_\pi r_0} \quad [A\text{-}2]$$

$$a = \frac{r_\pi + r_0}{2r_\pi r_0} \quad [A\text{-}3]$$

$$\Psi' = \frac{2P(u)}{u^2} \quad [A\text{-}4]$$

and the prime indicates differentiation with respect to u. The above expression Eq. A-1 is evaluated at $u = a$. For the case of the oblate planet

$$P(u) = \mu u^2\,[1 + J(Ru)^2 + (3/7)D\,(Ru)^4] \quad [A\text{-}5]$$

to second order. For a nearly circular orbit, $\delta = (r_\pi - r_0)/2r_\pi r_0 = 0(J)$. It can also be shown that

$$\frac{1}{\Psi' - a\Psi''}\left[\frac{a\Psi'''^2}{\Psi' - a\Psi''} + 3\Psi^{iv} - \frac{4\Psi''\Psi'''}{\Psi'}\right] = 0(J^2) \quad [A\text{-}6]$$

Hence, to second order, Eq. A-1 becomes

$$\Phi = \frac{\pi}{\sqrt{1 - a(\Psi''/\Psi')}} \quad [A\text{-}7]$$

The derivatives in Eq. A-7 are given by

$$\Psi' = 2\mu[1 + J(Ru)^2 + (3/7)D\,(Ru)^4] \quad [A\text{-}8]$$

and

$$\Psi'' = 2\mu\,[2JR^2\,u + (12/7)DR^4\,u^3] \quad [A\text{-}9]$$

Using these expressions evaluated at $u = a = (r_\pi + r_0)/2r_\pi r_0$ yields

$$a\frac{\Psi''}{\Psi'} = \frac{r_\pi + r_0}{2r_\pi r_0}\left\{\frac{JR^2[(r_\pi + r_0)/r_\pi r_0] + (3/14)\,DR^4[(r_\pi + r_0)/r_\pi r_0]^3}{1 + JR^2[(r_\pi + r_0)/2r_\pi r_0]^2 + (3/7)\,DR^4[(r_\pi + r_0)/2r_\pi r_0]^4}\right\} \quad [A\text{-}10]$$

This can be reduced to

$$a\frac{\Psi''}{\Psi'} = 2\left(\frac{r_\pi + r_0}{2r_\pi r_0}\right)^2\left[JR^2 - J^2R^4\left(\frac{r_\pi + r_0}{2r_\pi r_0}\right)^2 + \frac{6}{7}\,DR^4\left(\frac{r_\pi + r_0}{2r_\pi r_0}\right)^2\right] \quad [A\text{-}11]$$

Expanding the denominator in Eq. A-7 gives the desired result for apsidal angle

$$\Phi = \left[1 + J\left(\frac{R}{r_0}\right)^2\left(\frac{r_\pi + r_0}{2r_\pi}\right)^2 + \frac{J^2}{2}\left(\frac{R}{r_0}\right)^4\left(\frac{r_\pi + r_0}{2r_\pi}\right)^4 + \frac{6}{7}\,D\left(\frac{R}{r_0}\right)^4\left(\frac{r_\pi + r_0}{2r_\pi}\right)^4\right]\pi \quad [A\text{-}12]$$

Now Eq. 37 with $\xi = \pi$ becomes

$$\Phi = \pi\left[1 + J\left(\frac{R}{r_0}\right)^2\frac{1}{c^4} + \frac{5}{2}J^2\left(\frac{R}{r_0}\right)^4\frac{1}{c^8}\left(1 + \frac{\eta^2}{6}\right) + \frac{3}{14}\,D\left(\frac{R}{r_0}\right)^4\frac{1}{c^8}(4 + 3\eta^2)\right] \quad [A\text{-}13]$$

$$= \pi\left[1 + J\left(\frac{R}{r_0}\right)^2\frac{1}{c^4} + \frac{5}{2}J^2\left(\frac{R}{r_0}\right)^4\frac{1}{c^8} + \frac{6}{7}\,D\left(\frac{R}{r_0}\right)^4\frac{1}{c^8}\right] \quad [A\text{-}14]$$

for a nearly circular orbit since $\eta = 0(J)$. To get this expression in terms of r_π and r_0, as is Tisserand's result, it is necessary to use Eq. 44 to first order

$$c^2 = \frac{2r_\pi}{r_\pi + r_0}\left[1 + \frac{J}{3}\left(\frac{R}{r_0}\right)^2\left(\frac{r_\pi^2 + r_0r_\pi + r_\pi^2}{r_\pi^2}\right)\right] \quad [A\text{-}15]$$

from which

$$\frac{1}{c^4} = \left(\frac{r_\pi + r_0}{2r_\pi r_0}\right)^2\left[1 - \frac{2}{3}J\left(\frac{R}{r_0}\right)^2\left(\frac{r_\pi^2 + r_\pi r_0 + r_0^2}{r_\pi^2}\right)\right] \quad [A\text{-}16]$$

and

$$\frac{1}{c^8} = \left(\frac{r_\pi + r_0}{2r_\pi r_0}\right)^4 \quad [A\text{-}17]$$

to zero order. Substituting these expressions into Eq. A-14 yields

$$\Phi = \pi\left[1 + J\left(\frac{R}{r_0}\right)^2\left(\frac{r_\pi + r_0}{2r_\pi}\right)^2 - \frac{2}{3}J^2\left(\frac{R}{r_0}\right)^4\left(\frac{r_\pi + r_0}{2r_\pi}\right)^2\left(\frac{r_\pi^2 + r_\pi r_0 + r_0^2}{r_\pi^2}\right) + \frac{5}{2}J^2\left(\frac{R}{r_0}\right)^4\left(\frac{r_\pi + r_0}{2r_\pi}\right)^4 + \frac{6}{7}\,D\left(\frac{R}{r_0}\right)^4\left(\frac{r_\pi + r_0}{2r_\pi}\right)^4\right] \quad [A\text{-}18]$$

Adding to A-18 the fourth-order term $J^2\left(\frac{r_\pi - r_0}{r_\pi}\right)^2\frac{\pi}{6}\left(\frac{R}{r_0}\right)^4\left(\frac{r_\pi + r_0}{2r_\pi}\right)^2$

which does not affect the second-order analysis, gives the result

$$\Phi = \pi\left[1 + J\left(\frac{R}{r_0}\right)^2\left(\frac{r_\pi + r_0}{2r_\pi}\right)^2 - 2J\left(\frac{R}{r_0}\right)^4\left(\frac{r_\pi + r_0}{2r_\pi}\right)^4 + \frac{5}{2}J^2\left(\frac{R}{r_0}\right)^4\left(\frac{r_\pi + r_0}{2r_\pi}\right)^4 + \frac{6}{7}\,D\left(\frac{R}{r_0}\right)^4\left(\frac{r_\pi + r_0}{2r_\pi}\right)^4\right] \quad [A\text{-}19]$$

$$= \pi \left[1 + J \left(\frac{R}{r_0} \right)^2 \left(\frac{r_\pi + r_0}{2r_\pi} \right)^2 + \frac{J^2}{2} \left(\frac{R}{r_0} \right)^4 \left(\frac{r_\pi + r_0}{2r_\pi} \right)^4 + \frac{6}{7} D \left(\frac{R}{r_0} \right)^4 \left(\frac{r_\pi + r_0}{2r_\pi} \right)^4 \right] \quad [A\text{-}20]$$

which is identical to Tisserand's result.

Appendix B

Apsidal Motion

The purpose of this appendix is to show that Eq. 74 for a circular orbit with the mean motion given by

$$n = \frac{2\pi}{P} = \left[1 - \frac{J}{1 - \eta} \left(\frac{R}{r_0} \right)^2 \right] n_s \quad [B\text{-}1]$$

is identical to Brouwer's result

$$\frac{d\pi}{dt} = \left[J \left(\frac{R}{r_0} \right)^2 - \frac{J^2}{2} \left(\frac{R}{r_0} \right)^4 + \frac{6}{7} D \left(\frac{R}{r_0} \right)^4 \right] n_s \quad [B\text{-}2]$$

The condition for a circular orbit, Eq. 57, to first order

$$\eta = c^2 - 1 = J \left(\frac{R}{r_0} \right)^2 \quad [B\text{-}3]$$

yields

$$c^2 = 1 + J \left(\frac{R}{r_0} \right)^2 \quad [B\text{-}4]$$

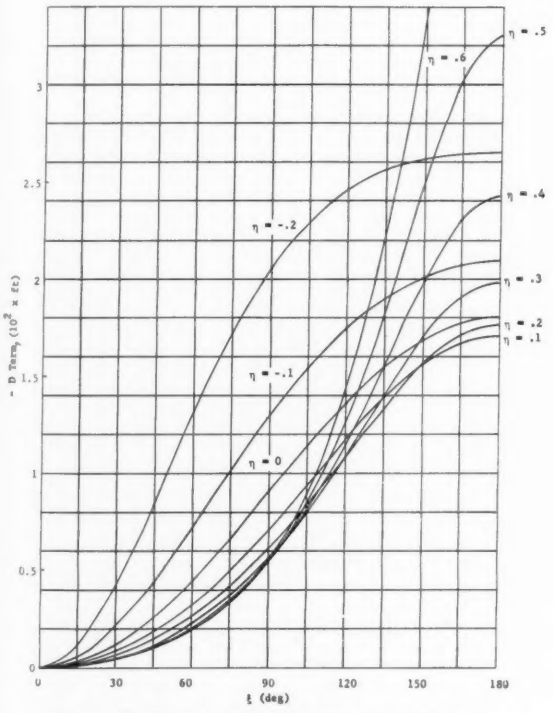

Fig. 3 Decrease in radial distance due to D term

Substituting Eqs. B-1 and B-4 into Eq. 74 yields

$$\frac{d\pi}{dt} = \left\{ J \left(\frac{R}{r_0} \right)^2 \left[1 - J \left(\frac{R}{r_0} \right)^2 \right]^2 + \frac{5}{2} J^2 \left(\frac{R}{r_0} \right)^4 + \frac{6}{7} D \left(\frac{R}{r_0} \right)^4 \right\} \times \left\{ 1 - J \left(\frac{R}{r_0} \right)^2 \left[1 + J \left(\frac{R}{r_0} \right)^2 \right] \right\} n_s \quad [B\text{-}5]$$

correct to second order. Performing the indicated operations yields

$$\frac{d\pi}{dt} = \left[J \left(\frac{R}{r_0} \right)^2 - \frac{J^2}{2} \left(\frac{R}{r_0} \right)^4 + \frac{6}{7} D \left(\frac{R}{r_0} \right)^4 \right] \quad [B\text{-}6]$$

which is identical to Brouwer's result.

Nomenclature

- e = eccentricity = $|\eta|$ for the nonoblate case
- G = Newton's universal gravitational constant
- g = gravitational acceleration at surface = μ/R^2
- g_c = centrifugal acceleration at surface = $\omega^2 R$
- h = angular momentum per unit mass (constant in this analysis)
- i = inclination of satellites orbital plane to the equatorial plane of the planet
- M = mass of the oblate spheroid
- r = radial distance to particle
- r_0 = radial distance to particle at initial apse
- R = equatorial radius of oblate spheroid
- R_p = polar radius of oblate spheroid
- v_c = $\sqrt{\mu/r_0}$, circular speed above a spherical body at $r = r_0$
- Φ = angular displacement from an apse
- μ = gravitational constant = GM
- ξ = independent variable used instead of Φ in eliminating secular items

A dot above a variable indicates differentiation with respect to time while a prime, unless otherwise stated, indicates differentiation with respect to ξ.

The subscript 0 refers to initial conditions, and s to results obtained for a spherically symmetric mass distribution.

References

1 Anthony, M. L. and Fosdick, G. E., "Planar Motions About an Oblate Planet," ARS JOURNAL, vol. 31, no. 9, September 1961.

2 Anthony, M. L. and Fosdick, G. E., "Escape in the Equatorial Plane of an Oblate Planet," Martin-Denver Research Rep., R-60-3, March 1960.

3 Jeffreys, H., *The Earth, Its Origin, History, and Physical Constitution*, 3rd ed., Cambridge Univ. Press, London, 1952.

4 King-Hele, D. G. and Merson, R. H., *Nature*, vol. 183, p. 881, March 1959.

5 Garfinkel, B., *Astronom. J.*, vol. 64, September 1959.

6 DeMoraes, D., "Effects of the Earth's Oblateness on the Orbit of an Artificial Satellite," *Anals de Academia Brasileira de Ciencias*, Vol. 30, Univ. of San Paulo, 1958.

7 Tisserand, F., *Traité de Méchanigue Céleste*, Gauthier-Villars and Son, Paris, 1889.

8 Allen, C. W., *Astrophysical Quantities*, Univ. of London Press, 1955.

9 Ehricke, K. A., *Space Flight*, Van Nostrand Co., Princeton, N. J., 1960.

10 Wollard, A. J., *Astronom. J.*, vol. 51, p. 33–36, 1944.

11 Brouwer, D., "The Motion of a Particle With Negligible Mass Under the Gravitational Attraction of a Spheroid," *Astronom. J.*, vol. 51, p. 223–231, 1946.

12 Sampson, R. A., "Theory of the Four Great Satellites of Jupiter," *Memoirs of the Royal Astronaut. Soc.*, Vol. 63, p. 1–270, 1921.

Recent Developments in Bio-Medical Instrumentation

H. L. WOLBERS[1]

Douglas Aircraft Company, Inc.
El Segundo Division
El Segundo, Calif.

This paper considers new techniques of sensing and analyzing physiological changes in human subjects. Bio-electronic recording techniques that have been developed to record the stress of pilots of high performance vehicles are described. These techniques have been used to supplement standard performance measurements in the evaluation of aircraft instrument displays. "Mini sensors" combining the sensing device (electrodes or energy transducers), signal amplification stages and an FM transmitter have been developed in packages smaller than 0.15 cu in. These units are used to transmit physiological changes over distances of 50 ft or more. It is suggested that body surface potentials from electrocardiac responses and/or electromyographic responses may be used as the primary power sources for miniaturized transmitters and receivers of bio-electronic information. The possibilities of improving the data analytic methods for processing physiologic measurements is illustrated by applying the techniques of frequency-amplitude-time pattern analysis used in the detection and classification of sonar returns to the description and analysis of sound patterns obtained from phonocardiac records of humans. Using the sensing and data analysis techniques developed to date, a "quickened" system for controlling human effectiveness is suggested wherein information on cellular changes, tissue changes, organic changes, body system changes, environmental control functions and task performance may be used to establish the relationship between the work capacity of and the work load on the individual operator.

FOR THE past seven years the Douglas Aircraft Co. has been engaged in a research program to develop a simplified form of information presentation for the operators of complex man-machine systems. The program was initiated when the Navy became concerned with the excessive demands being placed on pilots in the operation of high performace aircraft.[2] These operational work loads were approaching the level at which the human could no longer react and respond effectively. It was evident that ways had to be found to unburden the pilot, minimize stress, and delay the onset of fatigue.

It was observed that in many cases the accuracy with which a pilot could fly a flight simulator in the laboratory was relatively constant from one form of instrumentation presentation system to another. The usual performance measures, such as root mean square (rms) tracking error and accuracy of altitude or attitude control, did not reflect statistically significant performance differences. The subjects did, however, have definite opinions as to their likes and dislikes, or in their beliefs that they were working harder with one display configuration than with another. Since subjective opinion is unreliable, it was desired that a more objective index of effort, or fatigue, or stress, be determined.

In reviewing the past work on fatigue and allied phenomena, one general conclusion of investigators in the field (borne out by the simulation studies mentioned above) has been that neither fatigue nor impairment of organic functioning can be measured entirely by the work output of the "intact" organism. Activity may be used as a direct measure of impairment only when such systems as isolated nerve muscle preparations are used in ergographic studies. In these cases very definite indications of change in such parameters as muscle potentials can be demonstrated between a relaxed and active state. When considering the entire organism, however, investigators generally have found it necessary to distinguish among: 1) the physiological impairment of tissues; 2) the psychological aspects of fatigue; and 3) the changes in the work output of the integrated organism. These three factors, fatigue, impairment, and work output, are semi-independent variables. The experience of fatigue may arise either through impairment as an immediate after effect of exercise or as a conditioned feeling of boredom, distraction or other conflict.

One of the astonishing things is the extent to which the human organism can continue to perform adequately under extremely unfavorable conditions. Accordingly, it was decided that performance criteria be supplemented with indices of physiological and psychological change.

It was known that emotion is characterized by many combinations of bodily change, and it seemed that perhaps some of the more psychological aspects of fatigue might also be indicated from measures of autonomic activity. Fortunately, all body functions can be measured directly as potential changes, or can be converted to electrical form by the use of proper transducers. Some phenomena, such as brain waves, muscle potentials, galvanic skin responses, electrocardiograms, and eye blinks, can be measured directly as electric potentials. Other phenomena, such as skin temperature, can be transduced to electrical form by means of thermocouples. In similar fashion, respiration and blood pressure can be transduced

Presented at the ARS 15th Annual Meeting, Washington, D. C., Dec. 5–8, 1960; revision received July 5, 1961.

[1] Chief, Equipment and Safety Research.

[2] This effort is currently sponsored by the Office of Naval Research and the Army Signal Corps, Contract Nonr 1076(00).

by microphones and strain gages. Emphasis was placed on the use of direct bio-electronic measures in view of their advantage in minimizing the latent response time of the recording system. Physiologic factors initially considered were: electromyographic responses; galvanic skin response; plethysmographic responses (blood pressure and volume); the electro-cardiogram and heart rate; respiration rate; and skin temperature.

Development of Sensing Techniques

In the early studies conducted at Douglas, electrodes and other sensors on the subjects were wired to graphic recording devices. A portable data-recording cart was developed to give greater flexibility to the equipment, permitting it to be easily moved from one location to another. Initial studies, wherein the tasks assigned involved measuring physiologic responses during a graduated series of pencil and paper problems, gave very encouraging results. The next step was to place the individual in a dynamic simulator (Figs. 1 and 2) and present a series of tracking tasks which increased in difficulty level. To give the most faithful replication of waveform, d-c amplifiers were used, and the data was fed to tape recorders and/or graphic recorders. In some cases, analog computing equipment was used to integrate tracking errors and physiologic changes over a given time period. Respiratory rate, for example, was integrated on a cycle by cycle basis. Digital voltmeters were used to transform information from analog to digital form, and digital printouts were used for data processing.

Conventional sensors left much to be desired. In particular, the wiring harness was unwieldly and distracting to the subject. Accordingly, using some of the more advanced techniques of circuitry design and packaging, small integral units consisting of a sensor, amplifier and FM transmitter were designed. These so-called *mini sensors* could be readily attached to the subject to detect bio-electronic changes and transmit them to a remote receiver 50 ft or more away. The sensor transmitter unit occupied a volume of less than 0.15 cu in. At the present time, work is underway in the calibration and validation of these sensing devices. Early results look very promising.

The development of improved sensing techniques also permits extending the range of sensitivity for analytic purposes. As an example, in the investigation of heart sounds it was found that valuable information could be obtained from the very low sound frequencies. These were the sounds most characteristically associated with the muscle operation. On examining the threshold of audibility, it is found that the ear by itself cannot hear much of the vibratory spectrum of the heart (Fig. 3). Through the use of special microphones these unheard sounds can be detected and displayed to the medical diagnostician in a more usable form.

Development of Data Processing Techniques

Concurrently with the development of sensing devices, effort is also being expended toward applying the data processing techniques used in engineering studies to the faster analysis of physiologic data. The manual reduction of data from physiologic records is a tedious and time consuming task. In laboratory simulation and flight test work, the effective use of the data gathered is considerably reduced unless it can be made available in meaningful form in a very short time.

The area of cardiac disorders might be considered as an example of the possibilities in improving the analytic techniques for processing physiologic measurements. In a study at Douglas, an attempt was made to apply the same techniques of frequency-amplitude-time pattern analysis used in the detection and classification of sonar returns to the

Fig. 1 Dynamic simulator

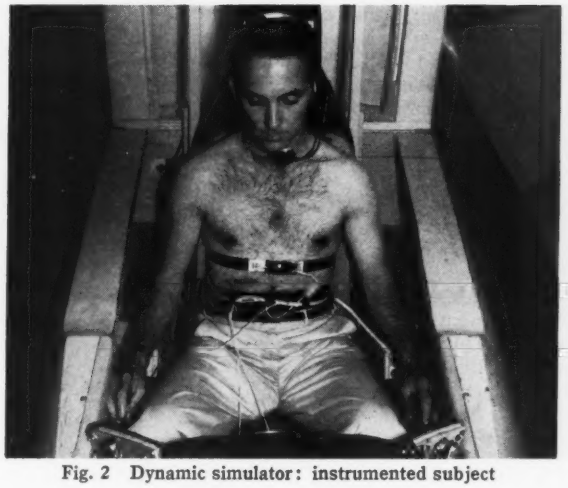

Fig. 2 Dynamic simulator: instrumented subject

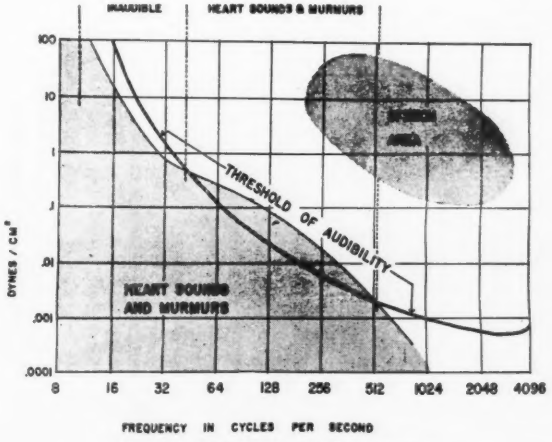

Fig. 3 Threshold audibility curve

description and analysis of sound patterns obtained with phonocardiac pickups on human subjects.

Standard demonstration magnetic tapes of various cardiac disorders were obtained from the American Heart Association. To illustrate the approach taken, consider a presystolic gallop and a pericardial rub. The envelopes of the sound wave pattern of each of these disorders are very similar (Fig. 4). If one were to listen to them they would sound very much the same, since both have a characteristic rhythm reminiscent of a horse galloping. If these complex wave forms are sent through a series of band pass filters and a rough frequency analysis performed, certain differences in the composition of the sound structure become evident. The presystolic gallop has a heavy loading of frequencies in the 50 to 125 cycle range, whereas the pericardial rub has a heavy loading of frequencies in the 100 to 200 cycle range (Fig. 5). The frequency patterns suggest one way of differentiating between the disorders. When frequencies, amplitudes, and time relationships are considered, it becomes possible to develop logic circuits which can trigger a particular display for a given response pattern. Thus, the diagnostician using this approach to data analysis could be provided much more information than he is now able to obtain with conventional recordings.

A feasibility unit was developed wherein several of the disorders, i.e., systolic murmur, diastolic murmur, presystolic gallop and pericardial rub, could be distinguished from normal heart sounds. Much more study and data analysis would be required of normal and abnormal heart conditions under controlled conditions before these analytic techniques could be validated. The important point, however, is the great promise demonstrated for analytic techniques used in engineering and the physical sciences to be directly applied to medical research.

Development of Display Techniques

Another major area requiring engineering development is the problem of the display of the data obtained. The objective of improving displays is to present the data being processed in a form that can be most readily interpreted and understood by the attending research personnel.

Conventional techniques usually involve direct writeout devices such as pen recorders. First order improvements can be made by computing and displaying integrated signals, rms errors or digital readouts (Fig. 6). The ultimate display, however, must be a device providing information in an even more meaningful form than digital readouts to the researcher or to the diagnostician. When given temperature, blood pressure, EKG, etc., at the present time, the physician must, through analysis, attempt to logically process this information and make a diagnosis from the various symptoms observed. Some delay in analysis and information presentation may be tolerated in the clinical case, but in monitoring the performance of individuals being subjected to stressful conditions, such as test pilots or astronauts in space capsules, a real time analysis and data presentation system is needed. Not only would it be desirable to have an immediate index of the individual's work capacity in these situations, but it would be even better to have a prediction of his work capacity for some time in the future, seconds, minutes or hours away. Fig. 7 illustrates one proposed configuration, called a Bio-Electronics Surveillance System, which might provide an integrated station receiving transduced and transmitted physiologic data from remote sources, processing the data, and providing a continuous up to date, second by second analysis of the physiological state of the individual being monitored.

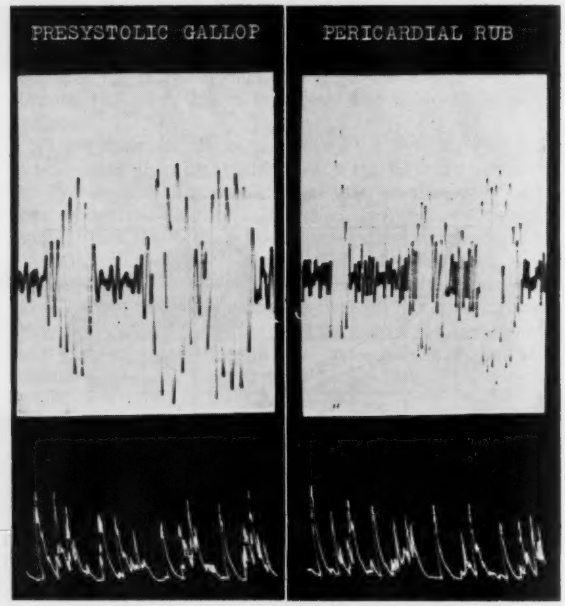

Fig. 4 Standard phonocardiographic presentation with rectified display

System for Monitoring Performance

Physiology teaches that each of the parts of the human body function, not in isolation, but as a highly interrelated and interdependent organizational structure. The outstanding trait of the human body is the mutual dependence within it of part on part, organ with organ. This interrelationship is achieved mechanically and by connective tissues, and it is also achieved through the actions of the chemical agencies such as the endocrine glands (the thyroid, parathyroid, pituitary, et al.). The balance of the correct relations among the elements of the body is achieved on a knife edge. An infinitesimal imbalance in the endocrine glands, for example, can result in a misshapen skeleton or an idiot. By the same token, any environmental change can, over an extended period of time, have as radical a set of consequences on man's ability to function as an effective component of the man-machine system. Although these comments are related to the monitoring of man's performance in advanced systems, the same problems are faced daily by the medical diagnosticians.

In monitoring man's performance, two classes of information are required: descriptive information and predictive information. In the case of the medical practitioner, all available information describing the state and past history of the patient is taken during the examination and, from this information, an attempt is made to diagnose the disorder. From the descriptive diagnosis, therapeutic action which the physician predicts will correct the malfunction is taken. In the case of a man operating in an unusual or extraterrestrial environment, the same problems of description and prediction are encountered. It is necessary to adequately describe his present state, and from this description it is desired to predict the effect at some future time (perhaps seconds, perhaps hours away) which his current status will have upon his personal well-being and upon his capacity to function effectively as an integral part of any man-machine system.

In attempting to describe the physiological reactions of mammals, or in attempting to develop predictive devices, the investigator is faced with a complex of contradictory and paradoxical phenomena. Respiratory rate can increase with exercise or with inactivity. The heart rate and cardiac output can increase while the blood flow in a given region increases, decreases, or remains the same. The glucose concentration of the blood may rise while the carbohydrate reserves are being augmented or depleted. Behind all of

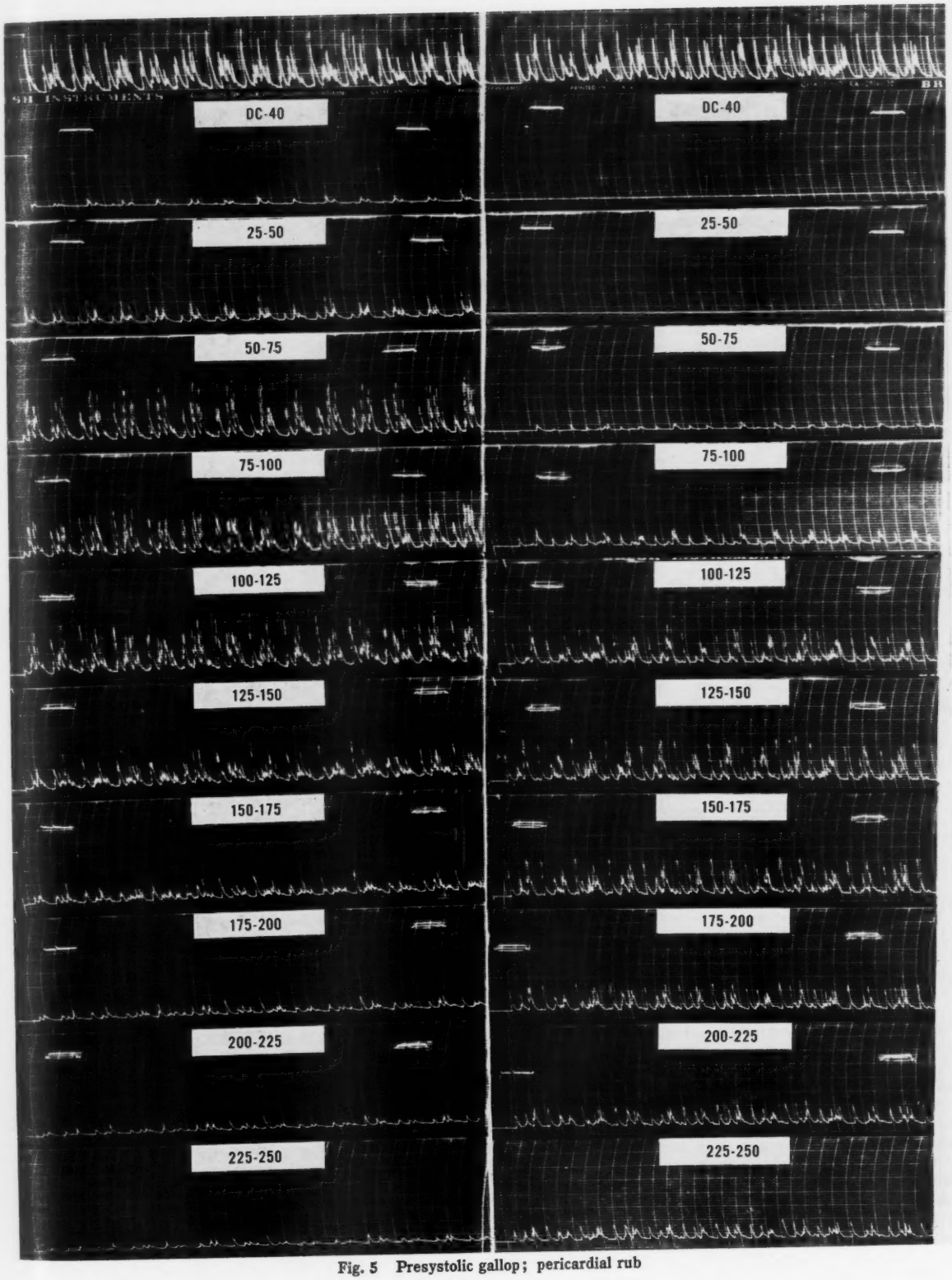

Fig. 5 Presystolic gallop; pericardial rub

DIRECT WRITEOUT:

THE DIRECT PEN-TYPE WRITEOUT OF "RAW" PHYSIOLOGICAL RESPONSE DATA IS PRESENTLY FOUND IN MOST LABORATORIES. HOWEVER, THIS APPROACH INVOLVES TEDIOUS INFORMATION EXTRACTION TECHNIQUES OR SUBJECTIVE DATA INTERPRETATION.

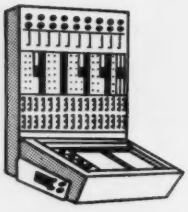

COMPUTED WRITEOUT:

THE USE OF A COMPUTER PERMITS A WRITEOUT OF DATA WHICH IS AT LEAST PARTIALLY PROCESSED, DIGESTED, AND RENDERED INTO A MORE IMMEDIATELY MEANINGFUL AND USEFUL FORM.

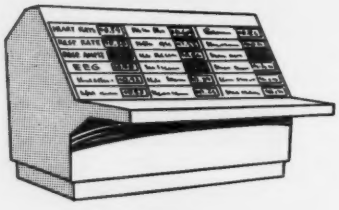

DIGITAL READOUT:

SPECIFIC PHYSIOLOGICAL MEASURES CAN BE ANALYZED AND PRESENTED AS INSTANTANEOUS VISUAL READOUTS AND PRINTOUTS. A STANDARD SCORE TYPE OF PRESENTATION MAY BE USED WITH COLOR CODING (VARIABLE COLOR BACK-LIGHTING) TO HELP INDICATE EXTREME DEVIATION.

FUNCTIONAL READOUT:

THE RESPONSES OF A PHYSIOLOGICAL FUNCTION OR ORGAN SYSTEM (I.E. CARDIOVASCULAR) MAY BE ANALYZED AND COMPARED WITH THAT WHICH IS NORMALLY EXPECTED AND THAT WHICH IS FOUND UNDER CERTAIN CONDITIONS OF STRESS, MALFUNCTION, OR DISEASE. IF CERTAIN CRITICAL SIGNS OR SCORES ARE FOUND, THE APPROPRIATE PRE-PROGRAMMED MESSAGE DISPLAY UNITS ARE THEN ENERGIZED.

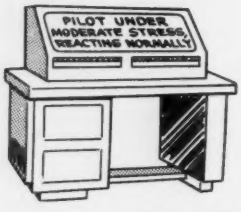

INTEGRATED DISPLAY:

A MORE SOPHISTICATED BIO-ELECTRONIC SYSTEM CAN BE ENVISIONED WHICH WOULD BE ABLE TO EVALUATE THE RESPONSES OF SEVERAL PHYSIOLOGICAL FUNCTIONS OR ORGAN SYSTEMS IN RELATION TO THE ENVIRONMENTAL CONDITIONS TO WHICH THE ORGANISM IS EXPOSED. A COMPARATIVELY FLEXIBLE MESSAGE DISPLAY UNIT (OR EVEN A PICTORAL ANALOG) WOULD PRESENT THE FINAL EVALUATION OF THE TOTAL SITUATION FOR THE INFORMATION AND ACTION OF THOSE CONCERNED.

Fig. 6 Development trends in bio-electronic display devices

these phenomena, however, are the homeostatic aspects of the body's regulatory mechanisms. The internal body temperature remains fixed, although the temperature of the external environment can vary considerably. Consequently, the thermo-dependent reactions of cells are protected from external changes. The acidity of the blood remains remarkably constant. A slight shift toward acidity would result in coma and death; a shift toward greater alkalinity would produce convulsions. The bloods of the various animals are closely similar in their ionic compositions, pH, and glucose concentrations. These facts suggest that the conditions under which life is possible are very restricted and have not changed substantially since life first began. The criticality of the proper body functioning is indicative of the difficulty to be encountered in detecting or sensing changes when the monitoring of human performance is desired.

There is a great deal in common between monitoring, describing, and predicting behavior in the operational sense, and describing and predicting the results of therapy in the clinical sense. In the former case, typical of performance evaluation as well as preventive medicine, it is desired to deal with individuals functioning normally, and it is desired that they be kept that way. In the latter case, individuals are considered who are in an abnormal state and wish to be returned to a normal condition. The data processing and display problems are very much the same. The measurement or sensing problem is considerably more difficult, however, in the case of monitoring normal individuals. Here, observed variations or variations from a population mean may or may not be perfectly normal for the individual concerned. Furthermore, symptoms are not causes. Measuring symptoms removes the diagnostician one step further

from the cause. To understand and control performance it becomes necessary to investigate the underlying cause, and this implies eventually going into the cellular structure itself. Microsensors may ultimately permit this.

In a recent project at Douglas, a team of specialists examined this problem under a small study contract with the Navy.[3] As a portion of this effort, a survey was conducted of some 38 aero-space medical specialists throughout the country to attempt to determine what the "experts" felt should be measured. It was interesting to note that each of the measurable physiological parameters or group of parameters had proponents among the people interviewed. Parameters suggested to be measured were respiratory rate (amplitude and rate change), index ratio, changes in alveolar ventilation, heart rate, plethysmograph, phonocardiographic signature, electro-cardiograph, blood pressure, pulse pressure, electroencephlograph, skin and body temperatures, electromyographic potentials, color discrimination, electrooculargram, blood O_2 saturation.

This much is certain, the development of a satisfactory system to predict behavior is predicated upon the ability to measure bodily change. Furthermore, the complexity of the interactions of the autonomic nervous system, the cerebrospinal system, and the endocrine glands, makes it clear that there is a long way to go before being able to measure bodily change in a definitive and exhaustive way. Effort must be made to develop procedures reasonably representative of the activity of the organism as a whole.

The concept of homeostasis was referred to earlier as the self-regulation of all of the bodily functions to maintain a steady state condition. When stability is threatened, even slightly, delicate indicators give the alarm and activate the appropriate corrective agencies, so that oscillations to either side of the homeostatic norm are slight. The effector organs react as if they were directed toward nullifying a disturbing condition. When bodily security or survival is seriously threatened, the internal fluid matrix is altered. If noxious stimili occur, such as bacteria, toxic drugs, or physical damage, the organism responds by altering the proportions of the protective white blood corpuscles, by augmenting the protective antibodies, and by elevating the body temperature. If perceptible foes arouse fear or rage, a number of internal readjustments unify and integrate the activities of the body for its maximal physical effort, flight or combat: blood sugar is increased; the circulation to special regions is greatly augmented; respiration is accelerated; extra red blood cells are mobilized to carry the extra oxygen; and adrenalin is produced to reinforce the adaptive nerve impulses.

These reactions may seriously disturb the internal environment, but they disturb it in such a way as to render the organism temporarily more effective in a contest that may end in life or death. The ultimate total stability of the organism is therefore defended, even at the cost of temporary disturbance to the welfare of its component parts. Environmental changes that affect the body affect the brain, which directs the activities of one or more of the body systems. The system responses structure, and are structured by, the organ responses which, in turn, place demands on the tissue structure which, in turn, requires cellular responses. Furthermore, the response of each stage in the body mechanism to some initial environmental change or stressful condition or work overload situation takes a finite amount of time. These factors influence or limit the manner in which information can be meaningfully displayed. The typical approach is to measure and display either environmental changes directly or record gross physiological changes, such as, skin resistance, blood pressure, blood flow and blood volume, respiration, temperature, et al., and infer body state or environmental changes from these measures. These measures by themselves are after the fact. If the causal factor is environmental change, then the damage is done before corrective action can be taken. What is actually required is the same type of "quickened" display that has been found so useful in higher order control systems with many required integrations.

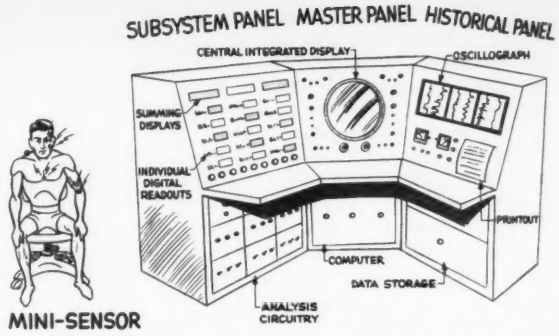

Fig. 7 Proposed bio-electronic surveillance system

In control dynamics, a quickened display is considered as one wherein the operator is provided with immediate knowledge of the results of his own control actions before they become available from sensing the system's actual output. Fig. 8 schematically describes a quickened display. The moving indicator on the display X_d represents the scan of the machine output X_m and its derivations. X_d is obtained by placing feedback loops from the machine output and each of its own derivatives back to the display. In a perfectly quickened system, the display tells the operator where to position his control. It shows what he should do with his control, but not the actual state of the system. One note of caution, however: a quickened display is not sufficient by itself, since the operator or monitor must know not only what he should do, but what the current system state is.

As an example of the need for quickened displays in some man-machine systems, consider the case of a submarine. In the older fleet type submarines, the position of the planesman's control directly affects the rate of change of the control surface (diving plane); the control-surface angle directly affects the acceleration of pitch; and pitch directly affects the rate of change of depth. Hence, the planesman is actually controlling the fourth derivative of depth. This is known as a "fourth order" control system.

Ideally there should be one term in the quickened display for each order of the control system. In some systems, such as certain types of guided missiles, it is impossible to sense directly some of the derivatives of output, and it is extremely difficult to obtain these derivative measures indirectly by such means as differentiating the output or installing rate gyros. Such systems cannot be fully quickened, but it has still been found advantageous to partially quicken the system to as great a degree as possible. The closer the feedback items can be to the machine output, the better the accuracy, assuming no intervening terms are skipped. Drawing an analogy with the quickened display system, it would seem

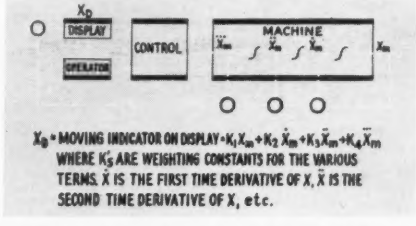
X_D
DISPLAY
OPERATOR
CONTROL
MACHINE
X_m
X_D = MOVING INDICATOR ON DISPLAY = $K_1X_m + K_2\dot{X}_m + K_3\ddot{X}_m + K_4\dddot{X}_m$
WHERE K_S ARE WEIGHTING CONSTANTS FOR THE VARIOUS TERMS. $\dot{X}$ IS THE FIRST TIME DERIVATIVE OF X, $\ddot{X}$ IS THE SECOND TIME DERIVATIVE OF X, etc.

Fig. 8 Generation of a quickened display

[3] Contract N123-(61756)24946A(PMR).

reasonable to propose a real time performance monitoring console, which would provide the monitor with sufficient information that appropriate corrective action to reduce the demands on the operator could be taken before an overload condition arises. For any mission it is to be expected that the operator's work capacity will decrease with time as a function of fatigue or continuing stress (Fig. 9). On the other hand, the work load will fluctuate on a time base in accordance with the requirements of the mission. When the work load approaches or exceeds the work capacity of the operator, a critical point in the success or failure of the mission arises. A quickened system (Fig. 10) for controlling operator effectiveness might be proposed wherein information on cellular, tissue, organic, body system, environmental control functions, and task performance would be fed back with proper weighting of each term to the monitor's display console. This master display console would describe and predict the relation between work capacity and work load on the individual operator. A major step forward in the development of a "real time" display could be taken by feeding as much as possible of the derivative information back to the central display.

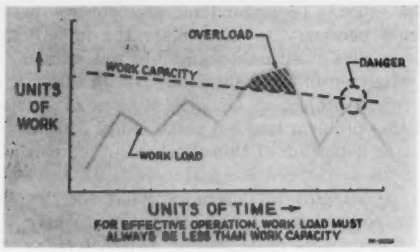

Fig. 9 Work load vs. work capacity

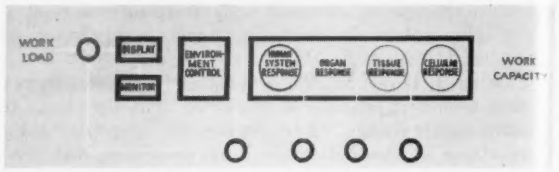

Fig. 10 A quickened system for controlling operator effectiveness

Conclusion

While the original orientation of the work which has been described in this paper has been directed toward developing techniques for measuring the physiological impairment of tissues, the psychological aspects of fatigue and the changes in the work output of the integrated organisms, it is believed that the bio-medical sensing devices, data processing techniques and bio-medical display devices have wide applicability to medical and psychological research.

Another vast area, wherein new developments from the electronic industry can make major contributions, is the field of stimulus generation. With the advent of miniaturized components, it now becomes feasible to develop remotely controlled, implanted, stimulus generators capable of stimulating end organs upon command. Applications to such devices as defibrillators and cardiac pacemakers are obvious.

The exceedingly low power requirements (0.01 w or less) of microcircuitized components, whether transmitters or receivers, suggest the fascinating possibility of using body surface potentials from EKG's and EMG's as the primary power sources. The concept of the self-winding watch might well be applied to the activation of bio-electronic devices.

By the very nature of its basic area of interest, the American Rocket Society is concerned with developing the methods and techniques for extending man's domain into space. With such tremendous achievements at his fingertips, we must not forget that man is a fragile thing. On any absolute physical scale, the deviations which man can tolerate in the temperature, pressure, and gas composition found in his normal terrestrial environment are infinitesimal.

To meet the challenge of the future, better sensing devices, data processing techniques and information displays are necessary. As knowledge of man increases with advances in research and as better instrumentation for man is developed, we will be able to use him more effectively in the exotic systems of the future.

Selected Bibliography

1 Catton, W. T., *Physical Methods in Physiology*, Philosophical Library, New York, 1957.

2 Dempsey, E. W., "Homeostasis," Chap. 6 in *Handbook of Experimental Psychology*, S. S. Stevens (ed.), John Wiley & Sons, Inc., New York, 1951.

3 Eason, R. G., "An Electromyographic Study of Impairment and Estimates of Subjective Effort Associated with Voluntary Muscular Contractions," R and D Rep. 898, Navy Electronics Laboratory, San Diego, Calif., May 1959.

4 Ely, J. H., Bowen, H. N. and Oelansky, J., "Man-Machine Dynamics," WADC Tech. Rep. 57-582, November 1957.

5 Glassner, H. F. and Peters, G. A., "Effects of Mental Task Difficulty on Physiological Response," Engng. paper no. 848, El Segundo, Calif., Douglas Aircraft Co., August 1959.

6 Glassner, H. F. and Peters, G. A., "Bio-Electronic Analysis of Performance," Engng. paper no. 897, El Segundo, Calif., Douglas Aircraft Co., presented at the Aerospace Medical Assn., Miami, Florida, May 9, 1960.

7 Grings, W. W., *Laboratory Instrumentation in Psychology*, The National Press, Palo Alto, Calif., 1954.

8 Lindsley, D. B., "Emotion," Chap. 14 in *Handbook of Experimental Psychology*, S. S. Stevens (ed.), John Wiley & Sons, Inc., 1951.

9 Mayo, A. M. and Wolbers, H. L., "Applications of the Army-Navy Instrumentation Program to Transport Aircraft," Engng. paper no. 969, El Segundo, Calif., Douglas Aircraft Co., presented at the Annual Meeting of the Soc. of Automotive Engrs., Los Angeles, Calif., Oct. 10–14, 1960.

10 Randall, J. E., *Element of Biophysics*, The Year Book Publishers, Chicago, Ill., 1958.

11 Whitfield, I. C., *Electronics for Physiological Workers*, MacMillan & Co., Ltd., London, 1959.

Optimum Conditions for Photosynthesis in Optically Dense Cultures of Algae[1]

A. G. FREDRICKSON[2]
A. H. BROWN[3]
R. L. MILLER[4]
H. M. TSUCHIYA[5]

University of Minnesota
Minneapolis, Minn.

The efficiency of use of radiant energy by cultures of algae is defined, and the physical variables upon which the efficiency depends are introduced. Expressions for the efficiency in a rectangular growth chamber are derived from considerations of an assumed mechanism of photosynthesis, the rate of respiration, and the conditions of agitation in the culture. Both unstirred and completely stirred cultures are considered. From the equations for efficiency in the two cases, methods are developed for finding the optimum physical conditions of light intensity, population density, length of light path, and temperature under which to propagate algae. In the unstirred culture, the treatment shows that a low light intensity is required; in the completely stirred culture, the treatment shows that a very high light intensity is required. The calculated efficiency is somewhat higher in the completely stirred case.

THE CHEMISTRY and mechanism of the photosynthetic reaction have been the subjects of intense study; particular attention has been given to photosynthesis in the microscopic algae and has led to the view that an algal culture may support the demand of animal life for oxygen and foodstuffs in a space vehicle or space station. It is the purpose of this paper to develop an approximate method for the optimum design of such extraterrestrial life support systems.

General Features of Photosynthesis in Algal Cultures[6]

The rate of photosynthesis in an algal cell is strongly influenced by the intensity of light incident upon the cell and by the availability of carbon dioxide, as well as other nutrients. At low light intensities, the rate increases with increasing intensity; at higher intensities, the rate becomes light saturated (1).[7] The rate shows a similar dependence on the concentration of carbon dioxide near the cell. We assume in this paper that the rate is carbon dioxide saturated, so that the concentration of carbon dioxide is eliminated as a variable.

It is impossible to establish a uniform light intensity in a culture of algae. If the intensity is high near a light source, it will be low far from a source because of absorption and scattering of light by the culture. Hence, the rate of photosynthesis will be different in different regions of the culture. It has been repeatedly conjectured (2,3) that turbulence in an optically dense[8] algal culture will increase the efficiency of light utilization by photosynthesis. This conjecture is based presumably on the so-called *flashing light effect.*

Flashing light effects arise, presumably, from the fact that photosynthesis does not cease the instant that light is removed, but continues until the energy absorbed in previous light periods has been used. In a turbulent, optically dense culture, individual algal cells are subjected to a pattern of light and darkness; hence, one may expect the flashing light effect to influence the overall rate of photosynthesis, provided the time scale characterizing the turbulent motion of algal cells is of the right order of magnitude. Experimentally, Davis et al. (4) found that turbulence can indeed increase the *rate* of photosynthesis; whether or not it can materially increase the *efficiency* of photosynthesis is one of the questions which this paper will attempt to answer.

Kinetics of the Photosynthetic Reaction

Discussions of the mechanism of photosynthesis and its allied reactions have been given by Tamiya (5), Hill and Whittingham (6), Rabinowitch (1), Kok (3), and Lumry and Rieske (7). The simplest mechanism proposed by Lumry and Rieske is

$$T \xrightarrow{k_{L'I}} T^*$$

$$T^* \xrightarrow{k_{D'}} \{OH\} + \{H\} + T$$

$$\{H\} + \text{Oxidant} \xrightarrow{\text{fast}} \text{Reduced Oxidant}$$

$$\{OH\} \xrightarrow{\text{fast}} O_2 + H_2O \qquad \ldots\ldots [1]$$

Received July 31, 1961.
[1] This work was supported by NASA, Contract No. NAS w-70, grant no. Ns G 79-60.
[2] Assistant Professor, Department of Chemical Engineering.
[3] Professor, Department of Botany.
[4] Research Fellow, Department of Chemical Engineering.
[5] Associate Professor, Department of Chemical Engineering. Member ARS.
[6] Much of this material is taken from the book of Rabinowitch (1) and an article by Myers (2).
[7] Numbers in parentheses indicate References at end of paper.
[8] That is, a culture which absorbs a significant part of the light incident upon it.

In this scheme T represents a *trapping center* for excitation energy—an assemblage of pigment molecules or an enzyme associated with such an assemblage which absorbs excitation energy. A plant reactant, which may be a water molecule associated with some acceptor molecule, forms a reducing agent {H} and an oxidizing agent {OH} upon reception of excitation energy. The oxidizing agent forms water and molecular oxygen by a series of fast reactions; the reducing agent is fed into a cycle of biochemical reactions such as those described by Bassham and Calvin (8). The end products of the photosynthetic reaction are of course molecular oxygen and new cellular material. Rieske, Lumry, and Spikes (9) found that kinetic expressions derived from the above mechanism described the rate of the Hill reaction, i.e., the reduction of certain oxidizing agents, such as ferricyanide, by chloroplast fragments in the presence of light. However, the situation prevailing in algal photosynthesis is probably more complicated than indicated by Eq. 1; thus, one fault of the mechanism is its failure to take explicit account of the effect of light color. Again, the rate of photosynthesis is influenced by the physiological condition of algal cells. Hence, the equations which we derive are only a first approximation to the true situation which obtains.

Let $[T_i^*]$ and $[T_i]$ be the molar concentrations of excited and unexcited trapping centers in the ith cell of a culture of algae. If T_{i_o} is the total molar concentration of trapping centers in the ith cell of a culture, then the rate of formation of excited trapping centers in the ith cell is

$$\frac{d[T_i^*]}{dt} = k_L' I_i [T_i] - k_D' [T_i^*]$$
$$= k_L' I \{T_{i_o} - [T_i^*]\} - k_D' [T_i^*] \qquad [2]$$

where I_i is the intensity of light incident upon the ith algal cell at time t, and k_D' and k_L' are rate constants for photosynthesis which are based on unit volumes of cells.

At this point the kinetic treatment of photosynthesis must depart from the usual methods, that is, the assumption of a steady-state concentration of activated molecules. If there is any movement[9] of the algal cells, the light intensity I_i seen by the ith cell will not be independent of time, and no steady state of reaction is possible. Hence, one must solve the unsteady state Eq. 2.

The general solution of Eq. 2 is readily found to be

$$[T_i^*] = k_L' T_{i_o} \exp(-[k_D' + k_L' \bar{I}_i(t)]t)$$
$$\int_0^t I_i(\tau) \exp([k_D' + k_L' \bar{I}_i(\tau)]\tau)\, d\tau +$$
$$K \exp(-[k_D' + k_L' \bar{I}_i(t)]\, t) \qquad [3]$$

where K is a constant of integration, τ is a dummy variable of integration, and

$$\bar{I}_i(t) = 1/t \int_0^t I_i(\tau) d\tau \qquad [4]$$

Clearly, the quantity $\bar{I}_i(t)$ is a kind of time-average[10] light intensity seen by the ith algal cell in its travels through the culture. For the present, the time t is left unspecified.

The rate of the photosynthetic reaction per unit volume of the ith algal cell is

$$R_{i_p}(t) = k_D' [T_i^*] \qquad [5]$$

whence from Eq. 3 one has

$$R_{i_p}(t) = k_D' k_L' T_{i_o} \exp(-[k_D' + k_L' \bar{I}_i(t)]t)$$
$$\int_0^t I_i(\tau) \exp([k_D' + k_L' \bar{I}_i(\tau)]\tau) d\tau +$$
$$R_{i_p}(0) \exp(-[k_D' + k_L' \bar{I}_i(t)]t) \qquad [6]$$

[9] This may even include rotations of algal cells. However, we ignore the effects of rotation.

[10] A single bar over a quantity indicates the time-average of that quantity.

It is of interest to investigate the time scale required for changes in the light intensity to be felt in the rate of photosynthesis. This time scale can be established from Eq. 6. Thus, if the ith cell is subjected to a step change in the light intensity, one finds

$$\frac{R_{i_p}(t) - R_{i_p}(\infty)}{R_{i_p}(0) - R_{i_p}(\infty)} = \exp[-(k_D' + k_L' I)t] \qquad [7]$$

where

$$R_{i_p}(\infty) = \frac{k_D' k_L' T_{i_o} I}{k_D' + k_L' I} \qquad [8]$$

is the steady rate of photosynthesis approached as the intensity I is maintained for very long times.

The time constant for the response to changes in light intensity is then

$$1/(k_D' + k_L' I)$$

If the step change is a flash of light of intensity I_0, the time constant is

$$\theta_f = 1/(k_D' + k_L' I_0) \qquad [9]$$

On the other hand, if the step change is a cessation of illumination, as in the period following a flash, the time constant is

$$\theta_D = 1/k_D' \qquad [10]$$

Thus, the time constant θ_D is a measure of the speed of the dark reaction of photosynthesis, whereas the time constant θ_f is a measure of the speed of the entire photosynthetic reaction.

Macroscopic Rate Laws for Algal Cultures

Eq. 6 is the microscopic rate law of photosynthesis for an individual algal cell. Actually, what is determined by rate measurements is not the microscopic rate of a single cell, but rather the macroscopic rate as composed of photosynthesis in all cells of the culture. Since the various cells of a culture are exposed to different light intensities, the rates of photosynthesis of different cells differ, and the observed macroscopic rate represents an average of all the microscopic rates.

It is evident that the macroscopic rate of photosynthesis will depend to some degree on the conditions of agitation present in the culture. If the level of agitation is very low, individual algal cells will see a light intensity which is nearly constant, whereas for very high levels of agitation, individual algal cells will see what is essentially the average light intensity in the culture. These ideas were formulated in an intuitive manner by Rieske, Lumry, and Spikes (9); we shall attempt to give them a theoretical formulation.

Let θ_H be the hydrodynamic time of an algal culture. The hydrodynamic time is the average time required for agitation of a culture to move an algal cell from a region of low light intensity to a region of high light intensity and back again. If the level of agitation is high, θ_H will be small; if the level of agitation is low, θ_H will be large.

Two special forms of the macroscopic rate law may now be derived. In the case of an unstirred culture, the hydrodynamic time is much greater than the time constant θ_D of the dark reaction of photosynthesis. In the case of a completely stirred culture, the hydrodynamic time is much less than the time constant θ_D.

The procedure is as follows: the time-average rate of photosynthesis of a single algal cell is

$$\bar{R}_{i_p} = \frac{1}{t} \int_0^t R_{i_p}(\tau) d\tau \qquad [11]$$

For convenience, choose the time of averaging to be some multiple m of θ_D

$$t = m\theta_D$$

For the case of an unstirred culture, one has

$$m\theta_D \ll \theta_H$$

by definition. Hence, from Eq. 4, the average light intensity is essentially constant at I_i, since the cell travels only a very short distance in the time $m\theta_D$.

From Eqs. 6 and 11, we have then

$$\bar{R}_{ip} = \frac{k_D'k_L'T_{io}I_i}{m\theta_D}\int_0^{m\theta_D}\exp\left[-(k_D'+k_L'I_i)\xi\right]d\xi\int_0^{\xi}\exp\left[(k_D'+k_L'I_i)\tau\right]d\tau + \frac{R_{ip}(0)}{m\theta_D}\int_0^{m\theta_D}\exp\left[-(k_D'+k_L'I_i)\xi\right]d\xi \quad [12]$$

where ξ is a dummy variable of integration. Let I_0 be the intensity of light incident upon the culture. Then, since $I_i \leq I_0$, we have

$$\theta_D^{-1} = k_D' < (k_D' + k_L'I_i) < (k_D' + k_L'I_0) = \theta_f^{-1}$$

where θ_f is the time constant for a flash intensity of I_0. It follows that the last term in Eq. 12 is bounded by

$$R_{ip}(0)\,\frac{1-\exp\left[-(m\theta_D/\theta_f)\right]}{m\theta_D/\theta_f}\,\frac{R_{ip}(0)}{m\theta_D} < \int_0^{m\theta_D}\exp\left[-(k_D'+k_L'I_i)\xi\right]d\xi < R_{ip}(0)\,\frac{1-e^{-m}}{m}$$

Therefore, if m is chosen large enough, say about ten, the last term in Eq. 12 can be made negligible. Further, since the above conclusion was not based on any assumption as to the relative magnitude of the hydrodynamic time, the conclusion is also true for the case of a completely stirred culture.

Eq. 12 then becomes

$$\bar{R}_{ip} = \frac{k_D'k_L'T_{io}I_i}{k_D'+k_L'I_i}\left[1-\frac{(1-e^{-\alpha})}{\alpha}\right] \quad [13]$$

where

$$\alpha = m\theta_D(k_D'+k_L'I_i)$$

Since $\alpha > m$, the above expression becomes, for m sufficiently large

$$\bar{R}_{ip} = \frac{k_D'k_L'T_{io}I_i}{k_D'+k_L'I_i} \quad [14]$$

Eq. 14 has the same form as Eq. 8; hence, for an unstirred culture, each cell photosynthesizes in a sort of pseudo steady state. In other words, the motions of the cells are so slow that photosynthesis in a given cell responds instantaneously to changing conditions of light intensity. It follows therefore that Eq. 14 gives the local reaction rate at any point where the intensity is I_i.

Let v_i be the volume of the ith algal cell and let N be the number of cells present in unit volume of the culture. If we set

$$k_D = k_D'T_{io} \quad [15]$$

$$k_L = k_L'T_{io} \quad [16]$$

$$p = Nv_i \quad [17]$$

then the microscopic rate of photosynthesis R_p at the point where the light intensity is I is

$$R_p = \frac{k_Dk_L\,Ip}{k_D + k_LI} \quad [18]$$

which is the familiar rectangular hyperbolic rate law. Clearly, the macroscopic rate of a culture of volume V is just the space-average[11] of the microscopic rates:

$$\bar{R}_p = \frac{1}{V}\iiint_V R_p\,dV \quad [19]$$

The rate parameters k_D and k_L, and the volume of cells per unit volume of culture p which appear in Eq. 18 actually represent averages. Thus, not all cells of a culture are of the same size, nor do they contain equal concentrations of trapping centers, as we assumed in Eqs. 15, 16 and 17. In physiologically "old" cells, cell volume is large, but rate of photosynthesis low. The converse is true of physiologically "young" cells (10). Hence, it follows that k_D and k_L can only be considered constants over a certain range of experimental conditions.

Consider now the case of a completely stirred culture, i.e., the case for which

$$m\theta_D \gg \theta_H$$

If the order of integration in the expression for the average rate of photosynthesis is interchanged and a change of variable is made, one obtains

$$\bar{R}_{ip} = \frac{k_D'k_L'T_{io}}{m\theta_D}\int_0^{m\theta_D} I_i(\tau)\,d\tau\int_0^{m\theta_D-\tau}\exp\left(-\{k_D'\eta + k_L'[(\eta+\tau)\bar{I}_i(\eta+\tau) - \tau\bar{I}_i(\tau)]\}\right)d\eta \quad [20]$$

where η is a dummy variable of integration. We now note that for all but the smallest values of t, the function

$$\bar{I}_i(t) \approx \bar{I}_i \qquad \text{(a constant)}$$

since the averaging procedure of Eq. 4 quickly smooths out variations in light intensity in this case. Hence, to a good approximation

$$\bar{R}_{ip} \approx \frac{k_D'k_L'T_{i0}}{k_D'+k_L'\bar{I}_i}\cdot\frac{1}{m\theta_D}\times \int_0^{m\theta_D} I_i(\tau)\,\left[1-\exp\left[-(m\theta_D-\tau)(k_D'+k_L'\bar{I}_i)\right]\right]d\tau \quad [21]$$

Use of the same procedure as outlined above then leads to the result

$$\bar{R}_{ip} = \frac{k_D'k_L'T_{io}\bar{I}_i}{k_D'+k_L'\bar{I}_i} = \frac{k_Dk_L\bar{I}_i}{k_D+k_L\bar{I}_i} \quad [22]$$

In the completely stirred culture, the time-average light intensity is the same for all cells, and moreover, is equal to the space-average light intensity; e.g., see Laning and Battin (11)

$$\bar{I} = \frac{1}{V}\iiint_V I\,dV \quad [23]$$

Hence, the macroscopic rate of photosynthesis, per unit volume of algal culture is

$$\bar{R}_p = \frac{k_Dk_L\bar{I}p}{k_D+k_L\bar{I}} \quad [24]$$

Note that this equation preserves the form of the rectangular hyperbolic rate law mentioned earlier, but with the space-average light intensity replacing the local light intensity. This equation was found by Rieske, Lumry and Spikes (9) to

[11] A double bar indicates the space-average of that quantity.

describe the macroscopic rate of the Hill reaction in an agitated suspension of chloroplasts. Of course, the quantities k_D and k_L still represent averages over the various physiological states of cells in the culture; hence, they will once again be slowly varying functions of intensity and cell concentration.

Net Rate of Oxygen Production: Correction for Respiration

The macroscopic rate of photosynthesis $\bar{R}_p$ is expressed in terms of oxygen produced per unit volume of algal culture per unit time. However, not all of the oxygen produced by photosynthesis appears as molecular oxygen in the culture medium. While algal cells are photosynthesizing, they are also respiring, that is, consuming oxygen. Hence, the net rate of production of molecular oxygen by an algal culture is the difference between rate of production by photosynthesis and rate of consumption by respiration. If light intensity is very low, the rate of respiration may exceed the rate of photosynthesis and the net rate of oxygen production will be negative. The light intensity at which photosynthesis just balances respiration is called the compensating light intensity.

We shall assume that the rate of respiration is independent of light intensity. The biological and biochemical implications of this assumption have been stated by Brown and Weis (12). If one assumes further that the rate of respiration of a culture is proportional to the amount of algal mass present in the culture, the microscopic rate of respiration per unit volume of culture R_r may then be written as

$$R_r = k_r p \qquad [25]$$

where k_r is the rate constant for respiration.[12] If agitation of the culture is sufficient to maintain a uniform distribution of cells in the culture, then the macroscopic rate of respiration is simply

$$\bar{R}_r = k_r p \qquad [26]$$

Hence, the net macroscopic rate of oxygen production by a culture is

$$\begin{aligned} \bar{R} &= \bar{R}_p - \bar{R}_r \\ &= \bar{R}_p - k_r p \end{aligned} \qquad [27]$$

where R_p is given by Eq. 24 for a completely stirred culture or by Eqs. 18 and 19 for an unstirred culture.

Photosynthesis in an Unstirred Culture of Algae

Suppose a suspension of algae is contained in a rectangular growth chamber as shown in Fig. 1. A parallel beam of light of intensity I_0 is incident upon the suspension at the face whose area is A. If it is assumed that Beer's law holds for the algal suspension, then one has

$$I(x) = I_0 \exp(-\epsilon p x) \qquad [28]$$

where ϵ is the extinction coefficient of the algal culture.

In reality, Eq. 28 is valid only for monochromatic light, so that the relative intensities of light of different wavelengths are functions of depth. We shall assume, however, that Eq. 28 may be applied with an appropriate average value of ϵ for light of a given quality.

From Eqs. 18 and 28, the microscopic net rate of oxygen production per unit volume of unstirred culture at the depth x is

$$R = \left\{ \frac{k_D k_L I_0 \exp(-\epsilon p x)}{k_D + k_L I_0 \exp(-\epsilon p x)} - k_r \right\} p \qquad [29]$$

[12] Of course, k_r is an average, as are k_D and k_L; hence, k_r will vary with conditions also.

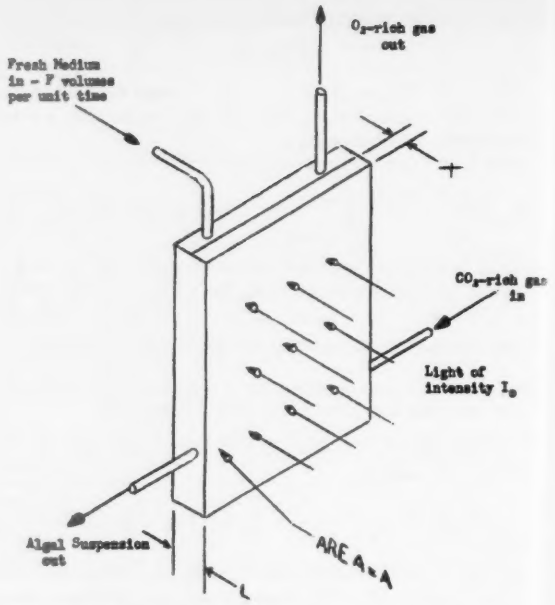

Fig. 1 Algal growth chamber as considered in text

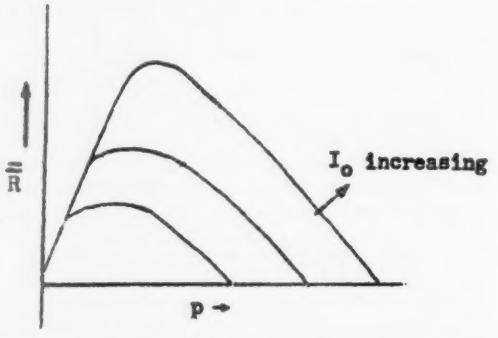

Fig. 2 Macroscopic rate of oxygen production in an unstirred algal culture as a function of population density; parameter is the incident light intensity

The statement that the culture is unstirred does not mean that no agitation is present, but merely that $m\theta_D \ll \theta_H$, as explained previously. Hence, no contradiction is involved if we assume that enough agitation is present to maintain a uniform distribution of algal cells throughout the culture. For a uniform distribution of cells, Eqs. 19 and 29 give

$$\bar{R} = \frac{k_D}{\epsilon L} \ln \left(\frac{k_D + k_L I_0}{k_D + k_L I_0 \exp(-\epsilon p L)} \right) - k_r p \qquad [30]$$

where L is the length of light path. See the culture chamber shown in Fig. 1. The first term on the right-hand side of Eq. 30 is the same as the expression found by Tamiya et al. (13) to describe the rate of batch growth of algae.

Fig. 2 is a plot of Eq. 30 for some reasonable values of k_D, k_L, k_r, and ϵL. Inspection of the figure shows that at low population densities, the net rate of oxygen production should be proportional to p. In this region, the culture is "optically thin."

As the population density is increased, the effects of light absorption and of respiration become more important, until the curve finally passes through a maximum. Such a maxi-

mum has been observed by Cook (14) and by Myers and Graham (15). It is to be noted that if the correction for respiration ($k_r p$ in Eq. 30) is omitted, then Eq. 30 will not predict a maximum in the rate vs. population density curves.

At very high population densities, respiration becomes predominant, and the rate of respiration exceeds the rate of photosynthesis. Eq. 30 shows clearly that the compensating light intensity depends on the population density.

The most important feature of Fig. 2 is the occurrence of the maxima in the curves. Clearly, there is an optimum population density for each light intensity used; as we shall see, there is also an optimum light intensity to use.

Optimum Conditions for an Unstirred Culture of Algae

For engineering purposes, a culture of algae may be said to be photosynthesizing in an optimum manner if the most efficient use is being made of the radiant energy supplied to the culture. This criterion is paramount in this paper. In practice, energy must be supplied not only in the form of radiation, but also for agitation of the culture and for removing the heat generated by absorption of radiation not used in photosynthesis. We assume, however, that power requirements for agitation and for heat removal are negligible in comparison with power requirements for illuminating the culture.

For the growth chamber shown in Fig. 1, the total rate of oxygen production is $\bar{R}AL$. The rate at which energy is supplied to the light source is AI_0/β, where β is the fraction of energy supplied to the light source which is converted to photosynthetically active radiation. The dimensional efficiency of light utilization E is then defined by[13]

$$E = \frac{\bar{R}AL}{AI_0/\beta} = \frac{\beta L}{I_0}\bar{R} \qquad [31]$$

Clearly, the optimum values of p, I_0, and L are those which make E a maximum.

Let
$$Z = \epsilon pL \qquad [32]$$

be the "optical thickness" of the culture (16). Then the efficiency of an unstirred culture is given by

$$E = \frac{\beta}{\epsilon I_0}\left\{k_D \ln\left(\frac{k_D + k_L I_0}{k_D + k_L I_0 e^{-Z}}\right) - k_r Z\right\} \qquad [33]$$

The efficiency is therefore a function of the two variables Z and I_0, and also of the temperature, since k_D and k_r are functions of temperature. Fig. 3 shows curves of efficiency vs. optical thickness for various values of incident intensity. It is apparent that corresponding to each value of I_0, there is an optimum value of Z and moreover, that there is one value of I_0 which makes E an absolute maximum.

The efficiency will be a maximum when Z and I_0 are chosen so that

$$\frac{\partial E}{\partial Z} = 0 \qquad [34]$$

and

$$\frac{\partial E}{\partial I_0} = 0 \qquad [35]$$

From Eqs. 33 and 34, one finds that Z and I_0 must be related by the equation

$$Z = \ln\left\{\frac{k_D - k_r}{k_D k_r} k_L I_0\right\} \qquad [36]$$

[13] The efficiency E as defined above is not to be confused with the quantum yield Q. The quantum yield is the *maximum* number of oxygen molecules which can be formed by the photosynthetic reaction per photon absorbed. One can show that the quantum yield is simply

$$Q = k_L/\epsilon$$

Then use of Eqs. 33 and 35 and elimination of Z by means of Eq. 36 leads to the transcendental equation

$$\frac{k_D k_L I_0}{k_D + k_L I_0} - k_r - k_D \ln\left\{\frac{k_D + k_L I_0}{k_D{}^2}(k_D - k_r)\right\} + k_r \ln\left\{\frac{k_D - k_r}{k_D k_r} k_L I_0\right\} = 0 \qquad [37]$$

The solution of this equation for I_0 gives the optimum light intensity.[14]

Inspection of Eq. 37 shows that at optimum light intensity, the group $k_L I_0/k_D$ is a function only of the ratio k_r/k_D. Fig. 4 is a plot of the solution of Eq. 37 for $k_L I_0/k_D$ as a function of k_r/k_D.

The procedure to establish the optimum conditions for an unstirred culture is as follows: The optimum value of I_0 is found from Fig. 4. The optimum intensity is a function of k_D, k_L, and k_r and therefore depends only on the temperature of the culture. One then determines the optimum value of Z from Eq. 36. Again, the optimum value of Z depends only on the temperature. The values of p and L finally chosen are arbitrary, subject to the restriction that the product ϵpL ($= Z$) must be equal to the optimum determined previously. The optimum population density is therefore inversely proportional to the length of light path L.

If a close approach to optimum conditions is desired, better values of the rate coefficients k_D, k_L, and k_r can be determined by experiments run near the optimum conditions calculated above. The optimization calculations can then be repeated, and a second approximation to the true optimum determined. It is apparent that this procedure minimizes the amount of experimental work required.

Optimum Conditions for a Completely Stirred Culture of Algae

Consider now the case of a completely stirred algal culture. If as before we assume the validity of Beer's law, then Eqs. 23 and 28 give

$$\bar{I} = I_0(1 - e^{-Z})/Z \qquad [38]$$

where Z is again the optical thickness of the culture. Hence, by combining Eqs. 24, 27, 31, and 38, we find the dimensional efficiency of a completely stirred culture to be

$$E = \frac{\beta Z}{\epsilon I_0}\left[\frac{k_D k_L I_0(1 - e^{-Z})/Z}{k_D + k_L I_0(1 - e^{-Z})/Z} - k_r\right] \qquad [39]$$

[14] In general, Eq. 37 will possess two real roots. One of these roots corresponds to $Z = 0$. Since Eq. 33 shows that $E = 0$ for $Z = 0$, this root gives a relative *minimum* efficiency and is not of interest.

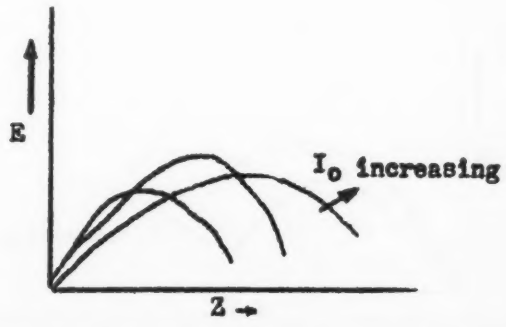

Fig. 3 Efficiency in an unstirred algal culture as a function of optical thickness; parameter is the incident light intensity

As with the unstirred case, the efficiency is a function of Z and I_0. Curves showing the variation of E with Z and I_0 as a parameter are given in Fig. 5.

The optimum conditions are found by applying Eqs. 34 and 35 to Eq. 39. Thus, Eq. 35 requires that

$$\frac{k_D^2 k_L \bar{I}}{(k_D + k_L \bar{I})^2} = \frac{k_D k_L \bar{I}}{k_D + k_L \bar{I}} - k_r \qquad [40]$$

Eq. 40 is a quadratic equation which may be solved for $\bar{I}$; for the case where $k_D > k_r$ (the only interesting case), the root is given by

$$k_L \bar{I} = \frac{k_D k_r}{k_D - k_r} \left\{ 1 + \sqrt{\frac{k_D}{k_r}} \right\} \qquad [41]$$

Hence, the optimum incident intensity is related to optical thickness by

$$k_L I_0 = \frac{Z}{(1 - e^{-Z})} \cdot \frac{k_D k_r}{k_D - k_r} \left\{ 1 + \sqrt{\frac{k_D}{k_r}} \right\} \qquad [42]$$

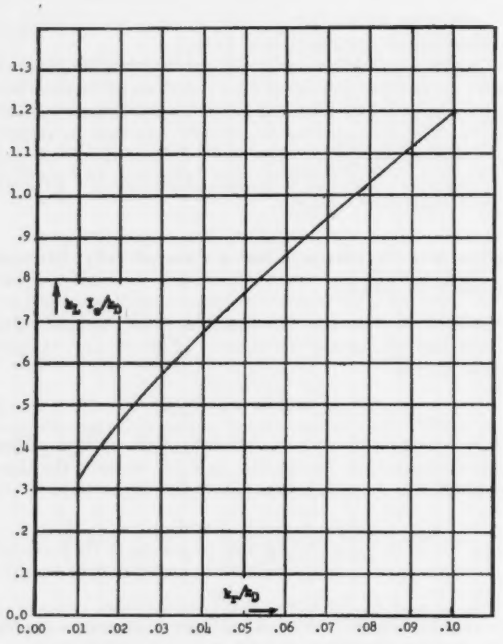

Fig. 4 Dimensionless plot of solution to Eq. 37

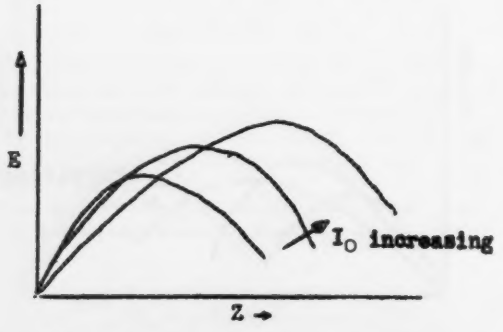

Fig. 5 Efficiency in a completely stirred algal culture as a function of optical thickness; parameter is the incident light intensity

Eq. 42 gives the locations of the maxima in the curves of Fig. 5.

Application of Eq. 34 to Eq. 39 and elimination of I_0 by means of Eq. 42 then shows that the optimum value of Z is a root of

$$Ze^{-Z} = 0 \qquad [43]$$

This equation possesses two real roots, $Z = 0$ and $Z = \infty$. The root $Z = 0$ corresponds to $E = 0$; that is, to a minimum efficiency. Hence, the optimum value of Z is infinite, and Eq. 42 shows that the optimum incident intensity is also infinite.

The maximum possible efficiency E_{max} for the completely-stirred case may be computed from Eqs. 39, 41, and 42. Thus, from Eqs. 41 and 42, one has

$$\lim_{Z \to \infty} \frac{k_L I_0}{Z} = \frac{k_D k_r}{k_D - k_r} \left\{ 1 + \sqrt{\frac{k_D}{k_r}} \right\} = k_L \bar{I} \qquad [44]$$

Substitution of Eq. 44 into 39 then gives

$$E_{max} = \frac{\beta k_L}{\epsilon} \left(\frac{M - 1}{M} \right)^2 \qquad [45]$$

where

$$M = \sqrt{\frac{k_D}{k_r}}$$

Numerical Examples

Tamiya et al. (13) have determined rate constants for the growth of the green alga *Chlorella ellipsoidea*. Data were reported in terms of growth rates rather than rates of oxygen production, but if one assumes that the formation of one liter of wet algal cells is accompanied by the evolution of 14 gm-mole oxygen, then the rate constants are $k_D = 0.0495$ moles-O_2/day-ml of cells; $k_L = 0.0166$ moles-O_2/day-kilolux-ml of cells at 25°C. If p is expressed in ml of cells/liter of culture, then the extinction coefficient is 0.944 liters/cm-ml of cells. The data of Tamiya and Chiba (17) show that the respiration rate of this alga should not be more than about 5% of the maximum possible photosynthetic rate at 25°C. Hence, suppose that $k_r = 0.05\ k_D = 0.00248$ moles-O_2/day-ml of cells.

Use of these rate constants with Fig. 5 then gives the optimum intensity at 25°C to be 2.28 kilolux (212 ft-c). This value of the incident intensity, which is considerably less than that obtained with ordinary fluorescent lamps, is remarkably low.

From Eq. 37 and the given value of ϵ, one finds that the product pL should be 2.84 cm-ml of cells/liter. Hence, if L is 1 cm, the optimum population density at 25°C is 2.84 ml of cells/liter.

Assume that an intensity of one kilolux corresponds to 0.000433 w/cm² (18), then the maximum possible efficiency of an unstirred culture at 25°C may be calculated from Eq. 33; the efficiency is then 0.0204β moles-O_2/watt-day. For fluorescent lights, the value of β is about 0.19, so that the maximum possible efficiency in an unstirred culture at 25 °C is 0.162 moles-O_2/kw-hr. Of course, this figure cannot be taken too seriously; nevertheless, the efficiency quoted may be taken as representative of the efficiencies to be expected with *Chlorella* cultures operating at optimum or near optimum conditions at 25 °C, but with low levels of agitation.

It is of interest to compare maximum efficiencies in the unstirred and completely stirred cases. Thus, for the same values of the rate constants and conversion factors given in the previous example, one finds $E_{max} = 0.195$ gram-moles of O_2/kw-hr, an increase of about 20% over the unstirred case. Since the expression for E does not account for energy spent in agitation or heat removal, it follows that the gain in efficiency of *total* energy utilization will be somewhat less than 20%, and may even be zero or negative, for the completely stirred case.

Discussion and Conclusions

The derivations of the preceding paragraphs show how one can find optimum conditions under which to grow an algal culture for two special cases—an unstirred culture and a completely stirred culture. In an unstirred culture, the equations show that the optimum light intensity is very low. This is a result of the phenomenon of light saturation; since there is a maximum rate at which algal cells can photosynthesize, the use of very high light intensities does not lead to proportionate increase in rate of photosynthesis, but merely succeeds in heating the culture.

With a completely stirred culture, the calculated optimum light intensity turns out to be infinite. Since the optimum optical thickness is also infinite, the macroscopic rate of photosynthesis under such conditions is not equal to the maximum (light saturated) rate, but is somewhat less.[15] The numerical examples given suggest that the increase in efficiency of light utilization caused by vigorous agitation is not very great, and when one considers the power required for agitation and heat removal, the gain in efficiency is of course somewhat less. It must be noted, however, that a completely stirred culture illuminated with a very intense light will give a much higher rate of photosynthesis than an unstirred culture operating at optimum conditions.

Clearly, the expressions derived for efficiencies and rates in unstirred and completely stirred cultures by no means exhaust the possibilities for theoretical analysis. There exist still the cases where the hydrodynamic time θ_H is of the same order of magnitude as the time constant θ_D. Theoretical analysis of such cases cannot be made unless one takes into account the details of the hydrodynamic situation prevailing in the culture. Analysis of the case where $\theta_H \sim \theta_D$ may show that the choice of agitation type and level is extremely critical in so far as one is concerned with the efficiency of light utilization. Thus, it may be that such a partially stirred culture will exhibit a higher efficiency than the completely stirred culture.

Detailed analysis of the hydrodynamic situation in a culture for the purposes enumerated in the preceding paragraph would also yield the numerical value of the hydrodynamic time θ_H. Quantitative knowledge of the hydrodynamic time is essential; if it is not known, one can only guess as to whether his culture is unstirred, partially stirred, etc. Very probably, such calculations would show that most present techniques yield partially stirred cultures; the unstirred case may not even exist.

Another area which has not been touched upon is the shape of the growth chamber. The rectangular vessel described above is not necessarily to be preferred over other geometries; it was chosen only to expedite the analysis. Other geometries may be preferable; thus, a cylindrical growth chamber has the advantage that the light intensity falls off somewhat less rapidly than exponentially with distance from the surface. Descriptions of pertinent experimental work and a literature survey on this subject are given by Myers et al. (20).

Since the ages of cells in a growing algal culture are not uniform but are distributed, the parameters k_D, k_L, k_r, and ϵ must be regarded as averages over the distribution, and hence will be weak functions of I and p. Use of the stepwise optimization procedure described above thus is necessary.

A more satisfactory procedure would be to determine the age distribution, either theoretically or empirically, and combine this with data, such as that of Nihei et al. (10) and Sorokin (21), on the variation of metabolic rates with degree of cell development. One consequence of a theory taking account of a distribution of ages and metabolic rates would be the prediction of light curves (plots of R_{ip} vs. I_i) which are not rectangular hyperbolae, even though the mechanism of Eqs. 1 was strictly followed. Much work remains to be done on this subject.

[15] This statement assumes that the effects of "solarization"—the irreversible bleaching of cells when subjected to light of very high intensity, e.g. Myers and Burr (19)—will not be important at practically realizable high intensities.

References

1 Rabinowitch, E. I., *Photosynthesis*, Vol. 2, 1, Interscience Press, New York, Chaps. 26–28.

2 Myers, J., "Growth Characteristics of Algae in Relation to the Problems of Mass Culture," Chap. 4 in *Algal Culture from Laboratory to Pilot Plant*, J. S. Burlew (ed.), Carnegie Inst. of Washington, Washington, D. C.

3 Kok, B., "Photosynthesis in Flashing Light," *Biochim. et Biophys. Acta*, vol. 21, 1956, pp. 245–258.

4 Davis, E. A., Dedrick, J., French, C. S., Milner, H. W., Myers, J., Smith, J. H. C. and Spoehr, H. A., "Laboratory Experiments on Chlorella Culture," Chap. 9 in Burlew *op cit.*

5 Tamiya, H., "Analysis of Photosynthetic Mechanism by the Method of Intermittent Illumination, Part II," *Studies from the Tokugawa Inst.*, vol. 6, 1949, pp. 43–132.

6 Hill, R. and Whittingham, C. D., *Photosynthesis*, Methuen, London.

7 Lumry, R. and Rieske, J. S., "The Mechanism of the Photochemical Activity of Isolated Chloroplasts, Part V," *Plant Physiol.*, vol. 34, 1959, pp. 301–305.

8 Bassham, J. A. and Calvin, M., *The Path of Carbon in Photosynthesis*, Prentice-Hall, Englewood Cliffs, N. J., 1957.

9 Rieske, J. S., Lumry, R., and Spikes, J. D., "The Mechanism of the Photochemical Activity of Isolated Chloroplasts, Part III. *Plant Physiol.*, vol. 34, 1949, pp. 293–300.

10 Nihei, T., Sasa, T., Miyachi, S., Suzuki, K. and Tamiya, H., "Change of Photosynthetic Activity of Chlorella Cells During the Course of Their Normal Life Cycle," *Arch. für Mikrobiol.*, vol. 21, 1954, pp. 156–166.

11 Laning, J. H., and Battin, R. H., *Random Processes in Automatic Control*, McGraw-Hill Book Co., New York, pp. 112–115.

12 Brown, A. H. and Weis, D., "Relation Between Respiration and Photosynthesis in the Green Alga, Ankistrodesmus Braunii," *Plant Physiol.*, vol. 34, 1959, pp. 224–234.

13 Tamiya, H., Hase, E., Shibata, K., Mituya, A., Iwamura, T., Nihei, T. and Sasa, T., "Kinetics of Growth of Chlorella," Chap. 16 in Burlew *op. cit.*

14 Cook, P. M., "Large Scale Culture of Chlorella," Chap. in *The Culturing of Algae*, J. Brunel, G. W. Prescott, and L. H. Tiffany (eds.), the C. F. Kettering Foundation, Yellow Springs, Ohio.

15 Myers, J. and Graham, J., "On the Mass Culture of Algae, Part II," *Plant Physiol.*, vol. 34, 1959, pp. 345–352.

16 Chandrasekhar, S., *Radiative Transfer*, Oxford at the Clarendon Press, Chap. 1.

17 Tamiya, H. and Chiba, Y., "Analysis of Photosynthetic Mechanism by the Method of Intermittent Illumination, Part I," *Studies from the Tokugawa Inst.*, vol. 6, 1949, pp. 1–42.

18 Tamiya, H., "Mass Culture of Algae," *Ann. Rev. Plant Physiol.*, vol. 8, 1957, pp. 309–334.

19 Myers, J. and Burr, G. I., "Studies on Photosynthesis: Some Effects of Light of High Intensity on Chlorella," *J. Gen. Physiol.*, vol. 24, 1940, pp. 45–67.

20 Myers, J., Phillips, J. N. and Graham, J., "On the Mass Culture of Algae," *Plant Physiol.*, vol. 26, 1951, pp. 539–548.

21 Sorokin, C., "Time Course of Oxygen Evolution During Photosynthesis in Synchronized Cultures of Algae," *Plant Physiol.*, vol. 36, 1961, pp. 232–239.

Technical Notes

Choice of Unperturbed Orbit in the Use of Encke's Method for the Effects of Oblateness and Drag

N. S. HALL[1]
H. F. GAWLOWICZ[2]
E. J. WALLMAN[3]

General Electric Co., Syracuse, N. Y.

Encke's method is applied to two unperturbed orbits of near Earth satellites in the presence of oblateness and drag. The first choice is the elliptical orbit corresponding to a spherical Earth for the given initial conditions. The second choice is the approximate orbit about an oblate Earth, neglecting terms of order J^2 and Je^4. Since the analytic theories for both choices contained equations dependent upon initial conditions, rectification is straightforward.

APPLYING Encke's method to the calculation of orbits about an oblate massive body in the presence of atmosphere, and using a Keplerian ellipse as the reference orbit, one finds that the altitude which is used for the estimation of atmospheric density may be in error by nearly 15 miles. This, in turn, can lead to a miscalculation of the density by a factor of 10. It would be expected, therefore, that this method would require frequent rectification for accurate results. This situation can be improved if an orbit corresponding to the oblate potential field is used instead of Keplerian ellipses. A suitable solution to the problem of orbits about an oblate attracting body is available in (1).[4]

This paper examines the improvements possible in the application of Encke's method for the combined effects of oblateness and drag when the orbits of (1) are used in place of Keplerian ellipses. In this comparison we shall deviate from the normal application of Encke's method by using the coordinate system of Fig. 1 instead of rectangular coordinates. In this system the variables used are:

- ρ = distance from the center of the Earth to the satellite
- v = speed of the satellite
- β = angle between the radius vector and the velocity vector
- η = inclination of the orbit plane to the polar axis
- ξ = longitude of the ascending node
- ζ = angle in the orbit plane between the radius to the point of maximum latitude and the radius to the satellite.

In addition, the independent variable will be chosen as ζ (true anomaly measured from maximum latitude). Although the time is obtainable by quadrature, this will not be done in the present work.

The differential equations for the motion of a satellite in this coordinate system are (to order J)

$$\frac{d\rho}{d\xi} = \rho \cot \beta - \frac{2K \sin^2 \eta \cos^2 \zeta \cos \beta}{\rho^2 v^2 \sin^3 \beta}$$

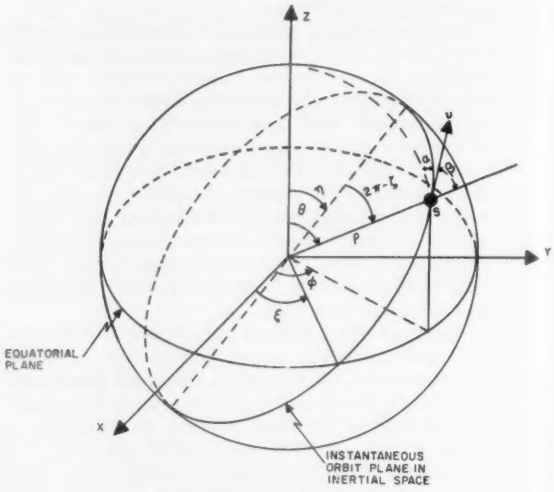

Fig. 1 Coordinate system

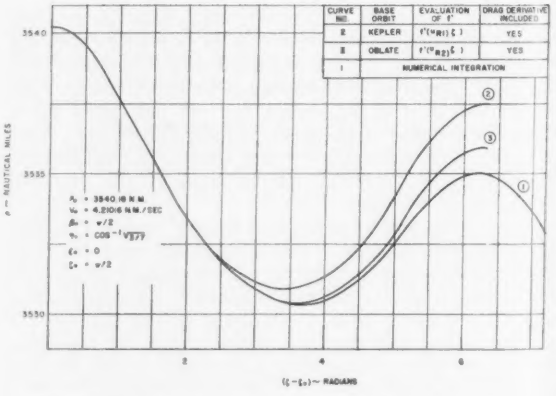

Fig. 2 Variation of radius ρ vs. central angle $\zeta - \zeta_0$

Presented at the ARS Semi Annual Meeting, Los Angeles, Calif., May 9–12, 1960; revision received June 27, 1961.

[1] Manager, Astrodynamics Unit, Defense Systems Dept. Member ARS.

[2] Engineer, Defense Systems Dept. Member ARS.

[3] Engineer, Computer Applications, Defense Systems Dept.

[4] Numbers in parentheses indicate References at end of paper.

EDITOR'S NOTE: The Technical Notes and Technical Comments sections of ARS JOURNAL are open to short manuscripts describing new developments or offering comments on papers previously published. Such manuscripts are usually published without editorial review within a few months of the date of receipt. Requirements as to style are the same as for regular contributions (see masthead page).

$$\frac{dv}{d\zeta} = -\frac{GM\cot\beta}{\rho v} + \frac{2KGM\cos\beta\sin^2\eta\cos^2\zeta}{\rho^4 v^3\sin^3\beta}$$

$$-\frac{3K\cot\beta}{\rho^3 v\,3}\left(\frac{1}{3}-\cos^2\eta\cos^2\zeta\right)+\frac{2K\cos^2\eta\sin\zeta\cos\zeta}{\rho^3 v}-\frac{C_D A\sigma\rho v}{2m\sin\beta}$$

$$\frac{d\beta}{d\zeta} = -1+\frac{GM}{\rho v^2}+\frac{2K(\rho v^2-GM)\sin^2\eta\cos^2\eta}{\rho^4 v^4\sin^2\beta}+\frac{3K}{\rho^2 v^2}\left(\frac{1}{3}-\cos^2\eta\cos^2\zeta\right)+\frac{2K}{\rho^2 v^2}\cot\beta\cos^2\eta\sin\zeta\cos\zeta$$

$$\frac{d\eta}{d\zeta} = -\frac{2K\sin\eta\sin\zeta\cos\eta\cos\zeta}{\rho^3 v^2\sin^2\beta}$$

$$\frac{d\xi}{d\zeta} = -\frac{2K\sin\eta\cos^2\zeta}{\rho^3 v^2\sin^2\beta} \qquad [1]$$

where

A = cross-sectional area of satellite
σ = atmospheric density
C_D = drag coefficient
m = mass of satellite
K = $JGMR^2$

The derivation of these equations are given in (1). It will be noted that these equations can be written in compressed notation in the form

$$\mathbf{U}' = f(U,\zeta) + \epsilon_1 g(U,\zeta) + \epsilon_2 h(U,\zeta)$$

$$\mathbf{U} = (\rho, v, \beta, \eta, \xi) \qquad [2]$$

The prime notation on $\mathbf{U}$ indicates differentiation with respect to ζ. In this form we identify the vector function f with the terms in Eqs. 1 which involve neither the oblateness constant J nor the atmospheric density; the vector function g is identified with those terms containing the oblateness parameter J; the vector function h is identified with the terms due to drag. In these differential equations, terms involving the product of J and the atmospheric density, as well as J^2 and σ^2, have been neglected.

We wish to subject Eqs. 2 to changes of variable

$$\mathbf{U} = \mathbf{U}_{R_i} + \Delta\mathbf{U}_i \qquad i = 1,2 \qquad [3]$$

where $\mathbf{U}_{R_1}$ is chosen as the solution corresponding to a spherical Earth

$$\mathbf{U}_{R_1}' = \mathbf{f}(\mathbf{U}_{R_1},\zeta) \qquad [4]$$

and $\mathbf{U}_{R_2}$ is chosen as the approximate solutions corresponding to an oblate Earth, i.e.

$$\mathbf{U}_{R_2}' = \mathbf{f}(\mathbf{U}_{R_2},\zeta) + \epsilon_1\mathbf{g}(\mathbf{U}_{R_2},\zeta) \qquad [5]$$

Let us first consider $\Delta\mathbf{U}_1$

$$\Delta\mathbf{U}_1' = \mathbf{f}(U_{R_1}+\Delta\mathbf{U}_1,\zeta) - \mathbf{f}(\mathbf{U}_R,\zeta) + \epsilon_1\mathbf{g}(\mathbf{U}_{R_1}+\Delta\mathbf{U}_1,\zeta) + \epsilon_2\mathbf{h}(\mathbf{U}_{R_1}+\Delta\mathbf{U}_1,\zeta) \qquad [6]$$

Evaluation of the first two terms of the right-hand member involves an inacceptable loss in precision. We follow the usual practice and apply the extended law of the mean.

The first of the resulting series developments is the analog in our coordinate system of the familiar Encke's series. This series may be truncated to whatever order is dictated by desired accuracy. It is recognized that severe truncation of Encke's theory would not be admissable in accurate orbital computation unless the magnitude of $\Delta\mathbf{U}$ is small; however, we wish to compare the choices represented by Eqs. 4 and 5, and for this purpose will fix upon the linear approximation

$$\Delta\mathbf{U}_1' = \sum_j \frac{\partial f^i(U_{R_1},\zeta)}{\partial U^j}\,\Delta U_2^j + \epsilon_1\mathbf{g}(U_{R_1},\zeta) + \epsilon_1\sum_j\frac{\partial g^i(U_{R_1}\zeta)}{\partial U^j}\,\Delta U_1^j + \epsilon_2\mathbf{h}(U_R,\zeta) + \epsilon_2\sum_j\frac{\partial h^i(U_{R_1},\zeta)}{\partial U^j}\,\Delta U_1^j \qquad [7]$$

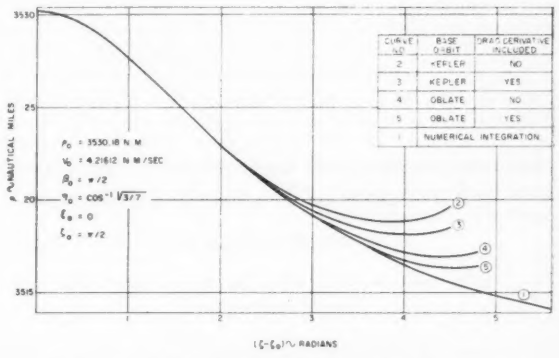

Fig. 3 Variation of radius ρ vs. central angle $\zeta - \zeta_0$

A similar equation arises if we apply the transformation represented by Eqs. 3 and 5; namely

$$\Delta\mathbf{U}_2' = \sum_j \frac{\partial f^i(U_{R_2},\zeta)}{\partial U^j}\,\Delta U_2^j + \epsilon_i\sum_j\frac{\partial g^i(U_{R_2},\zeta)\Delta U_2^j}{\partial U^j} + \epsilon_2\mathbf{h}(U_{R_2},\zeta) + \epsilon_2\sum_j\frac{\partial h^i(U_{R_2},\zeta)}{\partial U^j}\,\Delta U^j \qquad [8]$$

We shall ignore terms of order $\epsilon_1\Delta U_i$. But because of the extreme sensitivity of the drag terms to changes in altitude, we shall make calculations both with and without terms of order $\epsilon_2\Delta U_i$. In this work, the integration was performed on an IBM 704 using a Runge-Kutta-Gill numerical integration scheme. This program was devised to be extremely flexible to variations in step size, frequency of rectification interval, inclusion or omission of derivative of the perturbing terms, and choice of the reference orbit.

In Fig. 2 are presented the results of this numerical integration for an orbit under the following initial conditions:

$\rho_0 = 3540.18$ $\quad \eta_0 = \cos^{-1} 3/7$
$v_0 = 4.21016$ $\quad \xi_0 = 0$
$\beta_0 = \pi/2$ $\quad \zeta_0 = \pi/2$

These conditions would result in a circular orbit in the absence of oblateness or drag; the curves presented correspond to the choices indicated.

We note that the use of a reference orbit defined by Eq. 5 is a significant improvement over the use of one defined by Eq. 4. To obtain more detail on the effect of these initial conditions on the results of various possible combinations, consider Fig. 3. This represents the results of numerical integration of an orbit of lower altitude, which yields more severe drag perturbations; the initial conditions are

$\rho_0 = 3530.18$ $\quad \eta_0 = \cos^{-1} 3/7$
$v_0 = 4.21612$ $\quad \xi_0 = 0$
$\beta_0 = \pi/2$ $\quad \zeta_0 = \pi/2$

The results of five different calculations are presented in Fig. 3 namely:

1 Numerical integration of the differential equations of satellite motion (Runge-Kutta-Gill).

2 Encke's method using an elliptical base orbit, first Encke's series, and neglecting the derivation of the drag perturbation.

3 Encke's method using an elliptical base orbit, first order Encke's series, and including the derivative of the drag perturbations.

4 Encke's method using an oblate base orbit, first order Encke's series, and neglecting the derivatives of the drag perturbations.

5 Encke's method using an oblate base orbit, first order Encke's series, and including the derivative of the drag perturbations.

Reference

1 Hall, N. S. and Gawlowicz, H. F., "The Oblatory Perturbations of Satellite Orbits," presented at the Sixth Annual Meeting of the Amer. Astronaut. Soc., New York, January 1960 (preprint 60-29,).

Geomagnetic and Geoelectric Activity as a Function of Magnetic Latitude[1]

ROBERT SANDERS[2]

Communications Div., Hughes Aircraft Co.
Los Angeles, Calif.

A survey of world-wide geophysical data reveals a strong dependency of geomagnetic and geoelectric activity upon the magnetic latitude of the measuring site. Curves of geomagnetic and geoelectric activity are plotted as a function of magnetic latitude for quiescent conditions of Earth's electromagnetic field and for periods of terrestrial electromagnetic storms. These curves show the close correlation that exists between geomagnetic and geoelectric activity and the greater sensitivity of geoelectric activity to solar influences.

THAT the magnitude of geomagnetic and geoelectric activity varies with the magnetic latitude of the measuring site has been known to geophysicists for many decades. However, generalized curves showing this relationship, and the effect thereon of solar influences, heretofore have not been formulated.

A survey of world-wide geophysical data over the past three sunspot cycles provides the basis to describe variations in geomagnetic and geoelectric activity with the magnetic latitude. Profiles of geomagnetic activity (Fig. 1), and of geoelectric activity (Fig. 2), are shown as a function of the magnetic latitude for periods of terrestrial electromagnetic storms (upper curves, H_s and E_s), and during quiescent conditions (lower curves, H_q and E_q). In either case, the expected range of values for the functions plotted is determined from sunspot-cycle data, i.e., the upper limit of the curves corresponds to maximum sunspot activity, and the lower limit corresponds to minimum sunspot activity. Insufficient data from the polar cap regions permit only a crude estimation of geomagnetic and geoelectric effects above 75° magnetic latitude. The magnetic coordinate used for these determinations is that formulated by A. G. McNish (1).[3]

In Fig. 1, geomagnetic activity is shown as the variation of Earth's magnetic field intensity, measured in gammas. The variation is an average value for an idealized Earth which excludes geological inhomogeneities, such as localized magnetic anomalies (2). These may affect geomagnetic variations by a deviation factor as large as ten greater or smaller than the expected values, depending upon whether the local geomagnetic field intensity is reinforced or reduced.

In Fig. 2, geoelectric activity is shown as the variation of natural electric currents flowing in the Earth's crust, measured in mv/km. The geoelectric variation is also an average value for an idealized Earth. Generally, current flow is in the N-S direction, except in equatorial regions where the prevailing direction is E-W. Certain types of regional geological structures severely affect both the amplitude and the direction of flow of Earth currents (3). Likewise, unusual localized soil conditions may result in Earth resistivities which deviate significantly from the average value of the surrounding region. Possible influences of electrical currents flowing in the oceans must also be excluded from this model, because of insufficient experimental work from which suitable data may be derived.

These curves show the similarity that exists between geomagnetic and geoelectric activity. Quantitative results that define clearly the close relation between these two phenomena have been obtained recently by workers at the University of Alaska (4), which is located at 64.5° North

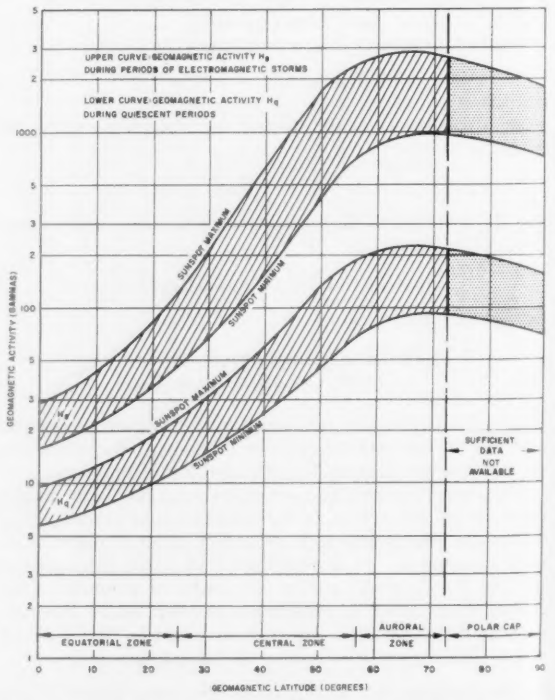

Fig. 1 Profile of geomagnetic activity as a function of magnetic latitude

Received Sept. 6, 1960.
[1] This study was supported by the United States Air Force under Contact AF 30(635)-12857.
[2] Member of the Technical Staff.
[3] Numbers in parentheses indicate References at end of paper.

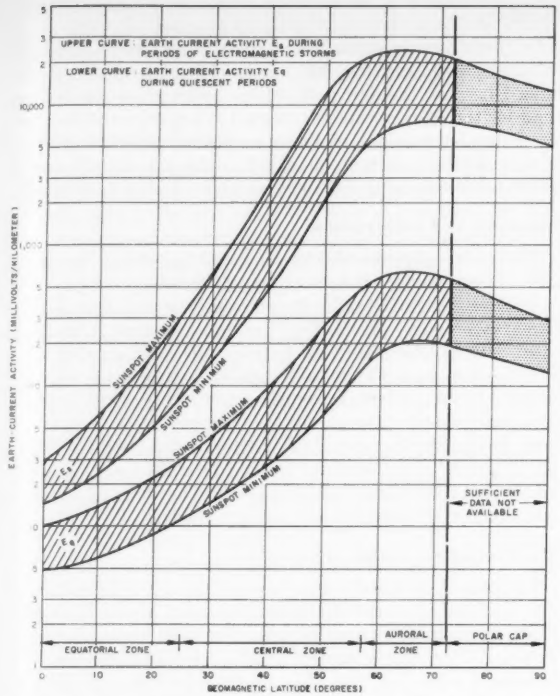

Fig. 2 **Profile of Earth-current activity as a function of magnetic latitude**

magnetic latitude. It is to be expected that similar statistical analyses of geomagnetic-geoelectric data for latitudes below the auroral zones will also yield high correlation coefficients. An interesting observation is that these curves show a greater sensitivity of the geoelectric variations to ionospheric activity, which is the primary cause of these phenomena. Indeed, during terrestrial electromagnetic storms, the range of geoelectric activity from the magnetic equator to the auroral zone is three orders of magnitude, whereas the range of geomagnetic activity is but two orders of magnitude. This would seem to confirm the contention of Russian workers (5) that some variations of the Earth's electromagnetic field, such as rapid fluctuations (0.02 to 1 cps) and micropulsations (1 to 50 cps), may best be investigated by means of Earth current measurements.

Permission to publish these results was granted through the International Telephone and Telegraph Communications Service, Inc., which is affiliated with the Hughes Aircraft Co. Communications Division. Much useful data were supplied by the British Post Office, the American Telephone and Telegraph Co., the Radio Corporation of America, and various geophysical observatories.

References

1 McNish, A. G., "Geomagnetic Coordinates for the Entire Earth," *Terrestrial Magnetism*, vol. 41, 1936, pp. 37–43.

2 Fleming, J. A., "Magnetic Anomalies and Geologic Features," *Physics of the Earth Series—Terrestrial Magnetism and Electricity*, McGraw-Hill Book Co., Inc., New York, 1939, pp. 28–33.

3 Card, R. H., "Earth Resistivity and Geological Structure," *Trans.* AIEE, vol. 54, 1935, pp. 1153–1161.

4 Hessler, V. P. and Wescott, E. M., "Correlation Between Earth-Current and Geomagnetic Disturbance," *Nature*, vol. 184, 1959, p. 627.

5 Troitskaya, V., "Earth Current Installations at the Stations of the USSR," *Annals of the IGY*, Vol. 4, Pergamon Press, New York, 1959, pp. 322–329.

High Temperature Fission Chambers and Ionization Chambers

G. M. B. BOURICIUS[1]

General Electric Co., Aircraft Nuclear Propulsion Dept.
Cincinnati, Ohio

A 700°C fission chamber built and tested showed the counting rate to decrease as the temperature increased from 30° to 700°C. The noise level shows no increase. The cause of the decrease in counting rate is under investigation, and it is the associated electronic circuitry that is suspect. Experimental current integrating type ionization chambers have been built and tested to 350°C. The background current increases with temperature, being about 3×10^{-9} amp at 350°C. Experimental a-c ionization chambers have been built and tested which show no adverse effects caused by background d-c leakage current. These are being readied for test at elevated temperatures.

Fission Chamber

THE NAME *fission chamber* comes from the physical principle operating the device. The design of a fission chamber is such as to use fission fragments. A fission chamber in cylindrical geometry with the signal output circuitry is shown schematically in Fig. 1. The two surfaces facing each other are coated with U^{235} and the space between is filled with a counting gas such as argon. The fission fragments ionize the gas. The electrons and ions are collected and the resultant signal current pulse is then amplified and displayed in some suitable manner. Since the fission chamber as described is a pulse device, it is easily operated at temperatures in the neighborhood of 700° C. At this temperature the resistance of the insulator is still sufficiently high; thus the signal pulse is not attenuated too much to be useful.

The cruxes of the problem of obtaining high temperature fission chambers are of materials and techniques.

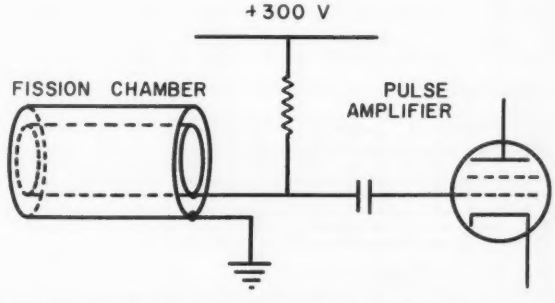

Fig. 1 **Circuit containing a fission chamber used as a neutron detector**

Presented at the ARS 15th Annual Meeting, Washington, D. C., Dec. 5–8, 1960.

[1] Supervisor, General Experimental Physics Unit.

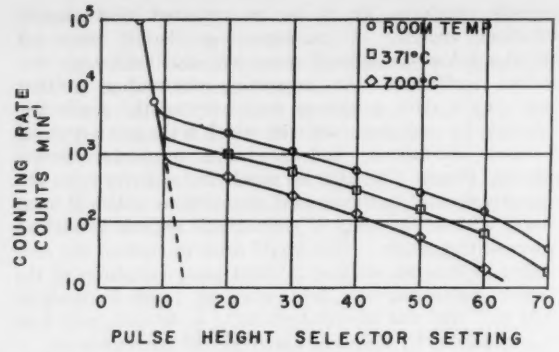

Fig. 2 Integral bias curves of a fission chamber as a function of temperature. These data were obtained using old style voltage pulse amplifier

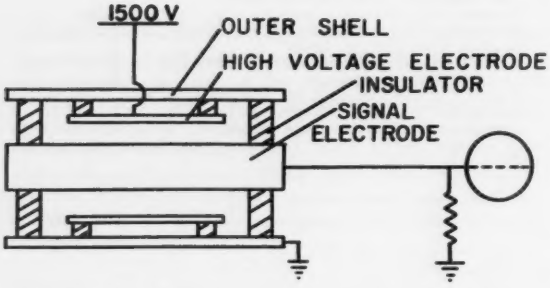

Fig. 3 Typical circuit containing an ionization chamber

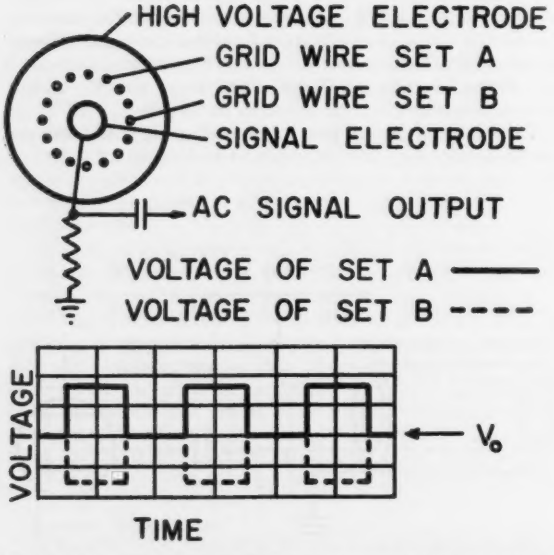

Fig. 4 Schematic of the construction of a cylindrical a-c ionization chamber and the relative voltages on the grid structures

Metals

Of the stainless steels tested, best results were obtained with 304, 310, and the 400 series. Nickel is more readily brazed because the dew point of the hydrogen is less critical than for the stainless steels. Nickel is a good metal because its thermal coefficient of linear expansion matches that of some ceramics quite well, but disadvantages are the softness of nickel when annealed and the ease with which it is annealed.

Ceramics and construction

Two types were found best for metal to ceramic hermetic seals. One is 96% Al_2O_3, the other 99% Al_2O_3. The ceramic to metal seals used in these fission chambers are all made in a two-step process. A coating of molymanganese is first applied. These parts are then brazed to the metal parts with silver or copper. The fit of the metal pieces to the ceramic pieces is very important, the tolerances being of the order of 0.002 to 0.004 in. These seals are then welded in place by an inert gas arc welding technique. After construction the chamber is baked out at 750°C for about 5 hr while being pumped and is next filled with 1 atm of argon. The filling tube is then sealed and the electrical leads are attached.

Mechanical test data

Vacuum tight welding was no problem. A nickel to stainless steel weld is somewhat easier to make than a nickel to nickel weld and is as easy as a stainless steel to stainless steel weld. All welding is more readily accomplished by using a gas shield of 85% A plus 15% H_2 than by using tank argon alone. Hydrogen brazing gave excellent results. Silver, copper, and GE81 brazes were used.[2] GE81 flows at about 1150 °C. Our experience has been that any torch brazing using a flux eventually fails at high temperatures.

Commonly, chamber diameters vary from $\frac{1}{4}$ to 2 in. and lengths from $\frac{1}{2}$ to 8 in.

Neutron response data

The size of the pulse is proportional to the energy that the fission fragment has transferred to the gas and is not the same from one fission event to the next. Consequently there will be a number distribution of pulses of various sizes. Integral bias curves taken at various temperatures are shown in Fig. 2. There is reason to suspect that with the newer current pulse amplifiers there would be little or no change in the integral bias curve with temperature. The only appreciable change in these curves as a function of hundreds of hours of time at a temperature of 700°C is a gradual falling off of the curve in the higher bias setting ranges.

The neutron responsivity of a fission chamber with a coating of U^{235} of 2 mg/cm² is about 0.0005 counts per unit ambient thermal neutron flux.

Ionization Chambers

An ionization chamber in cylindrical geometry with the signal output circuitry is shown schematically in Fig. 3. Ionization chambers usually contain B^{10} for measuring neutron fluxes and are most often used as current integrating instruments. The output is a direct current proportional to the ambient neutron flux. The high voltage electrode and the signal electrode are independently supported from the outer shell, which is at ground potential. This construction minimizes the leakage background current into the signal electrode.

Temperature effect on the signal

The background current limits the minimum signal which may be measured. At room temperature the output current is linear with neutron flux over a longer range than at high temperatures. At 350°C the background current of one particular chamber was about 3 x 10^9 amp and so neutron fluxes

[2] The GE81 is a boron free brazing compound developed at the Aircraft Nuclear Propulsion Dept., General Electric Co., Cincinnati, Ohio.

below about 10^6 cannot be readily measured with this chamber. Thus the range of fluxes to be measured will determine the allowable background current, which in turn determines the maximum temperature at which these fluxes can be measured.

A-C ionization chamber

If the d-c ionization chamber cannot be used because of temperature-induced background current, some other scheme must be used. One such scheme is the a-c ionization chamber. Fig. 4 shows the elements of an a-c ionization chamber and a graph of the voltages applied to the electrodes. There is a high voltage electrode and a collector or signal electrode as in a conventional d-c ionization chamber. An additional grid structure is placed between the two electrodes. The inner surface of the high voltage electrode is coated with B^{10}. The neutron interaction with the B^{10} surface causes ionization of the chamber gas in the region between the high voltage electrode and the grid structure. The grid wires are alternately connected together and a lead from each set of wires is brought out for electrical connection. When the two sets of wires are at the same potential V_0, then V_0 is adjusted so that normal d-c ion current flows to the signal electrode. Then the two sets of grid wires are driven to new potentials of the same change in voltage but opposite in polarity. Thus there is a gradient between the grid wires; therefore the ions are collected on the grid structures and the signal current decreases to about zero. In addition, since the grid sets change in opposite polarities and by the same amount, there is no net induced current in the signal electrode. The total signal will be d-c leakage current and a superposed a-c signal current. One can then choose the a-c signal and reject the leakage. Work is now going on to see how this scheme will work at high temperatures.

Thermal Diffusion Ratio in Dissociated Air[1]

SINCLAIRE M. SCALA[2]

General Electric Co., Missile and Space Vehicle Dept., Philadelphia, Pa.

Analysis

ALTHOUGH the mechanism of thermal diffusion has usually been neglected in studies of the diffusion process in the hypersonic laminar boundary layer (1,2),[3] the author has found that thermal diffusion can be important for nonequilibrium viscous flow (3,4).

Great interest has been focused recently on viscous effects at high altitude, including nonequilibrium viscous flow within shock waves, boundary layers and wakes (5,6,7). A realistic treatment of this type of chemically reacting flow requires a detailed consideration of the two competing rate processes, diffusion and chemical kinetics. Hence, it is appropriate that the mechanism of thermal diffusion be reviewed at this time and in particular, a number of approximations to the thermal diffusion ratio in binary mixture dissociated air will be presented here:

The equation for the conservation of species in a diffusing multicomponent chemically reacting gas mixture can be written

$$\frac{\partial \rho_i}{\partial t} + \nabla \cdot [\rho_i(\mathbf{v} + \mathbf{V}_i)] = \dot{w}_i \qquad [1]$$

where ρ_i is the partial density of species i, $\mathbf{v}$ is the macroscopic stream velocity, $\mathbf{V}_i$ is the diffusion velocity of species i, and $\dot{w}_i$ is the chemical source term. In first approximation, dissociated air may be treated as a binary mixture of air atoms and air molecules; hence only one equation, Eq. 1, required. Following Hirschfelder et al. (8) and neglecting external forces, one obtains for the diffusion flux vector in a binary mixture gas

$$j_i = \rho_i \mathbf{V}_i = \frac{n_t^2}{\rho} M_i M_j \mathfrak{D}_{ij}[\nabla X_j + (X_j - C_j)\nabla \ln p] - D_i^T \nabla \ln T \qquad [2]$$

where X_j and C_j are the mole fraction and mass fraction of species j, respectively. Eq. 2 includes the separate effects of ordinary (concentration) diffusion, pressure diffusion and thermal diffusion. All of these mechanisms of mass transfer are present, for example, within a normal shock wave.

Upon introducing the dimensionless thermal diffusion ratio (8)

$$K_T = \frac{\rho}{n_t^2 M_i M_j} \frac{D_i^T}{\mathfrak{D}_{ij}} \qquad [3]$$

one readily obtains for the diffusion flux vector

$$j_i = -\rho \mathfrak{D}_{ij} \left\{ \nabla C_i + \frac{M_i M_j}{\overline{M}^2} \left[\left(\frac{\overline{M} - M_i}{M_i} \right) C_i \nabla \ln p + K_T \nabla \ln T \right] \right\} \qquad [4]$$

where $\overline{M}$ is the mean molecular weight.

For dissociated air, the first approximation to the ordinary diffusion coefficient $\mathfrak{D}_{ij}$ (9) does not depend on the concentrations of the gaseous species, but as will be shown, K_T and hence D_i^T is highly concentration dependent.

For the evaluation of the diffusion flux, Eq. 4, there remains only a discussion of the thermal diffusion ratio K_T. Hirschfelder et al. (8) give as the first approximation to K_T

$$[K_T]_1 = \frac{X_1 X_2}{6K_{12}} \frac{S^{(1)}X_1 - S^{(2)}X_2}{\overline{X} + \overline{Y}} (6C_{12}^* - 5) \qquad [5]$$

The thermal diffusion ratio is a very complex function of the temperature, gas composition, the ratio of molecular weights of the species and the force law of the molecules. The primary dependence on gas composition is given by the product of the mole fractions X_1X_2, and to a smaller extent by $S^{(1)}X_1 - S^{(2)}X_2$. The primary dependence on the masses of the atoms and molecules is given by $S^{(1)}$ and $S^{(2)}$. The primary temperature dependence is given by $(6C_{12}^* - 5)$.

Received July 11, 1961.

[1] This note is based on work performed under the auspices of the Air Force Office of Scientific Research of the Air Research and Development Command, under Contract No. AF 49(638)-931. The Contract is administered by the Mechanics Div., AFOSR, with Milton Rogers acting as project officer.

[2] Manager, High Altitude Aerodynamics, Space Sciences Laboratory. Member ARS.

[3] Numbers in parentheses indicate References at end of paper.

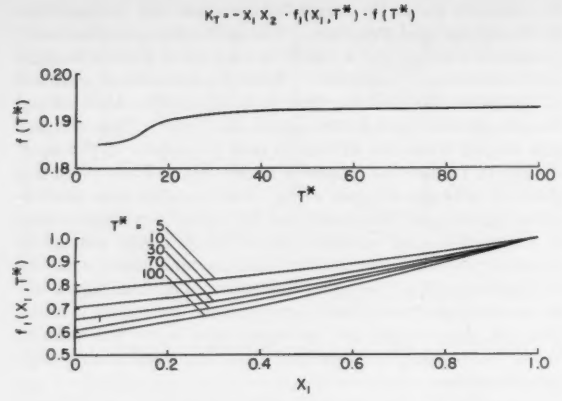

Fig. 1 Separable functions for thermal diffusion ratio

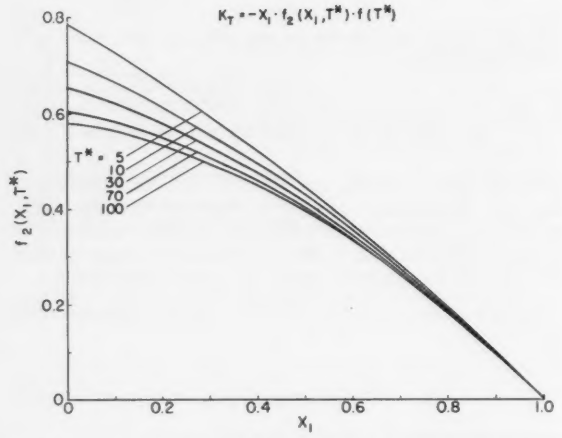

Fig. 2 Alternate functional dependence of K_T upon composition

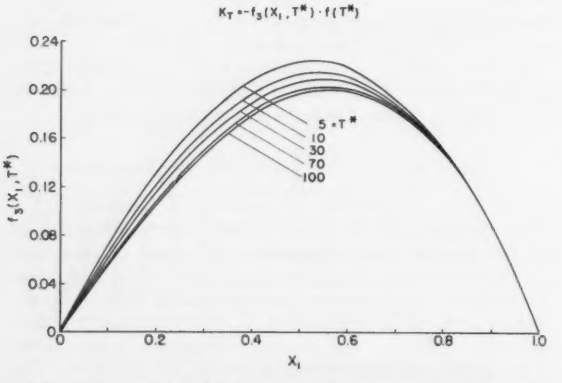

Fig. 3 Separable dependence of K_T upon composition

Since the thermal diffusion ratio can be either positive or negative, we note that the convention used by both Chapman and Cowling (10) and Hirschfelder et al. (8) is that when K_T is positive this signifies that component 1 tends to move into the cooler region and component 2 toward the warmer region. (The temperature at which the thermal diffusion ratio undergoes a change in sign is referred to as the inversion temperature).

In the following computations, it will be assumed that the air atoms behave like rigid spheres and that the interactions between molecules follow the Lennard-Jones 6:12 potential. Thus, for example the dependence of C_{12}^* upon T^* is appropriate to the Lennard-Jones model. For a detailed discussion of the effects of other force laws upon K_T and D_A^T, the reader may refer to either Hirschfelder, Curtiss and Bird (8) or to Grew and Ibbs (11). It is noted in passing, however, that if it had been assumed that the molecules obey a Maxwellian force law, rather than a Lennard-Jones model, then K_T would be identically zero.

Calculated Results

The constants used in the calculations include the collision diameters for the atoms and molecules $\sigma_1 = 2.92$ Å, $\sigma_2 = 3.59$ Å, the force constants utilized in the Lennard-Jones 6:12 potential function $\epsilon/k = 85°$K, and a ratio of specific heats for the air molecules $\gamma \approx 1.2$. The molecular weights of the atoms and molecules were taken as 15 and 30 lb/lb-mole respectively.

One then obtains the following results for K_T:

$$K_T = -X_1 X_2 \cdot f_1(X_1,T^*) \cdot f(T^*) \quad [6]$$

In effect, this equation shows that the effects of gas composition, intermolecular force law and temperature can be separated into the product of several functions, where the functions $f_1(X_1,T^*)$ and $f(T^*)$ are shown graphically in Fig. 1.

Since $X_2 = 1 - X_1$, one can absorb the mole fraction of molecules X_2 into a new function $f_2(X_1,T^*)$, in which case Eq. 6 becomes

$$K_T = -X_1 \cdot f_2(X_1,T^*) \cdot f(T^*) \quad [7]$$

where the function $f_2(X_1,T^*)$ is shown in Fig. 2.

Since K_T depends explicitly on the product $X_1(1 - X_1)$, both K_T and D_A^T vanish when X_1 is either unity (all atoms) or identically zero (all molecules). Further, K_T has a maximum when X_1 is approximately one half. This may be demonstrated by absorbing X_1 into $f_2(X_1,T^*)$ to obtain

$$K_T = -f_3(X_1,T^*) \cdot f(T^*) \quad [8]$$

where $f_3(X_1,T^*)$ is shown in Fig. 3. It has already been shown in Fig. 1 that $f(T^*)$ is nearly constant and equal to 0.19; hence Fig. 3 indicates that the peak value of K_T is of the order of -0.04, and occurs when X_1 is approximately 0.50. It is also seen that the dependence of K_T upon T^* is also most pronounced when the mole fraction of atoms is approximately one half.

Examination of all of the calculated data indicates that for binary mixture dissociated air, $f(T^*) \approx 0.19$, and $f_1(X_1,T^*) \approx 0.65 + 0.35X_1$. That is, when the explicit dependence of K_T upon T^* is neglected over a temperature range $600°\text{R} < T < 16{,}000°\text{R}$, one obtains

$$K_T = -0.124X_1(1 - X_1)(1 + 0.538X_1) \quad [9]$$

This equation can also be written in terms of the mass fraction of atoms C_1 by noting that $X_1 = 2C_1(1 + C_1)^{-1}$ and hence

$$K_T = -0.247C_1(1 - C_1)(1 + 2.08C_1)(1 + C_1)^{-3} \quad [10]$$

Since K_T is always negative for all values of $0 < C_1 < 1.0$, it is clear that according to the sign convention, $D_A^T < 0$, and hence the effect of thermal diffusion is to cause air atoms

to diffuse from cool regions to hot regions, and molecules to diffuse from hot regions to cool regions.

Acknowledgment

The author wishes to acknowledge the assistance of Leon Gilbert and John Wilson in deriving the results and in drawing the figures.

References

1 Lees, L., "Laminar Heat Transfer Over Blunt Nosed Bodies at Hypersonic Flight Speeds," JET PROPULSION, vol. 26, no. 4, 1956, p. 259.

2 Fay, J. and Riddell, F., "Theory of Stagnation Point Heat Transfer in Dissociated Air," *J. Aero. Sci.*, vol. 25, no. 2, 1958, p. 73.

3 Scala, S. M., "Hypersonic Heat Transfer to Catalytic Surfaces," *J. Aero. Sci.*, vol. 25, no. 4, 1958, p. 273.

4 Scala, S. M., "Hypersonic Stagnation Point Heat Transfer to Surfaces Having Finite Catalytic Efficiency," *Proc. of the Third U. S. National Congress of Applied Mechanics*, 1958, p. 799.

5 Talbot, L. and Scala, S. M., "Shock Wave Structure in a Relaxing Diatomic Gas," *Proc.* of the Second International Symposium on Rarefied Gas Dynamics, Berkeley, Calif., 1960.

6 Probstein, R. F. and Kemp, N. H., "Viscous Aerodynamic Characteristics in Hypersonic Rarefied Gas Flow," *J. Aero/Space Sci.*, vol. 27, no. 3, 1960, p. 174.

7 Feldman, S., "Trails of Axi-Symmetric Hypersonic Blunt Bodies Flying Through the Atmosphere," AVCO Research Rep. 82, December 1959.

8 Hirschfelder, J. O., Curtiss, C. F. and Bird, R. B., *Molecular Theory of Gases and Liquids*, John Wiley and Sons, Inc., New York, 1954.

9 Scala, S. M. and Baulknight, C. W., "Transport and Thermodynamic Properties in a Hypersonic Laminar Boundary Layer, Part I- Properties of the Pure Species," ARS JOURNAL, vol. 29, no. 1, 1959, p. 39.

10 Chapman, S. and Cowling, T. G., *Mathematical Theory of Non-Uniform Gases*, Cambridge Univ. Press, 1939.

11 Grew, K. E. and Ibbs, T. L., *Thermal Diffusion in Gases*, Cambridge Univ. Press, 1952.

Vacuum-Air Missile Boost

JAMES J. MURRAY[1]

Army Research Office, Durham, N. C.

SUDHIR KUMAR[2]

Duke University, Durham, N. C.

PRESENT-DAY missiles for satellite vehicles are normally launched from a static firing position wholly by their own propulsion system. The payload and the final velocity achieved are thus solely dependent on the propellant carried. For quite some time various ideas have been suggested for imparting initial velocities to missiles and rockets. Such ideas, if feasible and successful, would have the advantage of increasing either the range or the payload of the missile for a given amount of propellant. A historical account of early rockets and launchers is given by Willy Ley (1).[3] Also a popular article by Storko and Dorsey (2) gives an interesting compilation of ideas suggested in the past regarding launchers.

In this note, the authors suggest using the abundant potential energy conserved in the Earth's atmosphere for launching missiles. At sea level, the Earth's normal atmospheric pressure is 14.7 psi. Let us consider, for example, a missile of 16-ft span. For such a vehicle an initial thrust of more than 500,000 lb can be developed if it is launched from an evacuated tube of 16-ft diam, as shown in Fig. 1. For comparison purposes, the initial thrust of the presently suggested booster device and some missile rocket thrusts are given in Table 1. Particular attention is directed to missile no. 2, for which the effective air boost thrust is fourteen times as much as the effective rocket propellant thrust. Information in Table 1 is derived from (3). It may be noted that the thrust provided by the atmospheric boost in Table 1 is the value shown there only when the missile is not moving. Once the missile starts moving, the thrust will diminish, due to the air flow in the tube. There are several other factors that would have to be taken into account so as to have a more realistic estimate of the effective thrust while the missile is in flight within the tube. Some of the other major losses that should be taken into account are: the back pressure provided by the air remaining in the almost evacuated part of the tube around the missile; the friction losses; the Bernoulli loss; and shocks and vibration. An analysis considering all these factors is not given here, as extensive experimental information about these losses is not readily available. However, an elementary analysis which takes into account the first of these, i.e., the back pressure loss, is given. It is hoped that this will serve as a guide to judge the usefulness of the concept. Analysis of an air spring given by B. Sussholz (4) may also be found of interest in connection with the present problem.

Received April 3, 1961.

[1] Director, Engineering Sciences Div. Member ARS.

[2] Associate Professor, Department of Civil Engineering.

[3] Numbers in parentheses indicate References at end of paper.

Theoretical Analysis

As shown in Fig. 1, a missile of mass m is moving in a tube of length L and area of cross section A. The position of the missile at any instant, prescribed by its mass center, is measured by its distance x from the open end. If it is further assumed that the pressure acting on each end of the missile is uniformly distributed and is given by the atmospheric pressure P on the rear end and p_1 at the nose end, the equation of motion of mass m for a vertical tube may be written as

$$\frac{d^2x}{dt^2} + g = \frac{A}{m}(P - p_1) \qquad [1]$$

where g is acceleration due to gravity. Further, the enclosed air in the almost evacuated tube is taken to be under adiabatic compression. If the initial pressure in the tube after evacuation is p_1 (when $x = 0$), for $x > 0$, the subsequent internal

Table 1 Data on some major U.S. missiles

Missile number	Diam, in.	Span, ft	Rocket thrust, lb	Wt (W), lb	Static thrust of air boost (T), lb	Effective boost thrust (T-W), lb
1	120	16	60,000/300,000	255,000	540,000	285,000
2	72	12	75,000	62,000	239,300	177,300
3	105	..	150,000	110,000	127,000	17,000
4	54	..	130,000	28,000	33,650	5,650

pressure p_1 is given by

$$p_1 = \frac{p_i}{\left(1 - \frac{x}{L}\right)^{\gamma}} \qquad [2]$$

where γ is the adiabatic constant.

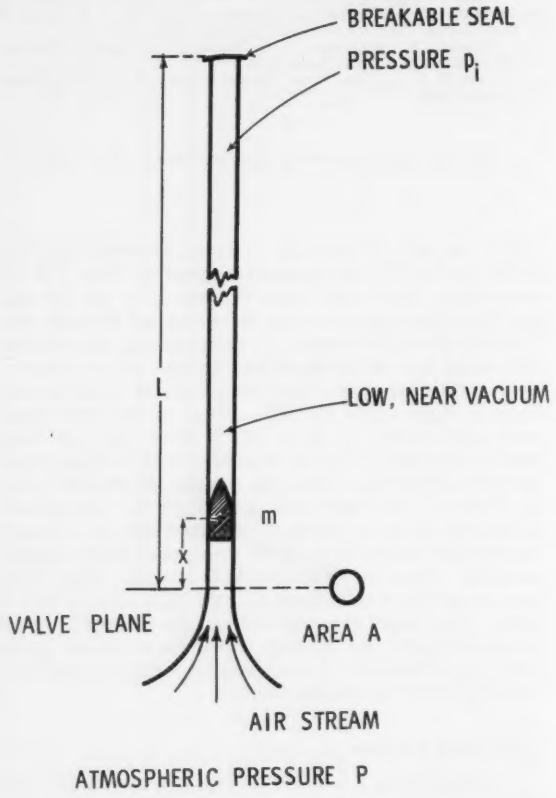

Fig. 1 Schematic representation of air boost rocket launcher

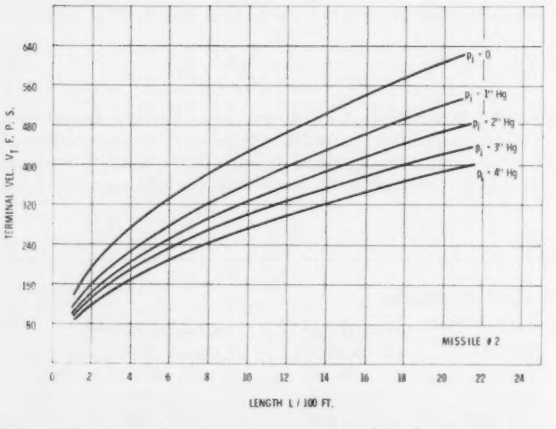

Fig. 2 Plot of terminal velocity vs. length of the launch tube for different degrees of vacuum computed for missile no. 2 and P = 14.7 psi

Thus Eq. 1 can be written as

$$\frac{1}{2}\frac{d}{dx}(v^2) = \frac{PA}{m}\left\{1 - \frac{p_i/P}{\left(1 - \frac{x}{L}\right)^{\gamma}}\right\} - g \qquad [3]$$

On integration, for the case when $\gamma \neq 1$, it becomes

$$v^2 = \frac{2PA}{m}\left\{x + \frac{L}{1-\gamma}\frac{p_i}{P}\left(1 - \frac{x}{L}\right)^{1-\gamma}\right\} - 2gx + C \qquad [4]$$

where C is a constant of integration.

Now, the initial conditions are

$$v = 0 \text{ at } x = 0 \qquad [5]$$

which gives

$$C = -\frac{2PA}{m}\frac{L}{1-\gamma}\frac{p_i}{P} \qquad [6]$$

For air, $\gamma = 1.4$, and so Eq. 4 becomes

$$v^2 = \frac{2PAL}{m}\left[\frac{x}{L} - \frac{1}{0.4}\frac{p_i}{P}\left\{\frac{1}{\left(1 - \frac{x}{L}\right)^{0.4}} - 1\right\}\right] - 2gx \qquad [7]$$

Eq. 7 gives the velocity of the missile at any location in the tube. To estimate the terminal velocity v_T with which the missile will come out of the tube, it is assumed that this velocity is acquired by the missile at a position x_T, where $p_1 = P$, the outside atmospheric pressure. So, using the adiabatic law, x_T is given by

$$P = \frac{p_i}{\left(1 - \frac{x_T}{L}\right)^{\gamma}}$$

which gives, with $\gamma = 1.4$

$$x_T = L\left\{1 - \left(\frac{p_i}{P}\right)^{1/1.4}\right\} \qquad [8]$$

Substituting for x from Eq. 8 in Eq. 7 and simplifying Eq. 8, the terminal velocity is obtained as

$$v_T^2 = \frac{2PAL}{m}\left[1 - \frac{mg}{PA} - q^{1/1.4}\left\{3.5 - \frac{mg}{PA}\right\} + 2.5\,q\right] \qquad [9]$$

where $q = p_i/P$ is a pressure ratio. Using Eq. 9 computations of terminal velocity have been made for missile no. 2, using the data in Table 1. These velocities are presented in Fig. 2 for several p_i. It is estimated roughly that under usual launching methods, for missile no. 2 to reach a velocity of 600 fps, about 5 tons of fuel would be consumed by the rocket engines. If this velocity is imparted to the rocket without using any of its fuel, the payload may be increased by a fraction of this amount with a corresponding reduction in the fuel and the load of the structure required to carry the fuel.

In order to achieve any appreciable velocities for heavy missiles, long tubes will have to be used under the present arrangement. However, the length of the tube can be kept smaller by doing either of the two things. First, the diameter of the tube may be increased, so that the total thrust, and therefore acceleration, increases, to give higher velocities in shorter tubes. The second approach could be using pressures greater than atmospheric. These pressures may be developed with a suitable controlled burning fuel. For small rockets or missiles, pressure tanks with control valves may be considered as a practical means of providing these higher pressures. Using the exhaust gases of the rocket for building pressure is another possibility that has been suggested in the past (2). Any of these ideas may be used for achieving the end desired. However, it is felt that there is a definite advantage in imparting an initial velocity to missiles or rockets where conditions permit.

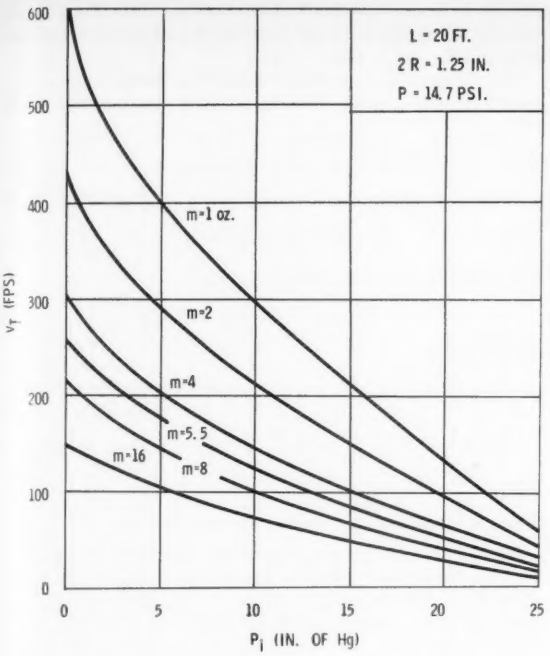

Fig. 3 Plot of terminal velocity vs. internal pressure for different masses in the experimental model

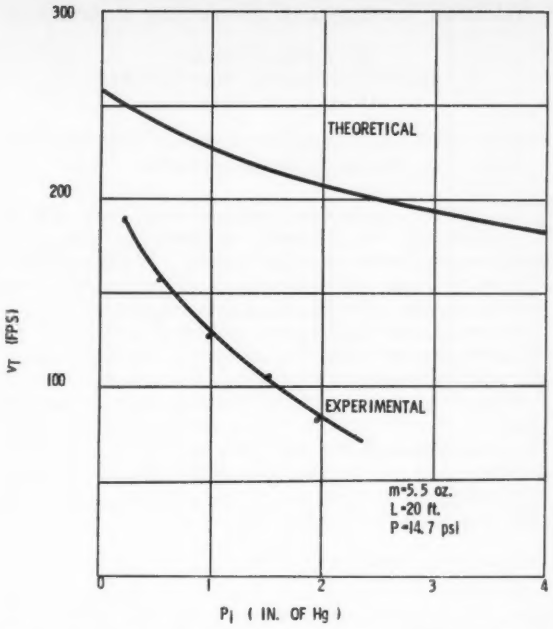

Fig. 4 Theoretical vs. experimental terminal velocities for the experimental model

Experimental Model

A small model was built for studying the feasibility of the atmospheric boost idea. A copper tube with a 1.25-in. ID and length 20 ft was mounted horizontally, and a missile-shaped projectile of teflon (this material was chosen in order to keep friction losses small) weighing 5.5 oz, was inserted at one end of the tube. A rubber stopper attached to a simple lever release mechanism was used to seal this end of the tube. At the muzzle end, which was machined flat, a thin plastic disk was affixed, coated with a silicone high vacuum grease. Air was evacuated from the tube by a standard forepump, and the internal pressure was measured by a mercurial pressure gage. When the rubber stopper was jerked out, the teflon projectile shot out of the tube, shattering the thin plastic cover. The velocity of the projectile was measured electrically with two wire probes near the muzzle of this air gun.

Eq. 9 giving terminal velocity, is applicable in this horizontal case when the gravity term is removed. Then

$$v_T^2 = \frac{2PAL}{m} [1 - 3.5\, q^{1/1.4} + 2.5q] \qquad [10]$$

This equation is used in Fig. 3 to plot the curves of v_T for different internal pressures and for projectile masses from one to 16 oz. In Fig. 4, the experimental and the theoretical curves for the 5.5-oz projectile are compared. The form of the two curves is similar; however, the magnitudes of v_T are different. The discrepancy becomes larger for higher p_i. It is recognized that this discrepancy is mainly due to the losses mentioned above and neglected in the present analysis. Other appreciable sources of loss of energy were friction, the shattering of the plastic seal, and compressing some air before hitting the seal. The results, however, do show considerable promise for the low internal pressures.

References

1 Ley, W., *Rockets and Space Travel*, The Viking Press, New York, 1947.
2 Storko, M. and Dorsey, J. W., "Rocket Catapult Facts and Fables," ASTRONAUTICS, vol. 5, no. 7, July 1960.
3 Ordway F. I. III and Wakeford, R. C., *International Missile and Spacecraft Guide*, McGraw-Hill Book Co., Inc., New York, 1960.
4 Sussholz, B., "Forced and Free Motion of a Mass on an Air Spring," *J. Appl. Mech.*, vol. 11, June 1944, pp. A-101 to A-107.

Attitude Control of Rotating Satellites

ROY DALE COLE[1]
MARY ELIZABETH EKSTRAND[2]
MICHAEL R. O'NEILL[3]

Aviation Ordnance Dept., U. S. Naval Ordnance Test Station, China Lake, Calif.

FOR MANY applications satellites must have attitude control, i.e., the orientation of particular components must be controlled in a specified manner. In this paper it is assumed that the whole satellite is to be controlled and that the satellite is a symmetric rotating rigid body.

The two fundamental aspects of attitude control are: 1) how given torques affect the orientation of a body, and 2) what torques are necessary to orient a body in a given manner. The standard classical works on rotating bodies are directed toward the former problem; this paper considers the latter. The same equations are used, only in reverse. The basic procedure is to write the six differential equations of motion in a condensed form that makes it simple to see how the desired control can be obtained.

Rotational Equations of Motion

The differential equations of motion of a symmetric body (1)[4] in a body rotating coordinate system xyz are given by the Euler equations

$$A\dot{\omega}_x + (C - A)\omega_y\omega_z = L_x \quad [1]$$

$$A\dot{\omega}_y - (C - A)\omega_x\omega_z = L_y \quad [2]$$

$$C\dot{\omega}_z = L_z \quad [3]$$

where ω_x, ω_y and ω_z are the components of angular rate; L_x, L_y and L_z are the components of torque; and A, A and C are the principal moments of inertia. Eqs. 1 and 2 can be combined to give the complex equation

$$\dot{\rho} - i\nu\rho = N \quad [4]$$

where

$$\rho = \omega_x + i\omega_y \quad [5]$$

$$N = L_x/A + iL_y/A \quad [6]$$

$$\nu = (C - A)\omega_z/A \quad [7]$$

In integral form

$$\rho = \rho_0 \exp\left(i\int_0^t \nu dt\right) + \left[\exp\left(i\int_0^t \nu dt\right)\right]\int_0^t N\left[\exp\left(-i\int_0^t \nu dt\right)\right] dt \quad [8]$$

In general, one wants to express the motion of a body in inertial coordinates; this problem usually proves to be more difficult than that of expressing the motion in body coordinates. Quite often position in inertial coordinates is described in terms of Euler angles. These angles are defined in the following way: Let 0 be the center of mass about which the body rotates, and let $0XYZ$ be a right-handed system of rectangular axes fixed in space. Let $0xyz$ be rectangular axes fixed in the body and coincident with $0XYZ$ before the displacement. Let $0K$ be perpendicular to the plane $z0Z$, drawn so that if $0Z$ is directed to the vertical and the projection of $0z$ perpendicular to $0Z$ is directed to the south, then $0K$ is directed to the east. Denote the angles $z0Z$, $Y0K$, $y0K$ by θ, ψ, ϕ, respectively; these are the three Euler angles defining the position of the axes $0xyz$ with reference to the axes $0XYZ$.

The differential equations relating the Euler angles and a body's angular rate expressed in terms of rotating coordinates are

$$\dot{\theta} = \omega_x \sin\phi + \omega_y \cos\phi \quad [9]$$

$$\dot{\psi}\sin\theta = -\omega_x \cos\phi + \omega_y \sin\phi \quad [10]$$

$$\dot{\phi} = \omega_z - \dot{\psi}\cos\theta \quad [11]$$

Eqs. 9 and 10 can be combined to give

$$\dot{\theta} + i\dot{\psi}\sin\theta = -i\rho\exp(i\phi) \quad [12]$$

or with Eq. 8

$$\dot{\theta} + i\dot{\psi}\sin\theta = -i\rho_0\exp\left[i\left(\phi + \int_0^t \nu dt\right)\right] - i\left\{\exp\left[i\left(\phi + \int_0^t \nu dt\right)\right]\right\}\int_0^t N\left[\exp\left(-i\int_0^t \nu dt\right)\right] dt \quad [13]$$

Torque Required for Specific Motion (2)

Eq. 13 can be used to find what torque is necessary to produce almost any desired angular rates $\dot{\theta}_1$ and $\dot{\psi}_1$, or at least rates that approach these desired rates. For simplicity in presenting the general method, let $L_z = \rho_0 = 0$.[5] Thus, Eq 13. becomes

$$\dot{\theta} + i\dot{\psi}\sin\theta = -i\{\exp[i(\phi + \nu t)]\}\int_0^t N[\exp(-i\nu t)]dt \quad [14]$$

If $\dot{\theta}_{10} = 0$, $\dot{\psi}_{10}\sin\theta_{10} = 0$, and $\theta_1 \neq 0$, then the required torque is found by replacing θ and ψ with θ_1 and ψ_1 in Eq. 14 and solving for N.

If $\dot{\theta}_{10} \neq 0$ or $\dot{\psi}_{10}\sin\theta_{10} \neq 0$, one may substitute into Eq. 14 values of $\dot{\theta}$ and $\dot{\psi}$ that will approach the desired rates, for example

$$\dot{\theta} = [\dot{\theta}_1(\theta,\psi,\ldots)](1 - \exp at) \quad [15]$$

$$\dot{\psi} = [\dot{\psi}_1(\theta,\psi,\ldots)](1 - \exp at) \quad [16]$$

where a is a negative real number. The value of N obtained from Eq. 14 gives a torque that will produce rates that approach the desired rates.

If $\theta = 0$ in Eq. 14, then the problem of defining ψ and ϕ exists. In general, an inertial coordinate system should be chosen so that $\theta \neq 0$; then rates in this coordinate system can be used to compute N from Eq. 14.

Although the mathematical method described in this section gives torques for the control of angular rate, it can be used to give torques for the control of angles; i.e., the angular rate can be selected so that particular angles are obtained and so that the rate approaches zero as the angles are approached (as in the next section). In general, once the desired angles are reached, a continuous torque is necessary to maintain them.

Torque Required for a Specific Example

Suppose one wishes to turn a satellite so that its axis of symmetry points in a given direction. If inertial coordinates are chosen so that Z coincides with this direction, then one way to turn the satellite is to have θ approach 0 while $\dot{\psi} = 0$, i.e., to rotate the z-axis in a plane.[6] Suppose the desired motion is $\dot{\theta}_1 = k\theta_1$, where k is a negative real number. This expression gives the desired end condition $\dot{\theta}_1 = 0$ at $\theta_1 = 0$, but $\dot{\theta}_{10} \neq 0$. Thus, Eqs. 14, 15, and 16 are used to solve for

Received April 7, 1961.

[1] Research Scientist and Consultant.
[2] Mathematician.
[3] Physicist.
[4] Numbers in parentheses indicate References at end of paper.

[5] Using Eqs. 3 and 11 one can modify the method to include ω_z as a variable; thus, theoretically, θ, ψ and ϕ can be controlled.
[6] Of course, if only the final direction is important for control, then various expressions for θ and ψ may be used.

N; for $\rho_0 = 0$, they give

$$N = ik\theta[\exp(-i\phi)]\{[(\dot{\theta}/\theta)(1 - \exp at) - a \exp at] - i[(\dot{\phi} + \nu)(1 - \exp at)]\} \quad [17]$$

and so

$$|N| = |k|\theta\{[k(1 - \exp at)^2 - a \exp at]^2 + [(\omega_z + \nu)(1 - \exp at)]^2\}^{1/2} \quad [18]$$

From Eq. 15

$$\dot{\theta} = k\theta(1 - \exp at) \quad [19]$$

thus

$$\theta = \theta_0 \exp [kt + (k/a)(1 - \exp at)] \quad [20]$$

Fig. 1 shows relative plots of $|N|/\theta$ and θ for a particular set of values.

The direction of the torque in the xy plane with respect to the x-axis is given by the angle μ, where

$$\sin(\mu + \phi) = \frac{k(1 - \exp at)^2 - a \exp at}{\{[(\omega_z + \nu)(1 - \exp at)]^2 + [k(1 - \exp at)^2 - a \exp at]^2\}^{1/2}} \frac{k}{|k|} \quad [21]$$

Fig. 1 shows a graph of $\mu + \phi$ for a particular set of values. Note that the initial value of $\mu + \phi$ is $-\pi/2$, and as time increases $\mu + \phi$ tends toward a constant value near π. It is of interest to compare this result with the simple approximate theory of gyroscopic action, which says that for a large spin rate a torque applied perpendicular to the spin axis produces rotation about an axis perpendicular to the torque axis; i.e., the z-axis turns into the resultant torque (3).

If $\rho_0 = \omega_0 \exp(i\tau) \neq 0$ and N is given by Eq. 17, then

$$\theta = \theta_0 \exp [kt + (k/a)(1 - \exp at)] + \exp [kt - (k/a) \exp at] \int_0^t \omega_0 \sin(\tau + \phi + \nu t) \exp [(k/a) \exp at - kt] dt \quad [22]$$

and

$$\dot{\psi} \sin \theta = -\omega_0 \cos(\tau + \phi + \nu t) \quad [23]$$

For certain examples the last term of Eq. 22 may not be sufficiently near zero. The torque could be modified from that given by Eq. 17 to include a term to damp out the effect of the initial ρ value. The ρ_0 term of Eq. 13 suggests that $\int_o^t N \exp(-i\nu t)\, dt$ could include a term such as $\rho_0 (\exp kt - 1)$. Then

$$N = ik\theta[\exp(-i\phi)]\{[(\dot{\theta}/\theta)(1 - \exp at) - a \exp at] + [(\dot{\phi} + \nu)(1 - \exp at)]^2\}^{1/2} + k\rho_0 \exp(kt + i\nu t) \quad [24]$$

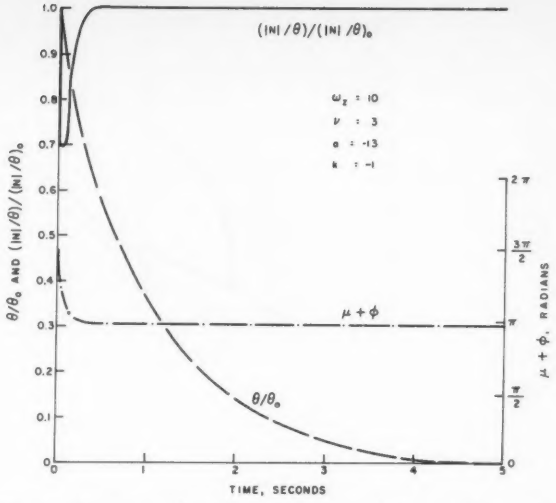

Fig. 1 Torque required for a particle control example; rates are in radians per sec

and

$$\theta = \theta_0 \exp [kt + (k/a)(1 - \exp at)] + \exp [kt - (k/a) \exp at] \int_0^t \omega_0 \sin(\tau + \phi + \nu t) \exp [(k/a) \exp at]\, dt \quad [25]$$

which should give sufficient damping. (Ref. 2 gives more information on damping of angular rates.)

Practical System Design

A mathematical method of finding torques for particular control applications is only a starting point for actual system design. The ideal of achieving the utmost in simplicity in hardware design requires comprehensive mathematical analysis. Such analysis also normally finds the majority of trouble spots that require special developmental effort. Our work at NOTS is directed toward these results.

References

1 Whittaker, E. T., *Analytical Dynamics*, 4th ed., Dover, New York.

2 Cole, R. D., Ekstrand, M. E. and O'Neill, M. R., "Motion of A Rotating Body, A Mathematical Introduction to Satellite Attitude Control," NAVWEPS Rep. 7619, U. S. Naval Ordnance Test Station, China Lake, Calif.

3 Page, L., *Theoretical Physics*, 2nd ed., Van Nostrand, New York, 1947, p. 146.

Preliminary Thrust-Time Curve for a Spherically Shaped Solid Propellant Rocket Motor

HOWARD M. SEGAL[1]

The Martin Co., Denver, Colo.

Received July 24, 1961.

[1] Assistant Project Engineer, Advanced Programs Div. Member ARS.

A systems engineer can now obtain a preliminary thrust vs. time curve for a spherically shaped grain (Fig. 1) by using the curves plotted in Figs. 2–4. Knowing only thrust, burning rate, specific impulse, and total impulse, he can select the proper thrust-time curve in less than one hour. Since the closures of any motor can be spherically shaped, the curves described in this paper can be used to predict the ballistic performance of a spherical motor, a cylindrical motor, or a segmented motor (Ref. 2).

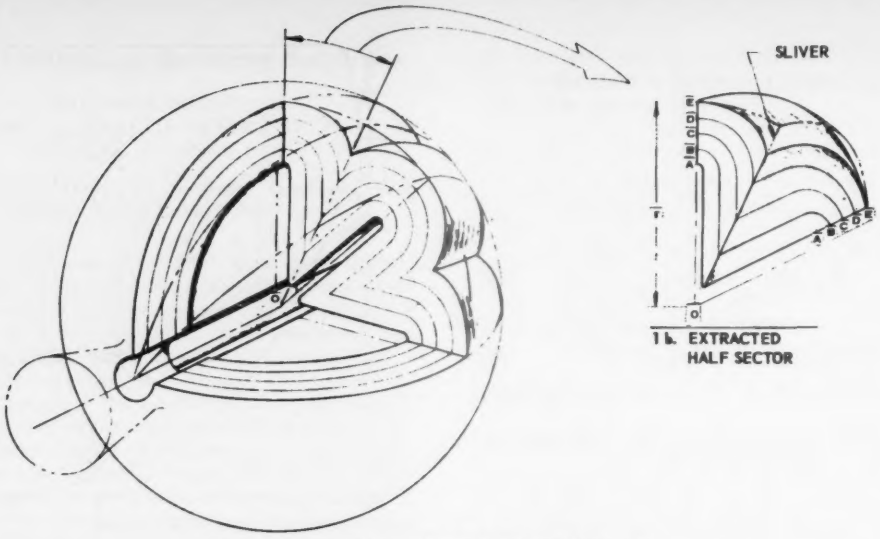

Fig. 1 Burnback positions of a melon-slice grain

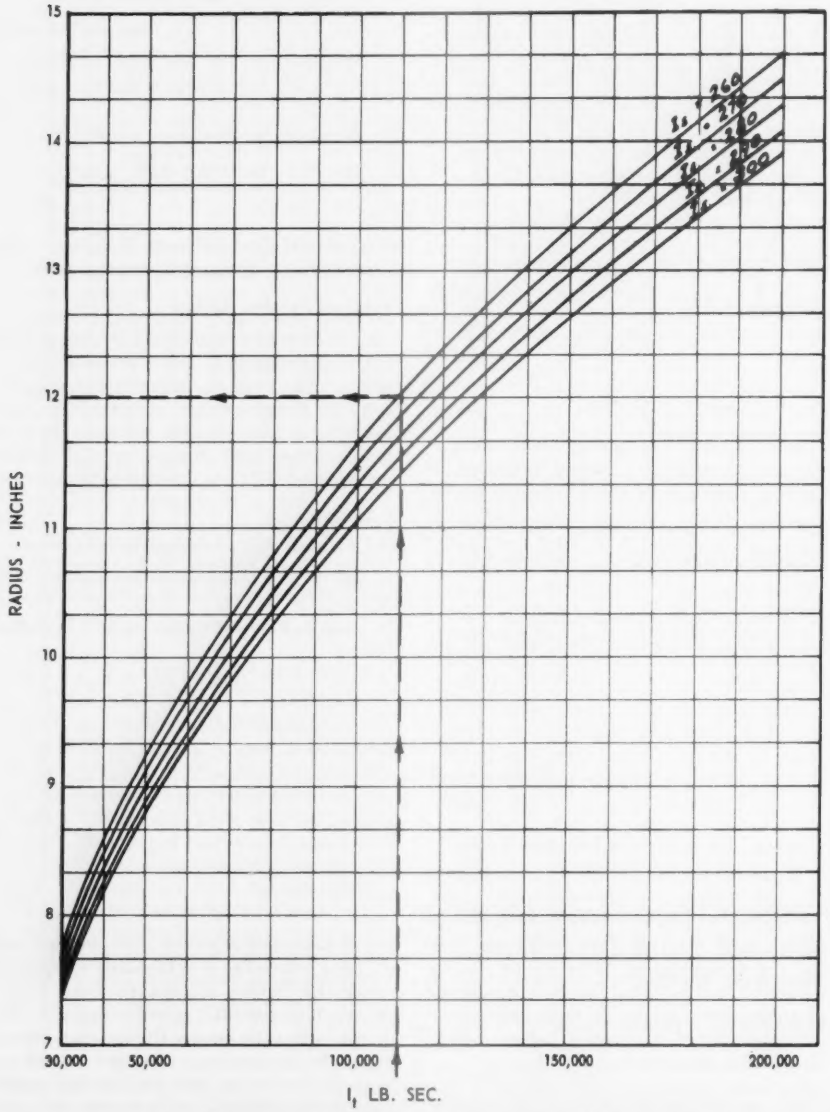

Fig. 2 Total impulse vs. chamber radius for different I_s (spherical motors)

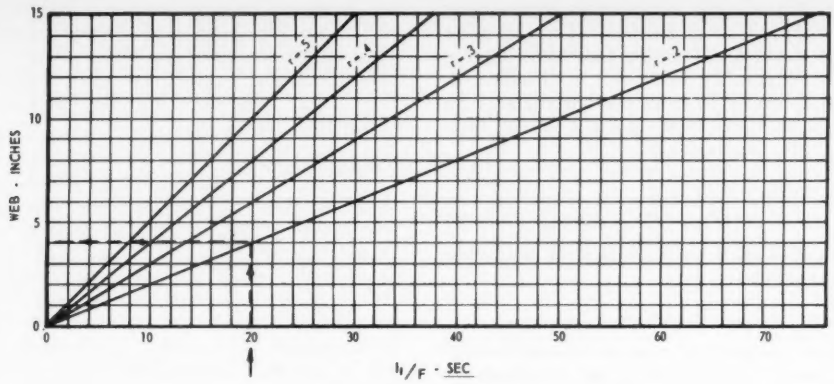

Fig. 3 Web vs. I_t/F for different burning rates

THE THREE curves of Figs. 2–4 are used in the following manner. With known thrust and total impulse, the radius can be selected from the curve of Fig. 2 and the web thickness selected from Fig. 3. Having now chosen a web thickness and a radius, a burning-area vs. web-thickness curve is selected from Fig. 4, which in turn is converted to a thrust-time curve by simple interior ballistic techniques.

Curve Explanation

Curves in Fig. 2 convert total impulse to grain radius by means of the following two mathematical relationships:

$$V_g = \frac{I_t}{I_s \times \rho \times \text{Loading}} \qquad [1]$$

$$R = (3V_g/4\pi)^{1/3} \qquad [2]$$

Web thickness derived from the curve shown in Fig. 3 is a graphical representation of the equation $w = rI_t/F$. Fig. 4 is the general solution of the burning area vs. web curve for any diameter spherical grain. It was obtained by developing curves for different web thickness using the method described in (1).[2] These curves were then made nondimensional and plotted in Fig. 4.

The burning area vs. web curve selected from Fig. 4 can be converted to a thrust vs. time curve in either of two ways. First, if rapid results are desired and the curve selected is essentially neutral, r can be considered constant, the thrust vs. time curve can be plotted proportional to the propellant area—fraction of web consumed curve. This is borne out by the mass-balance equation

$$A_p \rho r = \frac{F}{I_s} \qquad [3]$$

and the duration equation

$$w = r\Delta t \qquad [4]$$

For vacuum operation, with the above assumption that r is constant, all the terms in both equations are constant except for A_p and F in Eq. 3 and w and Δt in Eq. 4; therefore

$$A_p \sim F \qquad \text{in Eq. 3}$$

and

$$w \sim t \qquad \text{in Eq. 4}$$

If a more accurate thrust vs. time curve is desired, r cannot be considered constant. The propellant area and web at each instant during motor operation, or at each point of web burnback, must be calculated using Eqs. 3 and 4; an exact thrust-time curve will result.

[2] Numbers in parentheses indicate References at end of paper.

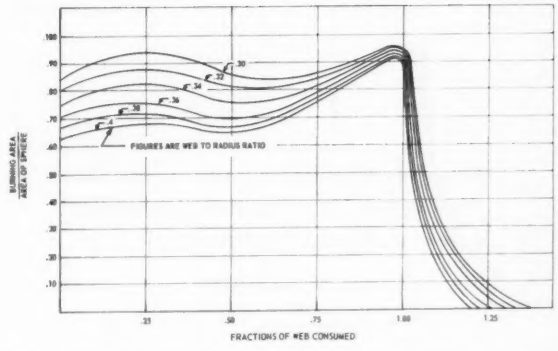

Fig. 4 Burning area ratio vs. fraction of web consumed for a spherical motor with web to radius ratio of 0.3 to 0.4

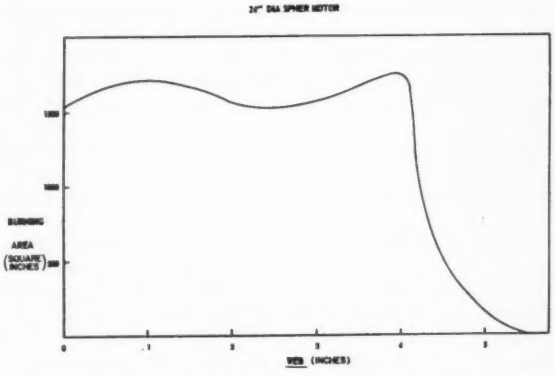

Fig. 5 Burning area vs. web

Sample Problem

Thrust and duration are usually given for a specific propulsion system. Let us assume a total impulse of 110,000 lbf-sec, a burning rate equal to 0.2 ips, a specific impulse of 260

sec, and a thrust of 5500 lbf. Fig. 2 shows that, by assuming these values, a radius of 12 in. is established. Then, by using the curve shown in Fig. 3 and knowing that total impulse divided by thrust is equal to 20, a web of 4 in. is indicated. All the information necessary to select the burning area vs. fraction of web-consumed curve shown in Fig. 4 has now been obtained.

$$\frac{w}{R} = \frac{4}{12} = 0.3$$

Since grain radius is 12 in., the area of the grain can be obtained by using the equation

$$A = \pi D^2 = 1810 \text{ sq in.}$$

The nondimensional ordinate and abscissa can now be converted to a dimensional propellant-area vs. web-thickness curve (Fig. 5), which in turn can be converted to a thrust vs. time curve by either of the two methods previously described.

Conclusion

The ballistic analysis of a melon slice grain (2) has been refined to the point where, by using the curves shown in Figs. 3 and 4, a thrust-time curve can be obtained for preliminary design purposes in less than an hour. If thrust and total impulse are known, Fig. 2 will yield the grain diameter; Fig. 3 will yield the required web; and Fig. 4 will permit selection of the properly shaped burning area vs. web-thickness curve (Fig. 5), which in turn can be converted to the end product—the thrust-time curve.

Nomenclature

Δt = duration
V_g = grain volume
I_t = total impulse
I_s = specific impulse
ρ = density
r = burning rate
w = web
F = thrust
A_p = propellant burning area
R = grain radius
A = surface area of sphere

References

1 Segal, H. M., "Design Method for Spherical Grains," ARS Journal, vol. 30, no. 4, April 1960, pp. 370, 371.

2 Segal, H. M., "Rapid Evaluation and Design of Spherical Motors," presented at the ARS Solid Propellant Conf., Salt Lake City, Utah, Feb. 1–3, 1961 (ARS preprint 1617–61).

Limitations on Space Vehicles Imposed by Communications Requirements

R. W. SANDERS[1]

Space-General Corp., Glendale, Calif.

THIS paper briefly discusses the limitations which are imposed on spacecraft design and operations by communication requirements, and suggests methods by which instrumentation facilities within the spacecraft and on the ground might be changed to overcome some of these limitations.

Usually, the most important limitation imposed on a spacecraft by the communication subsystem is the weight which must be carried aboard in order to supply the required data handling capability and the associated RF power generating equipment necessary to produce a required radiated power. In general, for a given modulation method it is necessary to increase the effective radiated power in direct proportion to the information rate which must be transmitted and as a square of the distance between the spacecraft and a ground receiver.

There are of course two methods by which increased radiated power can be achieved within a spacecraft: one is by increasing the size of the transmitter itself, whereas the other is by providing a large transmitted antenna gain. Assuming the effective radiated power in both cases is a linearly increasing function of the weight of the component involved, then the weight of the transmitter and its associated power supply should be made equal to the weight of the antenna if the objective is to minimize total spacecraft weight for a given effective radiated power. If the assumptions on the weight of transmitters and antennas are valid, it follows that the total radiated power is proportional to the square of the weight of these components if the optimum distribution of weights between them is used. Thus, to a first approximation, the range over which a spacecraft can communicate is directly proportional to the spacecraft weight, or at least to the transmitting and antenna portions of the total spacecraft weight (1).[2]

From this conclusion it might appear that in order to communicate over increasingly large distances we must continually increase the spacecraft weight. This conclusion is a valid one (for a fixed technology of power sources) only if one assumes that the modulation method and the data rate are not changed. However, the importance of a given information rate is closely associated with the type of mission involved and, more particularly, with the type of power source which is used aboard the spacecraft.

It is conceivable that in certain missions only a fixed and relatively small amount of total information must be transmitted from the spacecraft to Earth; however, it is easier to visualize missions where it is desirable to transmit to Earth as much information as possible. In this latter case there are two important aspects of the problem to be considered. In the case that power sources of a fixed lifetime are used, such as storage batteries, it is most important to consider carefully how much energy from the power source is required to transmit reliably one bit of information. In this case it is important to choose modulation techniques which provide the highest communication efficiency possible (2,3). If power sources are used which have an indefinite or a very long lifetime, such as solar cells or nuclear power sources, the important question to be asked is how much time can be afforded to transmit back from a spacecraft the desired information. If a time restriction is placed on transmitting a given amount of information, the communication problem immediately becomes the same as the one where storage cells are used for power. Again, in order to minimize spacecraft weight it is necessary to consider the communication efficiency question carefully.

It is not always the case that we must impose very confining limitations on the data rates which must be received from a spacecraft in order to consider a mission successful. For example, in a space probe that requires many months or even years to reach its destination, it is conceivable that data rates in the order of one bit per minute or even one bit

Presented at the ARS Missile and Space Vehicle Testing Conf., Los Angeles, Calif., March 13–16, 1961.

[1] Director, Satellite and Space Laboratories.

[2] Numbers in parentheses indicate References at end of paper.

per hour or per day might be perfectly reasonable data rates. However, transmitting at these rates involves another limitation imposed by a communication requirement that in many cases is just as fundamental and far reaching as any weight requirement; that is, the requirement of sufficiently stable oscillators at both ends of the link, and precise enough orbit determination techniques to allow very precise Doppler prediction methods to be used at the receiver.

A communication system with an average power limitation can be made to operate most efficiently if some type of matched filter detection method is used. However, for proper operation, matched filters must maintain a high degree of phase stability between the filter and the received waveform during the entire duration of the waveform. For example, if a 1000 mc is used as a carrier frequency in a spacecraft communication link, and it is assumed that oscillators at each end of the link are predictable in frequency to an accuracy of one part in 10^{10}, coherent matched filter detection methods can be used as long as the duration of each individual waveform is short compared to 10 sec. However, this example should not be taken to mean that systems cannot be built to operate at data rates of less than 1 bit transmitted every 10 sec. Such transmission rates are possible under the conditions of a 1000-mc carrier link and a one part in 10^{10} stability oscillators, although communication will not occur with as an efficient use of transmitter power as in the case that matched filter techniques are used. For example, consider Fig. 1. Here is shown the ratio of received power required to gaussian noise spectral density as a function of integration time per bit transmitted in an On/Off type PCM system. Here it is seen that as long as the integration time is small compared to 10 sec, coherent detection methods can be used and the required received power increases inversely as the first power of the integration time. However, if the duration of one bit becomes long compared with 10 sec, the receiver must make a judgment as to whether a signal is present within a bandpass which is larger than that required for a filter matched to the incoming waveform. In this case, since the precise frequency of the incoming waveform cannot be known, a chi-square distribution type, i.e., average energy type, of detector must be used. The received power required is related to the integration time per bit through an inverse square law relationship. Assuming that a noise spectral density is caused solely by a receiver which has an equivalent input noise temperature of 100°K, it is seen from the right-hand margin of Fig. 1 that with this type of modulation system, the minimum receivable signal possible using coherent detection techniques is approximately −170 dbm. However, if noncoherent techniques are used, the received signal level can be dropped to approximately −190 dbm, provided the bit rate is reduced to a point where one bit is transmitted each several hours.

Fig. 2 shows the results of this type of modulation and detection method as a function of transmitter to receiver range, assuming system constants as shown in the figure. In both figures are shown the amount of power and range which would be achieved if it were possible to design a so-called Shannon system, i.e., a system which is theoretically the most efficient possible communication system. Certainly it is seen that noncoherent detection of CW-like signals becomes extremely inefficient as the integration time becomes long compared to the reciprocal of the relative oscillator stabilities between the transmitter and the receiver in cycles per second.

These brief remarks indicate that in order to reduce the restrictions imposed upon spacecraft vehicle design and operations, state of the art advances must be made in those fairly obvious areas of increasing transmitter power, antenna gains, and receiver sensitivities. In addition, a very fruitful area in expanding communications capabilities to allow spacecraft operations at extreme ranges requires the development of more precise timing standards than are presently available, and in the end will require the utmost precision in the determination of the relative velocities between spacecraft and Earth based stations. Connected with the development of more stable clocks should be the use of more efficient modulation techniques, which include those methods which will approach the communication efficiency of Shannon type systems, and the inclusion of data processing equipments aboard the spacecraft to reduce the redundancy within data prior to its transmission. All of these methods can reduce the limitations presently imposed by communication requirements on spacecraft both as to extending their operating range and increasing their flexibility at medium ranges.

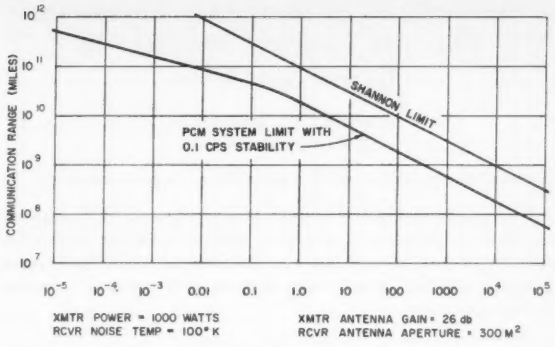
COMMUNICATION RANGE (MILES)
SHANNON LIMIT
PCM SYSTEM LIMIT WITH
0.1 CPS STABILITY
XMTR POWER = 1000 WATTS
RCVR NOISE TEMP = 100°K
XMTR ANTENNA GAIN = 26 db
RCVR ANTENNA APERTURE = 300 M²

Fig. 1 Integration time per bit sec

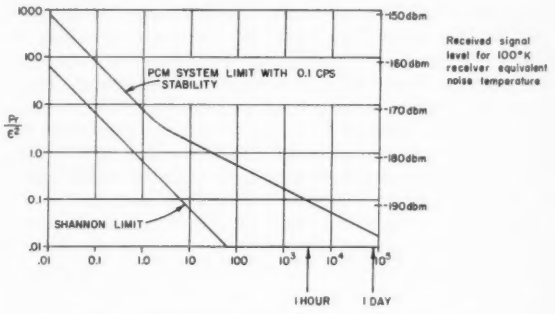

Fig. 2 Maximum information rate, bits per sec

References

1 Mueller, G. E., "A Pragmatic Approach to Space Communications," *Proc.* of the IRE, vol. 48, no. 4, April 1960.

2 Sanders, R. W., "Communication Efficiency Comparison of Several Communication Systems," *Proc.* of the IRE, vol. 48, no. 4, April 1960.

3 Sanders, R. W., "Digilock Communication System," *IRE WESCON Convention Record*, Part 5, August 1960.

Streamlines in Boundary Layers on Flat and Concave Surfaces in Hypersonic Flow[1]

ROBERT H. JOHNSON[2]
ELWIN C. BIGELOW[3]

General Electric Research Laboratory, Schenectady, N. Y.

Strong transverse secondary flows in the thick boundary layers on wedges in hypersonic helium flow are shown by means of oil streamers. Inhibition of this transverse boundary layer flow is demonstrated by use of concave wedge surfaces.

BOUNDARY layers on surfaces of some bodies at hypersonic speeds are very thick as a result of large temperature rises with corresponding density decreases caused by the viscous deceleration from high velocities. In addition to the much studied interaction between these viscous layers and the free stream flow field, the existence of the thick low kinetic energy layers on the body surface present additional complexities by providing flow area for propagating disturbances independent of the restrictions imposed by the very high Mach number external flow. Upstream and transverse flow leakage and propagation of disturbances within the boundary may become dominant features governing the aerodynamics of some hypersonic vehicle shapes and components.

Secondary flows within the boundary layer on the surface of a finite width plane and concave sharp wedges are described here. The experiments performed in the helium tunnel (1)[4] at Mach 28.9 show the extent of influence of model edges on the boundary layer flow pattern and demonstrate how this resulting secondary flow may be controlled by surface contours. The Reynolds number per inch was 0.7×10^6 for all runs with the boundary layer streamline trajectories traced by means of an oil streamer technique modified from that used in the shock tunnel by the Missile and Space Vehicles Dept., General Electric Co. (2).

Fig. 1 shows a photograph of the 10° half-angle wedge model with the oil strips applied to the surface before being placed in the helium tunnel. The concave surface is a deepening valley generated by two straight lines of decreasing angle from 180° to 140° between them on a model ¾-in. wide. The tunnel was run for approximately 4 sec per test. The length of the oil streamers gives a qualitative indication of shear stresses in the boundary layer on the model surface. The direction of the streamers indicate the boundary layer flow direction near the surface.

A schlieren photograph in Fig. 2 was taken with a vertical knife edge. The boundary layer on the plane wedge surface is clearly seen while only a small portion of the boundary layer at the leading edge of the concave surface is shown. The rest is skewed with respect to the light beam or is buried in the model valley.

The oil streamer patterns for the flat and concave wedge surfaces are given at the bottom of Fig. 2. On the flat wedge surface strong side flow within the boundary layer is shown by the oil streamer deflections. This side leakage occurs outside a region bounded by lines from the ends of the leading edge and back at approximately 30°, even though the Mach angle is only 2°. The gas on the wedge being at a pressure above the ambient pressure expands transversely into the lower free stream reservoir. However, after the gas experiences a Prandtl-Meyer expansion at the end of the wedge surface, the pressure is lower than the free stream value. This condition is seen by the inward deflection of the oil streamers on the flat surface downstream of the 10° plane wedge where gas from outside the boundary layer flows into it.

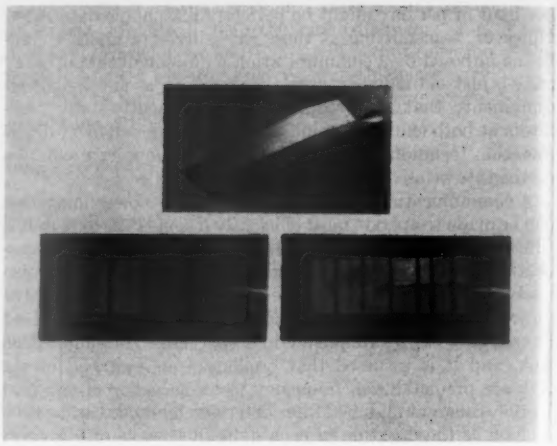

Fig. 1 Photographs of model and initial oil deposits

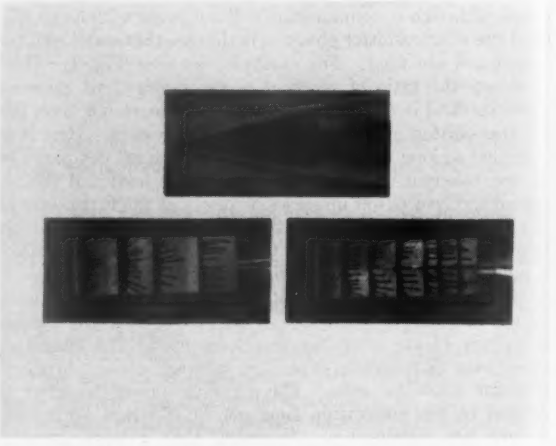

Fig. 2 Schlieren photograph at M = 28.9 and oil streamers on the flat and concave surfaces of the 10° half angle wedge

The side leakage of the boundary layer gas has been nearly blocked on the concave surface also shown in Fig. 2. The oil streamers are parallel to the main stream except very close to the model edge. That is, they exhibit an ever increasing realignment of the boundary layer flow pattern as the angle and depth of the groove becomes greater. The inward transverse pressure gradient caused by the lower flow deflection at the centerline balance the outward pressure gradient discussed above.

This suggests a means for controlling the side leakage flow in thick hypersonic boundary layers. Proper contouring of the concave surface will allow one to tailor the boundary layer velocity distribution and thereby give an added degree of control over the pressure acting on surfaces of finite width bodies.

Received June 18, 1961.
[1] This research was partially supported by the Ballistic Missile Div., U. S. Air Force, under contract AF 04(647)-269.
[2] Mechanical Engineer. Member ARS.
[3] Research Technician.
[4] Numbers in parentheses indicate References at end of paper.

References

1 Johnson, R. H., "A Hypersonic Helium Tunnel for Mach Numbers Above Twenty," G. E. Res. Lab. Rep. no. 58-RL-2089, September 1958.
2 Kaegi E. M., private communication.

One-Dimensional Overtaking of a Shock Wave by a Rarefaction Wave[1]

I. I. GLASS[2]
L. E. HEUCKROTH[3]
S. MOLDER[4]

Institute of Aerophysics, University of Toronto

WHEN a rarefaction wave $\vec{R}$ overtakes a shock wave $\vec{S}$ in a one-dimensional, inviscid, perfect gas flow ($1 \leq \gamma \leq 5/3$) it is possible to generate four final wave systems consisting of oppositely facing transmitted and reflected waves separated by a contact region C. Symbolically, these may be represented as follows (1):[5]

$\vec{R}\vec{S}$ a) $\overleftarrow{R}\vec{C}\vec{S}$, b) $\overleftarrow{S}\vec{C}\vec{S}$, c) $\overleftarrow{R}\vec{C}\vec{R}$, d) $\overleftarrow{S}\vec{C}\vec{R}$

The four cases are illustrated in the distance-time (x, t)-plane in Figs. 1 and 2. It is also possible to produce the limiting cases where either or both the reflected or transmitted waves are Mach waves.

Although these wave systems are shown to be possible in (1), the present note provides the analytical solutions in the form of algebraic equations, which make it possible to determine the final waves and quasi-steady states in terms of the initial conditions. The nonstationary penetration regions in the immediate vicinity of the interaction are not considered in the present analysis.

In obtaining the solutions, the following assumptions are made: the reflected compression waves coalesce and may be replaced by a shock front; the secondary Mach waves and contact surfaces that are generated during the formation of a reflected shock front may be considered as weak and do not affect the final states shown in Figs. 1 and 2. This latter assumption has been shown to be quite reasonable from experimental results, e.g. (3), and is similar to some steady flow analyses where the secondary Mach waves are neglected. If the initial states 1, 4, 5 and the waves $\vec{R}\vec{S}$ are specified, then the following four equations give a relation for the pressure ratio p_2/p_1 of the transmitted wave P_{21} in terms of the incident shock wave P_{51}, the overtaking rarefaction wave P_{45}, and the specific heat ratio γ.

For region A, Fig. 3

$$\overset{\vec{R}\vec{S}}{\left[\frac{1-P_{15}}{\sqrt{P_{15}(\alpha+P_{15})}}+\frac{1-P_{21}}{\sqrt{\alpha P_{21}+1}}\right]}\overset{\overleftarrow{R}\vec{C}\vec{S}}{\left[\frac{\beta P_{15}(P_{15}+\alpha)}{\alpha P_{15}+1}\right]^{1/2}}+ 2P_{45}{}^{\beta}-(P_{21}P_{15})^{\beta}-1=0 \quad [1]$$

For region B

$$\overset{\vec{R}\vec{S}}{\left[\frac{1-P_{15}}{\sqrt{P_{15}(\alpha+P_{15})}}+\frac{1-P_{21}}{\sqrt{\alpha P_{21}+1}}\right]}\overset{\overleftarrow{S}\vec{C}\vec{S}}{\left[\frac{\beta P_{15}(P_{15}+\alpha)}{\alpha P_{15}+1}\right]^{1/2}}+ P_{45}{}^{\beta}-\frac{\sqrt{\beta}\,P_{45}{}^{\beta}\left(\frac{P_{21}P_{15}}{P_{45}}-1\right)}{\sqrt{\frac{\alpha P_{21}P_{15}}{P_{45}}+1}}-1=0 \quad [2]$$

For region C

$$\overset{\vec{R}\vec{S}}{\left[\frac{\sqrt{\beta}\,(1-P_{15})}{\sqrt{P_{15}(\alpha+P_{15})}}+(1-P_{21}{}^{\beta})\right]}\overset{\overleftarrow{R}\vec{C}\vec{R}}{\left[\frac{P_{15}(P_{15}+\alpha)}{\alpha P_{15}+1}\right]^{1/2}}+ 2P_{45}{}^{\beta}-(P_{21}P_{15})^{\beta}-1=0 \quad [3]$$

For region D

$$\overset{\vec{R}\vec{S}}{\left[\frac{\sqrt{\beta}\,(1-P_{15})}{\sqrt{P_{15}(\alpha+P_{15})}}+(1-P^{\beta_{21}})\right]}\overset{\overleftarrow{S}\vec{C}\vec{R}}{\left[\frac{P_{15}(P_{15}+\alpha)}{\alpha P_{15}+1}\right]^{1/2}}+ P_{45}{}^{\beta}-\frac{\sqrt{\beta}\,P_{45}{}^{\beta}\left(\frac{P_{21}P_{15}}{P_{45}}-1\right)}{\sqrt{\frac{\alpha P_{21}P_{15}}{P_{45}}+1}}-1=0 \quad [4]$$

where

$$\alpha=\frac{\gamma+1}{\gamma-1} \qquad \beta=\frac{\gamma-1}{2\gamma}$$

Received June 7, 1961.
[1] The research was supported by DRB, Canada, and ONR, USN.
[2] Professor Aeronautics/Astronautics.
[3] Research Assistant.
[4] Research Assistant.
[5] Numbers in parentheses indicate References at end of paper.

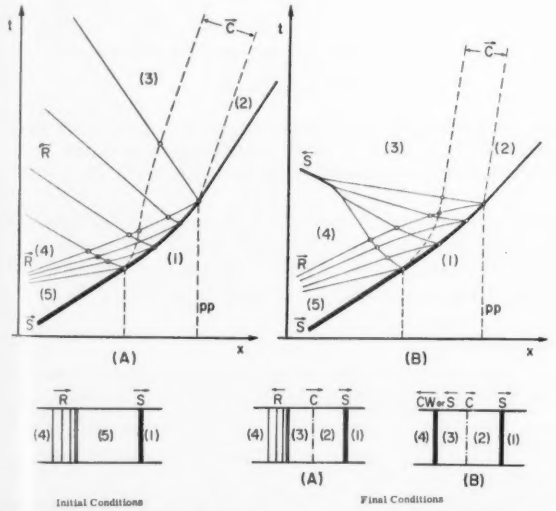

Fig. 1. Overtaking of a shock wave by a weak rarefaction wave

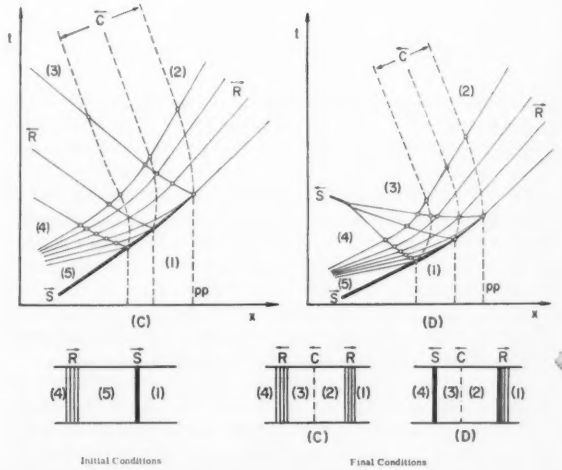

Fig. 2. Overtaking of a shock wave by a strong rarefaction wave

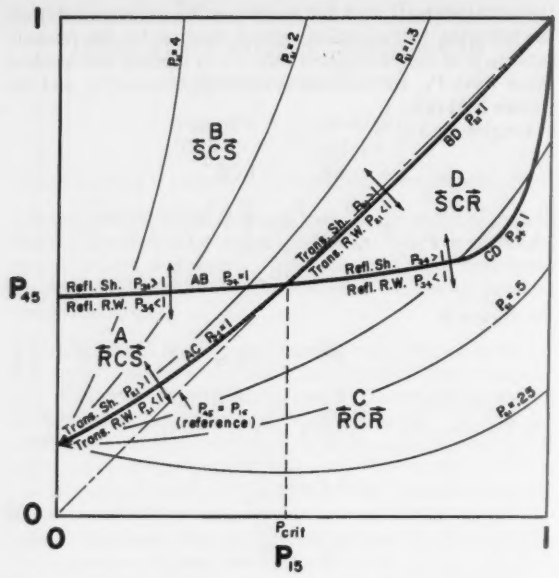

Fig. 3. Sketch of the four basic regions and their boundaries described by Eqs. 1 to 4

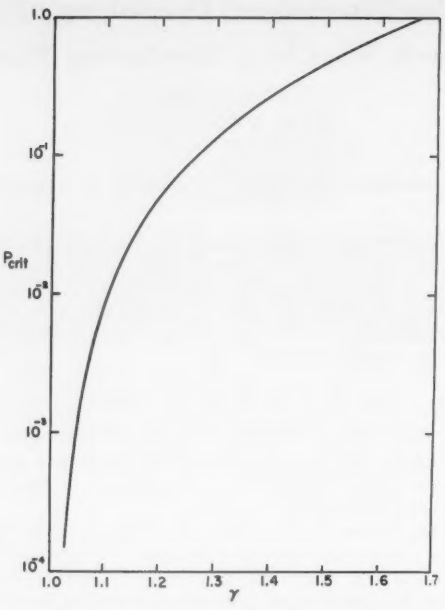

Fig. 4 Variation of P_{CRIT} with the specific heat ratio γ

The reflected wave strength P_{34} in all cases can be found from the condition that across the contact region the pressures are identical $p_2 = p_3$, or

$$P_{34} = P_{21} \cdot P_{15} \cdot P_{54} \qquad [5]$$

Eqs. 1, 2 and 5 describe the condition when the overtaking rarefaction wave is weak and a transmitted shock wave always results. Eqs. 3, 4, and 5 deal with the case when the overtaking rarefaction wave is strong and a transmitted rarefaction wave is always produced after the interaction.

If the above equations are plotted on a (P_{45}, P_{15})-plane, it can be shown (2) that they apply to four distinct regions, as indicated in Fig. 3. The boundary lines shown by the curves on which $P_{34} = 1$, a reflected Mach wave, and $P_{21} = 1$, a transmitted Mach wave, are obtained by allowing the respective waves, P_{34} and P_{21}, to approach unity in Eqs. 1–4, as required. In addition, the point of intersection of these two curves P_{CRIT} gives the condition for the unique case of a reflected and transmitted Mach wave, and may be obtained from any of the four basic equations by letting $P_{21} = 1 = P_{34}$, or

$$\sqrt{\beta}\,\frac{1 - P_{CRIT}}{\sqrt{\alpha P_{CRIT} + 1}} + P_{CRIT}^{\beta} - 1 = 0 \qquad [6]$$

From Eq. 5 it is seen that as a result $P_{15} = P_{45}$.

Eq. 6 is shown in Fig. 4. It is seen that P_{CRIT} is a monotonically increasing function of γ and has the limiting value for physical gases of $P_{CRIT} = 0$ for $\gamma = 1$, and $P_{CRIT} = 1$ for $\gamma = 5/3$. See (2) for a proof. The region of applicability of the various equations is discussed in detail in (2). Briefly, it can be seen from Fig. 3, that the extent of regions A to C in the (P_{15}, P_{45})-plane depends on the position of the point P_{CRIT}, whose locus is the 45° line $P_{45} = P_{15}$. In the limit when $P_{CRIT} = 0$, region A is nonexistent ($\gamma = 1$), and when $P_{CRIT} = 1$, region D vanishes ($\gamma = 5/3$). For all other gases ($1 < \gamma < 5/3$), all four regions are possible.

The above equations have been solved numerically on an IBM 650 digital computer for pressure ratios up to 1000 for perfect gases. (At the higher pressure ratios the results would not be valid for imperfect gas flows.) Specific heat ratios (γ) corresponding to monatomic (5/3), diatomic (7/5), carbon dioxide (1.30) and sulfur-hexafluoride (1.093) have been used

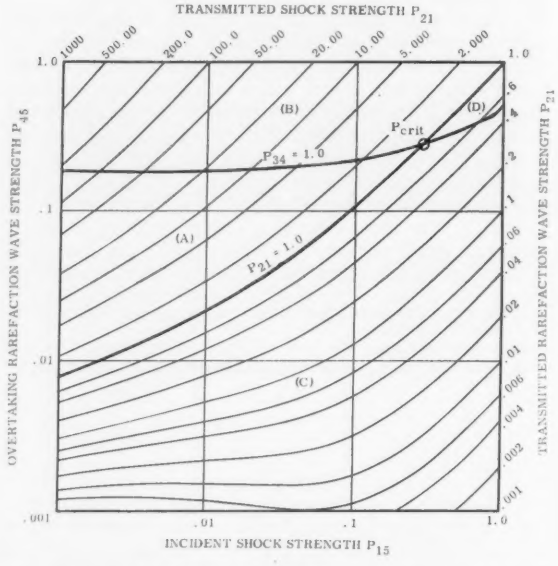

Fig. 5 Variation of the transmitted shock or rarefaction wave strength P_{21} with the initial overtaking rarefaction wave strength P_{45} and the incident shock wave strength P_{15} for $\gamma = 7/5$

in the computations to provide for an experimental means of checking the theory. A simplified plot for the case of $\gamma = 7/5$ is shown in Fig. 5. Further detailed plots can be found in (2). The complementary problem is treated in (4).

References

1 Courant, R. and Friedrichs, K. O., "Interaction of Shock and Rarefaction Waves in One-Dimensional Motion," OSRD Rep. 1567, 1943.

2 Glass, I. I., Heuckroth, L. E. and Molder, S., "On the One-Dimensional Overtaking of a Shock Wave by a Rarefaction Wave," UTIA Tech. Note no. 30, 1959.

3 Glass, I. I. and Hall, J. G., *Handbook of Supersonic Aerodynamics*, Section 18. "Shock Tubes," Navord Rep. 1488, vol. 6, U.S. Government Printing Office, Washington, D. C., 1959.

4 Bremner, G. F., Dukowicz, J. K. and Glass, I. I., "On the one-Dimensional Overtaking of a Rarefaction Wave by a Shock Wave," UTIA Tech. Note no. 33, 1960.

One-Dimensional Overtaking of a Rarefaction Wave by a Shock Wave[1]

G. F. BREMNER,[2]
J. K. DUKOWICZ[3]
I. I. GLASS[4]

Institute of Aerophysics, University of Toronto

WHEN a shock wave $\vec{S}$ overtakes a rarefaction wave $\vec{R}$ in a one-dimensional, inviscid, perfect gas flow, it is hypothetically possible to generate four final wave systems consisting of oppositely facing transmitted and reflected waves separated by a contact region C. Symbolically these may be represented as follows (1)[5]

$\vec{S}\vec{R}$ a) $\overleftarrow{R}C\vec{R}$, b) $\overleftarrow{S}C\vec{R}$, c) $\overleftarrow{R}C\vec{S}$, d) $\overleftarrow{S}C\vec{S}$

It was shown in (1), and in an alternate manner in (2) that for all physical gases with a specific heat ratio in the range $1 \leq \gamma \leq 5/3$, only two of the four wave systems are actually possible; that is, the two containing reflected shock waves b) and d). In this sense, the problem bears an analogy to the overtaking of two shock waves (3), where for the same range of γ, only reflected rarefaction waves are possible. If the initial overtaking shock wave is weak, the transmitted wave is a rarefaction wave, and if it is strong, the transmitted wave is a shock wave. The interactions are shown schematically in the distance-time (x,t)-plane in Figs. 1 and 2.

The present note provides analytical solutions to the interaction problem in the form of algebraic equations, which make it possible to determine the final waves and quasi-steady states in terms of the initial conditions. The nonstationary penetration regions in the immediate vicinity of the interactions are not considered. Two assumptions are also made: the reflected compression waves coalesce and may be replaced by a shock front; the secondary characteristic lines and contact surfaces generated as the reflected shock wave forms are weak and do not affect the final states shown in Figs. 1 and 2. Experimental evidence, e.g. (4), has shown that these assumptions are quite reasonable.

If the initial states (1,4,5) and waves $\vec{S}\vec{R}$ are specified, then the following equations provide the relation between the pressure ratio $p_3/p_4 = P_{34}$ of the reflected wave in terms of the pressure ratios of the incident rarefaction wave P_{51}, the overtaking shock wave P_{45} and the specific heat ratio γ.

For region B, Fig 3

$$\vec{S}\vec{R} \qquad \overleftarrow{S}C\vec{R}$$

$$\frac{1 - P_{34}{}^{\beta}P_{45}{}^{\beta}}{\sqrt{\beta}} + \frac{(P_{45} - 1)}{[1 + \alpha P_{45}]^{1/2}} + \left[\frac{P_{45}(\alpha + P_{45})}{1 + \alpha P_{45}}\right]^{1/2} \frac{(1 - P_{34})}{[1 + \alpha P_{34}]^{1/2}} = 0 \quad [1]$$

For region D

$$\vec{S}\vec{R} \qquad \overleftarrow{S}C\vec{S}$$

$$[1 - P_{51}{}^{-\beta}] - \frac{\sqrt{\beta}P_{51}{}^{-\beta}(P_{34}P_{45}P_{51} - 1)}{[1 + \alpha P_{34}P_{45}P_{51}]^{1/2}} + \left[\frac{\beta P_{45}(\alpha + P_{45}}{1 + \alpha P_{45}}\right]^{1/2} \frac{(1 - P_{34})}{[1 + \alpha P_{34}]^{1/2}} + \frac{\sqrt{\beta}\,(P_{45} - 1)}{[1 + \alpha P_{45}]^{1/2}} = 0 \quad [2]$$

where

$\alpha = (\gamma + 1)/(\gamma - 1)$
$\beta = (\gamma - 1)/2\gamma$

Received June 7, 1961.
[1] The research was supported by DRB, Canada and ONR, USN.
[2] Research Assistant.
[3] Research Assistant.
[4] Professor Aeronautics/Astronautics.
[5] Numbers in parentheses indicate References at end of paper.

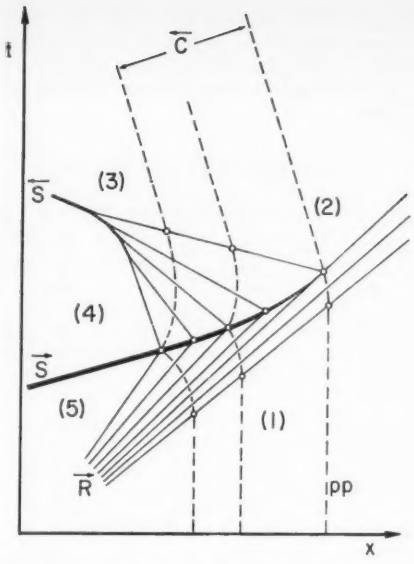

Fig. 1 Overtaking of a rarefaction wave by a weak shock wave

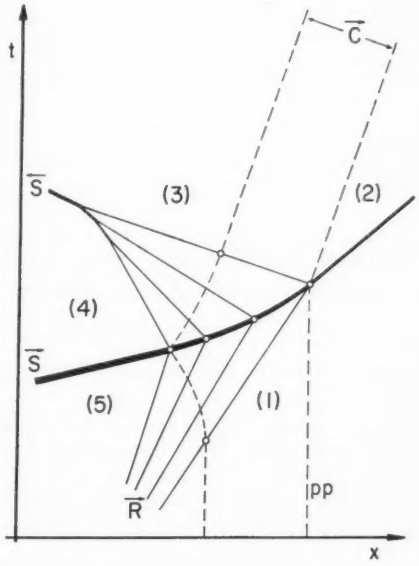

Fig. 2 Overtaking of a rarefaction wave by a strong shock wave

The transmitted wave strength P_{21} in both cases is found from the condition that across the contact region the pressures are identical $p_2 = p_3$, or

$$P_{21} = P_{34} \cdot P_{51} \cdot P_{45} \quad [3]$$

It is worth noting from Eq. 1 that the reflected shock strength P_{34} is independent of the incident rarefaction wave strength P_{51} as long as a rarefaction wave is transmitted. It can also be seen that Eq. 1 is obtainable from Eq. 2 by letting $P_{21} = 1$. Consequently, for purposes of computation it is only necessary to solve one equation to obtain a complete solution.

For the sake of completeness, Eq. 2 was solved on an IBM 650 digital computer for initial wave strengths up to 1000 for perfect gases. The results are not applicable to the higher

wave strength owing to imperfect gas effects. Specific heat ratios corresponding to monatomic (5/3) and diatomic (7/5) gases as well as carbon dioxide (1.30) and sulphurhexafluoride (1.093) were used to provide a basis for checking the theory experimentally.

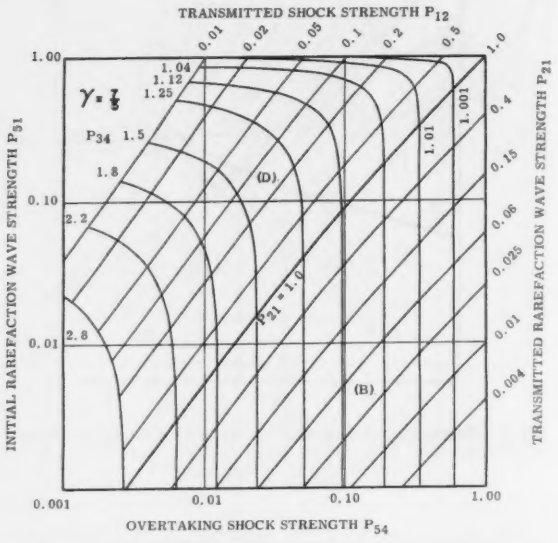

Fig 3. Variation of the reflected shock wave strength P_{34} and the transmitted wave strength P_{21} with the initial rarefaction wave strength P_{51} and the overtaking shock wave strength P_{54}

A simplified plot for the case of $\gamma = 7/5$ is shown on Fig. 3, in a (P_{51}, P_{54})-plane. The diagonal line marked $P_{21} = 1$, represents the case of a transmitted Mach wave and is the boundary between the cases of a weak and a strong overtaking shock wave. Below this line lies the region B of transmitted rarefaction waves ($P_{21} < 1$), and above it the region D of transmitted shock waves ($P_{21} > 1$). The lines of constant reflected shock strength P_{34} are vertical straight lines in region B, since here the reflected wave strength is independent of the initial rarefaction wave. In region D the lines of constant P_{34} depend on both initial waves, and consequently they are curved; but with increasing strength of the initial overtaking shock wave they tend to become horizontal, showing a decreasing dependence on this wave.

It can be seen that the reflected shock waves are quite weak over the entire range of interactions; this substantiates the assumption of using a shock front in place of a compression wave in the analysis. The results show that the reflected shock strength is greatest for gases with low specific heat ratios. Further details are given in (2). It is worth noting that the complementary problem is considered in (5).

References

1 Courant, R. and Friedrichs, K. O., "Interaction of Shock and Rarefaction Waves in One-Dimensional Motion," OSRD Rep. 1567, 1943.

2 Bremner, G. F., Dukowicz, J. K. and Glass, I. I., "On the One-Dimensional Overtaking of a Rarefaction Wave by a Shock Wave," UTIA Tech. Note no. 33, 1960.

3 Bull, G. V., Fowell, L. R. and Henshaw, D. H., "The Interaction of Two Similarly-Facing Shock Waves," UTIA Rep. no. 23, 1952.

4 Glass, I. I. and Hall, J. G., *Handbook of Supersonic Aerodynamics*, Section 18, "Shock Tubes," Navord Rep. 1488, vol. 6, U. S. Government Printing Office, Washington, D. C., 1959.

5 Glass, I. I., Heuckroth, L. E. and Molder, S., "On the One-Dimensional Overtaking of a Shock Wave by a Rarefaction Wave," UTIA Tech. Note no. 30, 1959.

Method for Determining Scale Heights in the Atmosphere

S. RUBIN[1]

Stanford Research Institute, Menlo Park, Calif.

This note describes a simple method for obtaining the atmospheric scale height from measurements of orbital parameters of satellites in moderate to strongly elliptical orbits. It is not necessary to know the drag coefficient of the satellite, nor is it necessary even to assume that it remains constant.

DETAILED analyses of the effects of air drag on generalized satellite orbits have been published by Roberson (1),[2] Sterne (2) and Baker (3). Most discussions of the measurement of upper atmosphere densities by use of observational data on satellites deal with the direct determination of the density, which requires a knowledge of the drag coefficient of the satellite. Roberson (4) described a method for determining the ratio of air densities at two different perigee altitudes traversed by a satellite, which does not require a priori knowledge of the drag coefficient, but he states that the method implicitly requires that the drag coefficient remain constant during the transfer. Michielsen (5), using a power function model of air density, derived an expression for the decay of perigee altitude per revolution which is applicable to slightly elliptic orbits.

One assumes that the orbit is sufficiently elliptic so that the orbit radius near perigee changes by the scale height over an angular range which is small compared with one radian. If one also assumes a nonrotating spherical atmosphere and Keplerian orbits, the following equations are derived for the change per revolution N, of the period T, the eccentricity e, the semimajor axis a and the perigee radius r_p

$$\frac{dT}{dN} = -3\sqrt{\frac{\pi}{2}}\left(\frac{C_DA}{m}\right)\rho_pH^{1/2}T\,a^{1/2}\left[\frac{(1+e)^{3/2}}{e^{1/2}(1-e)^{6/2}}\right] \quad [1]$$

$$\frac{de}{dN} = -2\sqrt{\frac{\pi}{2}}\left(\frac{C_DA}{m}\right)\rho_pH^{1/2}\,a^{1/2}\left[\frac{(1+e)^{3/2}(1-e)^{1/2}}{e^{1/2}}\right] \quad [2]$$

$$\frac{da}{dN} = -2\sqrt{\frac{\pi}{2}}\left(\frac{C_DA}{m}\right)\rho_pH^{1/2}\,a^{3/2}\left[\frac{(1+e)^{3/2}}{e^{1/2}(1-e)^{1/2}}\right] \quad [3]$$

$$\frac{dr_p}{dN} = -\sqrt{\frac{\pi}{2}}\left(\frac{C_DA}{m}\right)\rho_pH^{3/2}\,a^{1/2}\left[\frac{(1-e^2)^{1/2}}{e^{3/2}}\right] \quad [4]$$

where[3]

$\left(\frac{C_DA}{m}\right)$ = usual aerodynamic drag parameter

ρ_p = atmospheric density at perigee altitude

H = exponential scale height ($\rho_2 = \rho_1 e^{-\Delta h/H}$)

[1] Senior Physicist, Physics Dept. Member ARS.

[2] Numbers in parentheses indicate References at end of paper.

[3] Since the orbital parameters undergo step-like decrements at each pass through perigee, the derivatives in these formulas represent decrements per whole revolution or rates of change averaged over a large number of revolutions, and are not to be applied "microscopically" to a segment of an orbit.

The principal contribution to the drag occurs over an elevation interval of about one scale height above perigee, so that the value of H applies to this region of the atmosphere.

By taking the ratio of the rate of change of perigee radius to the other rates of change per revolution, three equations for H are derived

$$H = 3T\left[\frac{e(1+e)}{(1-e)}\right]\left(\frac{dr_p}{dT}\right) \qquad [5a]$$

$$H = 2e(1+e)\left(\frac{dr_p}{de}\right) \qquad [5b]$$

$$H = 2a\left[\frac{e(1+e)}{(1-e)}\right)\left[\frac{dr_p}{da}\right] \qquad [5c]$$

If the increments of r_p and T, e or a are measured over the same interval, effects of variations in the drag coefficient, due, for example, to changing aspect of a nonspherical satellite, will exactly cancel, since the decrement of every parameter is proportional to drag. In fact, since the velocity is essentially constant on each pass through the region near perigee where the drag is applied, the functional dependence of drag on velocity also has no effect on Eqs. 5. The effects of a rotating atmosphere and of nonsphericity of the atmosphere, which were neglected in deriving Eqs. 1–4, can be considered to be similar to fluctuations of the drag coefficient; therefore, these should also be cancelled from the ratio, at least to first order. In general, the experimental errors, particularly in the measurement of the rate of decay of perigee radius, may be expected to exceed the errors due to these approximations.

Although this analysis is formulated on the basis of aerodynamic drag, the only essential assumption is that the drag force is proportional to atmospheric density. Any drag process that is proportional to density will give the same result. Chopra (6) has discussed other possible satellite drag mechanisms in the upper atmosphere, and has pointed out that electrohydrodynamic effects may become important at altitudes above about 500 km. Strictly speaking, the H in Eqs. 5 is a scale height for drag force, and will not agree with the scale height derived from temperature and molecular weight if there are important drag forces which are not proportional to density.

The orbit eccentricity must be 0.1 or greater to satisfy the condition that essentially all the drag occurs within an angle around perigee such that $\theta^2 < 1$, which was assumed in deriving these equations.

This method was applied to data on the third Soviet satellite (1958 Delta II), reported by El'iasberg and Yastrebov (7). This satellite had a perigee altitude of about 225 km and an eccentricity of about 0.11.

Values of T, a, h_{max} and h_{min} were tabulated for eight particular revolution numbers over the range 39 to 255. Mean deviations of about 150 m in h_{max} and h_{min} were reported. Calculated values of r_p showed considerable scatter (Fig. 1), so, on the basis that r_p and h_{min} apply to the same point in each orbit, the estimated errors in h_{min} were applied to r_p. The fact that the values of r_p so determined fall within 25 m of a smooth curve is evidence of the validity of this procedure. From revolution 39 to about 140, the slope is 2.3 m per revolution; from 140 to 255, the slope is 2.1 per revolution.

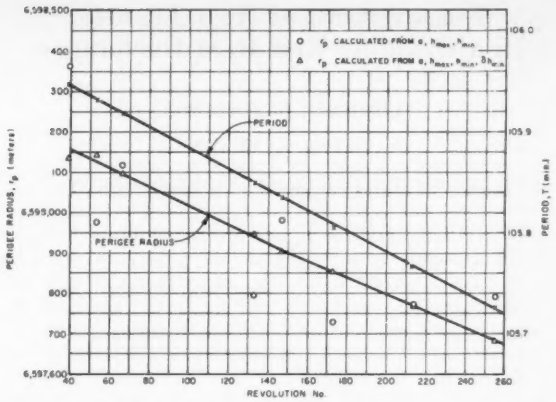

Fig. 1 Orbital data on 1958 Delta II. The points shown are based on the data of (7). The curve of perigee radius is fitted to values of r_p calculated from the formula: $r_p = a - (1/2)(h_{max} - h_{min}) - \delta h_{min}$; where δh_{min} is the reported estimate of the error in each of the tabulated values of h_{min}

Scale heights calculated from Eq. 5a for these two intervals are 98 and 88 km, respectively. Eqs. 5b and 5c each gave averaged values of about 100 km. The fact that this scale height is about double that derived by other methods suggests that the assumption of purely aerodynamic drag is not valid even in the region of 225 to 300 km altitude.

References

1 Roberson, R. E., "Effect of Air Drag on Elliptic Satellite Orbits," JET PROPULSION, vol. 28, 1958, pp. 90–96.

2 Sterne, T. E., "Effect of the Rotation of a Planetary Atmosphere Upon the Orbit of a Close Satellite," ARS JOURNAL, vol. 29, 1959, pp. 777–782.

3 Baker, R. M. L., Jr., "Three-Dimensional Drag Perturbation Technique," ARS JOURNAL, vol. 30, 1960, pp. 748–753.

4 Roberson, R. E., "Air Density Determination by Observation of a Satellite." JET PROPULSION, vol. 28, 1958, pp. 330–331.

5 Michielsen, H. F., "Orbit Decay and Prediction of the Motion of Artificial Satellites," LMSD-48360, Lockheed Aircraft Corp., Dec. 19, 1958.

6 Chopra, K. P., "Interactions of Rapidly Moving Bodies in Terrestrial Atmosphere," *Rev. Mod. Phys.*, vol. 33, 1961, pp. 153–189.

7 El'iasberg, P. E., and Yastrebov, V. D., "Upper Atmosphere Density Determination, Based on Flight Observations of the Third Soviet Artificial Earth Satellite," Supplement, ARS JOURNAL, vol. 31, 1961, pp. 706–713.

Measurement of Heat Transfer in a Graphite Rod Heat Exchanger

CHARLES B. JOHNSON[1]

FRANK L. CLARK[2]

NASA Langley Research Center, Langley Field, Va.

INCREASED attention is presently being directed toward the development of hypersonic test facilities which have capabilities of operation at high stagnation pressures and temperatures with sustained running time. The need for these elevated pressures and temperatures arises primarily from the pressure ratios necessary for satisfactory facility operation and the temperature levels necessary to avoid liquefaction of the flow medium upon expansion. It is the purpose of this paper to present some preliminary data results which were obtained during the operation of a high pressure, high temperature induction-type heat exchanger capable of sustained operation.

Basically the major components of the heat exchanger consist of a high pressure stainless steel chamber, water cooled induction coil and graphite heater element. Power to heat the graphite heater element is supplied to the graphite through the induction coil. Nitrogen was used as the flow medium in order to avoid oxidation of the hot graphite heater element. A photograph of the heater element is presented in Fig. 1a. Presented in Fig. 1b is a cross-sectional drawing of the element. The high pressure nitrogen enters the heater element at point A, swirls around the spiral to point B, passes down the straight tube section to point C where it exits the element. It is with this graphite heater element that this paper will be primarily concerned.

The total temperature of the hot exit gas T_2 was measured with a shielded thermocouple probe. In each case the mass flow of nitrogen through the system was held constant until the readout of the total temperature probe showed a steady state condition. The graphite surface temperature T_s was measured for a number of mass flows with an optical pyrometer. The viewing area of the pyrometer was the cylindrical surface from point B to C shown in Fig. 1b. The value of graphite surface temperature, as well as all data for heat transfer calculations, was taken only after the graphite surface temperature reached a steady state value. In applying the surface temperatures to the heat transfer analyses, it was assumed that the pyrometer readings could be applied to the internal wetted surface of the hot graphite element point A to C, Fig. 1b. The reasons for this assumption were the 1) high thermal conductivity of the graphite, 2) the excellent penetration quality of induction heating, and 3) the small distance between the graphite cylindrical surface and the spiral passage. Because of the complicated internal geometry of the heat exchanger, it was not feasible to calculate the change in temperature of the gas from the point it entered the heat exchanger pressure case to the point where it entered the hot graphite element (point A, Fig. 1b). Also, it would have been extremely difficult to measure the temperature of the gas at point A, Fig. 1b because of the radiation from the hot graphite to the surrounding environment and again because of the complicated internal geometry of the heater. To circumvent these problems the entrance temperature T_1, which corresponds to the gas temperature at point A Fig. 1b, was found by keeping the gas from flowing through the hot graphite element (point A to C Fig. 1b) and then measuring this exit gas temperature. With the gas bypassing the graphite element the implicit assumption was that the exit gas temperature was equal to the entrance gas temperature T_1 (point A Fig. 1b). The process employed in bypassing the hot graphite element allowed the gas to experience the same heating conditions that it would have experienced prior to entering the graphite element at point A Fig. 1b. The entrance temperature thus determined and the exit temperature with the hot graphite element in the heating cycle were then used to calculate the amount of energy which was absorbed as the gas passed through the graphite element. The average heat transfer coefficient was calculated from the experimental data by the following expression

$$h_{ave} = \frac{Q}{A_w(T_s - T_b)}$$

[1] Aeronautical Research Engineer.
[2] Aeronautical Research Engineer.

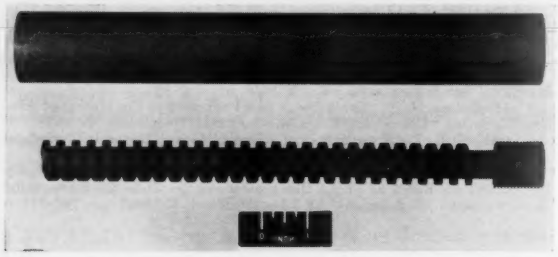

Fig. 1a Graphite rod heating elements; components disassembled

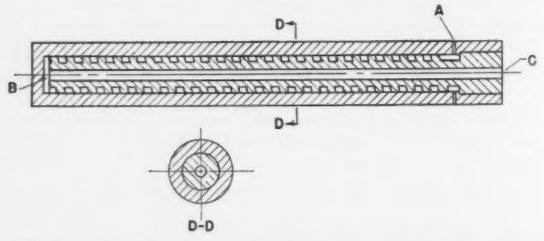

Fig. 1b Graphite rod heating elements; assembled cross-sectional view

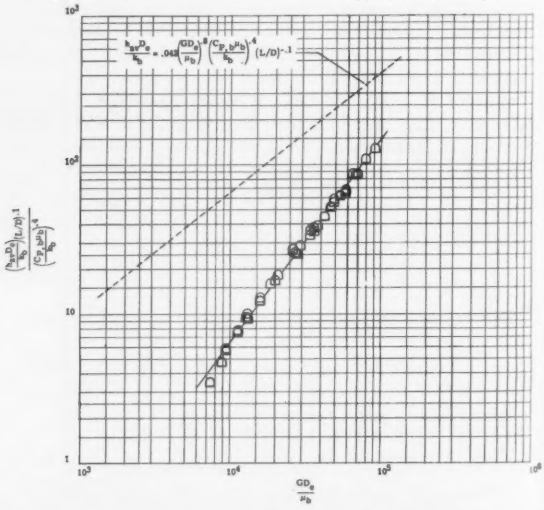

Fig. 2 Correlation of average heat transfer coefficients to nitrogen with the fluid properties evaluated at the bulk temperature T_b. Length-wall distance ratio 390

Table 1 Values of constants found from experimental correlated data

Fluid properties	c	m
Bulk (Fig. 2)	2.1791×10^{-5}	1.3670
Film (Fig. 3)	8.3637×10^{-5}	1.2757
Surface (Fig. 4)	7.7390×10^{-4}	1.1183

The results of the heat transfer analysis are presented in Figs. 2, 3, and 4 wherein $[\mathrm{Nu}(L/D)^{0.1}]/\mathrm{Pr}^{0.4}$ is plotted against Reynolds number with the fluid properties being evaluated at bulk, film, and surface temperatures, respectively. Included for comparison is the well known McAdams equation (1),[3] which has been modified to include the length-wall distance ratio $L/D = 390$ (dashed line on Figs. 2, 3, and 4). This equation may be expressed as

$$\mathrm{Nu} = 0.042(\mathrm{Rn})^{0.8}\,(\mathrm{Pr})^{0.4}(L/D)^{-0.1}$$

The constant 0.042 was obtained from the product of 0.023 from McAdams equation and $(L/D)^{0.1}$ yielding an expression similar to that found in (2).

It may be seen that when the fluid properties are evaluated at the graphite heater element surface temperature (Fig. 4) the data has the closest agreement with the reference line as predicted by the modified McAdams pipe flow equation. When the fluid properties are evaluated at bulk and film temperatures, the data is displaced even further from the predicted results. In (1) it is pointed out that the heat transfer for a somewhat similar configuration should be greater than that predicted by pipe flow equation. It may be seen that for the Reynolds numbers tested this was not the case; however, there will be a point where the experimental curves will intersect the reference curve and the heat transfer for the spiral configuration used in the present test will probably exceed pipe flow predictions. The difference between the experimental curves and reference curve can probably be attributed to the complicated geometry of the graphite heater element used in the present investigation as opposed to the simple geometry of the heater element used in pipe flow studies.

All three of the experimental curves may be represented by an equation in the form

$$\frac{\mathrm{Nu}(L/D)^{0.1}}{(\mathrm{Pr})^{0.4}} = C(\mathrm{Rn})^{m}$$

where C and m are constants which are tabulated in Table 1 for bulk, film, and surface temperature.

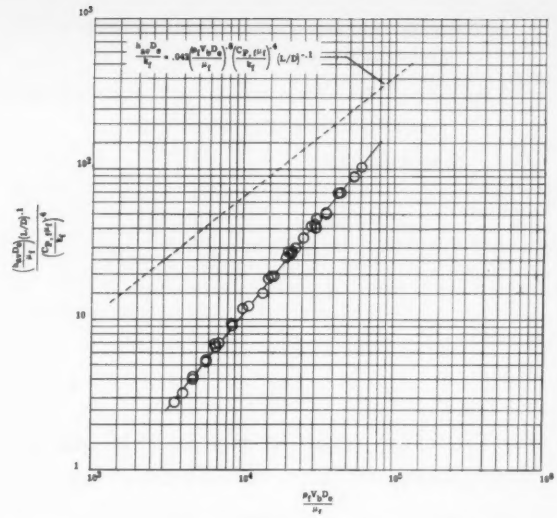

Fig. 3 Correlation of average heat transfer coefficients to nitrogen with the fluid properties evaluated at the film temperature T_f. Length-wall distance ratio 390

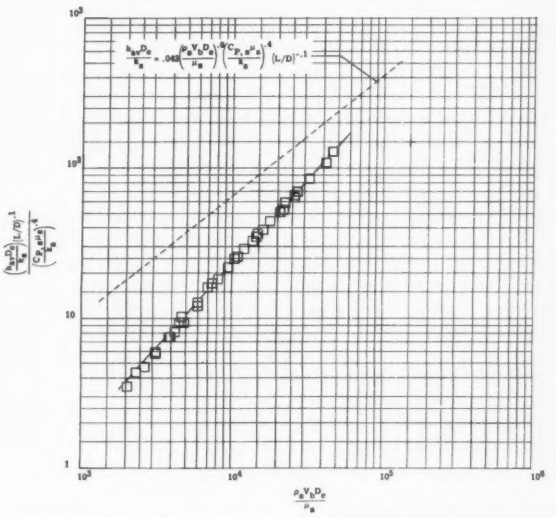

Fig. 4 Correlation of average heat transfer coefficients to nitrogen with the fluid properties evaluated at the surface temperature T_s. Length-wall distance ratio 390

Nomenclature

A_{cr} = cross-sectional area of spiral passage, sq ft
A_w = wetted area of graphite element, sq ft
C_p = specific heat of nitrogen at a constant pressure, Btu/lb-°F
D = longitudinal distance from wall to wall in spiral passage, ft
D_e = hydraulic radius ($4\,A_{cr}$/wetted perimeter), ft
G = mass velocity (mass flow per unit cross-sectional area)
h_{ave} = average heat transfer coefficient, Btu/hr-°F-sq ft
K = thermal conductivity of nitrogen, Btu/hr-ft-°R
L = length of wetted passage in graphite element, ft
Nu = Nusselt number, $\left(\frac{h_{ave}\,D_e}{K}\right)$
Pr = Prandtl number, $\left(\frac{C_p\,\mu}{K}\right)$
Q = rate of heat transfer to nitrogen, Btu/hr
Rn = Reynolds number, $\left(\frac{\rho V\,D_e}{\mu}\right)$
T = temperature, °R
T_b = average bulk temperature defined by $\left(\frac{T_1 + T_2}{2}\right)$, °R
T_f = average film temperature defined by $\left(\frac{T_s + T_b}{2}\right)$, °R
T_s = average graphite surface temperature, °R
V = velocity, ft/hr
μ = absolute viscosity of nitrogen, lb/hr-ft
ρ = density of nitrogen, lb/cu ft
$\frac{C_p\,\mu}{K}$ = Prandtl number
$\frac{G\,D_e}{\mu_b}$ = bulk Reynolds number, with fluid properties evaluated at the bulk temperature

[3] Numbers in parentheses indicate References at end of paper.

$\frac{\rho_f V_b D_e}{\mu_f}$ = modified Reynolds number, with fluid properties evaluated at the film temperature

$\frac{\rho_s V_b D_e}{\mu_s}$ = modified Reynolds number, with fluid properties evaluated at the surface temperature

$\frac{h_{av} D}{K}$ = Nusselt number

Subscripts

1 = graphite element entrance (point A in Fig. 1b)
2 = graphite element exit (point C in Fig. 1b)
b = bulk (when applied to fluid properties, it means evaluation at T_b)
f = film (when applied to fluid properties, it means evaluation at T_f)
s = surface (when applied to fluid properties, it means evaluation at T_s)

References

1 McAdams, W. H., *Heat Transmission*, 3rd ed., McGraw-Hill Book Co., Inc., 1954, p. 228.

2 Humble, L. V., Lowdermilk, W. H. and Desmon, L. G., "Measurements of Average Heat-Transfer and Friction Coefficients for Subsonic Flow of Air in Smooth Tubes at High Surface and Fluid Temperatures," NACA Rep. 1020, 1951.

Surface Behavior of Boron Nitride in High Temperature Arc Heated Gases[1]

P. BRO[2]
S. STEINBERG[3]

Avco Corp., Research and Advanced Development Div. Wilmington, Mass.

The interactions of boron nitride are described with a high velocity gas stream at temperatures of approximately 6000° to 7000°R and at atmospheric pressure. Erosion rates of 0.026 lb/sec-sq ft in nitrogen, 0.061 lb/sec-sq ft in a synthetic rocket exhaust, and 0.117 lb/sec-sq ft in air were observed with gas enthalpies of approximately 8000 Btu/lb. The erosion process is described in terms of a chemical surface spalling process. The erosion rates cannot be predicted from mass transfer considerations alone.

REFRACTORY materials may erode rapidly in chemically reactive environments at elevated temperatures, and the erosion mechanism is of considerable interest from a practical point of view. It has been shown (1)[4] that the rate of the surface reactions in gas-solid systems at elevated temperatures and at moderate pressures can be predicted reasonably well from mass transfer considerations when the erosion mechanism involves a solid → gas transformation. Here is presented experimental data on a system undergoing chemical solid → gas transformations as well as a thermally induced mechanical loss process. It will be shown that the loss rate cannot be predicted from any simple considerations.

Experimental Methods

The investigation was concerned with the behavior of boron nitride in contact with various gases at very high temperatures in a flow system. The experimental techniques involved the use of a high intensity electric discharge unit to heat the reactive and the inert gases to temperatures of 6000° to 7000°R; the details of the operating procedures have been described previously (1). The boron nitride specimens were cylindrical rods with a diameter of $\frac{3}{4}$ in. and a length of 4 in. The hot gas jet impinged on the flat ends of the rods, and the erosion rate was observed photographically.

The test gases were air, nitrogen, and a synthetic rocket exhaust mixture containing 53.7 at % hydrogen, 18.2 at % oxygen, 7.0 at % chlorine, 7.3 at % nitrogen, and 13.8 at % carbon. The exhaust mixture reacted to produce an equilibrium mixture at the temperature of the tests which were carried out at a pressure of 1 atm. The thermodynamic properties of the mixture were reported earlier (1).

Experimental Results

The loss rates of boron nitride under various conditions are reported in Table 1, and data on graphite filled specimens are included. The erosion rates of the boron nitride bodies were approximately the same under comparable conditions, being approximately 0.026 lb/sec-sq ft in nitrogen and 0.061 lb/sec-sq ft in reaction mixture A2. It may be seen that the effect of the chemical reactivity and the slightly higher heat transfer rates was to increase the erosion rate significantly. The rate of erosion of boron nitride in air with an average enthalpy of 8335 Btu/lb was 0.117 lb/sec-sq ft, which exceeded the rates in nitrogen and in mixture A2 by a considerable margin.

Observations during the runs indicated that the boron nitride did not melt when it eroded, and this confirmed predictions (2), based on thermodynamic analyses, that the material would sublime at very high temperatures. Furthermore, detailed examinations showed that extensive blistering occurred during the runs. Quite shallow blisters with diameters of approximately $\frac{1}{16}$ to $\frac{1}{32}$ in. would form, and boron nitride was removed mechanically by the rupture of the

Table 1 Erosion rates of boron nitride*

Sample	Gas	Gas enthalpy, Btu/lb	Cold wall heat transfer, Btu/sec-sq ft	Erosion rate, lb/sec-sq ft
BN	Air	3803	1231	0.300
BN	Air	5375	1162	0.132
BN	Air	7690	1147	0.095
BN	Air	8981	1090	0.139
BN	A2	7488	1617	0.0673
BN	A2	8114	1367	0.0676
BN	N_2	7439	1010	0.0361
BN	N_2	7884	1070	0.0121
BN + 20% C	A2	7293	1587	0.0557
BN + 20% C	A2	8517	1433	0.0510
BN + 20% C	A2	8081	1272	0.0511
BN + 20% C	N_2	7577	1022	0.0388
BN + 20% C	N_2	7669	1039	0.0109
BN + 45% C	A2	6986	1525	0.0576
BN + 45% C	A2	7757	1334	0.0720
BN + 45% C	A2	7749	1304	0.0547
BN + 45% C	N_2	7656	1037	0.0303
BN + 45% C	N_2	7580	1028	0.0272

* All the tests were performed at a gas pressure of 1 atm.

Received July 7, 1961.

[1] Based on work carried out under contract AF04(647)-258 with the Air Force Ballistic Missile Div., Inglewood, Calif.

[2] Assistant Section Chief, Physical Chemistry Sect.

[3] Senior Scientist, Physical Chemistry Sect., presently with Research Dept., General Mills, Inc., Minneapolis, Minn.

[4] Numbers in parentheses indicate References at end of paper.

blisters. This phenomenon will be referred to as superficial spalling. It appears to be caused by gas evolution below the reacting surface, and it is, therefore, different from bulk spalling.

Discussion of the Experimental Results

If no allowance is made for the scavenging effect of the cathode carbon (1) on the oxidation capacity of the reaction mixture A2, a maximum chemical loss rate of 0.004 lb BN/sec-sq ft can be calculated for the oxidation of BN under the test conditions. The corresponding maximum loss rate in air would be 0.041 lb BN/sec-sq ft. Since considerably greater loss rates were observed, it is concluded that processes other than gas-solid reactions dominated the behavior of boron nitride. The analysis below will include a consideration of the superficial spalling process as a contributor to the erosion of boron nitride.

The thermochemical heat of reaction of a material is defined by

$$q^* = q_c \frac{H - H_w}{H - H_c} \frac{1}{\rho V} - q_{rad} \frac{1}{\rho V} \qquad [1]$$

and its steady state value may be expressed in terms of a detailed energy balance

$$\begin{aligned} q^* V = {} & V C_p \Delta T && \text{(sensible heat in eroded material)} \\ & + V_G \Delta H_G && \text{(heat of vaporization and reaction)} \\ & + V_G \eta (H - H_w) && \text{(conventional transpiration effect)} \\ & + V_S \beta (H - H_w) && \text{(change in convective heat transfer by particle perturbations)} \end{aligned} \qquad [2]$$

It is assumed that the material removed by superficial spalling would reach a temperature equal to that of the reacting surface. Thus

$$q^* = C_p \Delta T + \frac{\Delta H_{vap} + \Sigma f_i \Delta H_i}{1 + (V_S/V_G)} + \frac{\eta + \beta(V_S/V_G)}{1 + (V_S/V_G)} (H - H_w) \qquad [3]$$

Eq. 3 is not very useful in its present form because of its many unknown parameters. In particular, the perturbations in the heat transfer rates caused by vaporization and superficial spalling cannot be evaluated from the experimental data with any degree of reliability. It may be seen that the contribution of this term vanishes as H approaches H_w, and under such conditions Eq. 3 may be reduced to

$$q^* H_w = C_p \Delta T + \frac{V_G}{V} (\Delta H_{vap} + \Sigma f_i \Delta H_i) \qquad [4]$$

This equation may be applied to the reaction rate data of boron nitride in air which extend over a sufficiently wide enthalpy range to allow an extrapolation to $H = H_w$ where $q^* H_w \sim 700$ Btu/lb. In order to illustrate the application of this equation, it will be assumed that the surface temperature of the boron nitride reached a steady state value of 3000°C. The values of C_p and ΔH_{vap} may be estimated from available thermodynamic data. Eq. 4 may then be reduced to

$$\frac{V_G}{V} (15{,}200 + \Sigma f_i \Delta H_i) + 1591 = 0 \qquad [5]$$

Two reactions of boron nitride in air must be considered

$$2BN(g) + \frac{3}{2} O_2(g) \rightarrow B_2O_3(g) + N_2(g)$$

$$\Delta F_{3000} = -359 \text{ kcal/mole}$$

$$\Delta H_{3000} = -21{,}600 \text{ Btu/lb BN} \qquad [6]$$

$$BN(g) \rightarrow B(g) + (1/2)N_2(g)$$

$$\Delta F_{3000} = -44 \text{ kcal/mole} \qquad [7]$$

The relative importance of these reactions under oxidizing conditions may be seen from the relation

$$P_B^2 = P_{B_2O_2} \exp(-39.4) \qquad [8]$$

which is obtained from the equilibrium constants with a partial pressure of oxygen of 0.21 atm. This shows that essentially all the dissociated boron nitride becomes oxidized, and that no reactions need to be considered in the energy balance other than reactions in Eq. 6. The following result is obtained

$$f_{ox} = 0.702 + 0.073 \frac{V}{V_G} \qquad [9]$$

In the absence of more detailed data, exact values cannot be assigned to V_S/V, but Eq. 9 shows that since $0.775 \leq f_{ox} \leq 1.00$, then

$$0 \leq \frac{V_S}{V} \leq 0.76 \qquad [10]$$

Thus, as much as 76% of the boron nitride may be removed by superficial spalling.

The thermochemical heat of reaction of boron nitride is given below

BN	$q^* = 49{,}500$ Btu/lb in nitrogen
BN + 20% C	$q^* = 36{,}000$ Btu/lb in nitrogen
BN + 46% C	$q^* = 19{,}200$ Btu/lb in nitrogen
BN	$q^* = 15{,}000$ Btu/lb in mixture A2
BN + 20% C	$q^* = 18{,}500$ Btu/lb in mixture A2
BN + 46% C	$q^* = 14{,}700$ Btu/lb in mixture A2

In nitrogen, the thermochemical heat of reaction decreased as the graphite concentration in BN increased. Earlier experiments had shown that graphite alone eroded quite slowly under comparable conditions, and if it is assumed that it acted as an inert filler, the corrected q^* values may be obtained on a graphite free basis

BN	$q^*_{corr} = 49{,}500$ Btu/lb BN in nitrogen
BN + 20% C	$q^*_{corr} = 45{,}000$ Btu/lb BN in nitrogen
BN + 46% C	$q^*_{corr} = 35{,}500$ Btu/lb BN in nitrogen

A considerably better agreement is thus obtained. A corresponding treatment of the data from the tests in mixture A2 gives a poorer agreement between the q^* values than shown above. It is possible to explain the increase of the q^*_{corr} values with graphite content in mixture A2 on the basis of the endothermic $C + H_2O \rightarrow CO + H_2$ reaction. However, it is doubtful whether the data are sufficiently precise for a reliable analysis of the variations within each group. The greater thermochemical heat of reaction in nitrogen relative to that in mixture A2 suggests that the endothermic dissociation of BN dominated the chemical behavior of BN in nitrogen and that exothermic reactions became important in the chemical erosion process in the oxidizing environment of mixture A2.

Conclusions

When boron nitride was exposed to hot gas streams at temperatures of 6000° to 7000°R and pressures of 1 atm it eroded

at an appreciable rate which depended upon the chemical composition of the hot gas. Although the highest erosion rates were observed in chemically reactive media, a superficial spalling process contributed most significantly to the deterioration of the boron nitride. Oxidizing gas-solid reactions could account for only a small fraction of the observed erosion rate.

A preliminary analysis of the superficial spalling process in air showed that as much as 76% of the boron nitride may have been removed by this means. The data indicated that the endothermic dissociation of boron nitride was the more important chemical erosion process in nitrogen, whereas exothermic reactions became important in the oxidizing environments.

Acknowledgment

We are indebted to T. Munson, who performed the thermodynamic calculations on the test gases and to C. Brine, who assisted with the experimental studies.

Nomenclature

β	=	particle perturbation coefficient
C_p	=	specific heat
η	=	transpiration coefficient
f_i	=	fraction of vaporized material undergoing reaction (i) at the surface of the sample
H	=	mean gas enthalpy
H_w, H_c	=	gas enthalpy at the wall and cold wall temperatures, respectively.
ΔH_G	=	heat of vaporization and reaction
ΔH_i	=	heat of reaction (i)
P_B, $P_{B_2O_3}$	=	partial pressures of boron and boric oxide
q^*	=	thermochemical heat of reaction
q_c, q_{rad}	=	cold wall and radiative heat transfer rates
ρ	=	density
ΔT	=	temperature difference between reacting surface and bulk specimen
V	=	total linear rate of erosion
V_S, V_G	=	linear rate of erosion by superficial spalling and vaporization, respectively

References

1 Bro, P. and Steinberg, S., "The Study of Chemical Surface Reactions in a High Temperature Flow System with Arc Heated Gases," to be published by ARS JOURNAL.

2 Panish, M. B., private communication.

Effect of Earth's Oblateness on the Anomalistic Period of a Satellite

M. M. MOE[1]
E. E. KARP[2]

Space Technology Laboratories, Inc.
Los Angeles, Calif.

MOST studies of satellite orbit perturbations derive expressions for the changes in the osculating elements (1, 2, 3),[3] but do not determine the anomalistic period explicitly. The purpose of this note is to obtain a first-order expression for the anomalistic period of a satellite orbit perturbed by Earth's oblateness. Only the second harmonic in Earth's gravitational potential will be considered.

In the absence of any perturbations, the anomalistic period T_A of an Earth satellite is simply that of a Kepler orbit

$$T_A = \frac{2\pi a^{3/2}}{\sqrt{\mu}} \qquad [1]$$

where a is the semimajor axis, $\mu = GM$, G is the universal gravitational constant, and M is Earth's mass.

Now consider the effect of a perturbing force. The acceleration caused by this force can be resolved into a component W normal to the instantaneous orbit plane[4] and components R and S in the instantaneous plane. R is the radial component (measured positive away from the center of Earth) and S is the transverse component (measured positive when making an angle less than 90° with the velocity vector). We can disregard the component W in our computations because W cannot, to first order, affect the magnitude of the angular momentum vector, only its direction. That is, it affects only the orientation of the instantaneous plane of the orbit and cannot affect either the length of an arc along the orbit or the speed at which the satellite describes that arc length. Therefore, W should not affect the perigee to perigee time (unless, of course, W is large enough to rotate the orbit plane so much that R and S deviate significantly from their values in a planar orbit). Accordingly, we consider the orbit to be planar and write the anomalistic period as

$$T_A = \int_{\text{perigee}}^{\text{next perigee}} dt = \int_0^{2\pi+\omega'(2\pi)} \frac{d\theta}{\dot{\theta}} \qquad [2]$$

where $\dot{\theta}$ is the instantaneous angular rate and $d\theta$ is the angle described in the infinitesimal time dt. The angle θ is measured in the orbital plane from perigee, and $\omega'(2\pi)$ is the angle by which perigee differs (after the satellite has completed a perigee to perigee revolution) from the position it would have had if there were no perturbing forces. The prime is used to distinguish ω' and ω which is the argument of perigee measured from the moving node on Earth's Equator. The essential point is that ω' is measured from the previous perigee rather than from the node. To evaluate the integral in Eq. 2 we write

$$\dot{\theta} = \frac{h}{r^2} \qquad [3]$$

where h is the instantaneous angular momentum and r is the instantaneous radial distance. Expressing h and r in terms of the osculating elements, we obtain

$$\frac{1}{\dot{\theta}} = \frac{1}{\sqrt{\mu}} \frac{a^{3/2}(1-e^2)^{3/2}}{(1+e\cos v)^2} \qquad [4]$$

where a and e are the semimajor axis and eccentricity of the osculating ellipse, and v is the satellite's true anomaly. We assume that v is equal to $\theta - \omega'(\theta)$, where $\omega'(\theta)$ is the angle by which the perigee of the osculating ellipse has moved when the satellite is at θ. Then Eq. 4 becomes

$$\frac{1}{\dot{\theta}} = \frac{1}{\sqrt{\mu}} \frac{a^{3/2}(1-e^2)^{3/2}}{[1+e\cos(\theta-\omega')]^2} = \frac{1}{\sqrt{\mu}} F(\theta) \qquad [5]$$

Received Jan. 27, 1961.

[1] Member of the Technical Staff.

[2] Member of the Technical Staff.

[3] Numbers in parentheses indicate References at end of paper.

[4] The instantaneous orbit plane is the plane passing through the satellite's velocity vector and the radius vector from the center of Earth to the satellite.

where a, e, and ω' are considered as functions of θ. Next we approximate $F(\theta)$ by the first terms in its Taylor series

$$F(\theta) = F_0(\theta) + \frac{\partial F}{\partial a}\bigg|_0 \delta a(\theta) + \frac{\partial F}{\partial e}\bigg|_0 \delta e(\theta) + \frac{\partial F}{\partial \omega'}\bigg|_0 \omega'(\theta) + \ldots \text{higher terms} \quad [6]$$

where the subscript zero indicates that all the orbital elements are evaluated at perigee and $\delta a(\theta)$, $\delta e(\theta)$, and $\omega'(\theta)$ are the deviations of these elements from their values at perigee. We assume that the perturbations are small enough that we may neglect higher order terms. $F_0(\theta)$ is the unperturbed $\sqrt{\mu}/\dot{\theta}$, which is simply the Kepler value. The partial derivatives are

$$\frac{\partial F}{\partial a} = \frac{3a^{1/2}(1-e^2)^{3/2}}{2[1+e\cos v]^2}$$

$$\frac{\partial F}{\partial e} = -\frac{a^{3/2}(1-e^2)^{1/2}[2(e+\cos v)+e(1+e\cos v)]}{[1+e\cos v]^3}$$

$$\frac{\partial F}{\partial \omega'} = -\frac{2e\,a^{3/2}(1-e^2)^{3/2}\sin v}{[1+e\cos v]^3}$$

.....[7]

When substituting these expressions in Eq. 6, we must choose the values of a and e at perigee and replace v by θ (since $\omega' = 0$ at perigee).

The expressions for $\delta a(\theta)$, $\delta e(\theta)$ and $\omega'(\theta)$ are obtained by an approximate integration of the usual formulas (4) for the time rate of change of the orbital elements. The rates of change are

$$\frac{da}{dt} = \frac{2}{n}\left[\frac{e\sin v}{\sqrt{1-e^2}}R + \frac{a\sqrt{1-e^2}}{r}S\right] \quad [8]$$

$$\frac{de}{dt} = \frac{\sqrt{1-e^2}}{na}\left[R\sin v + \frac{1}{ae}\left(\frac{a^2(1-e^2)}{r} - r\right)S\right] \quad [9]$$

and

$$\frac{d\omega}{dt} = -\frac{d\Omega}{dt}\cos i + \frac{\sqrt{1-e^2}}{nae}\left[-R\cos v + S\times\left(\frac{2+e\cos v}{1+e\cos v}\right)\sin v\right] \quad [10]$$

where n is the mean angular motion, i is the inclination of the orbit with respect to Earth's equatorial plane, and Ω is the longitude of the ascending node on the Equator. If we remove the term depending on the motion of the node in Eq. 10, we obtain

$$\frac{d\omega'}{dt} = \frac{\sqrt{1-e^2}}{nae}\left[-R\cos v + S\left(\frac{2+e\cos v}{1+e\cos v}\right)\sin v\right] \quad [11]$$

which is the rate at which perigee moves if we ignore perturbing forces normal to the instantaneous orbit plane. Let ϵ stand for any one of the orbital elements. Then the amount by which ϵ differs from its value at perigee is

$$\delta\epsilon(\theta) = \int_0^\theta \frac{d\epsilon}{dt}\frac{r^2}{h}\,d\theta$$

If we approximate all variables in the integrand by the values they would have in an unperturbed orbit, we obtain

$$\delta a(\theta) \cong \frac{2}{n^2a^2(1-e^2)}\int_0^\theta r^2\,[Re\sin v + S(1+e\cos v)]dv \quad [12]$$

$$\delta e(\theta) \cong \frac{1}{n^2a^3}\int_0^\theta r^2\left[R\sin v + \left(\frac{e+\cos v}{1+e\cos v} + \cos v\right)S\right]dv = \frac{(1-e^2)}{2ae}\,\delta a(\theta) - \frac{1}{n^2a^4e}\int_0^\theta r^3 S dv \quad [13]$$

and

$$\omega'(\theta) \cong \frac{1}{n^2a^3e}\int_0^\theta r^2\left[-R\cos v + S\left(\frac{2+e\cos v}{1+e\cos v}\right)\sin v\right]dv \quad [14]$$

where

$$r = \frac{a(1-e^2)}{1+e\cos v} \quad [15]$$

in which v is the only variable.

If we consider only the J term (or second harmonic) in the Earth's gravitational potential, the perturbing accelerations, R and S, are (1, 2, 3, 5)

$$R = -\frac{J\mu R_e^2}{r^4}\left[1 - 3\sin^2 i\sin^2(\omega+v)\right] \quad [16]$$

and

$$S = -\frac{J\mu R_e^2}{r^4}\sin^2 i\sin 2(\omega+v) \quad [17]$$

where R_e is Earth's equatorial radius and $J = 1.64\times10^{-3}$. If we place these components in Eqs. 12–14 (remembering that r and v are related by Eq. 15 and all other quantities are assumed constant), we find that all the integrals are elementary. The integrations yield lengthy results (6), omitted here because they are not essential to the discussion.

From Eqs. 2, 5, and 6, it is clear that the anomalistic period may be written as

$$T_A = \frac{1}{\sqrt{\mu}}\left\{\int_0^{2\pi+\omega'(2\pi)} F_0 d\theta + \int_0^{2\pi+\omega'(2\pi)}\left[\frac{\partial F}{\partial a}\bigg|_0\delta a(\theta) + \frac{\partial F}{\partial e}\bigg|_0\delta e(\theta) + \frac{\partial F}{\partial \omega'}\bigg|_0\omega'(\theta)\right]d\theta\right\} \quad [18]$$

The quantities $\partial F/\partial a|_0$, $\partial F/\partial e|_0$, and $\partial F/\partial\omega'|_0$, which are functions of θ, are taken from Eqs. 7 in which the elements are evaluated at perigee. The value of $\omega'(2\pi)$, obtained from Eq. 14 by setting $\theta = 2\pi$, is

$$\omega'(2\pi) = \frac{2\pi J\mu R_e^2(1-3/2\sin^2 i)}{n^2a^5(1-e^2)^2} \quad [19]$$

The first term on the right-hand side of Eq. 18 is simply

$$\int_0^{2\pi+\omega'(2\pi)} F_0 d\theta = \frac{2\pi a^{3/2}}{\sqrt{\mu}} + \frac{\omega'(2\pi)}{\dot{\theta}_p} \quad [20]$$

where $\dot{\theta}_p$, the angular velocity at perigee, is

$$\dot{\theta}_p = \frac{\sqrt{\mu}\sqrt{1-e^2}}{a^{3/2}(1-e)^2}$$

The second term in Eq. 18 is found by integrating from zero to 2π, since $\omega'(2\pi)$ in the upper limit adds only second-order terms.

Table 1 Comparison of anomalistic periods determined from Eq. 21 and numerical integrations

a, Earth radii	e	i, deg	ω, deg	T_K Kepler period, min	T_A Numerical integration, $J = 10^{-2}$, min	T_A Eq. 21, $J = 10^{-2}$, min	T_A Eq. 21, $J = 1.64 \times 10^{-3}$, min
1.2	0.01	90	60	111.065	112.11	112.06	111.23
1.2	0.01	45	20	111.065	110.65	110.41	110.96
1.2	0.05	90	60	111.065	112.21	112.31	111.25
1.2	0.05	45	20	111.065	110.35	110.32	110.94
1.2	0.10	90	60	111.065	112.41	112.39	111.28
1.2	0.10	45	20	111.065	110.21	110.19	110.92
1.2	0.10	45	50	111.065	110.94	110.94	111.05
1.2	0.10	60	20	111.065	110.29	110.29	110.94
1.2	0.10	10	30	111.065	110.04	110.03	110.90
2.2	0.50	60	60	275.705	278.86	278.84	276.22
2.2	0.50	45	20	275.705	271.99	271.95	275.09

The final expression for the anomalistic period becomes

$$T_A = \frac{2\pi a^{3/2}}{\sqrt{\mu}} \left\{ 1 - \frac{JR_e^2}{a^2(1-e)^2} (1 - 3\sin^2 i \sin^2 \omega) \right\} \quad [21]$$

To check our equations, we have compared Eq. 21 to the results provided by a numerical integration program in which all perturbing forces, except the J part of the gravitational force, were omitted. To guarantee meaningful numerical results, we chose a large value for J, 10^{-2}. The results are summarized in Table 1. In the last column of the table, we show the anomalistic period, calculated from Eq. 21, with the correct value of J, 1.64×10^{-3}, appropriate to Earth's oblateness.

Eq. 21 may be tested in the low eccentricity limit by considering perfectly circular motion in the equatorial plane. For such a motion it can be shown, by elementary mechanics, that the sidereal period is

$$T_S = \frac{2\pi a^{3/2}}{\sqrt{\mu}} \left[1 - 2J \left(\frac{R_e}{a} \right)^2 + \text{terms of order } J^2 \text{ and higher} \right] \quad [22]$$

The sidereal period can also be computed from Eq. 21 by subtracting the term contributed by the motion of perigee, i.e., the second term in Eq. 20. We obtain

$$T_S = \frac{2\pi a^{3/2}}{\sqrt{\mu}} \left[1 - 2J \left(\frac{R_e}{a} \right)^2 \right]$$

in agreement with Eq. 22.

Acknowledgment

The authors thank R. C. Booton Jr. for pointing out this problem. We also thank J. Titus for providing us with anomalistic periods determined by a numerical integration program and D. H. Cooper and L. J. Martin for checking some equations and doing the numerical computations. The helpful discussions with L. Blitzer and J. B. McGuire are appreciated.

References

1 Garfinkel, B., "The Orbit of a Satellite of an Oblate Planet," *Astronom. J.*, vol. 64, no. 9, November 1959, p. 353.

2 Kozai, Y., "The Motion of a Close Earth Satellite," *Astronom. J.*, vol. 64, no. 9, November 1959, p. 367.

3 Brouwer, D., "Solution of the Problem of Artificial Satellite Theory Without Drag," *Astronom. J.*, vol. 64, no. 9, November 1959, p. 378.

4 Moulton, F. R., *An Introduction to Celestial Mechanics*, The MacMillan Co., New York, 1914, pp. 404–405.

5 Blitzer, L., "The Orbit of a Satellite in the Gravitational Field of the Earth," STL/TR-60-0000-00264, Space Tech. Lab. Aug. 11, 1960.

6 Moe, M. M. and Cosnett, E. E., "The Effect of the Earth's Oblateness and the Sun and Moon on the Anomalistic Period of an Earth Satellite," STL/TR-60-0000-09099, Space Tech. Lab., April 20, 1960.

Capture Problem in Gravitational Attitude Control of Satellites

E. E. ZAJAC[1]

Bell Telephone Laboratories, Inc., Murray Hill, N. J.

For a satellite in a circular orbit, it is known that there exists an energy integral for motion relative to an Earth pointing rotating reference frame. This integral is used to obtain a set of orientation conditions. If the satellite is initially oriented so as to satisfy the first two conditions of the set, it will be captured by the gravitational gradient and all subsequent motion will be in a neighborhood of the desired orientation. Likewise, if it satisfies the third condition, it will never come to rest in the rotating reference frame.

Received July 2, 1961.

[1] Member of Technical Staff.

THE ENERGY integral of a simple pendulum allows one to conveniently characterize the pendulum's motion. For example, given enough energy the pendulum will revolve around and around rather than oscillate to and fro about the downward hanging position. Likewise, with sufficiently small energy the pendulum will be captured by gravity, and only oscillatory motion will occur.

It is well known that for a satellite in a circular orbit there also exists an energy integral for the motion about the satellite's mass center in an Earth pointing reference frame that rotates at the rate of one revolution per orbit (1).[2] Beletskiy (1) has used this integral to obtain bounds on the direction

[2] Numbers in parentheses indicates Reference at end of paper.

cosines between the satellite's principal axes and the axes of the rotating frame. However, from this integral one can obtain direct analogs of the above statements on the simple pendulum. Further, the analogs admit of a convenient geometric interpretation that is useful in attitude control, where one is interested in the capture of a satellite by the gravitational gradient.

Let x,y,z be the rotating reference frame (x-axis perpendicular to the orbital plane and z-axis along the local vertical, Fig. 1), and let ξ,η,ζ be the principal axes of the satellite with moments of inertia A,B,C respectively ($A > B > C$). Then the energy integral may be written

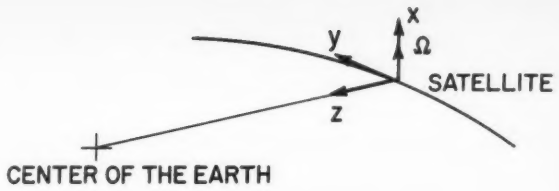

Fig. 1 Rotating reference frame

$$\frac{1}{2}\left[\omega_\xi^2 A + \omega_\eta^2 B + \omega_\zeta^2 C\right] + \frac{\Omega^2}{2}\left[A - (\mathbf{e}_\xi\cdot\mathbf{e}_x)^2 A - (\mathbf{e}_\eta\cdot\mathbf{e}_x)^2 B - (\mathbf{e}_\zeta\cdot\mathbf{e}_x)^2 C\right] + \frac{3}{2}\Omega^2\left[(\mathbf{e}_\xi\cdot\mathbf{e}_z)^2 A + (\mathbf{e}_\eta\cdot\mathbf{e}_z)^2 B + (\mathbf{e}_\zeta\cdot\mathbf{e}_z)^2 C - C\right] = E \quad [1]$$

where $\omega_\xi,\omega_\eta,\omega_\zeta$ are the ξ,η,ζ components of the satellite's angular velocity relative to the rotating x,y,z frame, the $\mathbf{e}$'s are unit vectors, Ω is the orbital rate and E is a constant. Here, we have adjusted the constant of integration so that $E = 0$ when the satellite is stationary in its stable orientation (ξ,η,ζ coincident with x,y,z). We recognize the first term of Eq. 1 as the satellite's kinetic energy T with respect to x,y,z. The third term, we recognize as the potential energy V with respect to x,y,z, i.e., the potential of the gravitational gradient if the satellite were held fixed in inertial space at the orbital radius. The second term we identify as a potential energy of rotation R. We may thus write the energy integral as $T + R + V = E$.

To describe the orientation of the body axes ξ,η,ζ with respect to the rotating axes x,y,z we use the Euler angles shown in Fig. 2. From these and Eq. 1 we obtain

$$V = \frac{3}{2}\Omega^2\sin^2\theta\left[A\cos^2\varphi + B\sin^2\varphi - C\right] \quad [2]$$

We note further the similarity between the bracketed parts of R and V in Eq. 1. In fact, in Fig. 2 we imagine a cyclic change in the coordinate labels x,y,z to y,z,x and ξ,η,ζ to η,ζ,ξ; and further we imagine a change in the angle labels θ,φ,ψ to α,β,γ. This gives an alternative set of Euler angles for the specification of ξ,η,ζ with respect to x,y,z. By analogy to Eq. 2, we then have, in terms of the alternative set

$$R = \frac{\Omega^2}{2}\sin^2\alpha\left[A - B\cos^2\beta - C\sin^2\beta\right] \quad [3]$$

Combining Eqs. 1, 2 and 3, we find

$$T + \frac{\Omega^2}{2}\sin^2\alpha\left[A - B\cos^2\beta - C\sin^2\beta\right] + \frac{3}{2}\Omega^2\sin^2\theta\left[A\cos^2\varphi + B\sin^2\varphi - C\right] = E \quad [4]$$

Since $A > B > C$ by assumption, we get from Eq. 4

$$\frac{\Omega^2}{2}(A-B)\sin^2\alpha + \frac{3}{2}\Omega^2(B-C)\sin^2\theta \le E - T \le T_0 + \frac{\Omega^2}{2}(A-C)(\sin^2\alpha_0 + 3\sin^2\theta_0) \quad [5]$$

where the zero subscript refers to values at some arbitrary initial time, and equality holds, e.g., if $\varphi = \frac{\pi}{2}$, $\beta = 0$, $\alpha = 0$, $\varphi_0 = 0$, $\beta_0 = \frac{\pi}{2}$, $\alpha_0 = \theta_0$, and $T = 0$. Further, we get from Eq. 5

$$\sin^2\theta \le \frac{2T_0}{3\Omega^2(B-C)} + \frac{1}{3}\left(\frac{A-C}{B-C}\right)(\sin^2\alpha_0 + 3\sin^2\theta_0) \quad [6a]$$

$$\sin^2\alpha \le \frac{2T_0}{\Omega^2(A-B)} + \left(\frac{A-C}{A-B}\right)(\sin^2\alpha_0 + 3\sin^2\theta_0) \quad [6b]$$

which is an analog of the statement on capture for the simple pendulum. Thus if the satellite is injected into orbit such that the right side of Eq. 6a is equal to $\epsilon^2(\le 1)$, then the principal axis of minimum moment of inertia will be captured in a cone whose generators make the angle $\sin^{-1}\epsilon$ with the local vertical. Likewise if the right side of Eq. 6b is $\delta^2(\le 1)$, then the principal axis of maximum moment of inertia will be captured in a cone whose generators make the angle $\sin^{-1}\delta$ with the perpendicular to the orbital plane. By making the right sides of Eqs. 6a and 6b sufficiently small, the satellite therefore can be captured near its stable orientation. In the absence of outside disturbances, such as meteorites, tumbling will not occur.

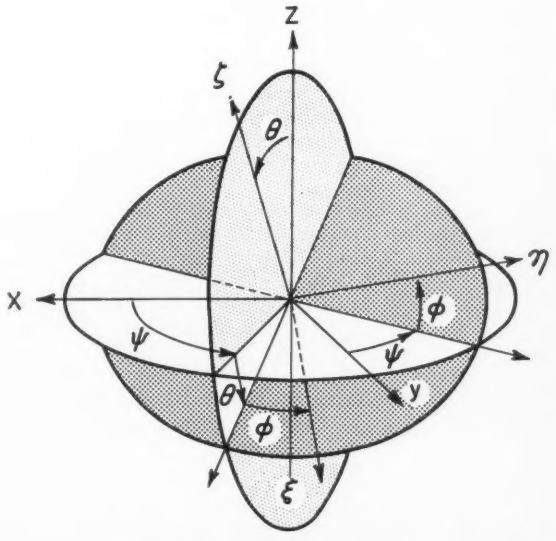

Fig. 2 Euler angles

On the other hand, we have from Eq. 4

$$T = E - R - V \geq$$

$$E - \frac{\Omega^2}{2}(A - C)(\sin^2\alpha + 3\sin^2\theta) \leq E - 2\Omega^2(A - C)$$

and finally, replacing E by its minimum possible initial value

$$T \geq T_0 + \frac{\Omega^2}{2}(A - B)\sin^2\alpha_0 + \frac{3}{2}\Omega^2(B - C)\sin^2\theta_0 - 2\Omega^2(A - C) \quad [7]$$

where equality is attained, e.g., if $\varphi = 0$, $\beta = \pi/2$, $\alpha = \theta = \pi/2$, $\varphi_0 = \pi/2$, $\beta_0 = 0$, $\alpha_0 = 0$. This expression gives an analog of the statement on around and around motion for the simple pendulum. Thus, if the right side of Eq. 7 is positive, the satellite will never come to rest in the rotating x,y,z frame.

We note that Inequalities 6 and 7 may be made sharper by taking into account φ_0 and β_0. However, in doing this it should be remembered that of the four variables, θ,φ,α and β, only three are independent.

Reference

1 Beletskiy, V. V., "The Libration of a Satellite" (in Russian), *Iskusstvennye Sputniki Zemli*, vol. 3, 1959, pp. 13–31, also NASA TTF-10 (English transl.), May 1960.

Technical Comments

Tentative Explanation of Irregular Burning in Solid Propellant Rockets[1]

J. VANDENKERCKHOVE[2]

University of Brussels, Brussels, Belgium

SEVERAL excellent survey papers have been presented recently by Clure, Price, and others on the important and difficult problem of unstable burning in solid propellant rockets.

Generally these authors emphasized the poor present understanding of the phenomena involved and the necessity of taking into account the burning mechanism of the propellant.

For the purpose here, their conclusions are summarized as follows:

1 Under certain conditions many, but apparently not all, propellants have the intrinsic ability to support oscillatory burning.

2 Actual initiation of oscillatory burning of an intrinsically unstable propellant results from an extremely delicate gain-loss energy imbalance which is influenced by numerous factors.

3 In many cases oscillatory combustion gives rise to irregularly burning characterized by large and erratic variations in mean chamber pressure.

The desirability of a clear distinction between oscillatory and irregular burning complicates the problem, and the greatest caution is imperative in this matter. Recent progress in understanding the steady-state burning mechanism of ammonium perchlorate propellants, however, has been sufficient for justifying a tentative phenomenological explanation.

Jaumotte and this author, studying the burning mechanism of ammonium perchlorate propellants, reached the conclusion that at low pressure the combustion surface consists in oxidizer crystals protruding over the fuel surface, while at high pressure the opposite situation exists: the crystals located at the bottom of small valleys and the apparent surface mainly consisting of sharp fuel peaks (1).[3] Conceivably, between these two extreme situations, the surface becomes first smoother and then rougher with increasing pressure.

Recently this behavior has been systematically observed and photographed by Barrère at O.N.E.R.A. and by Bastress, Hall and Summerfield at Princeton University (2). The latter group somewhat complicated the model by observing

Received March 27, 1961.

[1] This work has been supported by the Office of Scientific Research of the Air Research and Development Command, U. S. Air Force, under contract AF 61(052)-354.

[2] Lecturer, Institute of Aeronautics. Consultant for Poudreries Réunies de Belgique.

[3] Numbers in parentheses indicate References at end of paper.

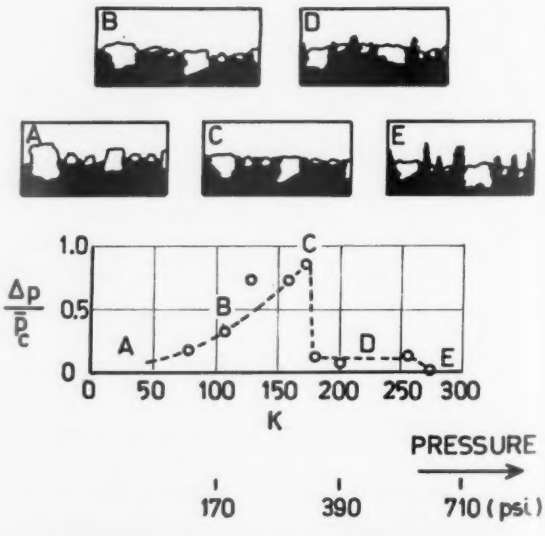

Fig. 1 Dependance of the severity of irregular burning on pressure as obtained at the JPL and the corresponding aspect of the combustion surface

the following: for very low pressures and very fine granulations the irregular surface is composed of fuel and no oxidizer particles are found, and for very fine granulations at medium pressure a plateau appears. A possible explanation for the first case lies in the detachment of very small crystals when the fuel regresses much faster than the oxidizer.

This improved understanding of steady-state burning of ammonium perchlorate propellants may also provide a plausible explanation for the intrinsic ability of a propellant to support oscillation and burn irregularly under certain conditions.

It seems reasonable, indeed, to expect that the surface erosivity, and possibly also acoustic admittance, i.e., response to small velocity and pressure perturbations, is much larger for a smooth surface than for a rough one.

Moreover roughness is not the only criterion; another most important surface characteristic is the nature of the protrusions. At low pressures, the surface protrusions are made of ammonium perchlorate which, alone, is a fair monopropellant capable of amplifying perturbations.

On the other hand, at high pressures, the apparent surface consists in fuel peaks generally made of rather inert substances whose regression one can hardly expect to be much influenced by small perturbations. However, this may not be true anymore for active fuels such as nitrocellulose.

The discussion is summarized by Fig. 1, which reproduces experimental data obtained by Landsbaum, Kuby, and Spaid (3). The severity of irregular burning is given, as measured by the ratio of the increase in pressure to the normal chamber pressure, as a function of combustion to throat area ratio K, which is itself a function of pressure (K = 100, 200 and 300, correspond respectively to $\bar{p}_c$ = 170, 390 and 710 psi). This figure also represents the type of surface which corresponds to the various behaviors, a nearly flat surface being assumed to give maximum instability.

One may be surprised by the sharp decrease in severity observed just above that particular pressure. A possible explanation is that, in this region, the rapid appearance of even a limited number of fuel peaks over the main surface almost completely prevents the establishment of small velocity oscillations over the active surface of the oxidizer.

The small amount of erosivity remaining in region D may be due to a few large crystals still slightly protruding (bimodal distribution), and in many instances the existence of this region has not been observed (3).

This theory assumes that small oscillations mainly affect the protrusions; this is consistent with the view that erosivity plays a predominant role in irregular burning, as emphasized by the stability of end burners and by the experiments described by Brownlee and Marble (4).

Although the acoustic admittance of the propellant can also be expected to depend on surface rugosity, this theory may not necessarily provide the complete explanation for oscillatory burning, and other factors, such as the gas phase reactions, may have to be taken into account, as proposed by Barrère (5).

It can be shown easily, through comparing burning rates of propellants and pure ammonium perchlorate, that an increase in oxidizer content or a decrease in crystal average size both result in a decrease in surface rugosity and a stronger tendency for the perchlorate to stay protruding above the surface, both factors favoring the ability to sustain irregular burning (1).

In this way, the influence of aluminum powder is suppressing irregular burning could be explained, tentatively, by an increase in surface roughness through cratering and the detachment of crystals away from the surface, as observed by Barrère (5).

This theory may perhaps also be applied to other formulations. Indeed, the flat active combustion surface of double base propellants may explain the apparent absence of any particularly orderly dependence of severity of erratic combustion on pressure, in tests on a variety of formulations, and the ripples observed by Price, among others, are second-order consequences irrelevent to the problem under consideration.

On the other hand the systematic protrusion of fuel peaks over the burning surface of ammonium nitrate propellants may be the origin of their stable behavior.

This theory is still somewhat speculative; However, there doesn't seem to be any major difficulty in attempting to prove its validity through systematic experimentation using a suitable method for interrupting the combustion of small samples (see the technique developed by M. Summerfield et al., Ref. 2).

If proved, it may provide a useful tool for predicting the ability of new high energy formulations to support irregular burnings.

Finally, it must be remarked that normal erosive burning, shortly after ignition, may also influence the surface, through some kind of smoothening action which would have to be studied in more detail (6).

References

1 Jaumotte, A. and Vandenkerckhove, J. A., "Remarks on the Burning Mechanism and Erosive Burning of Ammonium Perchlorate Propellants," Eighth Symposium on Combustion, Pasadena, Calif., 1960 (to be published).

2 Bastress, E. K., Hall, K. P. and Summerfield, M., "Modification of the Burning Rates of Solid Propellants by Oxidizer Particle Size Control," presented at the ARS Solid Propellant Rocket Conference, Salt Lake City, Utah, Feb. 1–3, 1961 (ARS preprint 1957-61).

3 Landsbaum, E. M., Kuby, W. C. and Spaid, F. W., "Experimental Investigations of Unstable Burning in Solid Propellant Rocket Motors," *Solid Propellant Rocket Research*, M. Summerfield (ed.), Academic Press, 1960.

4 Brownlee, W. G. and Marble, F. E., "An Experimental Investigation of Unstable Combustion in Solid Propellant Rocket Motors" *Solid Propellant Rocket Research*, M. Summerfield (ed.), Academic Press, 1960.

5 Barrere, M., presentation of an O.N.E.R.A. film on Combustion of Ammonium Perchlorate Propellants.

6 Vandenkerckhove, J. A., "Theoretical Investigation of Erosive Burning of Solid Propellants," Tech. Note NR.2, Contract NR.AF61(052)-354, July 1961, Publication de l'Institut d'Aeronautique, Universite de Bruxelles.

Integratable Form of Droplet Drag Coefficient

ABBOTT PUTNAM[1]

Battelle Memorial Institute, Columbus, Ohio

A CENTRAL problem in many combustion studies is the motion of spherical particles or droplets relative to the gas stream. The initial velocity of the droplet relative to the gas stream is usually the highest relative velocity. Using reasonable values of this velocity, the maximum expected droplet size and the minimum kinetic viscosity of the gas, the Reynolds number in many applications will not exceed 1000. Drag data covering the Reynolds number range up to this value are often approximated for numerical computational purposes by equations not mathematically tractable for integration. However, it should be noted that the relation

$$C_D R/24 = 1 + R^{2/3}/6$$

fits these data quite well and also is mathematically tractable.

As an example we might compute the projected distance of

Received July 10, 1961.

[1] Staff Mechanical Engineer, Mechanical Engineering Dept. Member ARS.

a droplet relative to the stream from the point of injection. Using Newton's law, the above relation, and designating initial conditions by the subscript 0, the ratio of velocity to initial velocity is given after one integration by

$$(V/V_0)^{-2/3} = (1 + R_0^{2/3}/6) \exp(12\mu t/\rho_d D) - R_0^{2/3}/6$$

where ρ_d is the droplet density and D is the droplet diameter.

The distance y traveled by the droplet from the point of injection relative to the stream is obtained by direct integration of the velocity over the transient time, with the result that

$$(\mu R_0^{2/3} y/\rho_d D^2 V_0) = 1 - [(1 + R_0^{2/3}/6)e^{\tau} - R_0^{2/3}/6]^{-1/2} + \sqrt{6}\, R_0^{-1/3} \left\{ \tan^{-1} \sqrt{6}\, R_0^{-1/3} - \tan^{-1} \left[\frac{(1 + R_0^{2/3}/6)\, e^{\tau} - R_0^{2/3}/6}{R_0^{2/3}/6} \right]^{1/2} \right\}$$

where

$$\tau = 12\, \mu t/\rho_d D$$

Eliminating τ from the above equation, the relation between velocity and distance is

$$R_0^{-1/3} (\rho/\rho_d)(y/D) = 1 - (V/V_0)^{1/3} - \sqrt{6}\, R_0^{-1/3} \tan^{-1} \left\{ \sqrt{6}\, R_0^{-1/3} \left[\frac{1 - (V/V_0)^{1/3}}{(V/V_0)^{1/3} + 6\, R_0^{-2/3}} \right] \right.$$

It is obvious that the maximum distance, given by $V/V_0 \to 0$, is

$$(\rho/\rho_d)(y_m/D) = R_0^{1/3} - \sqrt{6} \tan^{-1} (R_0^{1/3}/\sqrt{6})$$

Furthermore, at large values of R_0

$$(\rho/\rho_d)(y_m/D) \cong R_0^{1/3}$$

while, at small values of R_0

$$(\rho/\rho_d)(y_m/D) \cong R_0/18$$

The extension of these relations to obtain absolute values of distance of droplet travel is straightforward.

γ Large or Small

R. C. OLIVER[1]
S. E. STEPHANOU[2]

Aeronutronic Div. Ford Motor Co., Newport Beach, Calif.

The controversy on whether a large or small value of the isentropic expansion coefficient γ is desirable in an ideal propellant is noted. The conclusion is reached that generalizations regarding γ are not meaningful without careful prestatement of qualifying assumptions; the opinion is offered that attempts to separate the influence of γ in chemical rocket propellant systems are largely fruitless.

PERIODICALLY, articles appear in the literature (1,2,3)[3] in which attempts are made to describe an ideal propellant, or to estimate the potential of chemical propellants. In examining the factors involved, the authors generally come to some conclusion regarding the desirability of high or low values of γ, the isentropic expansion coefficient—an item which is *sine qua non* to the aerodynamicist although generally useless to the thermochemist. It is surprising that for such an apparently simple question various authors come to precisely opposite conclusions.

One author will argue, for example, that specific impulse is a function of the product of an enthalpy release term per unit weight and an efficiency term η based on γ and the pressure ratio

$$\eta = 1 - \left(\frac{P_e}{P_c}\right)^{(\gamma - 1)/\gamma} \qquad [1]$$

where p_e is the exhaust pressure and p_c is the chamber pressure. On examining this function, it appears that large values of γ are desirable in order to obtain high efficiency and thus high impulse. At 1000 psia chamber pressure and 14.7 psia exhaust, for example, the efficiency is calculated to be

γ	η
1.67	0.805
1.40	0.701
1.10	0.344

On this basis, a large value of γ is claimed to be desirable. The implication is clear; the ideal propellant should have a monatomic exhaust, for which $\gamma = 5/3$, the maximum value. Further, the advantages of a large γ can be shown with an example: the H_2-F_2 system with a specific impulse value of 410 sec (4)[4] has a γ of 1.33 (1); the H_2-O_2 system with a specific impulse of 391 sec (4), has a γ of only 1.26 (1).

The next author, however, goes one step further and points out that the enthalpy release per unit weight term can also be expanded, and states that the specific impulse is proportional to the square root of

$$\frac{RT_c}{M} \left(\frac{\gamma}{\gamma - 1}\right) \left[1 - \left(\frac{P_e}{P_c}\right)^{(\gamma - 1)/\gamma}\right] \qquad [2]$$

where R is the universal gas constant, T_c is the chamber temperature, and M is the molecular weight. When one examines this expression as a function of γ, however, it soon becomes clear that the $\gamma/(\gamma - 1)$ term overrides the "efficiency" term, and the total function increases with decreasing γ

γ	$\left(\frac{\gamma}{\gamma - 1}\right)\left[1 - \left(\frac{P_e}{P_c}\right)^{(\gamma - 1)/\gamma}\right]$
1.67	2.02
1.40	2.46
1.10	3.79

for the same pressure as used above.

Clearly we should have a system full of solid particles, thereby obtaining a low γ and high performance. Again, if we wished we could find an example to illustrate this point using one of the borohydride-amine systems. These systems give high theoretical performance with up to 87% solids and very low γ: Q.E.D.

We submit that this apparent problem arises from failure to adequately describe what is being discussed. To illustrate, let's start at the beginning and look at I_{sp} and γ.

The basic equation for I_{sp} is

$$I_{sp} = \sqrt{\frac{2J(H_c - H_e)}{g_c}} \qquad [3]$$

where

$H_c - H_e$ is the enthalpy difference between the chamber and exhaust, Btu/lbm
g_c is the gravitational constant, lbm-ft/lbf-sec^2
J is the mechanical equivalent of heat in ft-lbf /Btu

Received May 22, 1961.

[1] Senior Engineer. Member ARS.
[2] Supervisor, Propellant Chemistry. Member ARS.
[3] Numbers in parentheses indicate References at end of paper.
[4] Values shown are shifting impulse, 1000-14.7 psia.

For an ideal gas, with constant specific heat

$$H_c - H_e = C_p(T_c - T_e)$$

where

C_p, Btu/lbm-°R (Note that C_p is per lb mass.)
T, °R

To find the influence of γ at constant pressure ratio, write

$$\gamma = \frac{C_p}{C_p - R/M} \qquad [4a]$$

or

$$\gamma = \frac{MC_p}{MC_p - R} \qquad [4b]$$

where

R = 1.987 Btu/(lbm) (°R)
M = molecular weight

Examination of either of these equations shows that γ can approach 1.00 either as M approaches infinity at constant C_p, or as C_p approaches infinity at constant M. The two assumptions lead to quite different opinions regarding γ.

If, for example, M is assumed to be constant, we write

$$C_p(T_c - T_e) = \frac{RT_c}{M}\left(\frac{\gamma}{\gamma - 1}\right)\left[1 - \left(\frac{P_e}{P_c}\right)^{(\gamma - 1)/\gamma}\right] \qquad [5]$$

As was shown earlier, this function increases as γ decreases, leading to the opinion that low values of γ are desirable for high values of impulse, *provided that constant M and T_c are assumed.* At the limiting value of $\gamma = 1$, with this approach, it can be shown by L'Hospital's rule that the maximum I_{sp} is obtained according to the expression

$$I_{sp,\,\gamma=1} = \sqrt{\frac{2RT_cJ}{g_c M}}\sqrt{\ln\frac{P_c}{P_e}} \qquad [6]$$

If instead, C_p (per lb) is assumed to remain constant and variation in γ is caused by variation in molecular weight, the equation should be written

$$H_c - H_e = C_pT_c\left[1 - \left(\frac{P_e}{P_c}\right)^{(\gamma - 1)/\gamma}\right] \qquad [6a]$$

$$= C_pT_c\left[1 - \left(\frac{P_e}{P_c}\right)^{R/C_pM}\right] \qquad [6b]$$

since $(\gamma - 1)/\gamma = R/C_pM$ from Eq. 4. Here, as M increases (and γ decreases), the term $H_c - H_e$ decreases, leading to the opinion that low values of γ are undesirable. In this case, at $\gamma = 1$, $I_{sp} = 0$; maximum impulse is obtained with minimum molecular weight, which corresponds to the maximum γ.

In conclusion, it appears that neither approach to the γ question is correct or incorrect, but that both represent oversimplifications and imprecision as to what is implied by a change in γ. As a matter of fact, although γ or effective γ values can be useful, as for example, when comparing propellant systems at different pressure ratios, the authors feel that attempts to bring γ into discussion of ideal propellants are to a large extent fruitless. The difficulty is that γ is itself dependent on what could be termed more fundamental variables in the specific impulse relationship.

References

1 Tormey, J. F., "Liquid Rocket Propellants—Is There an Energy Limit?," *Ind. Eng. Chem.*, vol. 49, 1957, pp. 1339–1343.
2 Green, L., Jr. and Carter, J. M., "Performance Calculations for Hybrid Nuclear-Chemical Rocket Propulsion Systems," ARS JOURNAL, vol. 29, no. 3, March 1959, pp. 180–186.
3 Carter, J. M., "Isp: How High for Chemical Fuels?" ASTRONAUTICS, vol. 3, September 1958, pp. 26–27, 74–76.
4 Dobbins, T. O., "Thermodynamics of Rocket Propulsion and Theoretical Evaluation of Some Prototype Propellant Combinations," WADC TR-59-757, December 1959, p. 128.

Surface Temperatures of High Speed, Radiation Cooled Bodies in Dissociating Atmospheres

(ARS Journal, Vol. 31, No. 7, 1961, pp. 1013–1015)

Three typographical errors appearing in column 2 of page 1013 should be corrected as follows:

1) In Eq. 3e replace Q_* by θ_*.
2) In Eq. 3f replace α by σ.
3) In the first sentence of the section entitled Discussion, the condition $\theta > 1$ should read $\theta_* > 1$.

New Patents

George F. McLaughlin, *Contributor*

Thrust control for liquid propellant rocket engines (2,979,891). G. M. Widell, South Bend, Ind., assignor to The Bendix Corp. (ARS corporate member).

Metering valve controlling propellant flow as function of piston position. One diaphragm used to bias another to prevent thrust chamber overshoot during engine acceleration and deceleration.

Rocket-turbo engine convertible to ramjet (2,979,892). R. H. D. Chamberlin, R. E. Morris, A. L. Davies and L. R. Fletcher, London, England, assignors to D. Napier & Son, Ltd.

Unimpeded exhaust duct communicating with main combustion chamber. Compressor rotor windmills when turbine is stationary and unit is functioning as ramjet.

Power unit (2,979,896). H. E. Perkins Jr., and D. W. Haskins, East Alton, Ill., assignors to Olin Mathieson Chemical Corp. (ARS corporate member).

Cylindrical cartridge case of heat resistant elastometric material, and containing a slow burning propellant. One end of case closed by a refractory foraminous port for discharging high pressure gases.

Gyroscopic stabilizer for rocket (2,981,061). H. W. Lilligren, El Segundo, Calif.

Annular housing at exhaust end of rocket. Turbine vanes on rotor, responsive to gas flow through a nozzle, effect gyroscopic rotation of rocket.

Electromagnetically controllable fluid propellant type rocket motor system (2,986,004). J. D. McKenney (ARS member), assignor to Clary Corp.

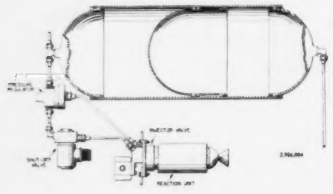

Variable thrust control for maneuvering or propelling a vehicle or space satellite. Thrust is proportional to value of electric signal applied from a point near motor or from a remote location.

Ullage compensators for pressurizing systems (2,979,897). W. R. Studhalter, L. M. Miller (ARS members) and W. O. Bergreen, Altadena, Calif., assignors to North American Aviation, Inc. (ARS corporate member).

Flexible wall ullage container near rocket propellant tank. Expansion and contraction of propellant in tank causes simultaneous compensating contraction and expansion of container before rocket actuation.

Editor's Note: Patents listed above were selected from the Official Gazette of the U. S. Patent Office. Printed copies of patents may be obtained from the Commissioner of Patents, Washington 25, D. C., at a cost of 25 cents each; design patents, 10 cents.

Missile terminal guidance system controller (2,984,435). W. O. Faith, H. W. Prier and A. E. Wasserman, Arlington, Tex., assignors to Chance Vought Corp. (ARS corporate member).

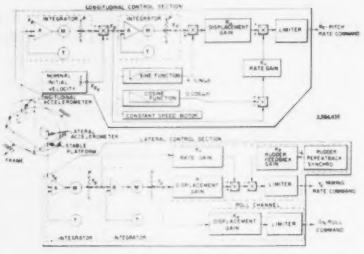

Inertial controller for guided missile having a pitch, yaw, and roll guidance system for controlling movements of the missile during its terminal maneuver between release point and target.

Expulsion bag tank for liquid propellant (2,980,177). W. J. Glasson, Los Angeles, Calif., assignor to Hughes Aircraft Co. (ARS corporate member).

Propelling gas supplied to an inflatable bag in fuel tank compartment. Rupturable diaphragm seals bag compartment from remainder of tank.

Fluid gyroscope for indicating orientation of a spinning missile (2,980,363). E. O. Schonstedt, Silver Spring, Md., assignor to the U. S. Navy.

Mercury in collapsible container communicates with interior of hollow sphere in missile. As missile is launched, mercury is injected into sphere where sensing means detects changes in direction of rotation.

Flying body for supersonic speed (2,980,370). F. Takacs, Caracas, Venezuela.

Ribbed nose cone of missile, each rib decreasing in height from base to apex, and arcuately concave in radial section. Control vanes mounted on base of cone.

Dual thrust chamber rocket (2,981,059). J. W. Horner (ARS member), and A. J. Rothenberg, Culver City, Calif., assignors to Thompson Ramo Wooldridge, Inc. (ARS corporate member).

Sustaining and boost levels of thrust for high altitude and low altitude flight. Sustaining nozzle leads to boost nozzle, both acting during time of sustaining flight.

Rocket construction (2,981,060). G. C. Barnes, Manchester, Conn., assignor to United Aircraft Corp. (ARS corporate member).

Solid propellants in a chamber, one of which alone will not support combustion, but together in close proximity will supply thrust. Distance between propellants may be varied.

Launcher (2,981,150). A. H. Miller Jr., Silver Spring, Md., assignor to the U. S. Navy.

Boom pivotally mounted on upper end of a central column supported by a tripod. Spaced plates under boom carry a track to releasably receive mating parts on a missile.

Aircraft with auxiliary launching aircraft (2,981,499). R. B. J. Janney II, Wilmington, Del., assignor to All American Engineering Co. (ARS corporate member).

Aerial jet engine powered pusher catapult for accelerating an aircraft from the ground. Aircraft has a catapult engaging means under the fuselage.

Servo control system for guided missile (2,981,500). A. G. Carlton, Silver Spring, Md., assignor to the U. S. Navy.

A first signal representing attitude of a missile is compared with a second signal representing a predetermined attitude. An error signal actuates an aerodynamic surface for control.

Missile handling and launching device (2,981,152). A. H. Miller, V. J. Dietz and D. M. Shipley, Hyattsville, Md., assignors to the U. S. Navy.

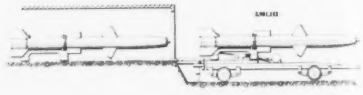

Plurality of underground launchers. Missiles stored in maximum degree of readiness because warmup power is supplied directly to missiles in launchers.

Automatic control of oxidizer and fuel turbopump system for rocket engines (2,984,968). W. W. Mower, G. P. Sutton, J. S. Newton (ARS members), W. C. Hunter Jr. and J. P. Morris, Long Beach, Calif., assignors to North American Aviation, Inc. (ARS corporate member).

Combustion chamber pressure controlled at a predetermined value by a servo between a pneumatic sensing means and a valve controlling flow of gas.

Afterburner control for a multispool gas turbine (2,984,969). B. N. Torrell, Wethersfield, Conn., assignor to United Aircraft Corp. (ARS corporate member).

Twin spool afterburning power plant. Means for varying area of exhaust nozzle combined with scheduling its area. Speed of low pressure spool regulates fuel flow.

Cooling system (2,984,994). D. L. Hankins, Bettendorf, Iowa, assignor to The Bendix Corp. (ARS corporate member).

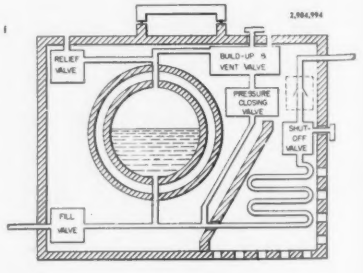

Portable unit for cooling, controlling the humidity, and circulating air in and through an aviator's suit. Converts liquid oxygen to gaseous oxygen.

Technical Literature Digest

M. H. Smith, *Associate Editor*
The James Forrestal Research Center, Princeton University

Propulsion and Power (Combustion Systems)

Symposium on Nondestructive Testing in the Missile Industry, San Francisco, Oct. 12, 1959 (ASTM Special Tech. Pub. no. 278), Philadelphia, ASTM, 1960, 71 pp.

Radiography of Large Solid Propellant Rocket Motors, by E. L. Criscuolo, J. A. Holloway, D. Polansky and C. H. Dyer, pp. 3–11.

Large Rocket Engines for Space Vehicles and Missiles, by S. K. Hoffman, *Royal Aeron. Soc., J.*, vol. 65, no. 605, May 1961, pp. 321–331.

Simple Method for Estimating First-Stage Boost Thrust and Specific Impulse, by Robert L. Doebler, ARS JOURNAL, vol. 31, no. 4, April 1961, pp. 550–551.

Ballistic Missile and Space Technology vol. 2: Propulsion and Auxiliary Power Systems (Symposium on Ballistic Missile Space Technology, 5th, Los Angeles, Aug. 1960) Donald P. Le Galley (ed.), Academic Press, New York, 1960, 441 pp.

Precision Determination of Vacuum Specific Impulse from Trajectory Data, by C. S. Powers, pp. 111–121.

Soviet Rocket Propulsion, by Donald J. Ritchie, pp. 55–86.

Propulsion and Power (Noncombustion)

The Effect of Variable Plasma Conductivity on MHD Energy Converter Performance, by W. B. Coe and C. L. Eisen, *Republic Aviation Corp., Plasma Propulsion Lab.*, PPL-TR-60-16 (176), Oct. 1960, 20 pp.

Experimental Performance of a Pulsed Gas Entry Coaxial Plasma Accelerator, by P. Gloersen, B. Gorowitz and W. Palm, *Gen. Electric Co., Missile and Space Vehicle Dept.* T.I.S. R61SD042, April 1961, 14 pp.

Comparative Measurements of Beam Power in Iron-Rocket Research, by E. A. Richley, V. A. Sandborn, L. V. Baldwin and E. E. Dangle, *NASA Tech. Note* D-845, May 1961, 32 pp.

Analysis of Thrust Measuring Devices for Pulse Systems, by Melvin Zaid, *Republic Aviation Corp., Plasma Propulsion Lab.* PPI-TR-60-17, Nov. 1960, 35 pp.

Achieving High Burn-Up in Fast Reactors, by L. R. Blake, *J. Nuclear Energy* (Parts A and B: Reactor Sci. and Tech.), vol. 14, no. 1, April 1961, pp. 31–48.

Pulsed Operation of a Fast Reactor, by I. I. Bondarenko and Yu. Ya. Stavisskii, *J. Nuclear Energy* (Parts A and B: Reactor Sci. and Tech.), vol. 14, no. 1, April 1961, pp. 55–58.

Essential Limitations and T-Nt Diagram for Self-Sustaining Fusion Systems, by Mitsuo Imoto, *J. Nuclear Energy* (Part C: Plasma Physics-Accelerators-Thermonuclear Res.) vol. 1, no. 1–2, Oct. 1959, pp. 19–30.

EDITOR'S NOTE: Contributions from Professors E. R. G. Eckert, E. M. Sparrow and W. E. Ibele of the Heat Transfer Laboratory, University of Minnesota, are gratefully acknowledged.

Measurement of Capacitor Charging Efficiencies Utilizing Ramp and Spike Charging Voltages, by D. Rigney, C. Cavalconte, I. Granet and A. Steinberg, *Republic Aviation Corp., Plasma Propulsion Lab.*, PPL-TR-61-2(257), Jan. 1961, 11 pp.

Proceedings (Advances in the Astronautical Sciences, U. S.), American Astronautical Society, Western National Meeting, Plenum Press, New York, 1960, 355 pp.

Shielding and Nuclear Propulsion, by Robert F. Trapp and Eugene B. Konecci, pp. 25–32.

Reaction Control Simulator, by Walter Kuehnegger, pp. 33–38.

Solar Photovoltaic Power Sources for Space Vehicles, by Douglas J. Sailor, pp. 149–156.

The Problem of Electrical Neutrality in Ion Beams, by Edward Fisher, pp. 157–165.

The Magnetic Pinch Engine for Space Flight, by Alfred E. Kunen and W. McIlroy, pp. 166–178.

General Research in Materials and Propulsion, Jan. 1959—Jan. 1960, Vol. 1, Propulsion Chemistry and Propulsion Physics, *Lockheed Aircraft Corp., Missiles and Space Div. Tech. Rep.* LMSD 288140, vol. 1, Jan. 1960, 154 pp.

Thermionic Theory and Technique, paper no. 1, by J. E. Cobb, W. H. Cutler and A. F. Dugan, 20 pp.

Ionic Propulsion an Assessment, paper no. 2, by G. B. S. Shook, 27 pp.

A Nuclear-Ionic System for Space Flight, paper no. 3, by J. E. Cobb, G. B. Shook and W. H. Cutler, 25 pp.

A Thermal-Electronic Converter, paper no. 5, by J. E. Cobb and W. H. Cutler, 23 pp.

Metallic Carbides as Emitter Materials in Thermal-Electronic Convertors, by G. C. Kuczynski, paper no. 6, 18 pp.

Radiator-Condenser for Space Environment, by A. M. Haire, L. G. Hayes and J. L. Collins, *Electro-Optical Systems, Inc., EOS Rep.* 310-Final (WADD TR 61-20) Oct. 31, 1960.

Investigations on the Direct Conversion of Nuclear Fission Energy to Electrical Energy in Plasma Diode, *Gen. Motors Corp., Res. Labs., Center Line, Mich., Final Rep.* Nonr-3109(00), Dec. 31, 1960.

Kiwi-A: The First Rocket Reactor Experiment, by R. E. Schreiber, *Inst. Aerospace Sci.*, Rep. 61-65, Jan. 23–25, 1961.

Safety Considerations for Nuclear Power in Aerospace, by J. A. Connor, *Inst. Aerospace Sci.* Rep. 61-67, Jan. 23–25, 1961.

Experimental Research on the Cesium Thermionic Converter, by N. S. Rasor, *Inst. Aerospace Sci.* Rep. 61-72, Jan. 23–25, 1961.

Thermionic Conversion of Heat to Electricity, by W. B. Nottingham, G. N. Hatsopoulos, and E. N. Carabateas, *Inst. Aerospace Sci.* Rep. 61-73, Jan. 23–25, 1961.

A Brief Study of Rocket-Powered Magnetohydrodynamic Generators and Energy-Storage Devices, by J. H. Huth, *Rand Corp.*, RM-2522-ARPA, May 19, 1960.

Propellants and Combustion

On the Stability of Detonation Waves at Low Pressures, by James A. Fay, *Princeton Univ. Project Squid*, MIT-25-R, May 1961, 15 pp.

Contact Surface Tailoring in a Chemical Shock Tube, by Howard B. Palmer and Bruce E. Knox, *Princeton Univ. Project Squid*, PSU-u-p, April 1961, 7 pp.

Shock Tubes in Fuels Research, by Howard B. Palmer, *Princeton Univ. Project Squid*, PSU-8-P, April 1961, 26 pp.

Fundamentals of Liquid Propellant Sensitivity, by T. A. Erikson and E. L. Grove, *Illinois Inst. Tech., Armour Res. Foundation*, ARF 3180 (Quar. no. 3), May 1961, 25 pp.

Studies on Deflagration to Detonation in Propellants and Explosives, *Bureau of Mines, Explosives Res. Lab.*, Quar. Rep., Jan. 1, 1961, to March 31, 1961, 11 pp.

Research on Combustion Phenomena at High Pressures, by W. A. Strauss and R. Edse, *Air Force Res. Div., Aeron. Res. Lab. Tech. Note* 60-132, Feb. 1961, 23 pp., 12 refs.

Internal Conversion Processes in Biacetyl, by Jean T. Bubois, *Air Force Res. Div., Wright Patterson AF Base*, ARL 8, Jan. 1961, 4 pp.

Bond Dissociation Energies in Small Hydrocarbon Molecules, by Bruce E. Knox and Howard B. Palmer, *Chem. Reviews*, vol. 61, no. 2, June 1961, pp. 247–256.

The Magnitude of the Primary Kinetic Isotope Effect for Compounds of Hydrogen and Deuterium, by F. H. Westheimer, *Chem. Reviews*, vol. 61, no. 2, June 1961, pp 265–274.

Symposium on Nondestructive Testing in the Missile Industry, San Francisco, Oct. 12, 1959 (ASTM Special Tech. Pub. no. 278), Philadelphia, ASTM, 1960, 71 pp.

An Ultrasonic Method to Detect, Count and Measure Fluid-Contaminating Particles, by Charles P. Albertson, pp. 53–56.

General Research in Materials and Propulsion, Jan. 1959-Jan. 1960, Vol. 1, Propulsion Chemistry and Propulsion Physics, *Lockheed Aircraft Corp., Missiles and Space Div., Tech. Rep.* No. LMSD-288140, vol. 1, Jan. 1960, 154 pp.

Phosphorus-Fluorine Oxidizers, paper no. 7, by C. J. Hoffman, 17 pp.

Investigation of Nitro Compounds as Oxidants for High-Energy Chemical Systems I, Lithium Dinitroethane, paper no. 8, by P. Noble Jr., 9 pp.

Investigation of Nitro Compounds as Oxidants for High-Energy Chemical Systems II, Methylene-Dinitramine, paper no. 9, by P. Noble Jr., 13 pp.

Condensation of Atomic and Molecular Hydrogen at Low Temperatures, by R. T. Brackmann and Wade L. Fite, *J. Chem. Phys.*, vol. 34, no. 5, May 1961, pp. 1572–1579.

Wiley BOOKS

DESIGN DATA IN AERONAUTICS AND ASTRONAUTICS

Edited by RICHARD B. MORRISON, *assisted by* MELVA J. INGLE, *both of the University of Michigan*. Brings together information previously unpublished or scattered widely throughout the literature. All data are presented in forms convenient for analysis and computation relating to the needs of industry, research, teaching, and the military. Correlated data and nondimensional parameters are given wherever possible, and graphs set forth material when graphs are the most useful form. Special feature—a Mollier Diagram for Equilibrium Air. *1961. Approx. 608 pages. Prob. $12.50*

BALLISTIC MISSILE AND SPACE VEHICLE SYSTEMS

By HOWARD S. SIEFERT, *Stanford University, and* KENNETH BROWN, *John Wiley & Sons, Inc.* This book offers a full coverage of engineering design principles of ballistic missiles and space vehicles which resemble each other in everything but their trajectories. It stresses the relationships among the many parts of a missile or space system, and presents a thorough survey of the ballistic problem—including vehicle stabilization, re-entry dynamics, and support system planning. Many illustrative examples and problems are included. *1961. 544 pages. $12.00*

Baker-Ryder-Baker: TEMPERATURE MEASUREMENT IN ENGINEERING, Volume II

Gives measurement methods on an engineering-design-technique basis. Also covers specific problems of measurement for laboratory, shop, field. *1961. 510 pages. $13.00*

Graham-McRuer: ANALYSIS OF NONLINEAR CONTROL SYSTEMS

Offers basic mathematical tools for analyzing problems of stability, accuracy, response. Illustrated with practical problems, design data. *1961. 482 pages. $9.75*

Peterson: STATISTICAL ANALYSIS AND OPTIMIZATION OF SYSTEMS

Analysis, synthesis, optimization of systems where statistical uncertainty is involved in process dynamics. Gives computing procedures, numerical results of specific examples. *1961. 190 pages. $9.75*

Markey-Hovorka: THE MECHANICS OF INERTIAL POSITION AND HEADING INDICATION

A rigorous treatment of synthesis of inertial navigation systems, for immediate practical application. *1961. 92 pages. $3.95*

Thomson: INTRODUCTION TO SPACE DYNAMICS

Stresses analysis in areas of coordinates for space motion; orbits; gyroscopic theory; generalized theory of dynamics from a variational approach; optimization techniques. *1961. Approx. 352 pages. Prob. $11.50*

Send now for your on-approval copies

JOHN WILEY & SONS, Inc.
440 PARK AVENUE SOUTH, NEW YORK 16, N. Y.

Effect of Molecular Oxygen on the Emission Spectra of Atomic Oxygen-Acetylene Flames, by S. L. N. G. Krishamachari and H. P. Broaida, *J. Chem. Phys.*, vol. 34, no. 5, May 1961, pp. 1709–1710.

Liquid Pumping Apparatus for Use in Studying Fast Chemical Reactions, by H. G. Weiss and C. W. Urmy Jr., *Radio Engng. and Electronics* (transl. of Radiotekhnika i Elektronika) vol. 5, no. 1, 1960, pp. 586–587.

Sputtering of Metals by Mass-Analyzed N_2^+ and N^+, by Michel Bader, Fred C. Witteborn and Thomas W. Snouse, *NASA Tech. Rep.* R-105, 1961, 30 pp.

Thermodynamics of Reactions Involving Light Metal Oxides and Propellant Gases, *Gabriel Rocket Power/Talco*, QR-1987-3, 3rd Quar. Rep., Nov. 1960-Feb. 1961, 26 pp.

Dissociation Energies of Gaseous Metal Dioxides, by Leo Brewer and Gerd M. Rosenblatt, *Chem. Reviews*, vol. 61, no. 2, June 1961, pp. 257–264.

Materials and Structures

Bibliography on the High Temperature Chemistry and Physics of Materials in the Condensed State, by J. J. Diamond, M. Foex, G. Hagg, H. Nowotny and J. P. H. Shaw, *Internat. Union of Pure and Appl. Chem., Comm. on High Temperatures and Refractories, Sub-Commission on Condensed States*, Jan.-March 1961, 36 pp.

A Preliminary Investigation of the Effect of Bumpers as a Means of Reducing Projectile Penetration, by John O. Funkhouser, *NASA Tech. Note* D-802, April 1961, 17 pp.

Electrical Characteristics of Four Ternary Platinum-Rhodium-Base Alloys Containing Chromium, Cobalt or Ruthenium, by Herman H. Lowell, Hubert W. Allen and Joe E. Jenkins, *NASA Tech. Note* D-867, May 1961, 17 pp.

The Behavior of Beryllium and Beryllium Copper in a 4,000°F Supersonic Air Jet at a Mach Number of 2, by William H. Kinard, *NASA Tech. Note* D-806, May 1961, 8 pp.

Maximum Stresses in Beams and Plates Vibrating at Resonance, by Eric E. Ungar, ASME paper 61-SA-14, June 11–14, 1961, 37 pp.

Maximum Stresses in Plates Vibrating at Resonance, by Eric E. Ungar, *Bolt, Beranek and Newman, Inc., Rep.* 724, Feb. 10, 1960, 34 pp.

Random Vibration of Beams, by Stephen G. Crandall and Asim Yildiz, *Mass. Inst. Tech.*, April 1961, 31 pp. (AFOSR 484).

Theoretical Elastic Stress Distributions Arising From Discontinuities and Edge Loads in Several Shell-Type Structures, by Robert H. Johns and Thomas W. Orange, *NASA Tech. Rep.* R-103, 1961, 63 pp.

Creep Analysis of Annular Plates, by B. Venkatraman and Sharad A. Patel, *Brooklyn, Polytech. Inst., Dept. Aerospace Engng. and Appl. Mech. Rep.* 588, March 1961, 26 pp., 3 figs. (AFOSR 518).

The Adhesion of Evaporated Metal Films on Glass, by P. Benjamin and C. Weaver, *Royal Soc., London, Proc.*, vol. A261, no. 1307, May 1961, pp. 516–531.

Conference on the Status of Radiation Effects Research on Structural Materials and the Implications to Reactor Design, Chicago, Oct. 15–16, 1959, *Atomic Energy Commission*, TID-7588, 1960, 306 pp.

Techniques for Measuring Reactor

Neutron Spectra, by J. B. Trice, pp. 1–15.

Neutron Flux Measurements for Materials Irradiation Experiments at ANL, BNL, ORNL and MTR, by L. E. Steele and J. R. Hawthorne, pp. 16–35.

Flux Measurements and Irradiation Assemblies Used in the LTTR, MTR and ORR Reactors, by J. C. Zukas and R. G. Berggren, pp. 36–55.

Neutron Radiation Embrittlement at 500°F and 650°F Reactor, by J. V. Alger and L. M. Skupien, pp. 56–90.

Radiation Effects in Ferritic Steels, by R. G. Berggren, pp. 91–127.

Studies at Harwell on Neutron Irradiation Effects in Steels, by D. R. Harries, pp. 128–139.

The Effect of Neutron Irradiation on the Charpy V and Drop-Weight Test Transition Temperatures of Various Steels and Weld Metals, by J. R. Hawthorne and L. E. Steele, pp. 140–176.

Effect of Irradiation on Mechanical Properties of Materials for Reactor Pressure Vessels, by L. P. Trudeau, pp. 177–188.

Programs on the Effects of Neutron Irradiation Upon the Mechanical Properties of Structural Materials, by E. E. Baldwin, pp. 189–204.

Tensile and Stress-Rupture Properties of Irradiated Stainless Steels and Inconel, by R. G. Berggren, W. E. Brundage, W. W. Davis, N. E. Hinkle and J. C. Zukas, pp. 205–217.

Practical Aspects of Reactor Pressure Vessel Design, by D. K. Davies, pp. 218–229.

Symposium on Nondestructive Testing in the Missile Industry, San Francisco, Oct. 12, 1959 (ASTM Special Tech. Publ. 278), Philadelphia, ASTM, 1960, 71 pp.

High Energy Radiography in the 6- to 30 Mev Range, by James H. Bly and Alfred E. Burrill.

Radiography of Weldments in Motion, pp. 40–46.

Ultrasonic Inspection of Adhesive-Bonded Aluminum Sandwich Structures, by C. Kammerer, pp. 47–52.

International Symposium on Stress Wave Propagation in Materials, State Univ. Pa., 1959, Proceedings, Normal Davids (ed.), Interscience Publishers, New York, 1960, 337 pp.

Propagation of an Elastic Strain Pulse in a Semi-Infinite Bar, by C. W. Curtis, pp. 15–44.

Viscoelastic Waves, by H. Kolsky, pp. 59–90.

Studies in Dynamic Photoelasticity With Special Emphasis on the Stress-Optic Law, by M. M. Frocht, pp. 91–118.

Edge Waves in Plates, by Sudhir Kumar, pp. 119–131.

Effects of Very Intense Stress Waves in Solids, by R. J. Eichelberger, pp. 133–167.

Experimental Studies in Armor Penetration, by James R. Kymer, pp. 169–181.

A Review of the Progress in the Measurement of Dynamic Elastic Properties, by K. W. Hillier, pp. 183–198.

The Theory of Wave Propagation in an Elastic Materials, by E. H. Lee, pp. 199–228.

Some Aspects of the Mechanism of Scabbing, by K. B. Broberg, pp. 229–246.

Some Problems of Transient Analysis of Waves in Plates, by Normal Davids, pp. 271–288.

Cinematography of Stress Waves, by H. Schardin, pp. 289–302.

Analysis of Dispersed Surface Waves, by Yasuo Sato, pp. 303–327.

General Research in Materials and Propulsion, Jan. 1959-Jan. 1960, Vol. 2, Metallurgy and Chemistry, *Lockheed Aircraft Corp., Missiles and Space Div. Tech. Rep.* LMSD-288140, vol. 2, Jan. 1960.

Electronic Structure of Beryllium, paper no. 1, by G. C. Kuczynski, 23 pp.

Electrical Resistivity of Beryllium, paper no. 2, by J. Ho and E. S. Wright, 19 pp.

Plastic Deformation in Beryllium, paper no. 3, by E. C. Burke, 13 pp.

Beryllium Analyzed for Trace Impurities by Gamma-Ray Activation, paper no. 4, by W. Bradshaw, R. Johnson and D. Beard, 21 pp.

High-Temperature Corrosion of Beryllium in Air, paper no. 5, by W. Bradshaw and E. S. Wright, 26 pp.

Stress Corrosion Cracking of Beryllium, paper no. 6, by C. M. Packer, 18 pp.

Grain Refinement in Beryllium by Alloying, paper no. 7, by D. Crooks and H. Sumsion, 32 pp.

Specific Heats of Beryllium and an Alloy at Room and Elevated Temperatures, paper no. 8, by E. Kanazawa and C. M. Packer, 19 pp.

Studies of the Gas Carburization of

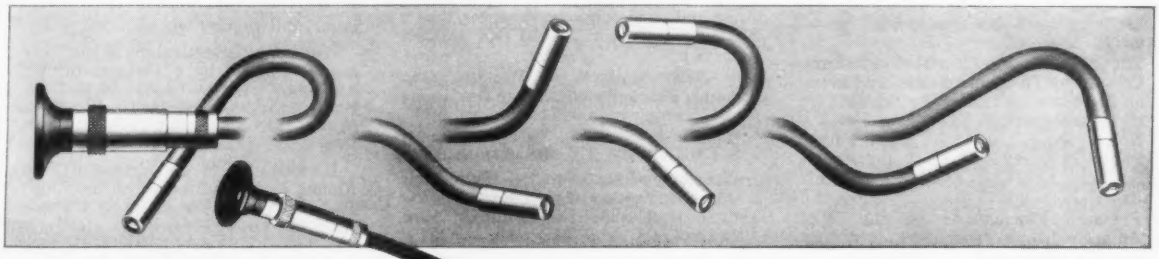

Focusing eyepiece for convenience of user.

For the ultimate in precision viewing of intricate, hard-to-reach areas . . .

A.C.M.I. Fiber Optic *Flexible* Borescopes

FOR visualization in inaccessible curved areas where a flexible instrument capable of adapting itself to irregular contours is required.

Fiber Optic Borescopes are equipped with focusing eyepiece and fixed or movable objective as required. Illumination can be provided by a flexible fiber optic light carrier with an external light source or an annular fiber optic light carrier attached to the image carrier. Fiber optic light carriers are particularly advantageous for transmission of intense cold light to inaccessible or hazardous areas.

Please send details and sketch of your requirements.

AMERICAN CYSTOSCOPE MAKERS, Inc.

8 Pelham Parkway, Pelham Manor (Pelham), N. Y.

Niobium, paper no. 9, by A. Ottenberg, 37 pp.

Study of Halide-Containing Oxide Films on Columbium, paper no. 10, by F. J. Clauss and S. Drake, 11 pp.

Ultrasonic Standards for the Evaluation of Missile Materials and Components, by T. Adams and J. W. Morris, pp. 57–71.

Properties and Handling Procedures for Rubidium and Cesium Metals, by T. D. Brotherton, O. N. Cole and R. E. Davis, *American Potash Chemical Corp., Trona Res. Lab.*, Feb. 28–March 2, 1961.

Expandable Structures for Space, by R. S. Ross, *Goodyear Aircraft Corp.*, GER 10073, Dec. 7, 1960.

Fluid Dynamics, Heat Transfer, and MHD

Naval Hydrodynamics, Hydrodynamic Noise, Cavity Flow (Symposium on Naval Hydrodynamics, 2nd, Washington, D. C., Aug. 1958) Ralph D. Cooper (ed.), Washington, D. C., Office of Naval Research, 1960, 583 pp.

Theory and Experiment in Aerodynamic Noise, With a Critique of Research on Jet Flows in Their Relationship to Sound, by Alan Powell, pp. 1–28.

A Theory of Turbulence Dynamics, by Robert H. Kraichnan, pp. 29–44.

Some Experimental and Theoretical Results Relating to Production of Noise by Turbulence and the Scattering of Sound by Turbulence or Single Vortices, by Ernst-August Muller, pp. 45–64.

Similarity Relations in Aerodynamic Noise Measurements, by E. Moll-Christensen and W. Liepmann, pp. 65–74.

Excitation of Acoustic Resonators by Flow, by Uno Ingrad and Lee W. Dean, pp. 137–150.

The Fluctuating Surface Pressure Created by Turbulent Boundary Layers on Hypersonic Vehicles, by Edmund E. Callaghan, pp. 127–136.

Noise Production in a Turbulent Boundary Layer by Smooth and Rough Surfaces, by Eugen Skudrayk and Gillian Haddle, pp. 75–106.

Pressure Fluctuations on the Wall Adjacent to a Turbulent Boundary Layer, by Mark Harrison, pp. 107–126.

Jets, Wakes, and Cavities, by Garrett Birkhoff, pp. 261–276.

Some Aerodynamic Cavity Flows in Flight Propulsion Systems, by William G. Cornell, pp. 391–424.

Radiative Transfer in the Flow of a Radiative Medium, by V. N. Adrianov and S. N. Shorin, *Purdue Univ., School of Aeron. and Engng. Sci., Radiative Transfer Proj., Transl. TT-1,* Feb. 1961, 16 pp. (transl. from Izvestiia Akademii Nauk SSSR OTN, no. 5, 46, May 1958).

An Analytical and Experimental Study of the Thermal Boundary Layer and Ebullition Cycle in Nucleate Boiling, by Yih-Yun Hsu and Robert W. Graham, *NASA Tech. Note* D-594, May 1961.

Free-Flight Aerodynamic-Heating Data to Mach Number 10.4 for a Modified von Karman Nose Shape, by William M. Bland Jr. and Katherine A. Collie, *NASA Tech. Note* D-889, May 1961, 28 pp.

Heat Transfer Tests of 20 Millimeter Projectiles at a Mach Number of 5 With an Analysis by Unsteady Scaling Laws to Predict Component Temperature Rises After Firing for Various Free-Flight Conditions, by Robert L. Trimpi, James G. Gallagher and Robert A. Jones, *NASA Tech. Note* D-758, May 1961, 30 pp.

Turbulent Skin-Friction and Heat-Transfer Coefficients for an Inclined Flat Plate at High Hypersonic Speeds in Terms of Free-Stream Flow Properties, by James F. Schmidt, *NASA Tech. Note* D-869, May 1961, 58 pp.

Exploratory Investigation of Transpiration Cooling of a 40° Double Wedge Using Nitrogen and Helium as Coolants at Stagnation Temperatures From 1,295°F to 2,910°F, by Bernard Rashis, *NASA Tech. Note* D-721, May 1961, 18 pp.

Compressible Flow Tables k = 1.20 Simple Gas Injection Without Forward Velocity y = 0, *Army Ballistic Missile Agency,* ABMA RA-TR-8-61, 14 April 1961, 89 pp.

Measurements of Aerodynamic Heat Transfer and Boundary-Layer Transition on a 10° Cone in Free Flight at Supersonic Mach Numbers up to 5.9, by Charles B. Rumsey and Dorothy B. Lee, *NASA Tech. Note* D-745, May 1961, 33 pp.

Heat Transfer, Temperature Recovery, and Skin Friction on a Flat Plate Surface With Hydrogen Release Into a Laminar Boundary Layer, by E. R. G. Eckert, A. A. Hayday and W. J. Minkowycz, *Minnesota Univ., Inst. Tech. Mech. Engng. Dept., Heat Transfer Lab. Tech. Rep.* 27, Feb. 1961, 35 Figs. (AFOSR TN 60–1417).

An Investigation of Transonic Flow Fields Surrounding Hot and Cold Sonic Jets, by George Lee, *NASA Tech. Note* D-853, April 1961, 39 pp.

Wave Functions for the Free Electron II. The Inclusion of Polarization and Exchange, by R. G. Breene Jr., *General Electric Co., Missile and Space Vehicle Dept.* T.I.S. R60SD478, Dec. 1960, 20 pp.

The Effect of Strong Magnetic Fields on Chemical Engineering Systems, by F. W. Camp and E. F. Johnson, *Princeton Univ., Plasma Physics Lab.*, MATT-67, March 1961, 97 pp.

A New Method of Treating Gas Dynamic Problems With Large Deviations From Thermodynamic Equilibrium, by F. Weitzsch, *Annalen der Physik,* vol. 7, no. 7–8, 1961, pp. 403–417 (in German).

Ultrasonic Relaxation in Polyatomic Gases and Vapours, by S. K. K. Jatkar and D. D. Deshpande, *British J. Appl. Phys.*, vol. 12, no. 5, May 1961, pp. 243–247.

Scattering of A Surface Wave by a Discontinuity in the Surface Reactance on a Right Angled Wedge, by F. C. Karal Jr., S. N. Karp, Ta-Shing Chu and R. G. Kouyou-Mjian, *Communications on Pure and Appl. Math.*, vol. 14, no. 1, Feb. 1961, pp. 35–48.

Diffraction by an Elliptic Cone, by Lester Kraus and Leo M. Levine, *Communications on Pure and Appl. Math.*, vol. 14, no. 1, Feb. 1961, pp. 49–68.

Hydrostatic Weighing of Liquids in Containers of Complex Shape, by L. P. Stepanov, *Measurement Techniques* (Trans. Izmeritel'naya Tekhnika) no. 9, Sept. 1960, pp. 742–743.

Gas and Heat Evolution From Thermally Unstable Materials, by O. B. Cecil and W. E. Koerner, *I/EC: Ind. Engng. Chem.*, vol. 53, no. 6, June 1961, pp. 475–478.

The Second Law of Thermodynamics, by Bruce Crawford Jr. and I. Oppenheim, *J. Chem. Phys.*, vol. 34, no. 5, May 1961, pp. 1621–1623.

A Resonance Method for Localizing and Heating a Plasma by Means of a Varying Electromagnetic Pressure, by G. A. Askaryan and M. S. Rabinovich, *J. Nuclear Energy* (Part C: Plasma Physics-Accelerators-Thermonuclear Res.), vol. 1, no. 3, March 1961, pp. 143.

On the Behaviour of Small Plasma Bunches in a Waveguide and Their Interaction With the Conducting Walls, by G. A. Askaryan, *J. Nuclear Energy* (Part C: Plasma Physics-Accelerators-Thermonuclear Res.) vol. 1, no. 3, March 1961, pp. 144–145.

Longitudinal Plasma Oscillations, by J. D. Jackson, *J. Nuclear Energy* (Part C: Plasma Physics-Accelerators-Thermonuclear Res.) vol. 1, no. 4, July 1960, pp. 171–179.

Longitudinal Plasma Oscillations in an Electric Field, by B. D. Fried, M. Gell-Mann, J. D. Jackson and H. W. Wyld, *J. Nuclear Energy* (Part C: Plasma Physics - Accelerators - Thermonuclear Res.) vol. 1, no. 4, July 1960, pp. 190–198.

A Twomode Variational Procedure for Calculating Thermal Diffusion Theory Parameters, by G. P. Calame, F. D. Federighi and P. A. Ombrellaro, *Nuclear Sci. and Engng.*, vol. 10, no. 1, May 1961, pp. 31–39.

On the Theory of Deionization of a Rarefied Gas in a Magnetic Field, by A. S. Syrgii and V. L. Granovskii, *Radio Engng. and Electronics* (Trans. of Radiotekhnika i Elektronika), vol. 5, no. 1, 1960, pp. 147–154.

Smear Camera Technique for Free-Surface Velocity Measurement, by W. C. Davis and B. G. Craig, *Rev. Scien. Instr.*, vol. 32, no. 5, May 1961, pp. 579–580.

Thermal Diffusion of Binary Gas Mixtures, by S. C. Saxena and S. M. Dave, *Reviews Modern Phys.*, vol. 33, no. 2, April 1961, pp. 148–152.

Dynamics of a System of Articulated Pipes Conveying Fluid, I, Theory; II, Experiments, by T. B. Benjamin, *Royal Soc., London Proc.*, vol. A261, no. 1307, May 1961, pp. 457–499.

Method of Investigation of the Flux of Atoms Emitted by a Plasma, by V. V. Afrosimov, I. P. Gladkovskii, Yu. S. Gordeev and others, *Soviet Phys., Tech. Phys.*, vol. 5, no. 12, June 1961, pp. 1378–1388.

Investigation of the Stream of Neutral Atomic Particles Emitted by the "Alpha" Plasma, by V. V. Afrosimov, I. P. Gladkovskii, Yu. S. Gordeev and others, *Soviet Phys., Tech. Phys.*, vol. 5, no. 12, June 1961, pp. 1389–1402.

The Energy Distribution of Fast Neutral Atoms Issuing From a Plasma, by O. V. Konstantinov and V. I. Perel', *Soviet Phys., Tech. Phys.*, vol. 5, no. 12, June 1961, pp. 1403–1411.

Longitudinal Vortices in Shear Flow, by G. S. S. Ludford, *Zeitschrift für Angewandte Math Mech.*, vol. 41, no. 4, April 1961, pp. 153–157.

Proceedings (Advances in the Astronautical Sciences, U. S.), American Astronautical Society, Western National Meeting, Plenum Press, New York, 1960, 355 pp.

Shock Tube Experiments Simulating Entry into Planetary Atmospheres, by R. W. Rutowski and K. K. Chan, pp. 346–356.

Transonic Wind-Tunnel Investigation of the Static Longitudinal Aerodynamic Characteristics of Several Configurations of the Scout Vehicle and of a Number of Related Models, by Thomas C. Kelly, *NASA Tech. Note* D-794, May 1961, 69 pp.

Investigation of Low-Subsonic Flight Characteristics of a Model of a Hypersonic Boost-Glide Configuration Having a

78° Delta Wing, by John W. Paulson and Robert E. Shanks, *NASA Tech. Note* D-894, May 1961, 31 pp.

Experimental Evaluation of Analytical Models for the Inertias and Natural Frequencies of Fuel Sloshing in Circular Cylindrical Tanks, by Robert W. Warner and John T. Caldwell, *NASA Tech. Note* D-856, May 1961, 35 pp.

An Experimental Investigation of the Damping of Liquid Oscillations in Cylindrical Tanks With Various Baffles, by Milton A. Silveira, David G. Stephens and H. Wayne Leonard, *NASA Tech. Note* D-715, May 1961, 28 pp.

Status of X-15 Aerodynamic-Heating Studies, by R. D. Banner and M. R. Kinsler, *ARS preprint* 1629-61, March 13–16, 1961.

Experimental Investigation of Lithium Hydride and Water Absorbers as Possible Heat-Sink Materials for Hypersonic and Re-Entry Vehicles, by R. O. Hickel, R. P. Cochran, C. R. Morse, and R. P. Dengler, *Inst. Aerospace Sci.* Rep. 61-3, Jan. 23–25, 1961.

Liquid Behavior in Zero-G Field, by T. Li, *Inst. Aerospace Sci.* Rep. 61-20, Jan. 23–25, 1961.

Viscous and Inviscid Non-Equilibrium Gas Flow, by R. J. Whalen, *Inst. Aerospace Sci.* Rep. 61-23, Jan. 23–25, 1961.

A Survey of Thermal Accommodation Coefficients, by J. P. Hartnett, *Rand Corp.*, RM-2585, March 19, 1960.

The Electrical Properties of the Air Around a Re-Entering Body, by G. F. Pippert, and S. Edelberg, *Inst. Aerospace Sci.* Rep. 61-40, Jan. 23–25, 1961.

Space Cooling Procedures, by M. Macklin, *Inst. Aerospace Sci.* Rep. 61-18, Jan. 23–25, 1961.

Excitation of Plasma Waves by Bodies Moving in an Ionized Atmosphere, by K. P. Chopra (Second Annual Meeting, Plasma Physics Div., Amer. Phys. Soc., Gatlinburg, Tenn., Nov. 2–5, 1960).

Physics of the Ionization Processes in Air, Part II: Dissociation and Recombination of Ions, an Annotated Bibliography, by G. R. Evans, *Lockheed Aircraft Corp., Missiles and Space Div.* SB-60-40, Part II, Dec. 1960.

Physics of the Ionization Processes in Air, Part III: Electron Theory, an Annotated Bibliography, by G. R. Evans, *Lockheed Aircraft Corp., Missiles and Space Div.* SB-60-40, Part III, Dec. 1960.

Physics of the Ionization Processes in Air, Part IV: (Other) Secondary Processes of Ionization, an Annotated Bibliography, by G. R. Evans, *Lockheed Aircraft Corp., Missiles and Space Div.* SB-60-40, Part IV, Dec. 1960.

Luminosity Studies of High Velocity Impact, by D. D. Keough, *Stanford Res. Inst., AF Cambridge Res Lab.* TR-60-415, Oct. 12, 1960 (ASTIA AD-247,074).

Production of Secondary Vortices in the Field of a Primary Vortex, by John R. Weske and Tom M. Rankin, *Maryland Univ., Inst. Fluid Dynamics and Appl. Math.* BN-244, April 1961, 18 pp. (AFOSR-623).

Measurement of the Dissociation Rates of Hydrogen and Deuterium, by Emmett A. Sutton, *Cornell Univ., Grad. School of Aeron. Engng.*, 1961, 50 pp.

Magnetogasdynamic Cone Flow for the Special Case of Infinite Conductivity and Aligned Fields, by Jerome J. Brainerd, *Cornell Univ., Grad. School of Aeron. Engng.*, 1961, 106 pp.

The Wave Motions of Small Amplitude in a Fully Ionized Plasma, Part III. With a Transverse Applied Magnetic Field, by S. I. Pai, *Maryland Univ., Inst. Fluid Dynamics, Tech. Note* BN 235, March 1961, 28 pp., 6 figs. (AFOSR-542).

Magnetic Field Interactions With a Moving Metal Slug, by Don Joel Wilen, *Princeton Univ., Proj. Squid,* MIT-24-R, May 1961, 16 pp.

Calculations of the One-Dimensional Non-Equilibrium Flow of Air Through a Hypersonic Nozzle (Interim Report), by Walter G. Vincenti, *Arnold Engng. Dev. Center Tech. Note* 61-65, 1961.

Charts for Air-Flow Properties in Equilibrium and Frozen Flows in Hypervelocity Nozzles, by Kenneth K. Yoshikawa and Elliott D. Katzen, *NASA Tech. Note* D-693, April 1961, 70 pp.

Experimental Heat Transfer and Pressure Drop of Liquid Hydrogen Flowing Through a Heated Tube, by R. C. Hendricks, R. W. Graham, Y. Y. Hsu and R. Friedman, *NASA Tech. Note* D-765, May 1961, 62 pp.

Note on Three-Dimensional Free-Mixing, by Martin H. Bloom, *J. Aerospace Sci.*, vol. 28, May 1961, pp. 430–431.

Flight Mechanics

Change of Satellite Orbit Plane by Aerodynamic Maneuvering, by H. S. London, *Inst. Aerospace Sci.* Rep. 61-5, Jan. 23–25, 1961.

Trajectory of a Vehicle Departing From a Circular Orbit, by R. B. Bowersox and D. Carter, *Lockheed Aircraft Corp., Missiles and Space Div.* LMSD-703049, July 1960.

Angular and Linear Deviation of Fin-Stabilized Rockets During the Burning Period, by J. V. Perry, *North Carolina State College Agric. Engng.*, March 3, 1961.

A Method for Determining Approximate Propulsion Cutoff Conditions for Ballistic Interplanetary Trajectories, by L. N. Rowell, *Rand. Corp.*, RM-2671, Dec. 29, 1960.

Measurements of Sphere Drag From Hypersonic Continuum to Free-Molecule Flow, by D. J. Masson, D. N. Morris and D. E. Bloxsom, *Rand. Corp.* RM-2678, Nov. 3, 1960.

Numerical Approximation to Equatorial Orbits, by J. L. Brenner, *Stanford Res. Inst.* SRI-3165-5(T), Dec. 1960.

Analog Computer Solution for the Equations of Powered Motion in Space, by R. C. Wingerson, *Wright Air Dev. Div., Propulsion Lab.* WADC TN 59-325, March 1960.

Application of Inequality Constraints to Variational Problems of Lifting Re-Entry, by E. S. Levinsky, *Inst. Aerospace Sci. Rep.* 61-21, Jan. 23–25, 1961.

On the PLK Method and the Supersonic Blunt Body Problem, by R. Vaglio-Laurin, *Inst. Aerospace Sci. Rep.* 61-22, Jan. 23–25, 1961.

Experimental Investigation of Stage Separation Aerodynamics, by Tobert A. Wasko, *NASA Tech. Note* D-868, May 1961, 24 pp.

Force and Pressure Tests of Two Elliptic Ogive Body Shapes at Mach Numbers 5, 6 and 8, by Jack L. Burk, *Arnold Engng. Dev. Center Tech. Note* 61-49, April 1961, 41 pp.

Predicted Shock Envelopes About Two Types of Vehicles at Large Angles of Attack, by George E. Kaattari, *NASA Tech. Note* D-860, April 1961, 34 pp.

A Semigraphical Method of Applying Impact Theory to an Arbitrary Body to Obtain the Hypersonic Aerodynamic Characteristics at Angle of Attack and Side-Slip, by Charlie M. Jackson Jr., *NASA*

ENGINEERS & SCIENTISTS

in the fields of space vehicle power and propulsion

The Propulsion and Power Systems Department of the Aerospace Vehicles Laboratory has several unusually interesting openings for engineers and scientists who are interested in the fields of space vehicle power and propulsion. The openings are at all levels of experience – from recent graduates to the senior staff level. Most of the positions will involve design and analysis of power and propulsion systems for satellite and space probe application. Specifically, some of the areas of specialization are:

1 SPACE POWER SYSTEMS
The positions will involve analysis and development of such energy sources as: photo voltaic, thermionic, thermoelectric, battery and advanced energy storage systems.

2 SPACE PROPULSION SYSTEMS
The positions will involve the preliminary and conceptual design and comparative analysis of all types of chemical and electric propulsion systems.

3 PROGRAM MANAGEMENT
The positions will be associated with the development of solid and liquid propellent rocket engines. Advanced degrees are preferred and considerable experience in the field will be required.

If you are interested and believe that you can contribute, please mail your resume to:

Robert A. Martin,
Supervisor of Employment
HUGHES
11940 W. Jefferson Blvd.
Culver City, California

We promise you a reply within one week.
An equal opportunity employer.

Creating a new world with Electronics

HUGHES

HUGHES AIRCRAFT COMPANY
AEROSPACE DIVISIONS

Tech. Note D-795, May 1961, 18 pp.

Effect of Free-Stream Vorticity on the Behavior of Viscous Boundary Layer on Blunt Body, by Li Ting Yi, *Rensselaer Polytech. Inst., Dept. Aeron. Engng.*, TRAE 6103, Feb. 1961, 27 pp. (AFOSR 425).

Regime of Frozen Boundary Layers in Stagnation Region of Blunt Re-Entry Bodies, by Norman T. Grier and Norman Sands, *NASA Tech. Note* D-865, May 1961, 37 pp.

Effects of Mass-Loading Variations and Applied Moments on Motion and Control of a Manned Rotating Space Vehicle, by William D. Grantham, *NASA Tech. Note* D-803, May 1961, 40 pp.

Experimental Evaluation of the Deceleration of Aluminum Cylinders Rotating in a Magnetic Field and Comments on Magnetic Damping of a Flywheel Control, by Donald G. Eide, *NASA Tech. Note* D-749, April 1961, 35 pp.

Aerodynamic Characteristics in Pitch and Sideslip of a 1/15-Scale Model of the Scout Vehicle at a Mach Number of 2.01, by Ross B. Robinson, *NASA Tech. Note* D-793, 37 pp.

Proceedings (Advances in the Astronautical Sciences, U. S.) American Astronautical Society, Western National Meeting, Plenum Press, New York, 1960, 355 pp.

An Analytical Method for Determining the Orbital Characteristics of a Nonlifting Body Which Passes Through the Lower Atmosphere of a Planet, by Geza S. Gedeon, pp. 325–337.

An Estimate of the Maximum Deviation for a Given Trajectory, by E. A. Barbashin, *Automation and Remote Control*, vol. 21, no. 10, Oct. 1960, pp. 945–952.

American Astronautical Society, Western National Meeting, Proceedings (Advances in the Astronautical Sciences, U. S.), Plenum Press, New York, 1960, 355 pp.

Dynamic Response Surfaces for Nonlinear Equations of Rocket-Powered Flight, by Robert E. Ross, pp. 116–137.

Round-Trip Trajectories for Mars Observation, by Paul G. Johnson and Roger L. Smith, pp. 181–205.

The Influence of Launch Conditions on the Friendly Rendezvous of Astro-Vehicles, by Robert S. Swanson and Norman V. Petersen, pp. 218–236.

Subsonic Longitudinal Aerodynamic Characteristics of Disks With Elliptic Cross Sections and Thickness-Diameter Ratio From 01225 to 0.425, by Fred A. Demele and Jack J. Brownson, *NASA Tech. Note* D-788, April 1961, 25 pp.

Low-Speed Static Stability Characteristics of Two Configurations Suitable for Lifting Reentry From Satellite Orbit, by John W. Paulson, *NASA Mem.* 10-22-58L, Nov. 1958, 17 pp. (declassified by authority of *NASA TPA* No. 45, May 11, 1961).

Static Longitudinal and Lateral Stability Parameters of Three Flared-Skirt Two-Stage Missile Configurations at a Mach Number of 6.86, by Jim A. Penland and C. Maria Carroll, *NACA Res. Mem.*, L57D15, June 1957, 48 pp. (declassified by authority of *NASA TPA* No. 45, May 11, 1961).

Static Longitudinal and Lateral Stability Characteristics of a Right Triangular Pyramidal Lifting Reentry Configuration at Transonic Speeds, by Walter B. Olstad, John P. Mugler Jr., and Maurice S. Cahn, *NASA Tech. Note* D-655, April 1961, 62 pp.

Analog Simulation of a Pilot-Controlled Rendezvous, by Roy F. Brissenden, Bert B. Burton, Edwin C. Foudriat and James B. Whitten, *NASA Tech. Note* D-747, April 1961, 51 pp.

Angular Motion of the Spin Axis of the Tiros I Meteorological Satellite Due to Magnetic and Gravitational Torques, by W. R. Bandeen and W. P. Manger, *NASA Tech. Note* D-571, April 1961, 6 pp.

Accuracy of Measuring Ballistic Missile Trajectories, by Frank Cooper, ARS JOURNAL, vol. 31, no. 4, April 1961, pp. 523–526.

Escape from Planetary Gravitational Fields by Use of Solar Sails, by Norman Sands, ARS JOURNAL, vol. 31, no. 4, April 1961, pp. 527–531.

Aeronautics and Astronautics (Proceedings Durand Centennial Conference, Stanford Univ., Aug. 5–8, 1959), Nicholas John Hoff and Walter Guido Vicenti (eds.), Pergamon Press, New York, 1960, 460 pp.

On the Motion and Ablation of Meteoric Bodies, by Julian Allen, pp. 378–416, 40 refs.

Ballistic Missile and Space Technology, vol. 3: Guidance Navigation, Tracking and Space Physics, Symposium on Ballistic Missile and Space Technology, Los Angeles, Aug. 1960), Donald P. LeGalley, (ed)., Academic Press, New York, 1960, 450 pp.

Analytical Perturbation Expressions for the Restricted Three-Body Problem, by Paul a Penzo, pp. 203–229.

Gravitational Librations of a Satellite and the Influence on Control System Design, by Robert R. Wolfe and Bernard Arrow, pp. 231–258.

The Motion of an Equatorial Satellite of an Oblate Planet, by J. L. Brenner, pp. 259–289.

Interplanetary Trajectory Simulation, by D. S. Merrilees and J. C. Walker, pp. 291–315.

Some Comparison of Sloshing Behavior in Cylindrical Tanks With Flat and Conical Bottoms, by H. Norman Abramson and Guido E. Ransleben Jr., ARS JOURNAL vol. 31, no. 4, April 1961, pp. 542–544.

Wall Pressure Distributions During Sloshing in Rigid Tanks, by H. Norman Abramson and Guido E. Ransleben Jr., ARS JOURNAL, vol. 31, no. 4, April 1961, pp. 545–547.

Optimal Powered Arcs in an Inverse Square Law Field, by D. F. Lawden, ARS JOURNAL, vol. 31, no. 4, April 1961, pp. 566–568.

A Study of Cotangential, Elliptical Transfer Orbits in Space Flight, by William Li-Shu Wen, *J. Aerospace Sci.*, vol. 28, no. 5, May 1961, pp. 411–417.

Effect of an Oblate Rotating Atmosphere on the Orientation of a Satellite Orbit, by G. E. Cook, *Royal Soc., London, Proc. (Series A. Math. Phys. Sci.)* vol. 261, no. 1305, April 1961, pp. 246–258.

Transit Angle for Low-Thrust Spacecraft, by Frank M. Perkins, *J. Aerospace Sci.*, vol. 28, May 1961, pp. 419–420.

A Note on the Motion of a Spinning Rocket With Eccentric Thrust, by A. G. Bennett, *J. Aerospace Sci.*, vol. 28, May 1961, pp. 426–427.

An Approach to Problem of Optimum Rocket Trajectories, by Samuel E. Moskowitz and Lu Ting, ARS JOURNAL, vol. 31, no. 4, April 1961, pp. 551–553.

Vehicle Design, Testing and Performance

Vanguard Satellite Separation Mechanisms, by Robert C. Baumann, *NASA Tech. Note* D-497, April 1961, 20 pp.

Calculation of Wind Compensation for Launching of Unguided Rockets, by Robert L. James Jr. and Ronald J. Harris, *NASA Tech. Note* D-645, April 1961, 52 pp.

Spaceflight Technology, (Commonwealth Spaceflight Symposium, 1st, London, 1959, Kenneth W. Gatland (ed.), Academic Press, N. Y., 1960, 365 pp.

Britain's Plans in Interplanetary Exploration, by John E. Allen, pp. 1–48, 93 refs.

The Economics of Spaceflight, by Derek Wragge Morley, pp. 49–68.

Some Remarks on Woomera as a Space Vehicle Tracking and Launching Station, by H. J. Higgs, pp. 107–112.

General Review of a British Spaceflight Programme Based on Blue Streak, by G. K. C. Pardoe, pp. 113–138.

Astronautics at Armstrong Whitworth's, by H. R. Watson, pp. 155–171.

Recovery of Earth Satellites, by D. E. Bailey, pp. 205–221.

Cabin Conditioning Equipment for a Manned Satellite, by George Beardshall and Peter W. Fitt, pp. 239–257.

Minimum Propulsion for Soft Moon-Landing of Instruments, by D. S. Garton, pp. 323–349.

Ballistic Missile and Space Technology, vol. 4, Reentry and Vehicle Design, Donald P. Le Galley (ed.), Symposium on Ballistic Missile and Space Technology, Los Angeles, Aug. 1960, Academic Press, N. Y., 1960, 422 pp.

Performance Considerations for a VTOL Boost Vehicle Using Turbo-Ramjet Engines, by W. R. Woodis, pp. 205–254.

Liquid Hydrogen Storage Parameters for a Lunar Voyage, by C. C. Love Jr., pp. 283–314.

Emphasis on Survival in the Design of Interplanetary Vehicles, by R. W. Connor and E. A. Smith, pp. 315–337.

Sea Launch of Large Solid-Propellant Rocket Vehicles, by J. E. Draim and C. E. Stalzer, pp. 339–375.

Economics of Booster Vehicle Design, by D. H. Mitchell, pp. 377–403.

Missile Systems Cost, by Herbert M. Reichert, pp. 405–422.

Optimum Staging Technique to Maximize Payload Total Energy, by Edgar R. Cobb, ARS JOURNAL, vol. 31, no. 3, March 1961, pp. 342–344.

Multistage Rocket Optimization, by Robert V. Ragsac and Paul L. Patterson, ARS JOURNAL, vol. 31, no. 3, March 1961, pp. 450–451.

Preliminary Calculation and Layout Method for Single and Multistage Ballistic and Space Rockets, by R. Schmidt, *Army Ballistic Missile Agency, Redstone Arsenal*, RA-TR-1-61, Feb. 10, 1961.

Nuclear Rocket Stages Increase Saturn's Payload Capability, by W. Y. Jordan, D. R. Saxton and P. G. Thomas, *Inst. Aerospace Sci. Rep.* 61-64, Jan. 23–25, 1961.

Temperature Control of Satellite and Space Vehicles: an Annotated Bibliography, by R. C. Gex, *Lockheed Aircraft Corp., Missiles and Space Div.* SB-61-5, Feb. 1961.

A Study of Manned Nuclear-Rocket Missions to Mars, by S. C. Himmel, J. F. Dugan, R. J. Weber and R. W. Luidens, *Inst. Aerospace Sci.* Rep. 61-49, Jan. 23–25, 1961.

Zero-G Devices and Weightlessness Simulator, by Siegfried J. Gerathewohl, *National Res. Council, Publ.* 781, Feb. 1960, 143 pp.

Symposium on Nondestructive Testing in the Missile Industry, San Francisco, Oct. 12, 1959 (ASTM Special Tech. Publ. no. 278), Philadelphia, ASTM, 1960, 71 pp.

Mobile Field Testing of Missiles and Aircraft, by A. Barath and D. J. Hagemaier, pp. 12–19.

Proceedings (Advances in the Astronautical Sciences, U. S.), American Astronautical Society, Western National Meeting, Plenum Press, New York, 1960, 355 pp.

Panel Discussion: Probing Space, by Homer E. Newell Jr., Donald D. Flickinger, A. G. Wilson and J. G. Beerer, pp. 5–14.

Scientific Significance of Deep Space Exploration, by E. T. Benedikt, pp. 98–115.

Design Optimization of Thermal Radiators for Space Vehicles, by Robert A. Cornog, pp. 141–148.

A Systematic Approach to a Matrix of Space Research Vehicles, by O. W. Nicks, pp. 206–217, 19 refs.

Effect of Re-Entry Technique on the Design of a Space Vehicle, by J. Stalony-Dobrzanski, pp. 237–247.

A Design Study of the Inflated Sphere Landing Vehicle, Including the Landing Performance and the Effects of Deviations From Design Conditions, by E. Dale Martin, *NASA Tech. Note* D-692, April 1961, 82 pp.

A Preliminary Study of the Solar-Probe Mission, by Duane W. Dugan, *NASA Tech. Note* D-783, April 1961, 58 pp.

Balancing Vanguard Satellites, by A. Simkovich and Robert C. Baumann, *NASA Tech. Note* D-498, April 1961, 23 pp.

Vanguard Satellite Spin-Reduction Mechanism, by Robert C. Baumann, *NASA Tech. Note* D-496, April 1961, 20 pp.

Aeronautica and Astronautics, Proceedings (Durand Centennial Conference, Stanford Univ., Aug. 5–8, 1959) Nicholas John Hoff and Walter Guido Vincenti (eds.), Pergamon Press, New York, 1960, 460 pp. (AFOSR TR 59-108).

The Advent of Astronautics, by W. B. Klemperer, pp. 435–460.

Ballistic Missile and Space Technology, vol. 1: Bioastronautics and Electronics and Invited Addresses (Symposium on Ballistic Missile and Space Technology, 5th, Los Angeles, Aug. 1960) Donald P. LeGalley (ed.), Academic Press, New York, 1960, 494 pp.

The Importance of Management in the Ballistic Missile and Space Vehicle Programs, by Bernard A. Schriever, pp. 11–16.

The Space Challenge, by T. Keith Glennan, pp. 17–24.

A Summary of U. S. Achievements in Space, by John H. Rubel, pp. 25–36.

The Life and Times of the Crash Program, by Simon Ramo, pp. 37–48.

Ballistic Missile and Space Technology, vol. 3: Guidance Navigation, Tracking and Space Physics (Symposium on Ballistic Missile and Space Technology, Los Angeles, Aug. 1960) Donald P. LeGalley (ed.), Academic Press, New York, 1960, 450 pp.

The Effect of Outage on Missile Performance, by D. G. Stechert, pp. 103–123.

Regions Accessible to a Ballistic Weapon, by F. L. Beckner, pp. 317–363.

Data Capsule Ejection Through a Re-Entry Body Wake, by Leonard C. MacAllister and Anthony M. Smith, *Aero/Space Engng.*, vol. 20, no. 5, May 1961, pp. 8–9, 66–69.

Nuclear Rocket Stages Increase SATURN's Payload Capability, by Willis Y. Jordan Jr., Donald R. Saxton and Paul G. Thomas, *Aero/Space Engng.*, vol. 20, no. 5, May 1961, pp. 14–15, 38–43.

Aerospace Nuclear Power Safety Considerations, by Joseph A. Connor Jr., *Aero/Space Engng.*, vol. 20, no. 5, May 1961, pp. 26–27, 58–60.

Radiation Shielding of Lunar Spacecraft, by T. G. Barnes, E. M. Finkelman and A. L. Barazotti, *Astronaut. Sci. Rev.*, vol. 3, no. 1, Jan.-March 1961, pp. 11–18.

Guidance and Control

Operational Standards for Radio Command Control, Inter-range Instrumentation Group, Tele-Communications Working Group, Radio Command Control Sub-Group, *Interrange Instrumentation Group, Recommendation* 104–59, 1959, 9 pp.

Input-Output Cross-Correlation Functions for Some Memory-Type Nonlinear Systems With Gaussian Inputs, by Harold R. Leland, *Amer. Inst. Elect. Engrs. Paper* 60-115, 1960.

Time-Variable Dynamics of Human Operator Systems, by Thomas B. Sheridan, *Mass. Inst. Tech., Dynamic Analysis and Control Lab.*, DACL-R-124, March 1960, 113 pp., 37 refs.

An Analytical Approach to the Design of an Automatic Discontinuous Control System, by Lawrence W. Taylor Jr. and John W. Smith, *NASA Tech. Note* D-630, April 1961, 59 pp.

Proceedings, The Self Adaptive Flight Control System Symposium, *Wright Air Dev. Center*, March 1961, 462 pp. (*ASTIA AD* 209,389)

ARDC Plans and Programs, by P. C. Gregory, pp. 8–10.

USASRDL Flight Control Programs, by J. P. Gilmore, pp. 11–15.

The Systems Dynamics Research Airplane, by E. C. Foudriat and S. A. Sjoberg, pp. 16–29.

NASA Adaptive Control System Program, by W. C. Triplett, pp. 30–32.

On an Adaptive Autopilot Using a Nonlinear Feedback Control System, by J. D. McLean, pp. 33–44.

Supervisory Control System, by R. L. Cosgriff, pp. 45–54.

MIT Presentation, by H. P. Whitaker, pp. 58–79.

Sperry Adaptive Flight Control System, by S. S. Osder, pp. 81–122.

Honeywell's History and Philosophy in the Adaptive Control Field, by O. H. Schuck, pp. 123–147.

A Technique for Analyzing an Adaptive Flight Control System Containing a Bi-Stable Element, by L. T. Prince, pp. 148–170.

Discussion of the Honeywell Adaptive Flight Control System by D. L. Mellon, pp. 171–180.

A Review of Optimizing Computer Control, by I. Lefkowitz and D. P. Eckman, pp. 181–197.

Recent Adaptive Control Work at the General Electric Company, by M. F. Marx, pp. 201–215.

Dodco Research in Optimum Adaptive Flight Control, by R. L. Barron and Anthony J. Pennington, pp. 216–250.

Convair Analysis of a Linear, Self Adaptive, Stability Augmentation System, by M. Dandois, pp. 254–337.

UCLA Program in Basic Research in Adaptive Control Theory, by M. Margolis, pp. 338–342.

Cornell Aeronautical Laboratory Presentation, by P. A. Reynolds, pp. 343–347.

The Aeronutronic Self-Optimizing Automatic Control System, by G. W. Anderson, R. N. Buland and G. R. Cooper, pp. 349–406.

Adaptive Control Systems Philosophy, by Y. T. L., pp. 407–431.

Trajectory Control in Rendezvous Problems Using Proportional Navigation, by Luigi S. Cicolani, *NASA Tech. Note* D-772, April 1961, 44 pp.

The Effect of Lift on Entry Corridor Depth and Guidance Requirements for the Return Lunar Flight, by Thomas J. Wong and Robert E. Slye, *NASA Tech. Rep.* R-80, 1961, 17 pp.

Spaceflight Technology, Commonwealth Spaceflight Symposium, 1st, London, 1969, Kenneth W. Gatland (ed.), Academic Press, N. Y., 1960, 365 pp.

Space Navigation, by P. R. Wyke, pp. 313–322.

Ballistic Missile and Space Technology, vol. IV. Reentry and Vehicle Design,

CHANGE-OF-ADDRESS NOTICE

In the event of a change of address, it is necessary to include both your old and new addresses, as well as your membership number and coding, when notifying ARS headquarters, in order to insure prompt service. If you are moving or have moved, send the following form to Membership Dept., American Rocket Society, 500 Fifth Ave., New York 36, N. Y.:

Name_____

Membership Card No _____ Coding _____

Old Address_____

_____

New Address_____

_____

Donald P. LeGalley (ed.,) Symposium on Ballistic Missile and Space Technology, Los Angeles, Aug. 1960, Academic Press, N. Y., 1960, 422 pp.

Propulsive Control of Atmospheric Entry Lifting Trajectories, by Murray Dryer, pp. 113–134.

Alignment of an Internal Autonavigator, by L. R. McMurray, ARS JOURNAL, vol. 31, no. 3, March 1961, pp. 356–360.

Celestial Rate Sensing, by Hans K. Karrenberg and Robert E. Robertson, ARS JOURNAL, vol. 31, no. 3, March 1961, pp. 440–441.

On the Motion of Gyroscopic Devices Under the Influence of Random Forces, by Ia. N. Roitenberg, *Appl. Math. Mech.* (*PMM*), vol. 24, no. 3, 1960, pp. 677–690.

Stability of a Gyroscope Having a Vertical Axis of the Outer Ring with Dry Friction in the Gimbal Axes Taken into Account, by V. V. Krementulo, *Appl. Math. Mech.* (*PMM*), vol. 24, no. 3, 1960, pp. 843–855.

On the Stability of Motion of a Heavy Gyroscope on Gimbals, by A. M. Tabarovskii, *Appl. Math. Mech.* (*PMM*), vol. 24, no. 3, 1960, pp. 856–860.

Automatic Opening Mode Optimization of a Class of Systems with Respect to Statistical Performance Criteria, by S. A. Doganovskii, *Automation and Remote Control*, vol. 21, no. 8, Aug. 1960, pp. 779–784.

Two Types of Optimum-Extremal Systems, by L. N. Fitsner, *Automation and Remote Control*, vol. 21, no. 8, Aug. 1960, pp. 786–790.

On a Problem of Optimum Control, by I. A. Litovchenko, *Automation and Remote Control*, vol. 21, no. 8, Aug. 1960, pp. 791–798.

On the Stability of the Periodic Motion of Piecewise Linear Automatic Control Systems, by K. K. Belya, *Automation and Remote Control*, vol. 21, no. 8, Aug. 1960, pp. 799–308.

Reduced Equivalent Amplification Factor of a Nonlinear Element in the Presence of Noise, by B. D. Kislov, *Automation and Remote Control*, vol. 21, no. 8, Aug. 1960, pp. 804–809.

Servomechanism-Compensation by Using Discrete Calculating Devices, by L. I. Volgin and L. I. Smolyar, *Automation and Remote Control*, vol. 21, no. 8, Aug. 1960, pp. 816–820.

Remote Control of Several Objects Located at Different Places, by V. A. Il'in, *Automation and Remote Control*, vol. 21, no. 8, Aug. 1960, pp. 826–831.

Determination of Parameters of Combined Linear Control Systems, by V. Ya. Rotach, *Automation and Remote Control*, vol. 21, no. 8, Aug. 1960, pp. 858–862.

Hydraulic Servomotor Motion in Automatic Control Systems with a Jet Amplifier, by V. I. Gol'traf, *Automation and Remote Control.*, vol. 21, no. 8, Aug. 1960, pp. 863–866.

Continuous Extremum Control Systems in the Presence of Random Noise, by A. A. Pervozvanskii, *Automation and Remote Control*, vol. 21, no. 7, July 1960, pp. 673–677.

Investigation of a Servosystem with an Electromagnetic Induction Clutch which Operates with Low Null Currents, by P. F. Klubnikin, *Automation and Remote Control*, vol. 21, no. 7, July 1960, pp. 678–684.

The Maximum Dynamic Characteristic Values of Servomechanism Components of Servosystems, by G. A. Nadzhafova, *Automation and Remote Control*, vol. 21, no. 7, July 1960, pp. 685–690.

Calculation of Static Characteristic Values of "Nozzle-Baffle" Elements, by E. A. Andreeva, *Automation and Remote Control*, vol. 21, no. 7, July 1960, pp. 691–700.

Dynamic Characteristics of a "Jet Amplifier-Servomechanism" System, by B. D. Kosharskii, *Automation and Remote Control*, vol. 21, no. 7, July 1960, pp. 701–708.

Autocompensation of Errors in Gyros and Accelerometers, by J. M. Slater, *Control Engng.*, vol. 8, no. 5, May 1961, pp. 121–122.

Statistical Design of Linear Discrete-Data Control Systems Via the Modified Z-Transform Method, by Julius T. Tou, *Franklin Inst. J.*, vol. 271, no. 4, April 1961, pp. 249–262.

Jump Resonance in a Third Order Nonlinear Control System, by Wellingron W. Koepsel, *Franklin Inst. J.*, vol. 271, no. 4, April 1961, pp. 292–298.

An Analysis of Errors and Requirements of an Optical Guidance Technique for Approaches to Atmospheric Entry With Interplanetary Vehicles, by David P. Harry, III and Alan L. Friedlander, *NASA Tech. Rep.* R-102, 1961, 131 pp.

Design and Flight Tests of an Adaptive Control System Employing Normal-Acceleration Command, by Walter E. McNeill, John D. McLean, Daniel M. Hegarty and Donovan R. Heinle, *NASA Tech. Note* D-858, April 1961, 39 pp.

Transmission Device for Reversibility of Rotation With Extremely Fast Action, by J. Boehm, A. L. Herrmann and J. F. Blanche, *NASA Tech. Note* D-603, May 1961, 28 pp.

The Optimum Response of Full Third Order Systems With Contactor Control, by I. Flugge-Lotz and H. A. Titus Jr., *Stanford Univ. Div. Engng. Mechanics, Tech. Rep.* 129, March 1961, 34 pp. (AFOSR 442).

A Vector Method for Calculating One Class of Control Systems, by S. M. Levin and L. G. Manusevich, *Automation and Remote Control*, vol. 21, no. 10, Oct. 1960, pp. 962–970.

Controlling a Servodrive Using One Null Indicator Which Performs the Functions of Two Null Indicators, by V. D. Vershinin, *Automation and Remote Control*, vol. 21, no. 10, Oct. 1960, pp. 979–983.

Synthesis of Circuits Whose Operation is Described by Boolean Time Functions, by D. A. Pospelov, *Automation and Remote Control*, vol. 21, no. 10, Oct. 1960, pp. 989–999.

An Optimal Strategy for a Saturating Sampled-Data System, by C. A. Desoer and J. Wing, *Inst. Radio Engrs., Trans. Automatic Control*, vol. AC-6, no. 1, Feb. 1961, pp. 5–15.

Proceedings (Advances in the Astronautical Sciences, U. S.) American Astronautical Society, Western National Meeting, Plenum Press, New York, 1960, 355 pp.

Fuel Requirements for Crude Interplanetary Guidance, by John V. Breakwell, pp. 53–65.

Guidance Requirements for Interplanetary Flight, by Friend H. Kierstead Jr., pp. 66–81.

Satellite Orbit Control System, by Mary C. Fitz-Gibbon, pp. 82–97.

Time-Optimal Control of Hither-Order Systems, by F. B. Smith Jr., *Inst. Radio Engrs., Trans. Automatic Control*, vol. AC-6, no. 1, Feb. 1961, pp. 16–21.

Control System Performance Measures: Past, Present, and Future, by W. C. Schultz and V. C. Rideout, *Inst. Radio Engrs., Trans. Automatic Control*, vol. AC-6, no. 1, Feb. 1961, pp. 22–34.

A Simulator Study of a Two-Parameter Adaptive System, by R. J. McGrath and V. C. Rideout, *Inst. Radio Engrs., Trans. Automatic Control*, vol. AC-6, no. 1, Feb. 1961, pp. 35–42.

Optimum Prediction With a Mean Weighted Square-Error Criterion, by Clarence C. Glover, *Inst. Radio Engrs., Trans. Automatic Control*, vol. AC-6, no. 1, Feb. 1961, pp. 43–48.

Design Aspects of Attitude Control Systems, by M. F. Marx, *Inst. Radio Engrs., Trans. Automatic Control*, vol. AC-6, no. 1, Feb. 1961, pp. 67–72.

A Study to Determine the Feasibility of a Self-Optimizing Automatic Flight Control System (*Ford Motor Co., Aeron. Div.*) *Wright Air Dev. Center, Tech. Rep.* 60-201, June 1960 (ASTIA AD 240,992).

A Method for Controlling the Attitude of a Spin-Stabilized Satellite, by L. H. Grasshoff, *ARS preprint* 1501-60, 1960, 5 pp.

A Reaction Spheres Attitude Control System, by Ralph D. Ormsby and Mahlan C. Smith, *ARS preprint* 1500-60, 1960, 20 pp.

Radio Command Control Equipment Catalog, vols. 1 and 2, *Inter-Range Instrumentation Group, White Sands Proving Ground, N. M.*, No. 105-59, Nov. 1959, 150, 65 pp.

Ballistic Missile and Space Technology, vol. 1: Bioastronautics and Electronics and Invited Addresses (Symposium on Ballistic Missile and Space Technology, 5th, Los Angeles, Aug. 1960) Donald P. Le Galley (ed.), Academic Press, New York, 1960, 494 pp.

Earth Viewer for Exospheric Navigation Trainer, by Allan L. Bernstein and Joseph H. Gifford, pp. 77–90.

A Self-Adaptive Control System for a Large Elastic Missile, by F. S. Nyland, pp. 187–218.

Design Analysis Considerations for Space Vehicle Attitude Control, by Walter O. Darby, pp. 219–238.

The Development of a Rote Diagnostic Process for the Atlas Guidance Computer System, by Howard R. Nonken, pp. 313–327.

Investigation of Digital Computer Reliability Utilizing Intermittent Operation on Long Missions, by G. C. Randa, pp. 329–339.

Analog Simulation of Digital Control Loops, by Arthur Freilich, pp. 457–469.

Ballistic Missile and Space Technology, vol. 3: Guidance Navigation, Tracking and Space Physics (Symposium on Ballistic Missile and Space Technology, Los Angeles, Aug. 1960) Donald P. Le Galley (ed.), Academic Press, New York, 1960, 450 pp.

Interplanetary Injection Guidance, by C. G. Sauer Jr., pp. 55–71.

The Problem of Satellite Navigation by Use of a Doppler Receiver, by Otto Spies, pp. 73–101.

Analog Simulation of Radio Guidance and Space Communication Systems, by J. P. Frazier and J. M. Lambert, pp. 169–199.

A Comparison of Fixed and Variable Time of Arrival Navigation for Interplanetary Flight, by Richard H. Battin, pp. 3–31.

Gyro Damping—Its Part in Platform Design, by E. M. Fischel, *Aero/Space*

Engng., vol. 20, no. 5, May 1961, pp. 16–17, 75–82.

Error Analysis Considerations for a Satellite Rendezvous, by W. M. Duke, E. A. Goldberg and I. Pfeffer, ARS JOURNAL, vol. 31, no. 4, April 1961, pp. 505–513.

Optimum Steering Program for the Entry of a Multistage Vehicle Into a Circular Orbit, by Stephen Jurovics, ARS JOURNAL, vol. 31, no. 4, April 1961, pp. 518–523.

Stratoscope II Telemetry and Command, by Alan B. Wissinger, ASTRONAUTICS, vol. 6, no. 5, May 1961, pp. 38–41, 98, 102, 104.

Analyze Nonlinear Controls With Saturation Functions, by S. Manabe, *Control Engng.*, vol. 8, no. 2, Feb. 1961, pp. 83–86.

Two vs. Three-Gyro Guidance Platforms—I: How they Compare, by E. M. Fischel, *Control Engng.*, vol. 8, no. 2, Feb. 1961, pp. 92–96.

The Effect of a Voltage With Rapidly Varying Frequency on an Intertial System, by I. S. Gonorovskii, *Radio Engng. Electronics* (Trans. of Radiotekhnika i Elektronika) vol. 5, no. 6, 1960, pp. 29–44.

The Possible Use of Atomic Nuclei as a Direction Reference in Inertial Space, by W. H. Culver, *Rand Corp.*, RM-2592, Dec. 13, 1960.

Instrumentation and Communications

An Investigation of the Use of Semiconductors as Detectors of Unclear Radiation, by Edward Weber Ivy, *Texas Agricultural Mech. College*, Aug. 1960, 61 pp., 29 refs., (*ASTIA AD* 244,336, Thesis, M.S.)

Hot-Wire Calorimetry: Theory and Application to Ion Rocket Research, by Lionel V. Baldwin and Virgil A. Sandborn, *NASA Tech. Rep.* R-98, 1961, 85 pp.

A Narrow-Band Spectral Analyzer for Random Waveforms, by D. S. Whitehead, *Gt. Brit. Aeron. Res. Council Tech. Rep.* 22,120, Aug. 1960, 14 pp.

Proceedings of the 1st All-IRIG Symposium, *Inter - Range Instrumentation Group, White Sands Proving Ground*, N. M., Oct. 1956, pp. (*IRIG Doc.* 104–56).

Evolution of Range Instrumentation, by Joachim W. Muehlner, pp. 22–34.

On Data Reduction and Computing, pp. 35–54.

State of the Art and Trends of Electronic Trajectory Measurement Systems, pp. 56–66.

Status of the Frequency Coordination Problem, pp. 69–77.

Report of the Meteorological Working Group, pp. 78–88.

Report of the Optical Systems Working Group, pp. 89–96.

Report of the Photographic Processing Working Group, pp. 97–113.

Report of the Radio Propagation Working Group, pp. 115–126.

Presentation by the Telecommunications Working Group, pp. 127–133.

Radio Telemetry for Guided Missiles, pp. 135–165.

Proceedings of the Second All-IRIG Symposium, Monterey, Calif., *Inter-Range Instrumentation Group, White Sands Proving Ground, N. M.*, Oct. 1958, 156 pp. (*IRIG Doc.* 107–58).

Earth Satellites and their Scientific Implications, by J. P. Hagen, pp. 13–20.

Long-Range Telemetry Data Acquisition, by E. H. Broome, pp. 21–37.

Target Acquisition for Space Tracking, by E. T. Hatcher, pp. 38–47.

Real Time Data Processing for the Space Age, by H. N. Morris, pp. 48–54.

Satellite Tracking, by L. A. Kurtz, pp. 55–57.

The Case for a Staging Station, by E. Levin, p. 58.

Trajectory Measurements in the Space Age, by F. Stoklas, pp. 62–83.

Optical Range Instrumentation in the Space Age, by J. A. Clemente, pp. 84–87.

Meteorology in the Space Age, by H. F. Tompson, pp. 88–91.

From Mouse to Moon, by E. F. Wiebke, pp. 92–98.

Electromagnetic Propagation in the Space Age, by Fred Hanson, pp. 99–109.

Coordinates in Space, by C. F. Gilchrist, pp. 110–124.

Effect of Deflection of the Vertical on the Location and Orientation of Instrumentation, by N. T. Halmark, pp. 125–130.

Telemetry in the Space Age, by R. T. Merrian, pp. 131–139.

Standard Frequency Transmission and Time Signals, by W. D. George, pp. 140–146.

Radio Command Control in the Space Age, by G. L. Meredith, pp. 147–151.

Instrumentation in the Space Age, by DR and CWG, p. 152.

Papers Presented at the Data Handling Meeting, AGARD Avionics Panel, Aachen, Germany, 1959, *North Atlantic Treaty Organization, Adv. Group for Aeron. Res. and Dev., AGARDograph* no. 43, Sept. 1959, 600 pp.

Minitrack, by Harry E. Carpenter Jr. and Jeremiah J. Madden, pp. 3–28.

Space Track, by G. R. Miczaika, pp. 29–34.

Some Aspects of Data Acquisition and Handling in 'Able' Space Probes, by John E. Taber, pp. 35–44.

Tracking and Data Handling for the Pioneer III and Pioneer IV Firings, by Manfred Eimer and Robertson Stevens, pp. 45–68.

The Venus Radar Experiment, by Robert Price, pp. 69–88.

An Experimental Automatic Radar Target Detection and Digital Coded Plot Extarction and Transmission System, by G. L. F. Winckley, pp. 95–110.

The Coordinated Synthetic Presentation of Radar Data and Flight Progress Information, by C. D. Colchester, pp. 171–182.

Centralized Recording and Computation of Propulsion System Research Data, by Robert E. Tozier, pp. 331–354.

Some Developments in Techniques Related to Data Handling, by L. Airey, pp. 355–372.

An Equipment for Automatically Processing Time-Multiplexed Telemetry Data, by J. H. Russell, pp. 535–546.

Design for Reliability in Data Handling Systems, by A. Davison and R. Threadgold, pp. 547–570.

Spaceflight Technology, Commonwealth Spaceflight Symposium, 1st, London, 1959, Kenneth W. Gatland (ed.), Academic Press, N. Y., 1960, 365 pp.

Scientific Instrumentation of Unmanned Earth Satellites, by P. Barratt, D. Rothwell and E. V. Somes Charlton, pp. 259–298.

The Jodrell Bank Radio Telescope as a Space Communicator, by J. H. Thompson, pp. 299–308.

Satellite Tracking by Optical Methods, by A. P. Willmore, pp. 309–312.

Measurement of Thickness of Thin Transparent Films Using Fluorescence, by B. P. Bunt, *Brit. J. Appl. Phys.*, vol. 12, no. 4, April 1961, pp. 175–177.

The Coupling Factor of Piezoelectric Ceramic Disks, by D. S. Campbell and A. M. MacSwan, *Brit. J. Appl. Phys.*, vol. 12, no. 4, April 1961, pp. 188–192.

Improved Standard for the Calibration of Vibration Pickups, by R. R. Bouche, *Experimental Mech.*, vol. 1, no. 4, April 1961, pp. 116–121.

Linearizing the Output of Resistance Temperature Gages, by D. R. Mack, *Experimental Mech.*, vol. 1, no. 4, April 1961, pp. 122–126.

Photoelastic Strain Gages, by G. U. Oppel, *Experimental Mechanics*, vol. 1, no. 3, March 1961, pp. 65–73.

Satellite-Borne Instrumentation for Observing Flux of Heavy Primary Cosmic Radiation, by P. Schwed, M. A. Pomerantz, H. Hanson and H. Benjamin, *Franklin Inst., J.*, vol. 271, no. 4, April 1961, pp. 275–291.

Measurement of Noise Power Spectra by Fourier Analysis, by A. Ziva Akcasu, *J. Appl. Phys.*, vol. 32, no. 4, April 1961, pp. 565–567.

Propagation in a Plasma, by P. A. Clavier, *J. Appl. Phys.*, vol. 32, No. 4, April 1961, pp. 578–582.

Use of 'Air-Bleed' When Measuring Pressure in Vacuum Processes in Which Condensable Vapours are Present, by H. Wycliffe, *J. Scien. Instr.*, vol. 38, no. 4, April 1961, pp. 126–129.

A Level Controller for Liquid Nitrogen, by D. Miller and H. C. Evans, *J. Scien. Instr.*, vol. 38, no. 4, April 1961, pp. 162.

Coaxial Cylinder Viscometer for Non-Newtonian Fluids, by John C. Harper, *Rev. Scien. Instr.*, vol. 32, no. 4, April 1961, pp. 425–428.

Propagation and Generation of Low-Frequency Electromagnetic Waves in the Upper Atmosphere, by B. N. Gershman and V. A. Ugarov, *Soviet Phys.: Uspekhi*, vol. 3, no. 5, March-April 1961, pp. 743–764.

On the Combination Reception of Signals Separated by the Angle of Arrival of the Ray in Long Distance Tropospheric Ultra-Short Wave Transmission, by A. S. Nemirovskii, *Telecommunications*, no. 8, 1960, pp. 853–864.

On the Possibility of Controlling the Capacity Ratio of High Frequency Quartz Resonators, by G. B. Al'shuller, *Telecommunications*, no. 8, 1960, pp. 864–874.

Methods of Calculating the Transfer Characteristics of Systems With Phase Distortions, by V. G. Alekseyeva, *Telecommunications*, no. 8, 1960, pp. 875–887.

Instrument to Measure Density Profiles Behind Shock Waves, by W. J. Witteman, *Maryland Univ., Inst. Fluid Dynamics Appl. Math., Tech. Note* BN-232, Feb. 1961, 18 pp. (*AFOSR* 364).

Refractory Metal Thermocouples, by J. C. Lachman, *ASME Paper* 59-HT-21, Aug. 1959, 10 pp.

Thermocouples for 5000°F Using Rhenium Alloys, by J. C. Lachman and J. A. McGurty, *Gen. Electric Co., Aircraft Nuclear Propulsion Dept.* (Presented at the Electrochemical Society Symposium on Rhenium, Chicago, Ill.), May 4, 1960, 24 pp.

Interaction Between a Radio Wave and a Plasma in the Presence of a Uniform Magnetic Field, by Toyoki Koga, *Southern Calif. Univ., Engng. Center Rep.* 83-204, Jan. 1961.

Telemetry Standards (Range Commanders' Conference Inter-range Instrumentation Group), *Inter-range Instrumentation Group, White Sands Missile Range, N. M., Doc.* 106-60, April 1961, 81 pp.

Nonstationary Signal Flow Graph Theory, by E. B. Stear and A. R. Subberud, *Calif. Univ., Los Angeles, Dept. Engng. Rep.* 60-64, Nov. 1960, 33 pp. (*AFOSR* 161)

Analysis of a Four-Station Doppler Tracking Method Using a Simple CW Beacon, by Clifford L. Frick and Carl W. Watkins, *NASA Tech. Note* D-748, April 1961, 38 pp.

A Sensor for Obtaining Ablation Rates, by Clyde W. Winters and Emedio M. Bracalente, *NASA Tech. Note,* D-800, April 1961, 17 pp.

The Mina Martin Aeronautical Student Fund, First Award Student Papers, *Inst. Aeron. Sci.,* 1960, 216 pp.

The Response Characteristics of Simulated Pneumatic Missile Pressure Sensing Systems Subjected to Continuous, Impulse and Shock-Type Inputs, by David A. Pirie and George W. Stone, pp. 128-158.

International Institute of Refrigeration Problems of Low Temperature Physics and Thermodynamics, Proceedings of the Meeting of Commission of the International Institute of Refrigeration, Delft, 1958, Pergamon Press, N. Y., 1959, 341 pp.

A Temperature Scale Down to 20°K Using Platinum Resistance Thermometers, by G. C. Lowenthal, W. R. G. Kemp and A. F. A. Harper, pp. 107-116.

A Variable Sensitivity Gas Thermometer for Use at Low Temperatures, by F. Rothwarf and J. Steinberg, pp. 117-128.

The Thermal E. M. F. of Several Thermometric Alloys, by R. L. Powell and M. D. Bunch, pp. 129-136.

A Practical Interpolation Procedure for Carbon Thermometry Between 1.5 and 30°K, by A. R. de Vroomen, pp. 137-144.

Temperature Measurements With an Acoustical Thermometer, by A. Van Itterbeek, G. Forrez, C. G. Sluijter and Miss G. Vaes, pp. 155-164.

Thermistors as Sensing Elements for Low Temperatures, by H. B. Sachse, pp. 145-154.

Space Trajectories, A Symposium, edited by *Radiation, Inc., Research Div.,* Academic Press, N. Y., 1960, 298 pp.

Space Trajectory Instrumentation, Present and Future, by Walter H. Manning Jr., pp. 269-274.

Methods and Apparatus for the Measurement of the Lowest Gas Pressures, VI. Different Vacuum Gages With Amplification, by Helmut Schwarz, *Appl. Sci. Res.,* Section A, vol. 10, no. 2, 1961, pp. 25-28 (in German).

Suggestion for Satellite Observations With Simple Electronic Apparatus, by G. Schiffner, *Astronautica Acta,* vol. 6, no. 5, 1960, pp. 266-272 (in German).

Deep-Space Communications, by Eberhardt Rechtin, ASTRONAUTICS, vol. 6, no. 4, April 1961, pp. 37, 42, 44, 46-47, 50.

Instrumentation for the First Anglo-American Scout Satellite, by A. P. Willmore, *Brit. Interplanetary Soc., J.,* vol. 18, no. 1, Jan.-Feb. 1961, pp. 11-16.

Ground Equipment for Radio Observations on Artificial Satellites, by B. G. Pressey, *Brit. Interplanetary Soc., J.,* vol. 18, no. 1, Jan.-Feb. 1961, pp. 20-27.

Designing Communication Links for Space Vehicles, by F. Sinnott, *Control Engng.,* vol. 8, no. 3, March 1961, pp. 155-160.

Effect of Pressure on emf of Thermocouples, by F. P. Bundy, *J. Appl. Phys.,* vol. 32, no. 3, March 1961, pp. 483-489.

Reference Equipment for Checking Vacuum Gauge Measuring Units, by A. V. Eryukhin, *Measurements Techniques* (Transl. of *Izmeritel'naya Tekhnika*) no. 8, Aug. 1960, pp. 657-658.

A Constant Forced Return in Moving Elements of Measuring Instruments, by N. P. Zakaznov, *Measurement Techniques* (transl. of *Izmeritel'naya Tekhnika*) no. 8, Aug. 1960, p. 659.

Strain-Gauge Acceleration Transducers, by V. P. Nenyukov, A. S. Zhumur and G. L. Lyapin, *Measurement Techniques* (transl. of *Izmeritel'nya Tekhnika*) no. 7, July 1960, pp. 590-592.

Differences in the Relation Between Resistance and Temperature of Several Brands of Platinum in the Range of 10.8 to 273.16°K, by D. I. Sharevskaya, P. G. Strelkov, A. S. Borovik-Romanov, etc., *Measurement Techniques* (transl. of *Izmeritel'naya Tekhnika*) no. 7, July 1960, pp. 598-602.

Checking the Sensitivity of Differential Resistance Thermometers in Unbalanced Bridge Circuits, by L. G. Kachurin, *Measurement Techniques* (transl. of *Izmeritel'naya Tekhnika*) no. 7, July 1960, pp. 603-605.

Instrument to Measure Density Profiles Behind Shock Waves, by W. J. Witteman, *Rev. Scien. Instr.,* vol. 32, no. 3, March 1961, pp. 292-296.

Transducer for the Measurement of Thermal Power, by B. L. Mattes and T. A. Perls, *Rev. Scien. Instru.,* vol. 32, no. 3, March 1961, pp. 332-334.

Design for Spinning Gonimeter Automatic Direction Finding, by W. J. Linsay and D. S. Heim, *J. Res. National Bur. Standards* (*D. Radio Propagation*), vol. 65, no. 3, May-June 1961, pp. 237-244.

Resolution Characteristics of Correlation Arrays, by Isham W. Linder, *J. Res. National Bur. Standards* (*D. Radio Propagation*), vol. 65, no. 3, May-June 1961, pp. 245-252.

Instrumentation for Propagation and Direction-Finding Measurements, by Edgar C. Hayden, *J. Res. National Bur. Standards* (*D. Radio Propagation*), vol. 65, no. 3, May-June 1961, vol. 65, no. 3, May-June 1961, pp. 253-254.

Brooke Variance Classification System for DF Bearings, by E. M. L. Beale, *J. Res. National Bur. Standards* (*D. Radio Propagation*), vol. 65, no. 3, May-June 1961, pp. 255-262.

Estimation of Variances of Position Lines From Fixes With Unknown Target Positions, by E. M. L. Beale, *J. Res. National Bur. Standards* (*D. Radio Propagation*), vol. 65, no. 3, May-June 1961, pp. 263-274.

Statistics of a Radio Wave Diffracted by a Random Ionosphere, by S. A. Bowhill, *J. Res. National Bur. Standards* (*D. Radio Propagation*), vol. 65, no. 3, May-June 1961, pp. 275-292.

Space Analysis of Radio Signals, by John B. Smyth, *J. Res. National Bur. Standards* (*D. Radio Propagation*), vol. 65, no. 3, May-June 1961, pp. 293-298.

Effect of Receiver Bandwidth on the Amplitude Distribution of VLF Atmospheric Noise, by Forrest F. Fulton Jr., *J. Res. National Bur. Standards* (*D. Radio Propagation*), vol. 65, no. 3, May-June 1961, pp. 299-304.

Reception of WWW and WWVH in Northern Canada, by J. R. Herman and R. B. Penndorf, *Avco Corp., Res. Advanced Dev. Div.,* Wilmington, Mass., RAD-TR-61-5, Jan. 1961 (AFCRL-15).

Final Report for the Collins Radio Company and Alpha Corporation Participation in Project Echo, *Collins Radio Co.,* CRR-234, Feb. 1, 1960.

Final Report on Evaluation of Auroral Propagation Factors Transmission Loss Phase, Part II: A Comparison of Artic HF Transmission Loss and VHF Riometer Data, by C. G. Little and R. Silberstein, *National Bur. Standards, Boulder Labs., NBS Rep.* 6743, Feb. 10, 1961.

The Design and Performance of Parametric Amplifier Antennas, by A. D. Frost and R. R. Clark, *New Hampshire Univ., Antenna Systems Lab.,* Sci. Rep. 3, Nov. 30, 1960 (AFCRL 11).

Threshold of Reliable Detection and Limiting Sensitivity of Radio Telescopes (Trans. from Akademiya Nauk Armyanskoy, SSR, Izvestia, Fizika Matematicheskaya, vol. 13, no. 1, 1960), by E. S. Burunsuzian, *Morris D. Friedman, Inc., Foreign Tech. Translations, West Newton, Mass.,* B-174, 1960 (AFCRL-35).

Interaction Between a Radio Wave and a Plasma in the Presence of a Uniform Magnetic Field, by T. Koga, *Southern Calif., Univ., Engng. Center, Los Angeles,* USCEC Rep. 83-204, Jan. 1961 (AFOSR 283).

The Determination of Noise Temperatures of Large Antennas, by D. Schuster, C. Stelzried and G. S. Levy, *Calif. Inst. Tech. Jet Propulsion Lab. Tech. Rep.* 32-97, 1961, 24 pp.

Damping Measurements With a Sting-Supported Bearing-Pivot Dynamic Balance, by C. J. Welsh, L. K. Ward and R. H. Urban, *Arnold Engng. Dev. Center Tech. Note* 61-52, May 1961, 14 pp.

Satellite Magnetic Field Mapping, by James P. Heppner, Joseph C. Cain, Ivan R. Shapiro and John D. Stolarik, *NASA Tech. Note* D-696, May 1961, 20 pp.

Selection of the Most Suitable Circuit for a Photoelectric Fluxmeter, by I. G. Gutovskii, *Automation and Remote Control,* vol. 21, no. 10, Oct. 1960, pp. 989-996.

Errors in Detection of RF Pulses Embedded in Time Crosstalk, Frequency Crosstalk, and Noise, by E. A. Marcatili, *Bell System Tech. J.,* vol. 40, no. 3, May 1961, pp. 921-950.

Time and Frequency Crosstalk in Pulse-Modulated Systems, by E. A. Marcatili, *Bell System Tech. J.,* vol. 40, no. 3, May 1961, pp. 951-974.

A Noise Investigation of Tunnel-Diode Microwave Amplifier, by A. Yariv and J. S. Cook, *Inst. Radio Engrs., Proc.,* vol. 49, no. 4, April 1961, pp. 739-743.

A Low-Noise X-Band Radiometer Using Maser, by J. J. Cook, L. G. Cross, M. E. Bair, and R. W. Terhune, *Inst. Radio Engrs., Proc.,* vol. 49, no. 4, April 1961, pp. 768-778.

Analysis and Synthesis Techniques of Oriented Communication Nets, by D. T. Tang and R. T. Chien, *Inst. Radio Engrs., Trans. Circuit Theory,* vol. CT-8, no. 1, March 1961, pp. 39-43.

Proceedings (Advances in the Astronautical Sciences, U. S.), American Astronautical Society, Western, National Meeting, Plenum Press, New York, 1960, 355 pp.

Global Communication Using Passive or Active Satellite Relay Stations, by Friedrich Vilbig, pp. 251–260.

Requirements for Data Transmission From a Martian Reconnaissance Vehicle, by C. H. Child, pp. 261–277.

Measuring Amplitude and Phase, by Nathaniel Roy Goodman, pp. 278–290.

Design Techniques for Space Television, by A. J. Viterbi, pp. 291–305.

Effect of Hard Limiting on the Probabilities of Incorrect Dismissal at the Output of an Envelope Detector, by P. Bello and W. Higgins, *Inst. Radio Engrs., Trans. Info. Theory,* vol. IT-7, no. 2, April 1961, pp. 60–66.

On the Asymptotic Efficiency of Locally Optimum Detectors, by Jack Capon, *Inst. Radio Engrs., Trans. Info. Theory* vol. IT-7, no. 2, April 1961, pp. 67–71.

Signal Detection by Adaptive Filters, by Edmund M. Glaser, *Inst. Radio Engrs., Trans. Info. Theory,* vol. IT-7, no. 2, April 1961, pp. 87–98.

A Note on Singular and Nonsingular Optimum (Bayes) Tests for the Detection of Normal Stochastic Signals in Normal Noise, by David Middleton, *Inst. Radio Engrs., Trans. Info. Theory,* vol. IT-7, no. 2, April 1961, pp. 105–111.

A Lower Bound for Error Detecting and Error Correcting Codes, by Peggy Tang Strait, *Inst. Radio Engrs., Trans. Info. Theory,* vol. IT-7, no. 2, April 1961, pp. 114–117.

Optimum, Linear, Discrete Filtering of Signals Containing a Nonrandom Component, by Kent R. Johnson, *Inst. Radio Engrs., Trans. Info. Theory,* vol. IT-2, no. 2, June 1956, pp. 49–55.

Effects of Signal Fluctuation on the Detection of Pulse Signals in Noise, by Mischa Schwartz, *Inst. Radio Engrs., Trans. Info. Theory,* vol. IT-2, no. 2, June 1956, pp. 66–71.

A Bibliography of Soviet Literature on Noise, Correlation and Information Theory, by Paul E. Green Jr., *Inst. Radio Engrs., Trans. Info. Theory,* vol. IT-2, no. 2, June 1956, pp. 91–95.

Probability Density Functions for Correlators With Noisy Reference Signals, by G. M. Roe and G. M. Shite, *Inst. Radio Engrs., Trans. Info. Theory,* vol. IT-7, no. 1, Jan. 1961, pp. 13–18.

On Coded Phase-Coherent Communications, by A. J. Viterbi, *Inst. Radio Engrs., Trans. Space Electronics and Telemetry,* vol. SET-7, no. 1, March 1961, pp. 3–14.

Data Transmission for the NRL Space Surveillance System, by M. G. Kaufman and F. X. Downey, *Inst. Radio Engrs., Space Electronics and Telemetry,* vol. SET-7, no. 1, March 1961, pp. 15–19.

The Role of the Jet Propulsion Laboratory in Project Echo, by W. K. Victor and R. Stevens, *Inst. Radio Engrs., Trans. Space Electronics and Telemetry,* vol. SET-7, no. 1, March 1961.

Propagation Studies Using Direction-Finding Techniques, by Edgar C. Hayden, *J. Res. National Bur. Standards (D. Radio Propagation),* vol. 65, no. 3, May-June 1961, pp. 197–212.

Diversity Effects in Long Distance High Frequency Radio Pulse Propagation, by S. A. Bowhill, *J. Res. National Bur. Standards (D. Radio Propagation),* vol. 65, no. 3, May-June 1961, pp. 213–224.

Influence of Ionospheric Conditions on the Accuracy of High Frequency Direction Finding, by P. J. D. Gething, *J. Res. National Bur. Standards (D. Radio Propagation),* vol. 65, no. 3, May-June 1961, pp. 225–228.

Phase Difference Observations at Spaced Aerials and Their Application to Direction Finding, by W. C. Bain, *J. Res. National Bur. Standards (D. Radio Propagation),* vol. 65, no. 3, May-June 1961, pp. 229–232.

Research at the National Bureau of Standards Applicable to Long-Distance Location and Direction-Finding Problems, by R. Silberstein, *J. Res. National Bur. Standards (D. Radio Propagation),* vol. 65, no. 3, May-June 1961, pp. 233–236.

Excitation of VLF and ELF Radio Waves by a Horizontal Magnetic Dipole, by Janis Galejs, *J. Res. National Bur. Standards (D. Radio Propagation),* vol. 65, no. 3, May-June 1961, pp. 305–309.

High-Sensitivity Recording Optical Density Meter, by K. E. Collins and D. J. Steele, *J. Scien. Instr.,* vol. 38, no. 5, May 1961, pp. 186–190.

Indium Resistance Thermometers, by B. Yates and C. H. Panter, *J. Scien. Instr.,* vol. 38, no. 5, May 1961, pp. 196–197.

Photoelectric Optical Pyrometer, by J. Middlehurst and T. P. Jones, *J. Scien. Instr.,* vol. 38, no. 5, May 1961, pp. 202–204.

Sensitive Method for Measuring Small Rotations of a Distant Object, by R. J. King, S. P. Middleton and I. M. G. Thompson, *J. Scien. Instr.,* vol. 38, no. 5, May 1961, pp. 207–208.

A Simple and Cheap Thermal Conductivity Apparatus, by D. W. Stops, *J. Scien. Instr.,* vol. 38, no. 5, May 1961, p. 221.

Dynamic Accuracy of Trigger Regulators With Unstable Pulses, by V. A. Shpolyanskii, *Measurement Techniques* (Trans. of Izmeritel'naya Tekhnika), no. 9, Sept. 1960, pp. 747–755.

A Bell Differential Manometer DKFM, by M. D. Gafanovich and B. Ya. Gorodetskii, *Measurement Techniques* (Trans. of Izmeritel'naya Tekhnika), no. 9, Sept. 1960, pp. 758–759.

An Autocompensated Thermal Vacuum Gauge, by V. I. Bakhtin and V. N. Mikhailin, *Measurement Techniques* (Trans. of Izmeritel'naya Tekhnika) no. 9, Sept. 1960, pp. 760–761.

Measurement of Accelerations by Means of Piezoelectric Transducers Working in Strain-Gauge Equipment, by B. A. Glagovskii, *Measurement Techniques* (Trans. of Izmeritel'naya Tekhnika) no. 9, Sept. 1960, pp. 762–763.

The Use of Alternating Currents for Calibrating Commercial Optical Pyrometers, by Yu. Ya. Donde and M. A. Pisarevskaya, *Measurement Techniques* (Trans. of Izmeritel'naya Tekhnika), no. 9, Sept. 1960, pp. 766–768.

Compensation for Temperature Effects in the EMF of Potentiometer Standard Cells, by A. Ya. Shramkov, *Measurement Techniques* (Trans. of Izmeritel'naya Tekhnika), no. 9, Sept. 1960, pp. 772–774.

Measuring Impedances by Means of Oscilloscopes, by K. P. Mikhailovskaya, *Measurement Techniques* (Trans. of Izmeritel'naya Tekhnika), no. 9, Sept. 1960, pp. 775–777.

Symmetrical Constant Pressure-Drop Flow Gauge, by D. N. Ulezko, *Measurement Techniques* (Trans. of Izmeritel'naya Tekhnika), no. 9, Sept. 1960, pp. 803–804.

An Ultrasonic Recorder of the Level of Liquids, by B. A. Syvak and V. A. Nosov, *Measurement Techniques* (Trans. of Izmeritel'naya Tekhnika), no. 9, Sept. 1960, pp. 805–806.

Certain Properties of Communication Systems With Fading Type Interference, by E. L. Blokh and A. A. Kharkevich, *Radio Engng.* (Trans. of Radiotekhnika), vol. 15, no. 9, 1960, pp. 1–9.

The Effect of the Parameters of a Transistor Blocking-Oscillator on the Shape of its Pulses, by E. E. Dovzhikov, *Radio Engng.* (Trans. of Radiotekhnika), vol. 15, no. 9, 1960, pp. 53–62.

Optimum Passband of a Filter in the Reception of Frequency-Modulated Signals With Follow-Up Tuning, by Ya. G. Rodionov, *Radio Engng.* (Trans. of Radiotekhnika), vol. 15, no. 9, 1960, pp. 63–73.

A Cascade Amplifier With a High Amplification Factor, by G. P. Petin, *Radio Engng.* (Trans. of Radiotekhnika), vol. 15, no. 9, 1960, pp. 74–78.

On the Theory of Cross-Distortion With Long-Distance Tropospheric UHF Propagation, by A. V. Prosin, *Radio Engng. and Electronics* (Trans. of Radiotekhnika i Elektronika), vol. 5, no. 1, 1960, pp. 27–45.

Receiving Equipment for the Measurement of Statistical Signal Characteristics With Tropospheric Propagation of Radio Waves, by L. T. Remizov, M. G. Golubtsov and L. S. Tiufiakin, *Radio Engng. and Electronics* (Trans. of Radiotekhnika i Elektronika), vol. 5, no. 1, 1960, pp. 46–56.

Free Electromagnetic Oscillations of a Spherical Resonator With Magnetized Ferrite Sphere in the Center, by A. A. Pistol'kors and Siui Ian'-Shen, *Radio Engng. and Electronics* (Trans. of Radiotekhnika i Elektronika), vol. 5, no. 1, 1960, pp. 77–87.

Excitation of Waveguide Systems by an Electron Stream With Prescribed Modulation, by V. A. Solntsev and A. S. Tager, *Radio Engng. and Electronics* (Trans. of Radiotekhnika i Elektronika), vol. 5, no. 1, 1960, pp. 100–118.

The Influence of Production Tolerances on the Bandwidth of a Diaphragmed Waveguide, by I. A. Grishaev and A. I. Zykov, *Radio Engng. and Electronics* (Trans. of Radiotekhnika i Elektronika), vol. 5, no. 1, 1960, pp. 231–234.

Oxygen Gauge, by J. Weissbart and R. Ruka, *Rev. Scien. Instr.,* vol. 32, no. 5, May 1961, pp. 593–594.

Development of High Temperature Strain Gages, by J. W. Pitts and D. G. Moore, *National Bur. Standards, Monograph* 26, March 17, 1961, 18 pp.

Potential Noise Stability in Short Wave Radio Telegraphy, by D. D. Klovskii, *Telecommunications,* no. 9, 1960, pp. 945–957.

Proceedings, Symposium on Advances in Fast-Pulse Techniques for Nuclear Counting, 2nd, Berkeley, Calif., Feb. 1959, Atomic Energy Commission, UCRL-8706, 1959, 125 pp.

High-Speed Photomultipliers and Electronic Devices, by George A. Morton, pp. 13–19.

A Millimicrosecond Light Source, by Albert L. Whetstone, pp. 24–28.

Analysis of Millimicrosecond Pulses by Use of a Charge-Storage Type of Pulse-Height Analyzer, by Louis Costrell, pp. 31–36.

Review of Image Intensifiers, by David O. Caldwell, pp. 37–42.

Time Sorting of Millimicrosecond Pulses, by Emilio Gatti, pp. 49–54.

A Time-Delay-to-Amplitude Converter, by Zoltan Bay, pp. 55–58.

Time-to-Pulse-Height Conversion, by John H. Neiler, pp. 59–61.

Many Coincidence Channels, by David Ritson, p. 62.

Multidimensional Pulse-Measuring Techniques, by Dan G. Maeder, pp. 63–67.

Millimicrosecond Gamma-Ray Detector and Oscilloscope System, by Robert B. Patten, pp. 71–77.

Fast-Oscilloscope Requirements, by Dick A. Mack, pp. 77–78.

Requirements on Fast Oscilloscopes, by Quentin A. Kerns, pp. 79–81.

The Design of a High-Speed Cathode Ray Tube With a Distributed Deflection System, by Jacob Goldberg, pp. 82–86.

Development of a Vertical-Deflection Amplifier for Fast Oscilloscopes, by John Kobbe, pp. 87–88.

Type-519 Oscilloscope, by Clifford Moulton, pp. 89–92.

Fast-Rise Sampling Oscilloscope and Pulse Generator, by Robert M. Sugarman, pp. 93–96.

Sampling Oscilloscopes, by Norman B. Schrock, p. 97.

Pulse Generators, by Quentin A. Kerns, pp. 98–104.

A Millimicrosecond Pulse Generator Capable of High Repetition Rates, by Michiyuki Nakamura, pp. 105–108.

Microwave-Gated Photomultipliers, by Donald I. Meyer, pp. 109–112.

Pulse-Height Analysis and Timing Measurements of Fast Pulses, by Henry H. Kendall, pp. 113–117.

Semiconductor Devices in Coincidence Circuits, by Val L. Fitch, pp. 118–119.

Simplified Coincidence Circuits Using Transistors and Diodes, by Richard H. Miller, p. 120.

Aeronautics and Astronautics, Proceedings, (Durand Centennial Conference, Stanford University, Aug. 5–8, 1959), Nicholas John Hoff and Walter Guido Vincenti (eds.), Pergamon Press, New York, 1960, 460 pp. (AFOSR TR 59-108).

Radar Astronomy (Exploration of the Solar System Using Man-Made Radio Waves), by Von R. Eshleman, pp. 207–226.

Observation Requirements for Precision Orbit Determination, by Samuel Herrick, pp. 417–436.

Ballistic Missile and Space Technology, vol. 1: Bioastronautics and Electronics and Invited Addresses (Symposium on Ballistic Missile and Space Technology, 5th Los Angeles, Aug. 1960), Donald P. Le Galley (ed.), Academic Press, New York, 1960, 494 pp.

Person-to-Person Communications in an Atmosphere-Free Environment, by R. J. Christman, pp. 49–62.

Gyro Spin-Axis Bearing Program at the General Motors Research Laboratories, by Donald R. Whitney, pp. 143–156.

A Miniature Accelerometer With a Fused Quartz Suspension, by A. R. Johnston, pp. 157–186.

The Effect of Hard Limiting in Satellite Repeaters on Signals Employing Angle Modulation, by R. E. Eachelbach, pp. 241–293, 14 refs.

Electronically Steerable Antenna for Space Vehicles, by Leo W. Procopio, pp. 295–310.

Lockheed Sampled-Data System for Optimum Telemetry Applications, by D. Hochman, L. K. Koehler and C. Kortman, pp. 343–363.

Estimates of Accuracy of Atlantic Missile Instrumentation, by Jerome P. Keuper, pp. 365–390.

Notes on Evaluation of an Impact Prediction and Location System, by Victor B. Kovac, pp. 391–408.

Theory of Scanning for Time and Frequency Synchronization, by John L. Hatcher, pp. 409–434.

Real-Time Multiprogramming in Project Mercury, by M. J. Buist and G. M. Weinberg, pp. 435–445.

Automatic Telemetry Magnetic Tape Editing Machine, by H. J. Hayes, pp. 447–455.

Ballistic Missile and Space Technology, vol. 3: Guidance Navigation, Tracking and Space Physics (Symposium on Ballistic Missile and Space Technology, Los Angeles, Aug. 1960) Donald P. Le Galley (ed.), Academic Press, New York, 1960, 450 pp.

Advanced Radar Information Evaluation System, by David L. Lovenvirth and William F. Holst, pp. 33–54.

Radar Velocity Tracking Systems Analysis, by Gregory O. Young, pp. 127–167.

Plasma Probes for Space Exploration, by Bernard Raab, pp. 367–392.

The Radio Noise Spectrum, Donald H. Menzel (ed.), Harvard Univ. Press, Cambridge, Mass., 1960, 183 pp.

Man-Made Radio Noise, by E. W. Allen, pp. 1–6.

The Aurora and Radio Wave Propagation, by Allen M. Peterson, pp. 7–42, 47 refs.

Ionospheric Scintillation of Radio Waves of Extra-terrestrial Origin, by Robert S. Lawrence, pp. 43–47.

Natural Background Noise at Very Low Frequencies, by Jules Aarons, pp. 111–122.

Noise of Planetary Origin, by B. F. Burke, pp. 129–140.

Correcting Noise Maps for Beamwidth, by R. N. Bracewell, pp. 141–150.

A Study on Cosmic Radio Noise, by Donald H. Menzel, pp. 151–176.

Deep-Space Communications, Part 2, by Eberhardt Rechtin, ASTRONAUTICS, vol. 6, no. 5, May 1961, pp. 26, 82–87.

Proceedings, Sponsored by the Professional Group on Space Electronics and Telemetry of the Institute of Radio Engineers, National Symposium on Space Electronics and Telemetry, San Francisco, Sept. 1959, Inst. of Radio Engineers, New York, 1959, vol. 1.

Design and Evaluation of Space Communications Systems Using Computer Simulation Techniques, by D. R. J. White, no. 1.1, 19 pp.

The Use of PCM in Data Links With Satellites, Space Vehicles and Long-Range Missiles, by R. L. Sink, no. 1.2, 21 pp.

Phase-Lock in Space Communications, by F. A. Ruegg and W. F. Sampson, no. 1.3, 5 pp.

A Communication System for a Small Interplanetary Vehicle, by M. I. Skolnik and L. Cartledge, no. 1.4, 14 pp.

Data Recovery—New Approaches Required for Re-Entry Vehicle Instrumentation, by P. L. Lathrop, no. 3.1, 18 pp.

Analysis and Prediction of Radio Signal Interference Effects Due to Ionized Layer Around a Re-Entry Vehicle, by W. C. Taylor, no. 3.2, 20 pp.

Radio Frequency Propagation to and From ICBM's and IRBM's, by F. S. Howell and W. H. Drake, no. 3.3, 16 pp.

A Diversity Combiner for Telemetry, by C. C. Hall, no. 3.4, pp.

Telemetry Diversity Reception Techniques, by V. A. Ratner, no. 3.5, 32 pp.

A Novel Concept Applied to Airborne Commutation, by E. H. Straehley, no. 4.1, 7 pp.

A Status Report on Missile Commutation, by R. J. Farrelly, no. 4.2, 16 pp.

An Improved Transistorized PDM Keyer for the Multi-Channel Data Acquisition System, by Boris Stefanov, no. 4.3, 7 pp.

Some New Techniques in Airborne Data Acquisition, by E. P. Brandeis and M. E. Harrison, no. 5.2, 14 pp.

Digital to Analog Conversion for PCM Telemetry and Digital Data Transmission Systems, by M. Palevsky, G. Slocomb and D. Block, no. 5.3, 5 pp.

Digilock Telemetry System, by R. W. Sanders, no. 6.3, 10 pp.

Telemetry Addition to the Azusa Tracking System, by E. W. Bush, no. 6.4, 10 pp.

A High Capacity PAM-FM-FM Telemetering System for the Saturn Booster, by O. B. King, no. 7.1, 10 pp.

SS-FM: A Frequency Division Telemetry System With High Data Capacity, by W. O. Frost and O. King, no. 7.2, 14 pp.

A Pulse Position Telemetry System, by L. Weisman and E. S. Teltscher, no. 7.3, 15 pp.

Some Methods of Obtaining More Vibration Data on Fewer Telemetry Channels, by W. D. Hancock, no. 7.4, 7 pp.

Extreme Environment Telemeter, by J. J. Weippert, J. S. Piontkowski and M. J. Huskey, no. 7.5, 12 pp.

A Solid State Decommutator, by J. H. Porter, no. 8.1, 10 pp.

An Advanced Decommutator System, by L. H. Beman, no. 8.2, 14 pp.

Crosstalk in Time Shared Systems as Affected by Discriminator Characteristics, by O. J. Ott, no. 8.3, 6 pp.

A Decommutation System for FM/FM Telemetry, by W. Kroll, no. 8.4, 6 pp.

Factors Affecting Choice of Loop Filters in Phase-Locked Loop Discriminators, by R. A. Runyan, no. 9.1, 7 pp.

Transistorized Sub-Carrier Oscillator Principles, by W. H. Swain, no. 9.2, 16 pp.

A Reactance-Modulated FM Transmitter for Space Communications or Telemetry, by R. Pasos and G. Heninger, no. 9.3, 7 pp.

A New Telemetry Transmitter Using a Voltage-Tuned Magnetron for Space Environment, by C. L. Jensen, no. 9.4, 8 pp.

A Tunable Airborne VHF Transmitter of High Stability for Wide Deviation FM With Low Distortion, by W. S. Swain and S. Fisher, no. 9.5, 8 pp.

Transit Program Results, by Richard B. Kershner, ASTRONAUTICS, vol. 6, no. 5, May 1961, pp. 30–31, 106–110.

Project Echo Results, by Leonard Jaffe, ASTRONAUTICS, vol. 6, no. 5, May 1961, pp. 32–33, 80.

Practical Problems of Satellite Communication, by John R. Pierce, ASTRONAUTICS, vol. 6, no. 5, May 1961, pp. 34–35, 90–96.

Dynasoar Communications and Data Link, by L. B. Garrett Jr., ASTRONAUTICS, vol. 6, no. 5, May 1961, pp. 42–43, 117–120.

Adaptive Aerospace PCM Telemetering, by John O. Bowers Jr., Donald H. Ellis and James M. Walter Jr., ASTRONAUTICS, vol. 6, no. 5, May 1961, pp. 44–45, 124–125.

Certain Relationships in Optimum Systems for Detecting Signals, by L. S. Gutkin, *Radio Engng. (Transl. of Radio-*

tekhnika) vol. 15, no. 4, 1960, pp. 34–43.

Maximum Interference Resistance of Systems With Discrete Signals, by N. L. Teplov, *Radio Engng.* (*Transl. of Radiotekhnika*) vol. 15, no. 4, 1960, pp. 4–60.

Linear Distortions in the Sampling of Continuous Signals, by V. A. Vol. *Radio Engng.* (*Transl. of Radiotekhnika*) vol. 15, no. 4, 1960, (pp. 61–69).

The Calculation of Radio Lenses With Constant Refractive Index, by Iu B. Molochkov, *Radio Engng. Electronics* (Transl. of Radiotekhnika i Elektronika) vol. 5, no. 6, 1960, pp. 45–52.

Current Distribution on the Reflector of a Reflector Antenna, by L. B. Tartakovskii and V. L. Tandit, *Radio Engng. Electronics* (Transl. of Radiotekhnika i Elektronika) vol. 5, no. 6, 1960, pp. 53–64.

Experimental Investigation of the Degenerate Regime of a Ferrite Amplifier, by V. P. Tychinskii, Iu. T. Derkach and V. V. Karpetskii, *Radio Engng. Electronics* (Transl. of Radiotekhnika i Elektronika) vol. 5, no. 6, 1960, pp. 90–106.

On Forced Oscillations of a Parametrically Regenerated System, by V. V. Migulin, *Radio Engng. Electronics* (Transl. of Radioteeknika i Elektronika) vol. 5, no. 6, 1960, pp. 107–116.

A Method of Increasing the Stability of Tuned Transistor Amplifiers, by I. U. Simonov, *Radio Engng. Electronics* (Transl. of Radiotekhnika i Elektronika) vol. 5, no. 5, 1960, pp. 153–161.

Computer Engineering, S. A. Lebedev (ed.) (Transl. from the Russian by Jane Stuart; translation edited by J. P. Cleave and F. A. Sowan) (Akademiia Nauk, SSSR) Pergamon Press, New York, 1960, 184 pp.

Digital Integrating Machines, by F. V. Maiorov, pp. 22–95.

Dynamic Flip-Flops and Their Use in Parallel Action Computers, by P. P. Golovistikov, pp. 96–133.

The Role of the Ferrite Core in a Matrix Storage Unit, by N. Ya. Matyukein and O. V. Rosnitskii, pp. 143–157.

Reliability of a Matrix Type Magnetic Store With Linear Selection, by Yu. N. Glukhov and O. V. Rosnitskii, pp. 158–169.

In What Cases Should Propagation or Refraction Calculations be Made in Data Reduction, and What are the Limitations of the Various Methods? Technical Presentation at Joint Session of Data Reduction and Computing and Electromagnetic Propagation Working Groups of IRIG, by Fred S. Hanson, *Inter-Range Instrumentation Group, White Sands Proving Ground, N. M.*, no. 101-58, Nov. 1958, 66 pp.

Initiation of the Meteorological Rocket Network, *Inter-Range Instrumentation Group, White Sands Proving Ground, N. M.*, no. 105-60, July 1960, 32 pp.

Catalogue of Data Reduction Film Reading Equipment, *Inter-Range Instrumentation Group, White Sands Proving Ground, N. M.*, no. 103-60, July 1960, 99 pp.

Proceedings, Sponsored by the Professional Group on Space Electronics and Telemetry of the Institute of Radio Engineers, National Symposium on Space Electronics and Telemetry, San Francisco, Sept. 1959, New York Inst. of Radio Engrs., 1959, vol. 1.

Encoding, Decoding and Recoding With Binary-Decimal Numbers, an Expanded View, by B. Lippel, no. 1.5, 13 pp.

Mathematical Approach to Hybrid Computing, by G. B. Birkel Jr., no. 2.1, 7 pp.

High-Speed Hybrid Computer, by M. C. Burns, no. 2.2, 9 pp.

High-Speed Plotter, by R. Sapirstein, no. 2.3, 4 pp.

Telemetry Data Processing at Convair-Astronautics, by R. G. Madsen, no. 2.5, 14 pp.

Atmospheric and Space Physics

Airborne Detection and Analysis of Primary Cosmic Particles With a Scintillation Device, by DeP. J. Corkhill and R. A. Hoffman, *AF Missile Dev. Center, Holloman AFB,* AFMDC-TN-60-12, July 1960.

Physics of the Van Allen Radiation Belts, by D. C. Hock, *AF Special Weapons Center, Kirtland AFB,* AFSWC TR-60-57, Dec. 1960.

Lunar Infrared Temperature Measurements During September 4, 5, and 6, 1960, by R. W. Shorthill and J. M. Saari, *Boeing Airplane Co.,* D7-2550-1, Jan. 30, 1961.

Carde IGY Rocket Measurements: The Height of the Sodium and Hydroxyl Airglow, by R. P. Lowe, *Canadian Armament Res. Dev. Establishment, Valcartier, Quebec, CARDE Tech. Mem.* 291/59, May 1960.

Electron Production in the E- and F-Regions, by K. Watanabe, *Geophysics Corp. of America, Bedford, Mass., GCA Tech. Rep.* 60-3-N, Dec. 1960.

Photoionization of Atomic Oxygen and Nitrogen, by A. Dalgarno, *Geophysics Corp. of America, Bedford, Mass., GCA Tech. Rep.* 60-5-N, Dec. 1960.

Note on the Geometry of Earth Magnetic Field Useful to Faraday Effect Experiments, by K. C. Yeh and V. H. Gonzalez, *Illinois Univ., Elect. Engng. Res. Lab.,* Feb. 10, 1960.

Ionospheric Electron Content and its Variations Deduced From Satellite Observations, by K. C. Yeh and G. W. Swenson, *Illinois Univ., Elect. Engng. Res. Lab.,* Nov. 15, 1960.

Tektites and Natural Satellites of the Earth, by J. A. O'Keefe and B. Shute, *Inst. Aerospace Sci.,* Rep. 61-78, Jan. 23–25, 1961.

A Satellite Borne Cadmium Sulfide Total Corpuscular Energy Detector, by J. W. Freeman, *Iowa State Univ.,* SUI 61-2, Feb. 1961.

Radiation Observations With Satellite 1958 Alpha (Explorer I), Vols. 1–4, *Iowa State Univ.,* SUI 61-3, Vols. 1–4, March 1961.

Further Evidence on Fibrous Nature of Exosphere From Guided HF Wave Propagation, by R. M. Gallet and W. F. Utlaut, *National Bur. Standards, Boulder Labs., NBS Rep.* 6747, Feb. 15, 1961.

Geophysics as Applied to Lunar Exploration: Final Report, by J. Green, *North Amer. Aviation, Inc., Space and Info. Systems Div.,* MD 59-277, June 30, 1960 (AFCRL-TR-60-409).

Inquiry Into the Feasibility of Weather Reconnaissance From a Satellite Vehicle, by S. M. Greenfield and W. W. Kellogg, *Rand Corp.,* R-365, Aug. 1960.

Geomagnetic Field Lines in Space, by E. H. Vestine and W. L. Sibley, *Rand Corp.,* R-368, Dec. 1960.

Summary of Orbital and Physical Data for the Planet Mars, by D. S. Kirby, *Rand Corp.* RM-2567, Aug. 1, 1960.

Research in Space Science, *Smithsonian Institution, Astrophys. Observatory, Cambridge, Mass., Special Rep.* 56, Jan. 30, 1961.

A Method of Analysis for Lens and Mirror Systems, by R. J. Davis, S. E. Strom, and K. M. Strom.

A Determination of the Ellipticity of the Earth's Equator From the Motion of Two Satellites, by I. G. Izsak.

Effects of Solar Radiation Pressure on the Motion of an Artificial Satellite, by Y. Kozai.

On the Stability of Planetary Scale Atmospheric Motions (Trans. from Akademiya Nauk SSSR, Izvestia, Seria Geofizicheskaya, No. 4, 1959) by M. B. Galin, *U. S. Dept. Commerce, Office of Tech. Services, Washington, D. C.,* OTS: 60-41, 095, Aug. 3, 1960 (JPRS: 5202).

Analysis of Project Hugo Test Firing December 5, 1958: Meteorological Satellite, Laboratory Report to the National Aeronautics and Space Administration, by L. F. Hubert, Appendix: Photogrammetry and Mathematics of Rocket Photograph Interpretation, by L. F. Hubert and J. Schuetz, *Weather Bureau, MSL Rep.* 2, Aug. 1960.

Summary Report, 1959 and 1960, Atmospheric Physics Program and Short Technical Reports on Exploratory Experiments, *Minnesota Univ., School of Physics,* March 1961, 58 pp.

Nitrogen and Oxygen Atomic Reactions in the Chemosphere, by Charles A. Barth, *Calif. Inst. Tech. Jet Propulsion Lab. Tech. Rep.* 32-63, April 1961, 13 pp.

Preliminary Study of Prediction Aspects of Solar Cosmic Ray Events, by Kinsey A. Anderson, *NASA Tech. Note* D-700, April 1961, 34 pp.

A Geoid and World Geodetic System Based on a Combination of Gravimetric, Astrogeodeteic and Satellite Data, by William M. Kaula, *NASA Tech. Note* D-702, May 1961, 23 pp.

Selenographic Coordinates, by B. E. Kalensher, *Calif. Inst. Tech., Jet Propulsion Lab. Tech. Rep.* 32-41, Feb. 1961, 31 pp.

Can There be a Shield for Gravitation? by W. F. G. Swann, *Franklin Inst. J.,* vol. 271, no. 5, May 1961, pp. 355–360.

Properties of Tropospheric Scattered Fields, by N. R. Ortwein, R. U. F. Hopkins and J. F. Pohl, *Inst. Radio Engrs., Proc.,* vol. 49, no. 4, April 1961, pp. 788–801.

On the Energy-Momentum Tensor of the Gravitational Field, by F. R. Tangherlini, *Nuovo Cimento,* vol. 20, no. 1, April 1961, pp. 1–19.

Interactions of Rapidly Moving Bodies in Terrestrial Atmosphere, by K. P. Chopra, *Reviews Modern Phys.,* vol. 33, no. 2, April 1961, pp. 153–189.

The Upper Atmosphere Above F2-Maximum, North Atlantic Treaty Organization, AGARDograph 42, H. Poeverlein (ed.), May 1959, 355 pp.

Information About the Gas Density in Space Derived From Radiation Measurements, by Herbert Friedman, pp. 3–10.

Ionization Above the F2-Peak, as Affected by the Interplanetary Gas, by Sydney Chapman, pp. 11–18.

The Structure of the Outer Atmosphere Including the Ion Distribution Above the F2-Maximum, by Francis S. Johnson, pp. 19–36.

Motions in the Magnetosphere of the Earth, by T. Gold, pp. 37–46.

Summary of Results on the Trapped Particle Zone, by Robert Jastrow, pp. 47–54.

Properties of the Upper Atmosphere and Their Relation to the Radiation Belts of the Earth, by S. F. Singer, pp. 55–66.

Measurement of Geomagnetically Trapped Particles of Natural and Artificial Origin, by Lew Allen Jr., pp. 67–82.

Atmospheric and Magnetic Loss Mechanisms for Geomagnetically Trapped Particles, by Jasper A. Welch Jr., pp. 83–94.

The Determination of the Directional Distribution of Charged Particles Trapped in the Magnetic Field of the Earth, by Russell D. Shelton, pp. 95–112.

Solar Flare Protons and Electrons and Their Interaction With the Geomagnetic Field, by John R. Winckler, pp. 113–138.

Hydromagnetic Theory of Geomagnetic Storms, by A. J. Dessler and E. N. Parker, pp. 139–150.

VHF Radio Wave Absorption in Northern Latitudes and Solar Particle Emissions, by Harold Leinbach and George C. Reid, pp. 151–164.

Travelling Disturbances Originating in the Outer Ionosphere, by K. Bibl and K. Rawer, pp. 165–174.

On the Interpretation of Very High Aurorae, by A. Omholt, pp. 175–182.

A Model of the F-Region Above H_{max} F2, by J. W. Wright, pp. 211–222.

Incoherent Scattering by Free Electrons as a Technique for Studying the Ionosphere and Exosphere: Some Observations and Theoretical Considerations, by Kenneth L. Bowles, pp. 223–242.

Electronic Density Less Than the F-Maximum, Deduced From the Emission of Satellites, by E. J. Vassy, pp. 263–270 (in French).

High-Latitude Studies of F-Layer and Outer Atmosphere Ionization, by L. Owren, H. Bates and J. Pope, pp. 271–284.

Ionospheric Electron Content From Refraction Measurements on Cosmic Radio Sources, by M. M. Komesaroff and C. A. Shain, pp. 285–290.

Radar Studies of the Cislunar Medium —Part I: Theoretical, by V. R. Eshleman, R. C. Barthle and P. B. Gallagher, pp. 291–300.

Radar Studies of the Cislunar Medium —Part II: Experimental, by P. B. Gallagher, R. C. Barthle and V. R. Eshleman, pp. 301–312.

Measurements of Ionospheric Electron Content by the Lunar Radio Technique, by Siegfried J. Bauer and Fred B. Daniels, pp. 313–320.

The Upper Atmosphere Above F2-Maximum, North Atlantic Treaty Organization, AGARDograph 42, H. Poeverlein (ed.), May 1959, 355 pp.

Optical, Electromagnetic and Satellite Observations of High-Altitude Nuclear Detonations, Part I, by Philip Newman, pp. 183–200.

Optical, Electromagnetic and Satellite Observations of High-Altitude Nuclear Detonations, Part II, by Allen M. Peterson, pp. 201–210.

The Faraday Effect and Satellite Radio Signals Propagated Through the Ionosphere, by W. T. Blackband, B. Burgess, I. L. Jones and G. J. Lawson, pp. 243–262.

Remark Concerning the Charge of a Satellite, by K. Rawer, pp. 321–322.

Hybrid Whistlers and the Problem of the Whistler Paths, by R. A. Helliwell, pp. 323–332.

Low-Frequency Electromagnetic Radiation Associated With Magnetic Disturbances, by G. R. S. Ellis, pp. 333–344.

Transparency of the Ionosphere and Possible Noise Signals From High Altitudes at Extremely Low Frequencies, by H. Poeverlein, pp. 345–354.

Radio-Star Scintillations and the Auroral Zone, by P. A. Forsyth and K. V. Paulson, *Canadian J. Phys.*, vol. 39, no. 4, April 1961, pp. 502–509.

Observations of Unusual Low-Frequency Propagation Made on 12 November, 1960, by J. S. Belrose and D. B. Ross, *Canadian J. Phys.*, vol. 39, no. 4, April 1960, pp. 609–613.

The Ionospheric Disturbance of November 12 and 16, 1960, by W. S. Campbell and P. L. Hubert, *Canadian J. Phys.*, vol. 39, no. 4, April 1961, pp. 614–616.

Hydrogen Emission During the Period November 9–16, 1960, by R. Montalbetti and D. J. McEwen, *Canadian J. Phys.*, vol. 39, no. 4, April 1961, pp. 617–618.

Geomagnetic Variations Between November 12 and November 16, 1960, by E. R. Niblett, *Canadian J. Phys.*, vol. 39, no. 4, April 1961, pp. 619–621.

Observations of Auroral Ionization During the Period November 11–16, 1960, by H. V. Serson and B. C. Blevis, *Canadian J. Phys.*, vol. 39, no. 4, April 1961, pp. 622–624.

Auroral Radar Observations at 48 Mc/s During the Period of the 12 November 1960, Solar Event, by A. G. McNamara, *Canadian J. Phys.*, vol. 39, no. 4, April 1961, pp. 625–627.

Propagation of Meteor Burst Signals During the Polar Disturbance of November 12–16, 1960, by L. A. Maynard, *Canadian J. Phys.*, vol. 39, no. 4, April 1961, pp. 628–629.

Ionospheric Absorption on November 12, 1960, by E. L. Vogan and T. R. Hartz, *Canadian J. Phys.*, vol. 39, no. 4, April 1961, pp. 630–634.

An Instrument to Measure the Solar Constant From a Satellite, by Rudolf A. Hanel, *NASA Tech. Note* D-674, April 1961, 15 pp.

IRIG System Standards for C-Band (5 CM) Instrumentation Radars and Beacons, *Inter-Range Instrumentation Group, White Sands Proving Ground, N. M., Electronic Trajectory Measurements Working Group, Beacon Committee, Recommendation* 106-59, May 1961, 65 pp.

Electronic Trajectory Systems Catalogue, Vol. 2, Radar Beacons, *Inter-Range Instrumentation Group, White Sands Proving Ground, N. M.*, No. 104-58, June 1958, 210 pp.

Electronic Trajectory Systems Catalogue, vol. 2 (A) Comparison Chart of Radar Beacons, *Inter-Range Instrumentation Group, White Sands Proving Ground, N. M.*, no. 105-58, June 1958, 56 pp.

Frequency Utilization Parameters and Criteria, *Inter-Range Instrumentation Group, White Sands Proving Ground, N. M., Recommendation* 102-56, Feb. 1956, 13 pp.

Rotating Pendulum Accelerometer, by Samuel Schalkowsky and Henry F. Blazek, ARS JOURNAL, vol. 31, no. 4, April 1961, pp. 469–473.

Optical Refraction With Emphasis on Corrections for Points Outside the Atmosphere, by Duane C. Brown, ARS JOURNAL, 31, no. 4, April 1961, pp. 549–550.

Methods and Apparatus for the Measurement of Low Gas Pressures VII. Ionization Manometer, by Halmut J. Schwarz, *Archiv für Techisches Messen*, no. 302, March 1961, pp. 49–52 (in German).

Seventeen Ways to Measure Acceleration, by H. B. Sabin, *Control Engng.*, vol. 8, no. 2, Feb. 1961, pp. 106–110.

The Solar Noise Burst of November 12, 1960, by A. E. Covington, G. A. Harvey and L. R. McNarry, *Canadian J. Phys.*, vol. 39, no. 4, April 1961, pp. 635–637.

Delayed Propagation of Solar Cosmic Rays on September 3, 1960, by L. R. Davis, C. E. Fichtel, D. E. Guss, and K. W. Ogilvie, *Phys. Rev. Letters*, vol. 6, no. 9, May 1, 1961, pp. 492–494.

Heavy Nuclei in Solar Cosmic Rays, by C. E. Fichtel and D. E. Guss, *Phys. Rev. Letters*, vol. 6, no. 9, May 1, 1961, pp. 495–496.

Electromagnetic Radiation in an Atmosphere in Arbitrary Electric Conductivity, by F. Reiche and H. F. Ludloff, *Phys. of Fluids*, vol. 4, no. 5, May 1961, pp. 618–621.

Investigating the Ionosphere by Vertical Probing Methods During the International Geophysical Year, by N. M. Boenkova, *Radio Engng.* (*Transl. of Radiotekhnika*) vol. 15, no. 4, 1960, pp. 28–33.

The U. S. Planetary Exploration Program, by Robert J. Parks, ASTRONAUTICS, vol. 6, no. 5, May 1961, pp. 22–25, 52–56.

Orbiting Astronomical Observatories, by Robert R. Ziemer, ASTRONAUTICS, vol. 6, no. 5, May 1961, pp. 36–37, 58–60.

Human Factors and Bio-Astronautics

Cosmic-Ray Monitoring of the Manned Stratolab Balloon Flights, by H. Yagoda, *AF Cambridge Res. Center*, AFCRL-TN-640, Sept. 1960 (GRD Res. Note 43).

Requirements for Artificial Gravity During Prolonged Space Flight-Impact on Vehicular Design and Operation, by A. M. Mayo, *Amer. Astron. Soc.* paper 61-13, Jan. 16–18, 1961.

Biological Systems in Interplanetary Environment: Semi-Annual Status Report, by C. A. Tobias, *Calif. Univ., Space Sciences Lab.*, Series 2, Issue I, Jan. 10, 1961.

Chimpanzee Temperature-Humidity Tolerance Tests, by Erwin R. Archibald and William E. Ward, *Air Force Missile Dev. Center, Tech. Rep.* 61-11, April 1961, 53 pp.

Proceedings (Advances in the Astronautical Sciences, U. S.) American Astronautical Society, Western National Meeting, Plenum Press, New York, 1960, 355 pp.

Human Factors in Probing Outer Space, by Henry A. Imus, pp. 15–24, 50 refs.

Human Factors in Spacecraft Technology, by Richard N. deCallies, pp. 39–50.

Ballistic Missile and Space Technology, vol. 1: Bioastronautics and Electronics and Invited Addresses (Symposium on Ballistic Missile and Space Technology, 5th, Los Angeles, Aug. 1960) Donald P. Le Galley (ed.), Academic Press, New York, 1960, 494 pp.

Genetics and the Reliability of Ecological Systems, by D. F. Mitchell, pp. 63–76.

Man Protection During Landing Impact of Aerospace Vehicles, by James W. Brinkley, pp. 91–106.

Human Experiments to Determine Human Tolerance to Landing Impact in Capsule Systems, by Galen A. Holcomb, pp. 107–142.

COMMUNICATIONS

HOW TO ADD DEPTH TO THE RF SPECTRUM

Faced with an almost unsolvable problem, Martin engineer McKay Goode helped parlay a unique concept and three years of research into a spectacular advancement in radio communications. • The problem turned over to Goode and a team of specialists was to design a flexible, interference-free, mobile communications system that would reliably perform in high-density military operations. • Their answer: a system called RACEP.* Here, speech signals are pulse-coded into millionth-of-a-second fragments, combined at random and transmitted all at once over the same frequency. Only receivers preset for the proper code can receive and reconstruct the fragments into normal speech. • *Result: Engineers working in the creative environment at Martin in Florida have given the almost saturated rf spectrum a new life.*

*Random Access and Correlation for Extended Performance

MARTIN
ORLANDO

Breakthroughs like this are achieved when men with talent are allowed to seek their own solutions. At The Martin Company in Orlando, Florida, there is a continuing need for engineers and scientists who can help push forward technological frontiers. • For information about your place in one of our six major missile and electronics systems, or in one of our future programs, write: C. H. Lang, The Martin Company, Orlando 81, Florida.

Immediate technical staff openings include:

COMMUNICATIONS / DIGITAL COMPUTER RESEARCH / HUMAN FACTORS / OPERATIONS RESEARCH / WEAPONS SYSTEMS ANALYSIS / GUIDANCE & CONTROL SYSTEMS / HIGH RESOLUTION RADAR / FLUID DYNAMICS / AEROSPACE DYNAMICS / INFORMATION THEORY

All qualified applicants will receive consideration for employment without regard to race, creed, color or national origin.

POWER CONVERSION SYSTEMS
The Power/Equipment Division of Aerojet-General offers a complete capability in advanced power systems for space missions, including:
• nuclear turbo-electric systems
• solar dynamic and static systems
• cryogenic dynamic systems
• advanced electrical and support equipment
Aerojet's nuclear SNAP-8 Electric Generating System for NASA converts reactor thermal energy to electrical energy for spacecraft, providing power for electrical propulsion, and scientific or military operations.
POWER/EQUIPMENT DIVISION
Aerojet-General
CORPORATION
Azusa, California
A SUBSIDIARY OF THE GENERAL TIRE AND RUBBER COMPANY
THE GENERAL TIRE

Engineers, scientists – investigate outstanding opportunities at Aerojet